Biofilm growth and electron storage at anodes

João Pereira

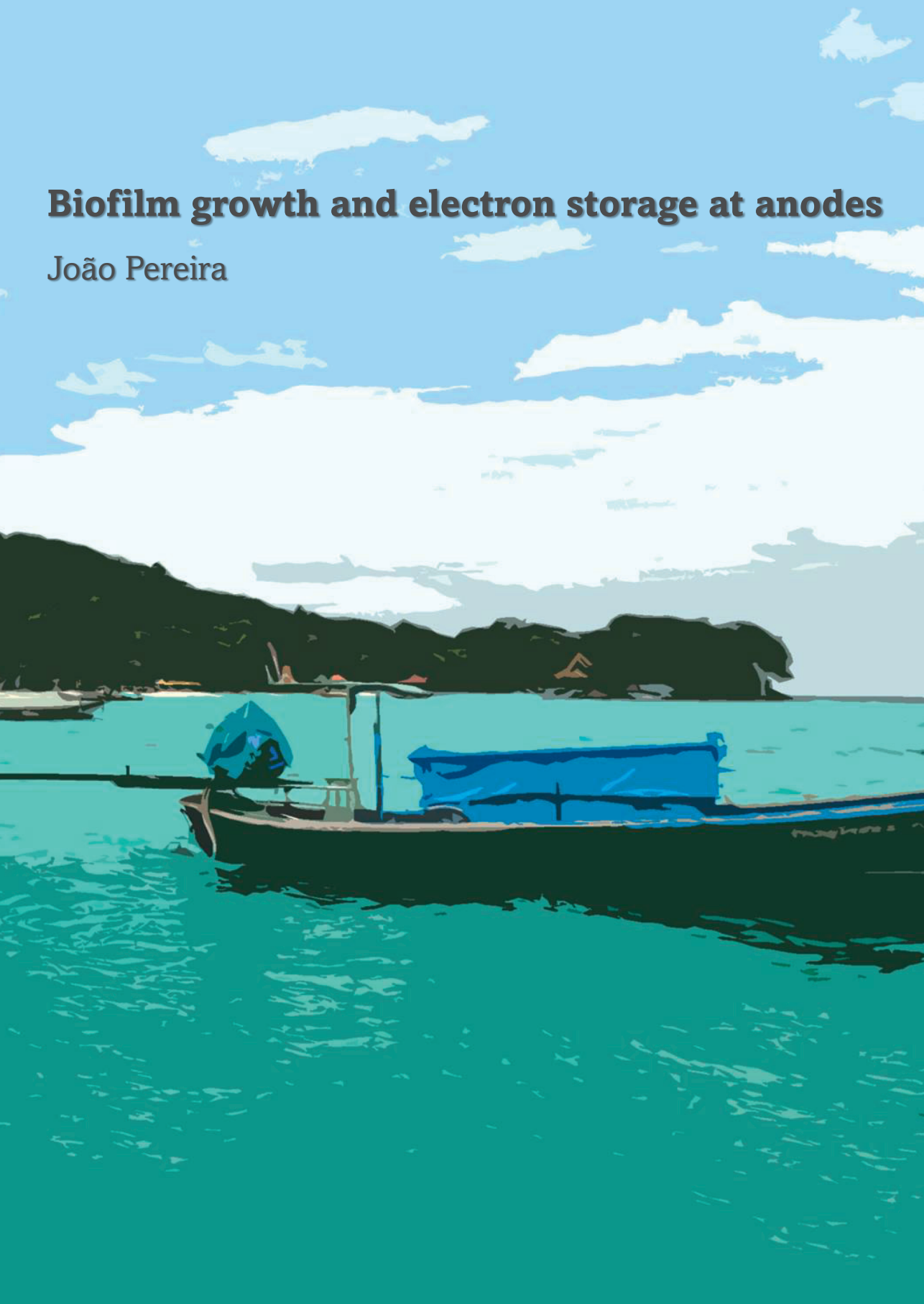

Propositions

1. Preventing the overgrowth of electro-active biofilms is essential to circumvent diffusion limited current at anodes.
   (this thesis)

2. Electrodes combined with visualization techniques are essential to better understand biological processes.
   (this thesis)

3. Scientific papers should not become an intellectual social media network.

4. Scientific equality is created by sharing and applying knowledge in low-income countries.

5. Interdisciplinarity is key to creativity in mature and biased minds.

6. Judgemental minds are obstacles to personal development.

7. Social pressure detaches voices from hearts.

8. Approaches to sustainability should not interfere with culture or human lifestyle.

Propositions belonging to the thesis, entitled

Biofilm growth and electron storage at anodes

João Pereira
Wageningen
11th September 2023

Biofilm growth and electron storage at anodes

João Pereira

Thesis committee

Promotor

Prof. Dr Annemiek ter Heijne

Professor of Biological Recovery and Re-use Technology, Wageningen University & Research

Co-promotors

Prof. Dr H.V.M (Bert) Hamelers

Special Professor, Electrochemical Resource Recovery

Wageningen University & Research

Dr T.H.J.A. (Tom) Sleutels

Scientific Project Manager

Wetsus, Leeuwarden

Other members

Prof. Dr RA (Ruud) Weusthuis, Wageningen University & Research

Prof. Dr A. (Abraham) Esteve-Núñez, University of Alcalá, Spain

Dr C. (Cornelia) Welte, Radboud University, Nijmegen

Dr B. (Benjamin) Erable, Laboratory of Chemical Engineering, Toulouse, France

This research was conducted under the auspices of the Graduate School for Socio-Economic and Natural Sciences of the Environment (SENSE)

Biofilm growth and electron storage at anodes

João Pereira

Thesis

submitted in fulfilment of the requirements for the degree of doctor

at Wageningen University,

by the authority of the rector Magnificus,

Prof. Dr A.P.J. Mol,

in the presence of the

Thesis Committee appointed by the Academic Board

to be defended in public

on Monday 11 September 2023

at 11 a.m. in the Omnia Auditorium.

João Pereira

Biofilm growth and electron storage at anodes

217 pages

PhD thesis, Wageningen University, Wageningen, The Netherlands (2023)

With references, with summary in English, Portuguese, and Dutch.

ISBN: 978-94-6447-732-0

DOI: https://doi.org/10.18174/632451

Table of contents

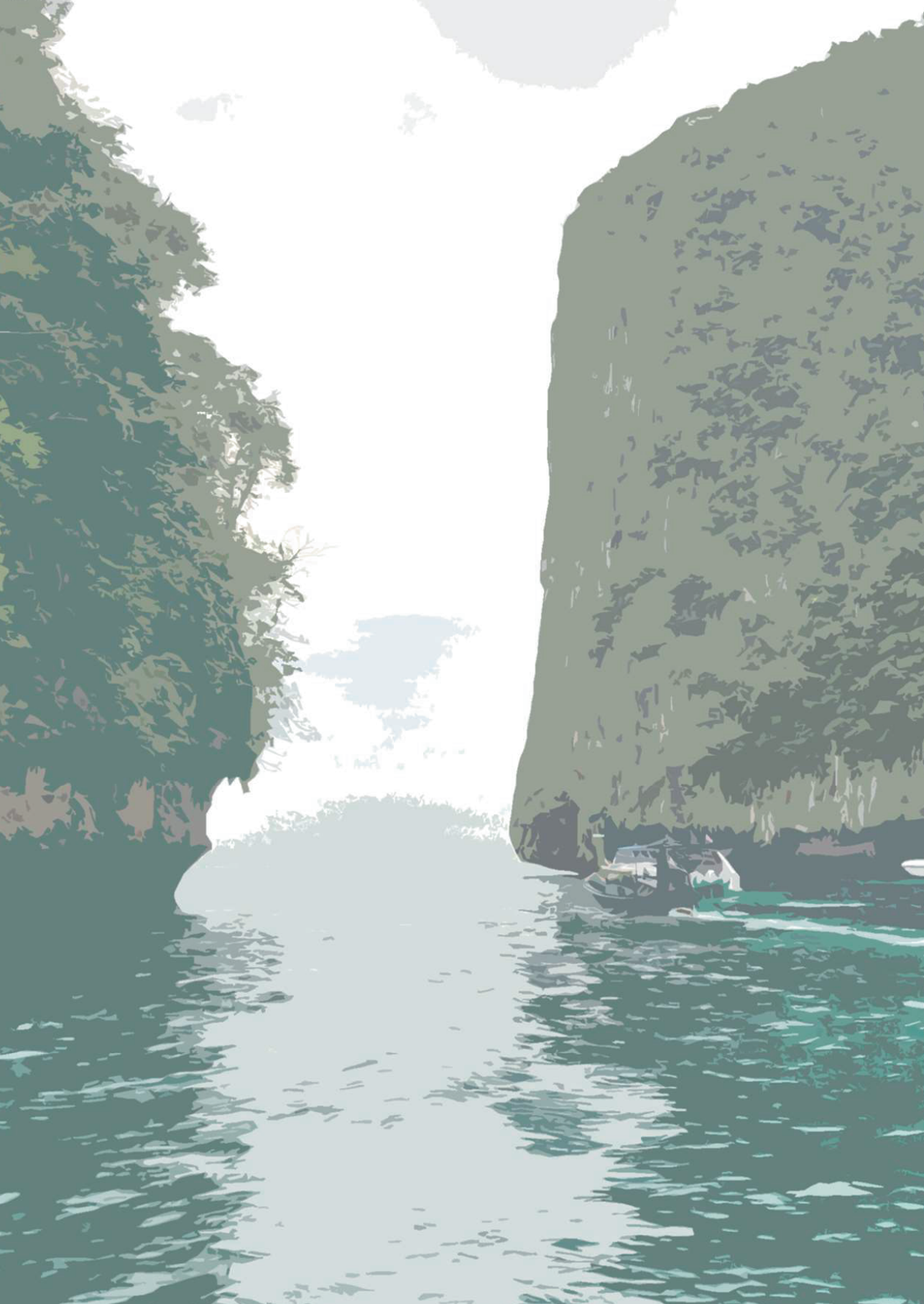

1 General introduction

In this chapter, the positioning of Bio-electrochemical Systems (BESs) as a green technology to tackle current environmental problems is discussed, including a brief explanation of the basic principles of the interaction between microorganisms and electrodes. Techniques to study electro-active microorganisms, their growth on electrodes, and their ability to store electrons are discussed as a means for understanding process limitations and opportunities for future applications.

1.1. The role of biological processes in an environmental context

Nowadays, the attention given to the environment keeps increasing as society tries to attenuate the consequences of an excessive and unweighted use of resources from previous, and also current, generations. Based on recent assessments of the planetary boundaries, it is clear that our planet is been pushed to its limits and that the boundaries of its safe operating space have been crossed.[1,2] This includes increasing risks in the categories of climate change, related to growing CO_2 emissions, freshwater change, as the water available for plants is getting scarce due to global warming, and novel entities, which are related to chemical industries for the production of e.g., plastics. The "red flags" are evident, and therefore, to tackle these challenges, while sustaining an increasing population, the consequences of the current and future use of resources to the environment need to be reconsidered. In order to guarantee the future of coming generations, it is thus important to tackle the current environmental issues and to implement a circular economy in which resources are recovered and reused as much as possible to bring our planet back to the safe operating space. Thus, this raises the call for new and sustainable technologies.

Biological processes play a crucial role towards sustainability. With microorganisms, sustainable energy can be generated, resources can be recovered, and remediation can be addressed. Examples of the contribution of biological processes are the recovery of energy from wastewater via anaerobic digestion, the removal and recovery of nutrients, e.g., nitrogen (N) and phosphorous (P), from wastewater, and the degradation of micropollutants.[3] Microorganisms are present in diverse environments (including different temperature ranges, or the presence or absence of oxygen) and are equipped with a molecular machinery that allows them to facilitate conversions, acting as catalysts in biological processes. Besides, processes based on microorganisms are associated with shorter life cycles of elements and lower environmental pollution when compared to non-biobased processes. For example, bioplastics have a shorter life cycle in comparison to chemically produced plastics due to the ability to regenerate the raw materials via biological degradation, allowing thus for a faster availability of raw materials to be reused in the same, or other, processes. As opposed, the degradation of non-biobased plastics takes longer and the raw materials these plastics are composed of are not regenerated (slowing down circularity), as these are typically incinerated for heat production, which consequently emits CO_2, thus resulting in higher environmental pollution when compared to biobased processes.

Bio-electrochemical Systems (BESs) have been introduced as a promising technology to address environmental problems.[4] These systems rely on the electron exchange between microorganisms and electrodes. Even though being widely acknowledged as a technology that allows to steer biological conversions towards the desired reactions and efficiencies, BESs are not yet used on big scales. Several factors including energy losses due to e.g., internal resistances, keeping competitive performances when scaling-up, and

cost-effectiveness still need to be addressed. Another important factor towards scalability, and to turn BES into a mature technology, is gaining more understanding of the underlying mechanisms between the microorganisms and electrodes as these can provide valuable insights towards increasing current densities and/or the production of more valuable compounds. As such, the aim of this thesis was to understand the relation between electron transfer and the growth of microorganisms on anodes and to explore electron storage mechanisms at anodes.

1.2. The principle behind the combination of electrodes and microorganisms

All reactions occurring in biological processes require the presence of an electron donor and an electron acceptor. Electrons are charged energy carriers, and they flow from the electron donor towards the electron acceptor. This forms a pair of reactions that is typically called redox reaction, in which in one reaction electrons are generated (the oxidation of the electron donor), and in another reaction the electrons are consumed (the reduction of the electron acceptor).[5] In redox reactions, electrons flow spontaneously from a high to a low energy status. Thermodynamically, electrons flow spontaneously when from an electron donor in which they have high energy (low redox potential) towards an electron acceptor in which they have low energy (high redox potential). However, when the opposite direction is wanted, energy is required to move an electron from a high to a low redox potential.

This energy associated with a given reaction can be calculated using Gibbs free energy (ΔG, in Joules). This can be calculated using Equation 1.1, in which ΔG^0 is the Gibbs free energy under standard conditions (298.15 K, 1 bar pressure, and 1 M concentration for all species), R is the universal gas constant (8.31447 J/mol/K), T is the temperature (in K), $[products]^x$ represents the product of the concentrations of the products (of partial pressures in the case of gaseous products) of the reaction to the power of their stoichiometric coefficients in the reaction (x), and $[reactants]^x$ represents the previously described for the reactants in the reaction.

$$\Delta G = \Delta G^0 + RTln(\frac{[products]^x}{[reactants]^x}) \quad \text{(Eq. 1.1)}$$

The energy associated with a reaction can be converted to a reaction potential (E), which represents the energy (or work) needed to move a charge in a reaction. Thus, the calculation of a given reaction potential considers the number of electrons transferred in a reaction. In Equation 1.2, the number of electrons exchanged in the reaction is given by n, and F is Faraday's constant (96485 C/mol$_{e^-}$). The standard potential of a reaction (E^0) can also be calculated when using ΔG^0.

$$E = -\frac{\Delta G}{nF} \quad \text{(Eq. 1.2)}$$

In redox reactions, when the difference between the potentials of the oxidation reaction (oxidation of the electron donor) and the potential of the reduction reaction (reduction of the electron acceptor) is positive, these reactions can happen spontaneously, and energy is generated. However, when this difference is negative, energy is required for the reaction to take place as the transfer of electrons is not spontaneous.[6]

In biological processes, common examples of electron donors are organic matter, and examples of electron acceptors are oxygen or nitrate. Their reactions and redox potentials are given in Table 1.1.

Table 1.1. Overview of common reactions (presented as reduction reactions) with standard (E^0) and actual (E) potential (with $[C_2H_3O_2^-]$, $[HCO_3^-]$, $[C_6H_{12}O_6]$, and $[NO_3^-]$=0.05 M, pO_2=0.2 bar, pH=7 and T=298K). All potentials are presented vs Normal Hydrogen Electrode (NHE).

Reactions	E^0 (V)	E (V)
Acetate oxidation		
$2\ HCO_3^- + 9\ H^+ + 8\ e^- \rightarrow C_2H_3O_2^- + 4\ H_2O$	0.187	-0.289
Glucose oxidation		
$6\ HCO_3^- + 30\ H^+ + 24\ e^- \rightarrow C_6H_{12}O_6 + 12\ H_2O$	0.104	-0.429
Oxygen reduction to water		
$O_2 + 4\ H^+ + 4\ e^- \rightarrow 2\ H_2O$	1.229	0.805
Protons reduction to hydrogen		
$2\ H^+ + 2\ e^- \rightarrow H_2$	0	-0.414
Nitrate reduction to nitrogen gas		
$2\ NO_3^- + 12\ H^+ + 10\ e^- \rightarrow N_2 + 6\ H_2O$	1.246	0.734

In biological processes in the presence of oxygen – in aerobic conditions – oxygen is typically the electron acceptor used by microorganisms due to its high redox potential (high tendency to receive electrons).[7] However, some microorganisms live in environments deprived of oxygen – anaerobic conditions, and in turn, other elements (with lower redox potential in comparison to oxygen) are used as final electron acceptor such as sulphate or nitrate.[8] The electron donor (also called energy source) can be an organic molecule (providing both electrons and carbon, in heterotrophic microorganisms) or an inorganic molecule providing only electrons (in lithotrophic microorganisms, e.g., hydrogen and sulphur) combined with a carbon donor (for instance CO_2, in chemolitho(auto)trophic microorganisms).[9] Regardless of the type of electron donor and acceptor used by microorganisms in a given biological process, the redox conditions are important to guarantee biological conversions. As can be seen in Table 1.1, protons (H^+) are involved in all reactions, meaning that pH plays an important role in biological conversions (as the actual concentration of protons affects the redox potentials). Besides the pH, in the case of depletion of electron donors and/or acceptors, biological conversions will be limited.

This is where electrodes can play a role in biological processes.[10] Electrodes are a solid conductive material (allowing thus electrons flow) that can be used as final electron

acceptor and/or electron donor. Hence, microorganisms can exchange the electrons derived from a biological oxidation with an electrode (electrode as a replacement of a final electron acceptor) or microorganisms can be provided with electrons from an electrode (electrode as a replacement of an electron donor).[11,12] This brings several advantages as when electrodes are used, the redox conditions can be controlled, and reactions can be steered. For example, in aerobic processes, oxygen can become limiting and thus limit the reaction rate and the performance of the process. When electrodes are used, this depletion can be circumvented as the electrode can be controlled at favouring redox conditions, allowing for the process to operate for longer times without becoming limited, reducing the costs for aeration, and allowing for the production of energy. In the same line of thinking, with electrodes, electrons can endlessly be provided to the microorganism guaranteeing that the microorganisms will not be limited in energy source. For example, it is theoretically expected that from the fermentation of one mol of glucose, twelve moles of hydrogen gas are formed.[13] However, in practice, the hydrogen yields are much lower (approximately 2 moles of hydrogen per mol of glucose), due to the formation of by-products such as acetate. With electrodes, this acetate could be converted into hydrogen (energetic output), increasing the hydrogen production yields and, in such a way, valorising organic matter and decreasing sludge yields in a wastewater treatment plant when compared to activated sludge processes.

As such, considering the ability to control the electrode potentials, electrodes can be used to provide favourable conditions for biological conversions. Besides facilitating conversions, different electrode potentials can also affect electron transfer mechanisms in the microorganisms, and thus, electrodes can ideally be used to control the conversions performed by microorganisms.

1.3. Biotechnological applications of microorganisms on electrodes and their environmental impact

In short, BESs and their applications are based on the decoupling of the oxidation and reduction reactions happening at two electrodes and on controlling the electron flow between this pair of reactions.[14] By decoupling a redox reaction into separate oxidation and reduction reactions, the use of electrodes allows to recover energy from redox reactions that are thermodynamically favourable and/or to enable reactions that are otherwise thermodynamically unfavourable.

The microorganisms that interact with and grow on electrodes are typically called electro-active microorganisms due to their ability to exchange electrons with a solid conductive material. Their interaction and exchange of electrons with the electrodes is the core working principle of BESs.[15,16] This has become of increasing interest as by exploring the fascinating capabilities of microorganisms that live on electrodes, alternative environmental solutions could be created to fight the demands and environmental threats of densely populated countries on food, and water pollution, and

therefore prevent uncontrolled climate change.[17] In the next sections, a detailed description of the working principles of BESs is provided. Besides, BESs applications and their link to the aimed environmental impact are described.

1.3.1. Working principles and performance parameters in BESs

A BES is composed of two electrodes: one anode where an oxidation reaction occurs and a cathode where a reduction reaction occurs.[18] On the electrodes, the reactions can be catalysed by electro-active microorganisms that exchange soluble chemical energy with electrical energy. Figure 1.1 shows a schematic of these systems including a bio-anode and a bio-cathode.

In a bio-anode, a soluble chemical is oxidized by microorganisms, and the electrons derived from this oxidation are given away to the anode. These electrons flow, via an external electrical circuit, from the anode to the cathode, where the same electrons are used to reduce an electron acceptor. In a bio-cathode, microorganisms are the ones performing the reduction reaction, by taking up the electrons provided by the cathode to reduce an electron acceptor to a reduced product.

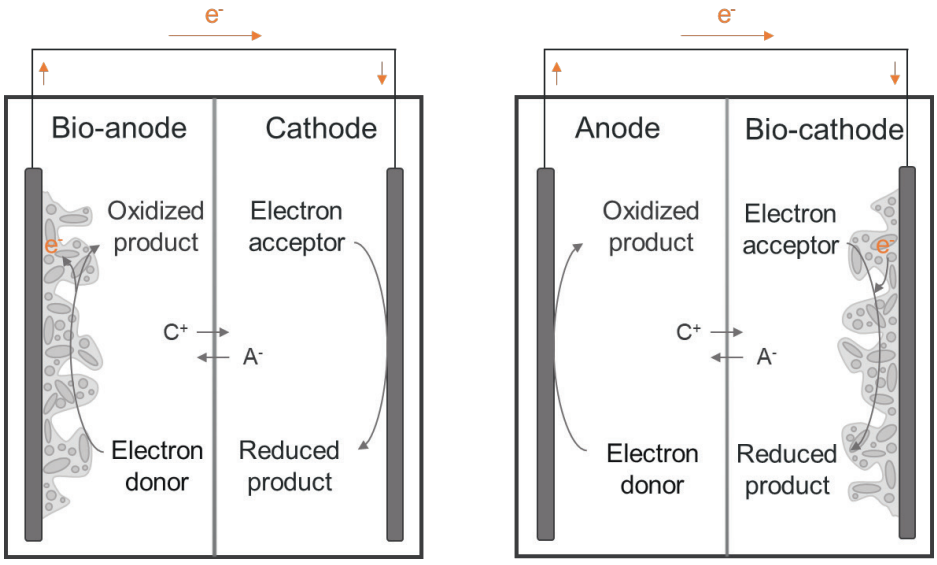

Figure 1.1. Schematic of BESs illustrating the electron exchange between chemical and electrical energy mediated by electro-active microorganisms in a bio-anode (left) and in a bio-cathode (right). The transfer of ions (C^+ cations and A^- anions) through an ion exchange membrane (line) is also represented.

Two parameters determine the energy efficiency of BESs: the Coulombic efficiency (CE) and the cell voltage (E_{cell}). The Coulombic efficiency is related to the electron efficiency. To reach high electron efficiencies, all the electrons generated by the oxidation reaction in a bio-anode should be recovered at the anode, whereas in a bio-cathode, all the

electrons provided by the cathode should end up in the desired reduced product (also called cathodic efficiency). This ratio between the electrons recovered and the electron provided is defined as CE. Equations 1.3 and 1.4 can be used to assess the performance of bio-anodes and bio-cathodes, respectively. It is wanted that CEs are close to 1 to have an efficient system. However, these are typically lower in practice as electrons are used for the growth of microorganisms and can also end up in other (unwanted) electron consuming processes.

$$CE_{anode} = \frac{electrons\ recovered\ at\ the\ anode}{electrons\ provided\ by\ the\ electron\ donor} \quad \text{(Eq. 1.3)}$$

$$CE_{cathode} = \frac{electron\ recovered\ in\ the\ reduced\ product}{electrons\ provided\ by\ the\ cathode} \quad \text{(Eq. 1.4)}$$

Besides the CE, the cell voltage is also relevant to evaluate the energy efficiencies of BES. Cell voltage (E_{cell}, Equation 1.5) is the difference between the electrode potentials, that, thermodynamically, should equal the difference between the potential of the reduction (E_{cat}) and oxidation (E_{an}) reactions occurring at the electrodes (in this case, named cell electromotive force).

$$E_{cell} = E_{cat} - E_{an} - (\eta_{cat} + \eta_{an} + IR) \quad \text{(Eq. 1.5)}$$

where η_{cat} is the overpotential at the cathode, η_{an} is the overpotential at the anode, and internal losses (IR). These overpotentials and internal resistance result in cell voltages lower than theoretically expected. The electrode overpotentials are related to activation losses (to active exchange between electrons from or to the electrodes), metabolic losses in the microorganism (through the electron transfer chain in the microorganism), and concentration losses (related to unbalances in the ratio of oxidized and reduced species at the electrodes). The ohmic losses are related to the resistance in electron flow in the electrodes and external electrical circuit, and the flow of ions between the electrolytes to keep electroneutrality (flow of C^+ and A^- in the electrolytes – anolyte in the anode and catholyte in the cathode).

The energy efficiency of a BES, which expresses the energy recovered from the energy input, is calculated by the product of the CE and E_{cell}. For high energy efficiency, it is important that both parameters are high and that overpotentials and internal resistances are kept low. Several system parameters such as the distance between the electrodes, electrode size and material, temperature, and the conductivity of the electrolyte influence overpotentials and internal losses. The electro-active microorganisms, being the catalysers of anode and/or cathode reactions, also affect the energy efficiency and are the focus of this thesis. The relevant aspects will be addressed in more detail in section 1.4, including the growth of microorganisms on the anode, and the electron transfer between the microorganisms and the electrode.

1.3.2. Examples of BESs and opportunities for environment impact

The first intended application using BESs was the generation of electrical energy in Microbial Fuel Cells (MFCs).[19] This principle linked the electron flow between the anode, which is used as an electron acceptor for the electrons generated from the microbial oxidation of acetate (organic energy), and the cathode, which is used as an electron donor to the reduction of oxygen to water. The electron flow between the two electrodes could thus be recovered as current in an external electrical circuit and used as an energy source for other applications. The combination of oxidation of acetate and reduction of oxygen is thermodynamically favourable, generating energy.[20] Based on Table 1.1, the cell electromotive force is given by

$$E_{emf}\ (V) = E_{cat} - E_{an} = +0.805V - (-0.289V) = +1.094V \qquad \text{(Eq. 1.6)}$$

The application of MFC was envisioned in wastewater treatment plants, where electroactive microorganisms would oxidize acetate (already present in wastewater effluents, that are discharged containing acetate concentrations of approximately 400 mg/L)[21] and recover energy in a sustainable and circular way from waste streams.[18] Even though this was posed as a promising source of renewable electricity, it soon became clear that the power (product of the current through the external circuit and the E_{cell}) obtained in such a system reached a maximum (maximum power point) determined by the internal resistance of the system, which in turn limited the maximum current density that could be reached.[22] After this point, higher current densities result in decreasing power outputs. In other words, this meant that the system had energy losses, such as electrode overpotentials and internal resistances as previously described. Therefore, work in this field moved mainly towards the optimization of electrode materials and reactor designs, for instance by decreasing the distance between electrodes and improving the cathodic reactions to improve power densities.[23–25]

The idea of an energy producing system was adjusted to the production of hydrogen at the cathode. Hydrogen is an energy carrier, and in a Microbial Electrolysis Cell (MEC) (Figure 1.2), the microorganisms would catalyse the conversion of acetate into the formation of hydrogen, with a little energy investment.[13]

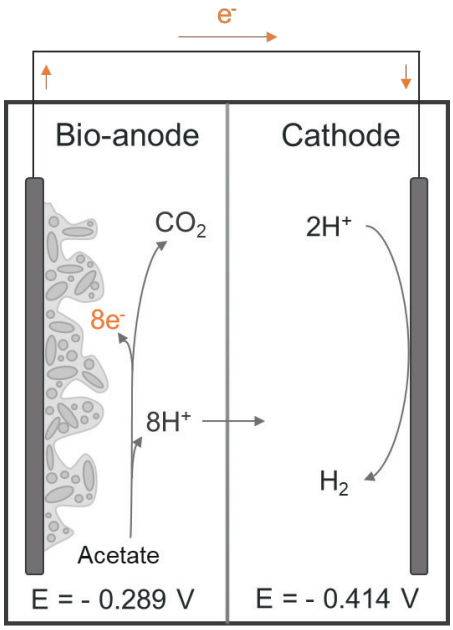

Figure 1.2. Scheme of a MEC in which microorganisms oxidize acetate in the anode and hydrogen is formed in the cathode (separated by a cation exchange membrane, illustrated by the grey line). Given the thermodynamics of the redox reactions, energy input is needed to drive the electrons from the anode to the cathode (reactions potentials from Table 1.2).

As opposed to the MFCs, the thermodynamics of this pair of reactions results in a negative electromotive force ($E_{emf}\ (V) = -0.414V - (-0.289V) = -0.125V$). Therefore, this reaction does not happen spontaneously. Even though not recovering energy from wastewater streams, this technology is still attractive due to the low energy input required. The production of H_2 is currently of high interest as this gas is considered to be a very important source of renewable energy for the coming generations.[26]

Besides bio-anodes, microorganisms can also grow on the cathode (bio-cathodes), in Microbial Electrosynthesis Systems (MES).[27,28] Here, the microorganisms take up electrons provided by the electrode, and use them as an energy source to reduce CO_2 and synthesize added value compounds. These include acetate and long chain fatty acids (caproate and butyrate) or energy storage compounds such as methane. Therefore, MESs might play an important role in providing raw materials to food industries and helping reduce CO_2 emissions, and thus global warming.[29] Besides CO_2 fixation, the formation of reduced compounds in the cathode as a form of energy storage is also very attractive due to the seasonality of current renewable energies (sun and wind energy).[30,31] When temporary excess of renewable electricity is used to form energy storage compounds, these could later be degraded and used as an energy source when

renewable energy becomes limiting. This a promising way to guarantee a constant use of green and sustainable energy.

1.4. Electro-active biofilms (EABfs) growing on anodes

Even though the wide range of possible applications for BESs and the continuous knowledge development in the field, the use of these systems on a large scale is still in its infancy.[32,33] Besides engineering aspects, the system deeply relies on its (bio)catalysers: electro-active microorganisms.[34]

In anodic EABfs, the exchange of the electrons derived from the oxidation of the electron donor (or substrate) with the anode, measured as current (or given as current density when normalized by the available anode surface area), is an important performance parameter.[35] Together with high CEs and cell voltages, the higher performance of bio-anodes depends on higher currents, which means a faster electron transfer rate between the EABf and the anode. This electron flow is mediated by microorganisms that, after catalysing the degradation of the organic donor, use charge carriers – these are redox groups in protein-based compounds such as cytochromes, or co-factors such as NAD+/NADH – to allow the electrons to reach the electrode and thus produce current. The transfer of electrons between the EABf and the anode can be completed via three different ways: 1) direct contact between the microorganisms and the anode, 2) mediated electron transfer by means of soluble charge carriers, and 3) via nanowires (or conductive pili structures) that are biological structures that allow electron tunnelling towards the anode.[36–38]

1.4.1. Anode potential control and its influence on anodic EABfs

To study and to better understand electron flows in anodic EABfs, the most convenient approach is to control the anode potentials and measure the exchange of electrons between the EABfs and the anode (as current) – this is called chronoamperometry.[39] From a research point of view, this strategy allows to control the anode potential and to study the microorganisms on the electrodes and their interaction with the electrode under a wide range of anode potential conditions.

The set anode potential is of crucial importance as this determines the energy available for the microorganism when using the anode ad final electron acceptor. As such, the energy gained by the microorganisms is determined by the difference between the energy of the electrons in the substrate (carbon source and electron donor) and the energy of the electrons in the final electron acceptor (the anode potential, which can be controlled). This means that, for a given electron donor, the higher the set anode potential, the higher the potential difference between the set anode potential and the oxidation potential of the electron donor (so-called overpotential), and consequently, more energy can be gained by the microorganism.[40] When acetate is used as an electron donor, the anode potential that allows microorganisms to gain energy by using the

anode as a final electron acceptor needs to be more positive than the oxidation potential of acetate (Table 1.1).

Besides the set anode potential, the anode potential can also be controlled at different regimes. For example, the anode potential can be continuously controlled, meaning that the anode is continuously available as a final electron acceptor, or the anode potential can be controlled intermittently. The last consists of alternating periods of anode potential control and Open Cell Potential (OCP, in which the external electrical circuit is opened and no current flows), meaning that the anode is only temporarily available as the final electron acceptor.

Both the set value and anode potential regime can affect the electron flow mechanisms from the electron donor to the electron acceptor, as the set potential determines the overall energy gain, and intermittent anode potential forces the EABf to temporarily deviate the electron flow to another electron sinks other than the anode (Figure 1.3).

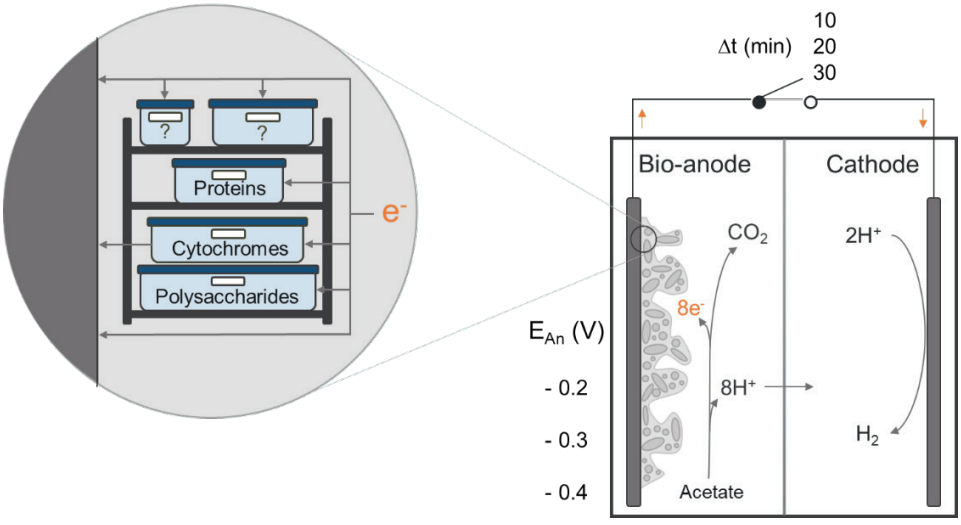

Figure 1.3. Example of an acetate fed bio-anode and illustration of possible alternative electron flows under different set anode potentials and when the anode is intermittently available as final electron acceptor. Electrons can be used, among others, for growth and the synthesis of proteins and polysaccharides (adapted from ter Heijne et al., 2020).

Alternative electron sinks include electrons used for microorganisms' growth, for the synthesis of polysaccharides and proteins, to reduce charge carriers, and, when present, alternative electron acceptors. These electron sinks decrease the charge recovered at the anode (lower CEs).

The flow of the electrons in the anode can be affected by the provided set anode potential and anode potential regime, suggesting that EABfs respond and can be controlled by the anode conditions. In theory, this control can be used to promote a

desired microbial response and favour certain biological conversions. However, in practice, this requires understanding and quantifying electron flows in the anodic EABf, e.g., by measuring microorganism growth and quantifying alternative electron consuming processes. This approach allows to understand the adaptations of EABfs to the anode conditions, related to produced currents and CEs, and can, ultimately, contribute to the optimization of electron transfer between the microorganisms and electrodes.

1.4.2. The growth of anodic EABfs

After their generation during acetate oxidation and before being exchanged with the anode, electrons flow inside the microorganisms and, via the tricarboxylic acid (TCA) cycle, energy is formed in the form of ATP (via phosphorylation) for the microorganisms.[42] This gained energy can be used, among others, for reproduction, and for maintenance and repair processes in the microorganisms. However, in anodic EABfs, as it is desired that the biggest fraction of electrons derived from the acetate are recovered as current at the anode (in other words, high CE), little growth (and negligible use of electrons in alternative processes) is preferred. Nevertheless, as electro-active microorganisms are the bio-catalysers in anodes, it is wanted that the whole anode surface is covered by microorganisms to increase electrons transfer to the anode, and to allow for more and faster acetate consumption. Therefore, microorganisms' growth is essential to increase electron transfer rates with the anode, but their growth leads to lower CEs and can also decrease produced currents.

When microorganisms grow on an electrode, these typically form a biofilm that is referred to as electro-active biofilm (EABf, as previously described).[43] This is an accumulation of microorganisms that inhabit the electrode surface and perform electron exchange with the electrode. Over time, and as the microorganisms grow, an EABf is formed that is composed of several layers of microorganisms embedded in a matrix. As such, being layers and layers of microorganisms piled up in an EABf, not all the microorganisms present in the EABf will be in direct contact with the electrode surface. The development of an anodic EABf increases thus the distance between the top layer of microorganisms and the anode surface, which translates into an increase in the distance between the electron donor (in solution) and the electron acceptor (the electrode). Particularly, this increases the distance between the bottom layers of microorganisms (the first layers of microorganisms on the electrode) and the electron donor, as well as the distance between the top layers and the electron acceptor. Consequentially, this can create different local conditions inside the EABfs which can affect biological conversions. For example, the consumption of acetate by the whole EABf can be affected if the acetate concentration in the EABf matrix is not homogeneous. Besides, as the acetate oxidation produces protons (that need to diffuse out of the EABfs matrix towards the cathode), pH gradients can be formed in the EABf matrix, affecting the activity of EABfs. As a consequence, the creation of the desired

environment for the microorganisms via controlling anode potentials becomes less effective, and consequently, the rate at which electrons are exchanged with the anode can decrease.

1.4.3. Electron storage in anodic EABfs

Besides being recovered at the anode or used for growth, electrons can take different pathways in anodic EABfs.[41] It has recently been suggested that intermittent anode potential regimes lead to electron storage in anodic EABfs. This was shown in a study in which anodic EABfs microorganism kept oxidizing acetate while under OCP.[44] As there is no current during OCP, anodic EABfs have a storage mechanism to allow continuous acetate oxidation when the anode is not available as the final electron acceptor.

Two different types of electron storage mechanisms in anodic EABfs have been suggested (Figure 1.4): 1) temporary and extracellular electron storage in charge carriers (such as flavins and cytochromes) that are located at the membrane of the microorganisms, and 2) intercellular electron storage in the form of reduced compounds such as biopolymers.

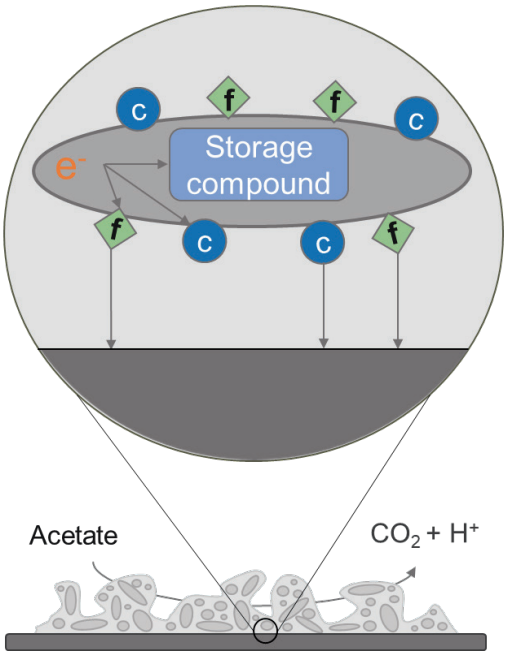

Figure 1.4. Electron storage in anodic EABfs: storage in reduced cytochromes (c) and flavins (f), and storage in intracellular compounds (adapted from ter Heijne et al., 2020).

The temporary storage is suggested to take place when the anode is not available as final electron storage (OCP conditions) for short intermittent periods (in the order of seconds or minutes). Consequently, the charge carriers remain reduced until the anode

potential is applied again (closed circuit conditions). At that point, the release of stored electrons from the EABfs towards the electrode takes place, which results in a measured peak current (also referred to as discharge of the EABf). This sequence of EABf discharges because of repeating intermittent cycles, has been suggested to increase current densities at the anode and to enrich the EABf in charge carriers.[45]

The intracellular storage in the microorganisms present in the anodic EABf is presumed to take place when the anode is not available for long intermittent periods of time (in the orders of hours). This storage can result in the formation of polymers and lipophilic inclusions, such as poly-hydroxyalkanoates (PHA), polyphosphate, triacylglycerol, and glycogen. These are typically produced when microorganisms have excess energy or when depleted in an essential growth element. These compounds are then biological storage mechanisms and can be a long-term reservoir of carbon and energy.

1.4.4. The effect of electron donor and electron acceptor imbalances on anodic EABfs

On the one hand, in the case of an intermittent availability of the anode as the final electron acceptor and a constant availability of acetate, anodic EABfs face an excess of acetate while limited in their access to the anode. On the other hand, in case of limited availability of acetate while the anode is constantly available as a final electron acceptor, anodic EABfs face starving conditions (which can also be stimulated by the absence of other essential growth elements, e.g., phosphate, rather than acetate) while having continuous access to the anode. Both scenarios create an imbalanced ratio between the electron donor and electron acceptor (Figure 1.5).[46]

These imbalances may create stressful conditions for the microorganisms, namely excess of electrons or lack of electron donor, that can thus promote the accumulation of electrons extracellularly (reduction of charge carriers), intracellularly in the form of storage compounds, or lead to the production of Extracellular Polymeric Substances (EPS) that will also accumulate extracellularly in the EABf matrix. Besides being a mechanism to cope with the anode and acetate conditions, the storage of electrons in the form of stored compounds can bring advantages to the microorganisms as these compounds can be oxidized and used as carbon and energy sources when in the absence of substrate.[47,48]

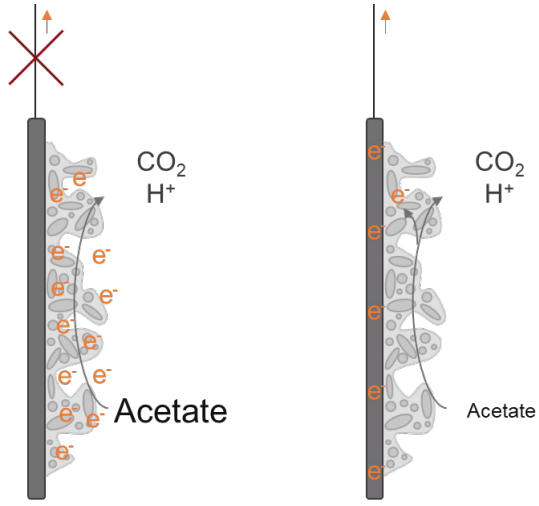

Figure 1.5. Imbalances between the electron donor and electron acceptor affect the exchange of electrons between the EABf and the anode and induce alternative electron flow such as electron storage. Excess of electron donor while limited availability of the anode is represented on the left, and limited access to the electron donor while constant availability of the anode is represented on the right.

Therefore, changing the set anode potential and exploring anode potential regimes, as well as different feeding modes, may influence electron flows by interfering with the exchange of electrons between microorganisms and the anode surface. This can affect the growth, morphology, and composition of the EABfs, as well as the amount of storage compounds in the EABfs. Even though these can be seen as undesired electron sinks, monitoring and quantifying these alternative electron flows provide more information towards the understanding of EABfs, and ultimately, it can be used as a tool to increase the flow of electrons towards the desired sink (the anode). Besides, this knowledge gained by understanding the biological response to different ratios between electron donor and acceptor can eventually be translated to other biological processes without electrodes.

1.5. The need to have a closer look at the EABfs on electrodes

As previously mentioned, specific operating conditions can prioritize a given electron pathway over another. However, since all the reactions (or in other words, the chosen electron pathways) are catalysed by microorganisms in the EABfs, more attention must be given to these microorganisms and their adaptation to the operating conditions over time, as these microorganisms can determine and explain system performances. For this purpose, several kinds of techniques can be used as shown in Figure 1.6.

EABfs are complex and dynamic.[49,50] Therefore, tracking and monitoring the growth and composition of EABfs on the electrode surface over time can provide a more complete

insight into the adaptations undergone by the EABfs during their development. Due to the electro-active attribute of these microorganisms, electrochemical techniques can be used to study their performances.[51] These techniques typically apply a current or potential and measure the respective potential or current response of the EABfs, therefore, characterizing the exchange of electrons between the EABfs and the electrode. In the anode, these electrons can thus be related to the electrons derived from substrate oxidation (typically measured by means of chemical analysis such as Chemical Oxygen Demand or chromatography), and in the cathode, related to the synthesis of a desired product to calculate conversion performances (CEs in anodes and cathodes, as described in Equations 1.3 and 1.4). Besides, with electrochemical techniques such as Cyclic Voltammetry and Electrochemical Impedance Spectroscopy (EIS), the presence of certain redox compounds can also be assessed.[52,53]

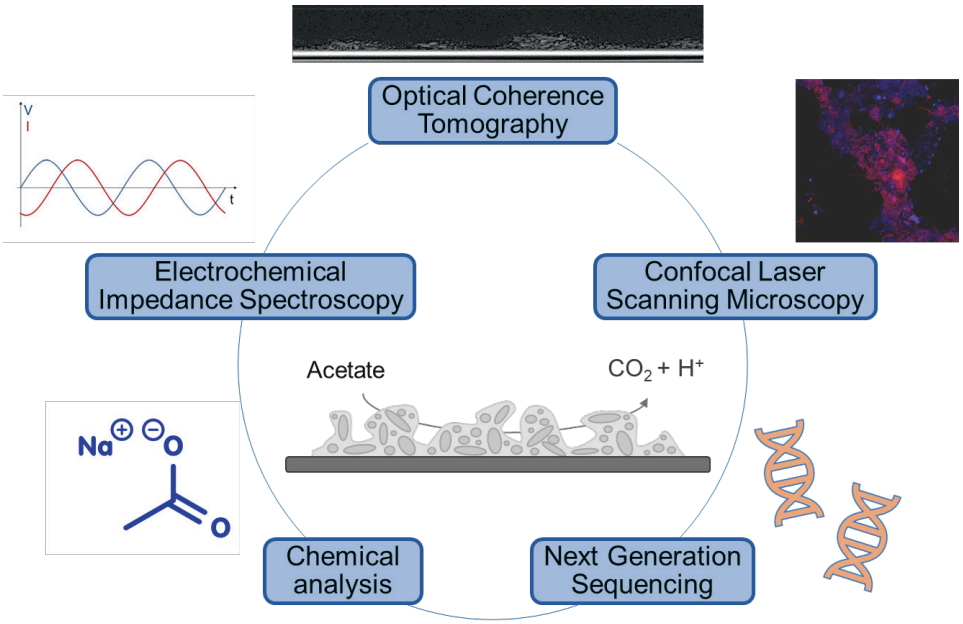

Figure 1.6. Tools to better understand the adaptation of anodic EABf to the electron donor feeding and electron acceptor regimes. The results from different techniques can be used to measure the consumption rate of the electron donor, quantify EABf growth and electron storage, and relate these to the produced current at the anode.

The quantification of the amount of EABf on an electrode surface is usually performed with visual techniques. These can be used for the quantification of electrons that ended up as growth, as well as the EABf composition, including intracellular and extracellular electron storage compounds.[54] In Figure 1.6, Optical Coherence Tomography (OCT) and Confocal Laser Scanning Microscopy (CLSM) are shown as two examples of visual

techniques: the thickness and morphology of EABfs can be visualized with OCT and CLSM, and the composition and microbial mapping can be visualized with CLSM.

Besides electrochemical and visual characterization, molecular techniques are frequently needed as EABfs can be constituted of mixed cultures (more linked to application studies) or pure cultures (with a more controlled environment for fundamental studies). A typical microorganism studied in anodic EABfs is *Geobacter sulfurreducens*, even though there are several other electro-active microorganisms.[55] DNA analysis of the microbial community present in the EABf is thus of crucial importance, as well as tracking how the community changes as a function of the operating conditions.

1.6. Research objective and Outline

The aim of this thesis was to study the development and characterisation of anodic EABfs over time to quantify electron flows and to better understand the electron exchange from acetate towards the anode. In brief, the effect of the amount of EABf on electron transfer was studied and electron storage mechanisms in anodic EABfs were explored by means of electrochemical and visual techniques.

In Chapter 2, an overview of several visual techniques is given and presented as a tool towards EABfs quantification on an electrode. A short description of the working principles, along with the advantages and disadvantages of each technique is described, aiming at conveying the importance of measuring the amount and composition of EABfs on an electrode and relating these to performance parameters. By referring to different types of techniques such as electrochemical and chemical, the combination of visual techniques with established methodologies was highlighted and introduced as a source of inspiration for future work in BES.

OCT was one of the visual techniques used in this thesis to quantify the growth of EABfs on the anode. With this technique, the thickness of the EABfs was measured under different operating conditions and related to the produced current at the anode. The relation between EABfs thickness and the produced current was explored using a simple dynamic model considering acetate and buffer diffusion in EABfs. In Chapter 3, acetate penetration depths in the EABf were calculated and related to the measured EABfs at different anode potentials and acetate concentrations. This allowed to compare the thickness of the EABf to the acetate penetration depth and to report the maximum acetate penetration depth (meaning the maximum thickness of a non-acetate limited EABf) under different operating conditions.

As protons are produced when acetate is oxidized, a similar approach was used to understand how deep phosphate buffer could penetrate the EABf and intervene in the diffusion of protons out of the EABfs. This is presented in Chapter 4, in which the effect of different buffer concentrations on EABf growth and current production was studied. In both Chapters 3 and 4, acetate and buffer diffusion rates are reported, as well as

specific acetate consumption rates, at different operating conditions. These are important parameters for future modelling works in EABfs, that can be extrapolated to cathodic EABfs and used as a tool to better characterize EABf in BESs.

In Chapter 5, the effect of intermittent anode potential regimes on electron flows in EABfs was studied as an approach to improve EABfs performance and study alternative electron flows. Here, EABfs were grown under different intermittent times, and a balance was set up to quantify electron sinks. This electron balance included electrons recovered at the anode, EABf growth (including planktonic cells), and electrons used to produce EPS. This study allowed to understand electron flows in the anode by monitoring EABfs response to the intermittent availability of the electrode as the final electron acceptor.

In Chapter 6, and to complement the previous chapter in which only electron acceptor regimes were experimented, EABfs were grown in continuous and batch feeding modes to further understand electron storage, including intracellular storage. CLSM was used as a visual technique to visualize and quantify storage in the form of PHA. These two aforementioned chapters, focussed on electron storage, open the door to new niches and possible applications of BESs towards the production of EPS and bioplastics.

Finally, a discussion on the knowledge gained in EABfs and its transition to application is given in Chapter 7. As the amount of EABfs on the anode was measured, allowing to calculate biomass growth yields, a short case study on the application of bio-anodes in wastewater treatment plants will be presented in this last chapter. Besides, challenges towards the application of anodic EABfs in wastewater treatment plants will be enumerated and discussed. These will include mass transfer limitations (acetate and buffer) and will be focussed on the thickness of the EABf and methodologies to control the growth of the EABfs. To conclude, a brief discussion on the metabolic pathways for EPS and PHA will be discussed and how these can be used in practice.

1.7. References

1. Wang-Erlandsson, L. *et al.* A planetary boundary for green water. *Nat. Rev. Earth Environ.* **3**, 380–392 (2022).
2. Persson, L. *et al.* Outside the Safe Operating Space of the Planetary Boundary for Novel Entities. *Environ. Sci. Technol.* **56**, 1510–1521 (2022).
3. AlSayed, A., Soliman, M. & Eldyasti, A. Microbial fuel cells for municipal wastewater treatment: From technology fundamentals to full-scale development. *Renew. Sustain. Energy Rev.* **134**, 110367 (2020).
4. Borole, A. P. *et al.* Electroactive biofilms: Current status and future research needs. *Energy Environ. Sci.* **4**, 4813–4834 (2011).
5. Korth, B., Rosa, L. F. M., Harnisch, F. & Picioreanu, C. A framework for modeling electroactive microbial biofilms performing direct electron transfer. *Bioelectrochemistry* **106**, 194–206 (2015).
6. Arends, J. B. A. & Verstraete, W. 100 years of microbial electricity production: Three

concepts for the future. *Microbial Biotechnology* vol. 5 333–346 (2012).

7. Kracke, F., Vassilev, I. & Krömer, J. O. Microbial electron transport and energy conservation - The foundation for optimizing bioelectrochemical systems. *Front. Microbiol.* **6**, 1–18 (2015).

8. Tharali, A. D., Sain, N. & Osborne, W. J. Microbial fuel cells in bioelectricity production. *Front. Life Sci.* **9**, 252–266 (2016).

9. Frühauf-Wyllie, H. M. & Holtmann, D. Geobacter sulfurreducens metabolism at different donor/acceptor ratios. *Microbiologyopen* **11**, (2022).

10. Babauta, J., Renslow, R., Lewandowski, Z. & Beyenal, H. Electrochemically active biofilms: Facts and fiction. A review. *Biofouling* **28**, 789–812 (2012).

11. Santoro, C., Arbizzani, C., Erable, B. & Ieropoulos, I. Microbial fuel cells: From fundamentals to applications. A review. *J. Power Sources* **356**, 225–244 (2017).

12. Hamelers, H. V. M. *et al.* New applications and performance of bioelectrochemical systems. *Appl. Microbiol. Biotechnol.* **85**, 1673–1685 (2010).

13. Logan, B. E. *et al.* Microbial Electrolysis Cells for High Yield Hydrogen Gas Production from Organic Matter. *Environ. Sci. Technol.* **42**, 8630–8640 (2008).

14. Erable, B., Duţeanua, N. M., Ghangrekar, M. M., Dumas, C. & Scott, K. Application of electro-active biofilms. *Biofouling* **26**, 57–71 (2010).

15. Das, D. *Microbial fuel cell: A bioelectrochemical system that converts waste to watts*. *Microbial Fuel Cell: A Bioelectrochemical System that Converts Waste to Watts* (2017). doi:10.1007/978-3-319-66793-5.

16. Cologgi, D. L., Otwell, A. E., Speers, A. M., Rotondo, J. A. & Reguera, G. Genetic analysis of electroactive biofilms. *Int. Microbiol.* (2021) doi:10.1007/s10123-021-00176-y.

17. Virdis, B. *et al. Microbial Fuel Cells*. *Treatise on Water Science* (2011). doi:DOI: 10.1016/B978-0-444-53199-5.00098-1.

18. Ramírez-Vargas, C. A. *et al.* Microbial electrochemical technologies for wastewater treatment: Principles and evolution from microbial fuel cells to bioelectrochemical-based constructed wetlands. *Water* **10**, 1–29 (2018).

19. Logan, B. E. *Microbial fuel cells*. (Wiley-Interscience, 2008).

20. Logan, B. E. *et al.* Microbial fuel cells: Methodology and technology. *Environmental Science and Technology* vol. 40 5181–5192 (2006).

21. Korth, B., Heber, C., Normant-Saremba, M., Maskow, T. & Harnisch, F. Precious Data from Tiny Samples: Revealing the Correlation Between Energy Content and the Chemical Oxygen Demand of Municipal Wastewater by Micro-Bomb Combustion Calorimetry. *Front. Energy Res.* **9**, 1–8 (2021).

22. Sleutels, T. H. J. A., Ter Heijne, A., Buisman, C. J. N. & Hamelers, H. V. M. Bioelectrochemical systems: An outlook for practical applications. *ChemSusChem* **5**, 1012–1019 (2012).

23. Ter Heijne, A., Hamelers, H. V. M. & Buisman, C. J. N. Microbial fuel cell operation with continuous biological ferrous iron oxidation of the catholyte. *Environ. Sci. Technol.* **41**, 4130–4134 (2007).

24. Heijne, A. Ter *et al.* Copper recovery combined with electricity production in a microbial fuel cell. *Environ. Sci. Technol.* **44**, 4376–4381 (2010).

25. Yang, L. *et al*. Building electrode with three-dimensional macroporous interface from biocompatible polypyrrole and conductive graphene nanosheets to achieve highly efficient microbial electrocatalysis. *Biosens. Bioelectron.* **141**, 111444 (2019).

26. Kadier, A. *et al*. A comprehensive review of microbial electrolysis cells (MEC) reactor designs and configurations for sustainable hydrogen gas production. *Alexandria Eng. J.* **55**, 427–443 (2016).

27. Pant, D. *et al*. Bioelectrochemical systems (BES) for sustainable energy production and product recovery from organic wastes and industrial wastewaters. *RSC Advances* vol. 2 1248–1263 (2012).

28. Schröder, U., Harnisch, F. & Angenent, L. T. Microbial electrochemistry and technology: Terminology and classification. *Energy Environ. Sci.* **8**, 513–519 (2015).

29. Thapa, B. Sen *et al*. Overview of electroactive microorganisms and electron transfer mechanisms in microbial electrochemistry. *Bioresour. Technol.* **347**, 126579 (2022).

30. Logan, B. E., Rossi, R., Ragab, A. & Saikaly, P. E. Electroactive microorganisms in bioelectrochemical systems. *Nat. Rev. Microbiol.* **17**, 307–319 (2019).

31. Baek, G., Kim, J., Lee, S. & Lee, C. Development of biocathode during repeated cycles of bioelectrochemical conversion of carbon dioxide to methane. *Bioresour. Technol.* **241**, 1201–1207 (2017).

32. Sultana, S. T., Babauta, J. T. & Beyenal, H. Electrochemical biofilm control: A review. *Biofouling* **31**, 745–758 (2015).

33. Holtmann, D. & Harnisch, F. *Electrification of biotechnology: Quo vadis? Advances in Biochemical Engineering/Biotechnology* vol. 167 (2019).

34. Korth, B., Rosa, L. F. M., Harnisch, F. & Picioreanu, C. A framework for modeling electroactive microbial biofilms performing direct electron transfer. *Bioelectrochemistry* **106**, 194–206 (2015).

35. Deeke, A., Sleutels, T. H. J. A., Heijne, A. Ter, Hamelers, H. V. M. & Buisman, C. J. N. Influence of the thickness of the capacitive layer on the performance of bioanodes in Microbial Fuel Cells. *J. Power Sources* **243**, 611–616 (2013).

36. Lovley, D. R. & Walker, D. J. F. Geobacter Protein Nanowires. *Front. Microbiol.* **10**, (2019).

37. Kotloski, N. J. & Gralnick, J. A. Flavin electron shuttles dominate extracellular electron transfer by Shewanella oneidensis. *MBio* **4**, 1–4 (2013).

38. Carmona-Martínez, A. A., Harnisch, F., Kuhlicke, U., Neu, T. R. & Schröder, U. Electron transfer and biofilm formation of Shewanella putrefaciens as function of anode potential. *Bioelectrochemistry* **93**, 23–29 (2013).

39. Kumar, S. S., Kumar, V. & Basu, S. Electroanalytical techniques for investigating biofilms in microbial fuel cells. *Bioelectrochemical Interface Eng.* 149–163 (2019) doi:10.1002/9781119611103.ch9.

40. Aelterman, P., Freguia, S., Keller, J., Verstraete, W. & Rabaey, K. The anode potential regulates bacterial activity in microbial fuel cells. *Appl. Microbiol. Biotechnol.* **78**, 409–418 (2008).

41. ter Heijne, A., Pereira, M. A., Pereira, J. & Sleutels, T. Electron Storage in Electroactive Biofilms. *Trends Biotechnol.* **39**, 34–42 (2020).

42. Doll, K., Jongsthaphongpun, K. L., Stumpp, N. S., Winkel, A. & Stiesch, M. Quantifying implant-associated biofilms: Comparison of microscopic, microbiologic and biochemical

methods. *J. Microbiol. Methods* **130**, 61–68 (2016).

43. Sharma, M. *et al.* A critical revisit of the key parameters used to describe microbial electrochemical systems. *Electrochim. Acta* **140**, 191–208 (2014).

44. Kubannek, F., Schröder, U. & Krewer, U. Revealing metabolic storage processes in electrode respiring bacteria by differential electrochemical mass spectrometry. *Bioelectrochemistry* **121**, 160–168 (2018).

45. Zhang, X., Prévoteau, A., Louro, R. O., Paquete, C. M. & Rabaey, K. Periodic polarization of electroactive biofilms increases current density and charge carriers concentration while modifying biofilm structure. *Biosens. Bioelectron.* **121**, 183–191 (2018).

46. Izadi, P., Gey, M. N., Schlüter, N. & Schröder, U. Bidirectional electroactive microbial biofilms and the role of biogenic sulfur in charge storage and release. *iScience* **24**, (2021).

47. Yates, M. D. *et al.* Microbial electrochemical energy storage and recovery in a combined electrotrophic and electrogenic biofilm. *Environ. Sci. Technol. Lett.* **4**, 374–379 (2017).

48. van Loosdrecht, M. C. M., Pot, M. A. & Heijnen, J. J. Importance of bacterial storage polymers in bioprocesses. *Water Sci. Technol.* **35**, 41–47 (1997).

49. Suidan, M. T., Rittmann, B. E. & Traegner, U. K. Criteria establishing biofilm-kinetic types. *Water Res.* **21**, 491–498 (1987).

50. Wanner, O. & Gujer, W. A Multispecies Biofilm Model. *Biotechnol. Bioeng.* **28**, 314–328 (1986).

51. Harnisch, F. & Rabaey, K. The diversity of techniques to study electrochemically active biofilms highlights the need for standardization. *ChemSusChem* **5**, 1027–1038 (2012).

52. de Smit, S. M., Buisman, C. J. N., Bitter, J. H. & Strik, D. P. B. T. B. Cyclic Voltammetry is Invasive on Microbial Electrosynthesis. *ChemElectroChem* **8**, 3384–3396 (2021).

53. Lazanas, A. C. & Prodromidis, M. I. Electrochemical Impedance Spectroscopy—A Tutorial. *ACS Meas. Sci. Au* (2022) doi:10.1021/acsmeasuresciau.2c00070.

54. Azeredo, J. *et al.* Critical review on biofilm methods. *Crit. Rev. Microbiol.* **43**, 313–351 (2017).

55. Howley, E., Ki, D., Krajmalnik-Brown, R. & Torres, C. I. Geobacter sulfurreducens' Unique Metabolism Results in Cells with a High Iron and Lipid Content. *Microbiol. Spectr.* **10**, (2022).

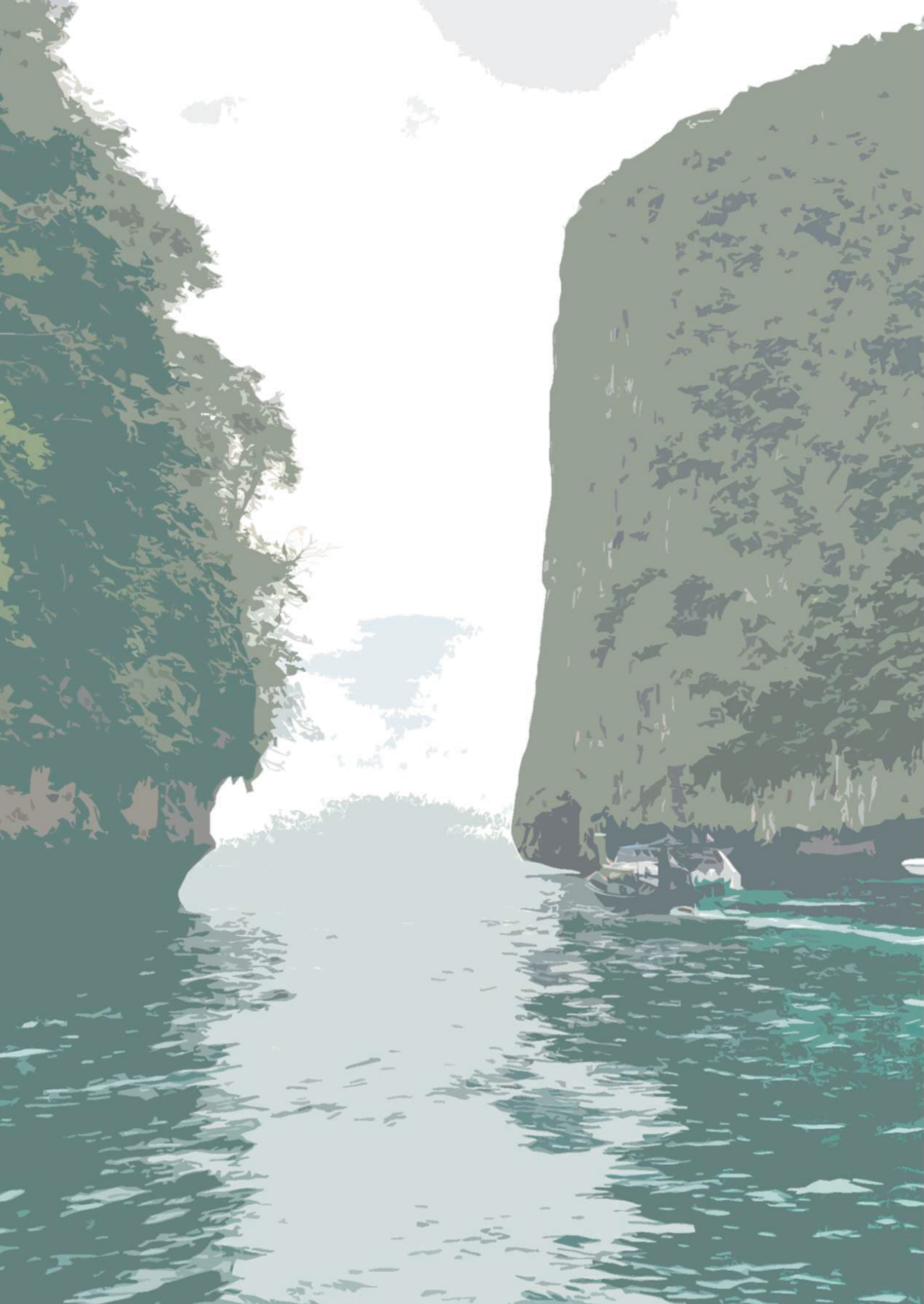

2 Opportunities for visual techniques to determine characteristics and limitations of electro-active biofilms

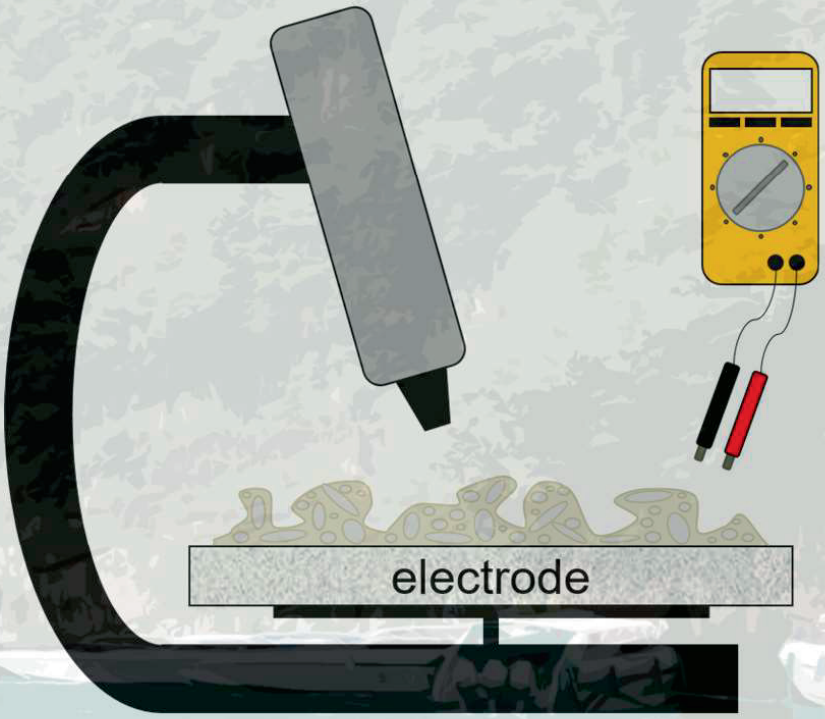

This chapter has been published as:

Pereira J, de Nooy S, Sleutels T, ter Heijne A. *Opportunities for visual techniques to determine characteristics and limitations of electro-active biofilms.* Biotechnol Adv 2022;60:108011.

Abstract

Optimization of bio-electrochemical systems (BESs) relies on a better understanding of electro-active biofilms (EABfs). These microbial communities are studied with a range of techniques, including electrochemical, visual, and chemical techniques. Even though each of these techniques provides very valuable and wide-ranging information about EABfs, such as performance, morphology and biofilm composition, they are often destructive. Therefore, the information obtained from EABfs development and characterization studies are limited to a single characterization of EABfs and often limited to one time point that determines the end of the experiment. Despite being scarcer and not as commonly reported as destructive techniques, non-destructive visual techniques can be used to supplement EABfs characterization by adding in-situ information of EABfs functioning and its development throughout time. This opens the door to EABfs monitoring studies that can complement the information obtained with destructive techniques. In this review, we provide an overview of visual techniques and discuss the opportunities for combination with the established electrochemical techniques to study EABfs. By providing an overview of suitable visual techniques and discussing practical examples of the combination of visual with electrochemical methods, this review aims at serving as a source of inspiration for future studies in the field of BESs.

2.1. Introduction

The increasing world population, global warming due to the increased greenhouse effect and depletion of fossil fuel reserves are making sustainable energy and research recovery technologies, such as recovery of energy and nutrients from wastewater, more pressing matters.[1,2] Bio-electrochemical systems (BESs) have gained substantial interest in the past two decades as they provide a new way to recover resources (e.g. nutrients) and energy from wastewater.[3,4] BESs are systems that make use of microorganisms that are able to use electrodes as external electron acceptors (exoelectrogens) or electron donors (electrotrophs) for chemical conversions.[5,6] These systems include the Microbial Fuel Cell (MFC) and Microbial Electrolysis Cell (MEC) for energy recovery in the form of electricity or hydrogen, and Microbial Electrosynthesis Cell (MES) for production of fuels or chemicals from CO_2.[7] They all base their working principle on electro-active microbial communities, with the difference that MFCs and MECs rely on exoelectrogens (at the anode), while MESs rely on eletrotrophs (at the cathode).[8,9]

Electro-active biofilms (EABfs) are a conglomerate/community of electro-active bacteria that develop on the surface of an electrode.10 These bacteria catalyze the conversion between electrical energy and chemical energy. Because of their crucial role in BESs, providing the most suitable operating conditions for bio-catalysis has been the focus of many studies.[11–13] We frequently see research resulting in the improvement of BESs performance using more suitable materials and optimized electrode designs to improve the interaction between EABfs and electrode surface.[14–17] However, being electro-active bacteria the key player that determine the exchange between electrical and chemical energy, it is pivotal not only to study the behavior of electro-active bacteria and EABfs as a response to operational conditions e.g., electrode designs and electrode current/potential, but also the relation between their characteristics to improved performance.

Several types of techniques, including electrochemical, visual, and chemical analyses, have been used to study EABfs. These techniques provide a wide range of information about EABfs: they give insights into, e.g., microbial activity, biofilm composition, structure and thickness, mass transfer limitations and conductivity.[18–20] Electrochemical techniques are used to determine the general performance indicators of EABfs, being the relationship between electric current and potential. Examples of commonly used electrochemical techniques are Cyclic Voltammetry (CV), potentiostatic control (also called chronoamperometry), and Electrochemical Impedance Spectroscopy (EIS), which can be performed at different stages of EABfs growth, and provide information about microbial activity, the presence of redox active compounds, and charge storage.[21–25] Chemical analyses are also frequently used in BESs to assess the concentration of substrate and/or products in the bioreactor. Linking these concentrations to the electrons exchanged at the electrode(s) gives information on the (Coulombic) efficiency of anodes and cathodes. Besides, these chemical techniques can

be used on EABfs themselves, to evaluate the composition of the biofilm by means of elemental analysis (with an elemental analyzer) or quantification of protein and polysaccharides present in the extracellular matrix of the biofilm (using Pierce BCA protein Assay Kit for proteins, and the phenol-sulphuric acid method for polysaccharides).[26] Well-known techniques to visualize biofilms have also been adopted and adapted to study electro-active biofilms on an electrode.[27] Among others, the use of Confocal Laser Scanning Microscopy (CLSM) and Optical Coherence Tomography (OCT) has been reported in EABfs works as tools to monitor biofilm thickness, investigate biofilm composition, and to localize microbial species and activities in the biofilm structure.

Even though there are many techniques to study EABfs, many of the available techniques are destructive. This means that the biofilm needs to be sacrificed to perform a given analysis and that the ongoing study needs to be interrupted and cannot be resumed after the analysis. As a result, using these destructive techniques means that EABfs cannot be monitored during the experiments and that these biofilms are monitored during their operation only using a typically "safe" and repetitively reported set of techniques. Added value can be brought to the field of BESs when in-situ techniques are used to visualize EABfs, since these can perform online monitoring of biofilm characteristics, and follow biofilm developments over time. Table 2.1 gives an overview of techniques that can be used to visualize biofilms on electrode surfaces, based on the criteria that are relevant for biofilm monitoring and characterization: quantification, 3D distribution, destructivity, and the possibility to detect/target specific compounds of interest. This table aims at providing a non-exhaustive summary of the general characteristics of the techniques that will be discussed in detail in this review. These six techniques, namely Confocal Laser Scanning Microscopy (CLSM), Optical Coherence Tomography (OCT), Raman Microscopy, Scanning Electron Microscopy (SEM), Scanning Transmission X-ray microscopy (SXRM) and Magnetic Resonance Imaging (MRI), have been selected due to their potential to add valuable information on electrochemical data and the positive trade-off between image quality and ease of use. More criteria, that are not included in Table 2.1, can be discussed when evaluating the suitability of a visual technique: its working methodology including the time invested for samples preparation and for visualization, and the equipment and operating costs. The information learned on EABfs from the use of other more costly and very sensible techniques is acknowledged and, therefore, some are mentioned and briefly discussed in section 2.3.

Table 2.1. Techniques that can be used to visualize electro-active biofilms. In green (✓), the aspects that can be covered with each technique; in red (x), the ones that are not.

Techniques	Quantify	3D distribution	Non-destructive		Specific compounds
Confocal Laser Scanning Microscopy (CLSM)	✓	✓	✓*	x	✓
Optical Coherence Tomography (OCT)	✓	✓	✓		x
Raman Microscopy	✓	✓	✓		✓
Scanning Electron Microscopy (SEM)	x	x	x		x
Scanning Transmission X-ray microscopy (SXRM)	✓	✓	✓		✓
Magnetic Resonance Imaging (MRI)	✓	✓	✓		x

*CLSM is non-destructive when using auto-fluorescent samples and no specific compounds are stained

Each visual technique provides specific information on the biofilm, at diverse resolutions and on different aspects of the biofilm. Their advantages and disadvantages for biofilm characterization differ: most techniques can be used for biofilm quantification, since they give insights into the 3D distribution of biofilms, while others are limited to 2D imaging and can require more destructive sampling procedures. From the techniques included in Table 2.1, CLSM is the most universal as it allows for visualization, quantification, 3D imaging and characterization of biofilm composition with a single apparatus. For a quick biofilm visualization, SEM is an appropriate technique as it allows for a qualitative description of the biofilm development on an electrode providing insights into the structure of the biofilm including size, shapes and distribution on an electrode surface. MRI and OCT allow for 3D imaging, to determine the biofilm distribution and its volume, and they have the advantage of not destroying the sample. Due to their non-destructive features, Raman and STXM are suitable options when aiming at studying biofilm composition. Even though their positive points, each technique has its intrinsic shortcomings. Therefore, choosing a suitable technique is challenging and a careful weighing is needed to assess what a certain technique can offer to meet the goal of the study.

EABfs can be very challenging to study as these biological matrixes, in which electro-active bacteria are embedded, have a unique composition and mechanical properties (depending on the operating conditions such as feed concentration and electrode potential). Moreover, the composition of their matrix is continuously changing with time as EABfs grow on an electrode, which makes characterizing EABfs and predicting their performance even more challenging. Therefore, using visual techniques to detect

specific compounds present in the extracellular matrix and to visualize the distribution of the biofilms as a function of time opens opportunities to better understand performance results obtained e.g. from an electrochemical measurement in electro-active biofilms. For example, monitoring the current profile during continuous polarization on an anode is a typical measure of the activity of EABfs. This activity can, for example, be associated with the amount of biofilm on the anode. Therefore, relating the activity of the biofilm with its thickness on the anode is an example of the added value derived from the combination of electrochemical and visual techniques. Besides, this combination helps in understanding how biofilm growth is affected by the operating conditions. High activities are also linked to a high concentration of c-type cytochromes on the membrane of electro-active bacteria.[28,29] Thus, staining these compounds and visualizing the biofilm with a suitable technique supplement and support the information derived from the electrochemical measurements. Moreover, the activity of EABfs can also be affected by other factors such as biofilm density, the microbial community the biofilm is composed of, and the positioning of species in the biofilm structure. For that purpose, visual techniques can be used to image the morphology and cellular density in the biofilm structure, identify species that are part of the biofilm and mapping their disposition in the biofilm. Especially the combination of electrochemical and visual techniques allows to acquire more knowledge about EABfs.

In this review, we describe visual techniques that have been used for EABfs studies combined with electrochemical techniques and discuss what information has been obtained. For the techniques introduced in Table 2.1, we provide a brief description of basic principles, how they have been applied to study electro-active biofilms (including limitations and practical implications), and what information/knowledge has been gained from their use. We also discuss other less often used visual techniques and summarize their applications to investigate EABfs. Finally, by providing an overview of suitable visual techniques and discussing practical examples of the combination of visual with electrochemical methods, this review aims at serving as a source of inspiration for future studies in the field of BESs.

2.2. Techniques for visualization of EABfs and outcomes of their use

Visual techniques in BESs are plentiful and cover very wide-ranging aspects of biofilms.[30–32] In this chapter, we will discuss six different techniques and their application for EABfs: CLSM, OCT, Raman, SEM, STXM, and MRI. Some more versatile techniques are a better choice for analysing diverse biofilm characteristics such as thickness and composition, and others stand out due to their high resolution. In many cases, these visual techniques provide additional information to electrochemical techniques, instead of offering an alternative way to measure similar characteristics of EABfs. In fact, the combination of these visual and electrochemical techniques gives more reliable and/or more comprehensive information on EABfs.

2.2.1. Confocal Laser Scanning Microscopy (CLSM)

Confocal Laser Scanning Microscopy (CLSM) is suitable for real-time, non-invasive, and in-situ measurement of biofilm characteristics. It is often considered the most powerful visual technique for biofilms.[27] CLSM uses a laser to excite fluorescent molecules (fluorophores) and it measures, subsequently, the light emitted when electrons fall back to their ground energy state.[33] It makes use of a pinhole to filter out light that is not in the optimal focal plane, also known as out-of-focus light. Due to the pinhole, the sub-micrometer resolution is high enough to visualize single cells. CLSM allows 1) imaging of live and hydrated samples, 2) sectional visualization of samples without invading the sample, and 3) performing 3D analysis of molecules and cells.[34–36] For EABfs, this translates into observing individual components such as proteins, polysaccharides and nucleic acids, pH mapping, viability and activity of cells, thickness, and 3D structures. Even though the ability to visualize biofilm samples at different depths, the penetration depth of the laser is one of the limitations linked to the use of CLSM. Samples thicker than 200 μm easily absorb all the laser light, leading to loss of visibility. The penetration depth is also affected by the presence of impurities in the samples such as sand, clay or precipitates.[37] A non-destructive visualization of biofilm structures with CLSM depends on the auto-fluorescence of the biofilm. Since biofilm samples have typically weak auto-fluorescence signals, their visualization with CLSM is dependent on the use of fluorescent probes and dyes. These probes, which are genetic sequences that bind to specific genome fragments (or to mRNA to target the expression of specific proteins), can be used to quantify the biofilm amount on an electrode. Biofilm samples can also be stained with dyes (generally chemical reaction-based interaction) to investigate their composition: for example, dyes to assess the species present in the biofilm and dyes to investigate the ratio of live/dead cells and proteins and polysaccharides content in the Extracellular Polymeric Substances (EPS). The use of these probes and dyes is not reversible. Once these bind to and/or react with their target compounds, namely DNA and/or mRNA and proteins and/or polysaccharides in the EPS, these can often not be unbound from the biofilm structure without affecting the activity and development of the biofilm on an electrode. On the one hand, these probes and dyes can be added to the biofilm for visualization at any moment of an ongoing experiment. Moreover, with this approach, the electrode does not necessarily need to meet the requirements for in-situ visualization as the study will not be resumed after biofilm staining. On the other hand, besides their costs and toxicity, the use of several fluorescent probes on a biofilm sample needs to ponder the overlapping of the emission spectra of the fluorophores (which may reduce the number of possible probes and dyes combinations to study one biofilm sample). In a non-destructive approach, the visualization can be performed in-situ with genetically modified bacteria: for example, with electro-active bacteria that incorporate a fluorescent probe such as Green Fluorescence Protein (GFP). However, in-situ visualization of electro-active bacteria with an incorporated fluorescent probe

requires a suitable transparent electrode with a flat surface to allow high resolution imaging.

Even though the need to dye biofilm samples, the use of this technique in EABfs studies is widely reported.[38–41] By including CLSM in their works, Franks et al., 2009 and Richter et al., 2009 were able to image the growth of *Geobacter sulfurreducers* biofilms and to determine the biofilm thickness on the electrode. Monitoring the growth of biofilm is an important tool to calculate biomass yields and to relate the amount of biofilm with produced current (so-called microbial specific activity). In addition to monitoring biofilm growth, CLSM has also been used to investigate the viability of the bacteria present on the electrode by means of Live/Dead kits.[44–46] Sun et al., 2016 combined Live/Dead staining with electrochemical measurements on an anodic biofilm and showed that the decreasing produced current at the anode was caused by a fast accumulation of dead cells in the electro-active biofilm (Figure 2.1). Since the thickness of the biofilm can also be measured with CLSM, the relation between biofilm thickness, maximum activity of the electro-active biofilm, and the presence of dead cells was also reported in this study: maximum activity was reached when the biofilm thickness was approximately 20 μm, and it decreased (due to the accumulation of dead cells) as the biofilm grew up until a final thickness of 45 μm.

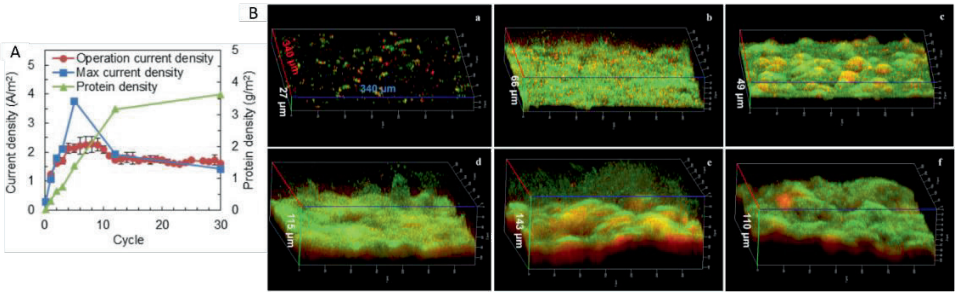

Figure 2.1. A) Current density as a function of time (in number of cycles) and B) Anode biofilms of *G. sulfurreducens* PCA visualized with CLSM after Live/Dead staining with BacLight™ Bacterial Viability Kit. Green are live and red are dead cells at sequential growth phases: a) beginning of initial phase (beginning of cycle 1), b) end of initial phase (end of cycle 1), c) fast cell accumulation (cycle 2), d) maximum activity (cycle 5), and e and f) mature phase (cycle 12 and 30, respectively) (adapted from Sun et al., 2016).

CLSM also allows to identify species present in the biofilm and their positioning on the electrode by using Fluorescent In-Situ Hybridization (FISH).[3,27,33,35] The information obtained using FISH can be used to give insights into how the accumulation of dead biomass and minority and/or unfavorable positioning of electro-active species on the electrode affects performance. The composition of the biofilm matrix also plays a role in the performance of EABfs.[48,49] Schmidt et al., 2017 and Esteve-Núñez et al., 2008 have used CLSM to image *G. sulfurreducens* biofilm and study the importance of c-type cytochromes in electron transfer mechanisms and their auto-fluorescent properties. As

recognized in literature, CLSM is thus a versatile and powerful technique that allows linking electrochemical data with the presence of redox compounds in EAB, composition of biofilm matrix (for example, proteins and polysaccharides), cells viability, and the mapping of microbial species on the electrode.

2.2.2. Optical Coherence Tomography (OCT)

Optical Coherence Tomography (OCT) is an imaging technique based on the scattering of light. This technique uses near-infrared light, and the light reflected from the samples is analyzed with an interferometer.[52] Based on its working principle, the delay in the reflected light has already been used to study flow and diffusion phenomena in colloidal suspensions.[53] OCT has a micrometer resolution and it allows imaging of large sample areas (several millimeters) without the use of fluorescent probes.[31,54] Even though in-situ visualization, quantification and 3D imaging are possible, the penetration depth of the OCT's signal is limited to around 2 mm thick samples and samples composition cannot be assessed.

The use of OCT as a tool to quantify the biofilm volume over time on a transparent anode has been reported by Molenaar et al., 2018. This work validated the use of this visual technique as a non-invasive and in-situ analysis to study EABfs. In this work, 54 scans of the transparent electrode with biofilm were taken with OCT, and then processed with a Matlab script that isolated and counted the biofilm pixels. The thickness of the biofilm on the electrode was calculated by averaging the 54 pixel counts and dividing this average by the pixel size. The biofilm volume was calculated by multiplying the thickness with the electrode surface area. By facilitating biofilm monitoring on an electrode, it allowed for linking biofilm growth/formation to local conditions and overall system performances. Positioning and morphologic changes on the biofilm structure as a response to operating conditions can also be determined. In a study that aimed at understanding the effect of intermittent anode potential on the morphology of EABfs, Pereira et al., 2021 used OCT to describe the response of the electro-active biofilms to this anode potential regime. In this study, irregular and patchy biofilm structures were observed on the anodes controlled with an intermittent anode potential, and regular and flat biofilm structures were observed on the anodes controlled with a continuous anode potential (Figure 2.2). By combining potentiostatic operation with OCT measurements and chemical analysis of the biofilms at the end of the experiments, a higher production of EPS by the intermittent EABfs was observed and quantified. Besides, measuring the acetate concentration in the anode and the amount of the biofilm on the electrode allowed to calculate biomass yields, which were higher for the intermittent EABfs.

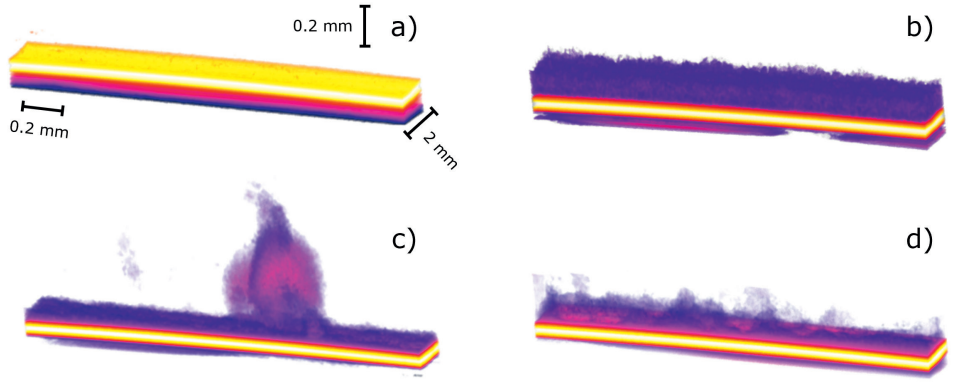

Figure 2.2. OCT visualization of biofilm morphology on a transparent glass electrode coated with Fluorine Tin Oxide: a) bare electrode, b) continuous anode potential, and c and d) intermittent anode potential regimes in which patchy forms can be observed (adapted from Pereira et al., 2021).

Xi et al., 2006 showed that it is also possible to obtain 3D images of the volume of the biofilm with OCT. More recently, Pereira et al., 2022 have identified mass transfer limitations in bio-anodes by monitoring the thickness of the biofilm at three different anode potentials and acetate concentrations. In this study, acetate diffusion rates in bio-anodes that can be used for modelling EABfs have also been reported.

2.2.3. Raman microscopy

Raman can be used to determine the chemical composition and molecular structure of a biofilm.[32] Raman microscopy uses monochromatic light and measures the scattering patterns of the light. Since the frequency of the scattered light differs per compound, the chemical composition of the biofilm can thus be assessed. It is a non-destructive method capable of real-time detection.[33] Raman is a highly sensitive technique to detect neutral chemical bonds such as C-C, C=C, and C-H, and it has a very high resolution (in the order of microns) without the need for staining. For some measurements though, the equipment needs to be optimized before use due to the weakness of the Raman effect (i.e., hardly detected changes in the vibration mode of chemical bounds) and the fluorescence of a given sample may readily distort the spectrum. Besides, even though biofilms share similar compounds, e.g.DNA, proteins, polysaccharides, and lipids, the vibration of the chemical bonds of a given compound varies among species.[58] Therefore, a more accurate and valid use of Raman to determine biofilm composition usually requires the recognition of a vibration pattern and the creation of a library for the specie of interest.

Raman has been used to monitor EABfs development at different growth stages based on the Raman resonance effect of c-type cytochromes (Figure 2.3).[59] In this study, they

showed that the redox state of cytochromes can be determined without interfering with the biofilm structure and used to measure the activity of the electro-active biofilm.

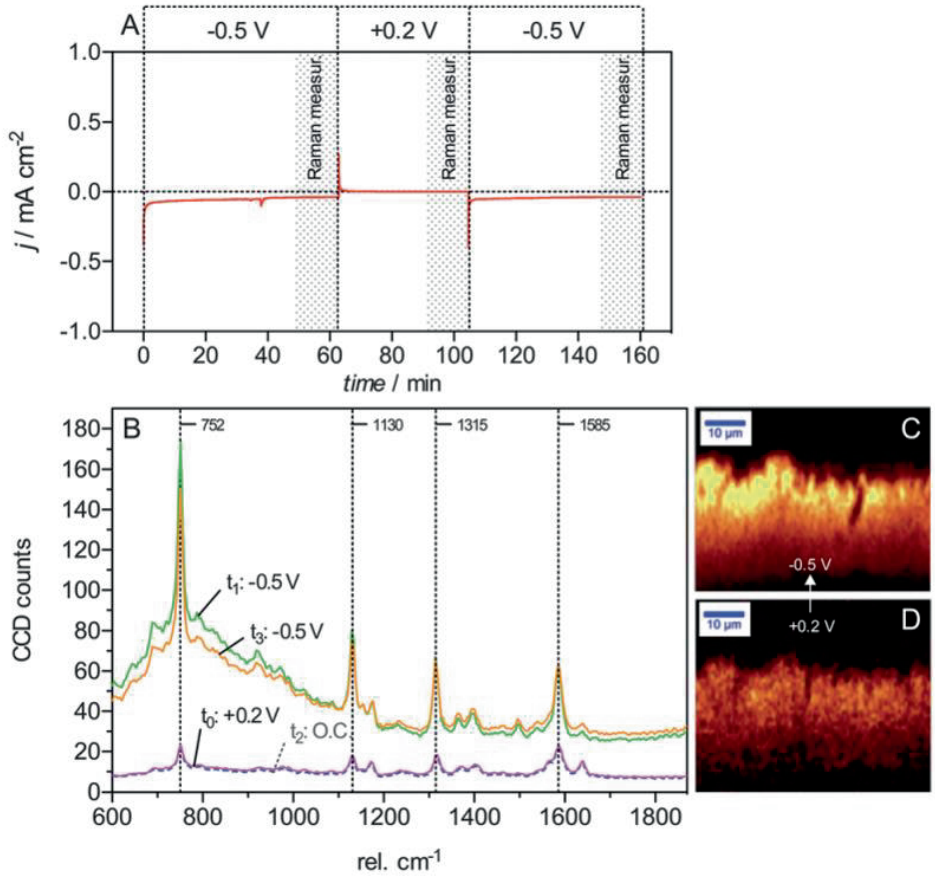

Figure 2.3. A) The reduced and oxidized states of the c-type cytochromes were tested by controlling the anode at -0.5 and +0.2 V vs. Ag/AgCl, respectively; B) Reduced (green and orange traces, t_1 and t_3) and oxidized (purple and blue traces, t_0 and t_2) states in biofilm under non-turnover conditions; C and D) Cross-sectional images of the biofilm at -0.5 V and +0.2 V vs. Ag/AgCl, respectively (adapted from Virdis et al., 2012).

In a follow up study, they related the oxidation state of the cytochromes with biofilm thickness.[60] They observed that cytochromes remained homogenously oxidized at early and middle stages of biofilm development (10 and 57 days, respectively) when the biofilm had a thickness of 70 µm. In the later stages (80 days) when the biofilm reached a thickness of 100 µm, the cytochromes were in a reduced state. This ability to monitor the redox state of cytochromes adds essential information to better understand electric characteristics of biofilms, and here it suggests electron transfer limitations as thick biofilms could not exchange the electrons with an oxidized redox compound or

electrode. More works have reported the use of Raman to show the presence of a redox gradient caused by cytochromes in the biofilm monitor, and to characterize *G. sulfurreducens* biofilms during electricity generation for both wild and mutant strains.[61,62]

Besides cytochromes, Keleştemur et al., 2018 used Raman to determine the concentration of protein and polysaccharides in EPS and to describe changes in the composition of polysaccharides into glycoproteins in EPS.

2.2.4. Scanning electron microscopy (SEM)

Scanning electron microscopy (SEM) is mostly used for qualitative analysis of biofilms.[40,64] SEM is based on spraying the sample with electrons, which will bounce back to a detector that will then produce an image of the surface of the sample. SEM allows for visualization at a nanometers scale. However, drawbacks of the use of this technique are the sample preparation that requires a pre-treatment/fixation, which may alter the structure of the sample, and the detection of the reflected electrons from non-smooth surfaces, which makes imaging rough surfaces of biofilms very challenging. However, this has been tackled by combining SEM with advanced segmentation methods to get better image quality. Vyas et al., 2016 applied machine learning to be able to calculate the area of a biofilm by distinguishing biofilm structure from the surface on which the biofilm had been developed.

SEM has been used in BESs not only to visualize electro-active bacteria but also electrode surfaces,[13,45,65] and the adhesion/interaction of the biofilm on different electrode surfaces.[66–68] In a study on anodic EABfs, Katuri et al., 2020 concluded that the electrode surface characteristics had a noticeable effect on biomass adhesion, activity, and morphology. They reported that the produced current on an anode was linked to the presence and growth of electro-active bacteria on the anode surfaces and that the produced current was promoted by hydrophilic surfaces, especially at early stages of biofilm development (Figure 2.4). From all the studies that use SEM to study EABfs, this study is here described given the combination of SEM with CLSM to determine the biofilm thickness. Particularly, the homogenous distribution of the biofilms on the electrode was visualized with SEM, and when later combined with CLSM, a thickness of approximately 22 μm was determined.

SEM can also be coupled with Energy-Dispersive X-ray spectroscopy (SEM-EDX) to investigate the composition of precipitates and the elemental composition of biofilm samples. Even though this approach is not commonly found in literature, the composition of the biofilm could be used to derive an experimental biomass elemental formula towards a more accurate mass balance in the bioreactors.

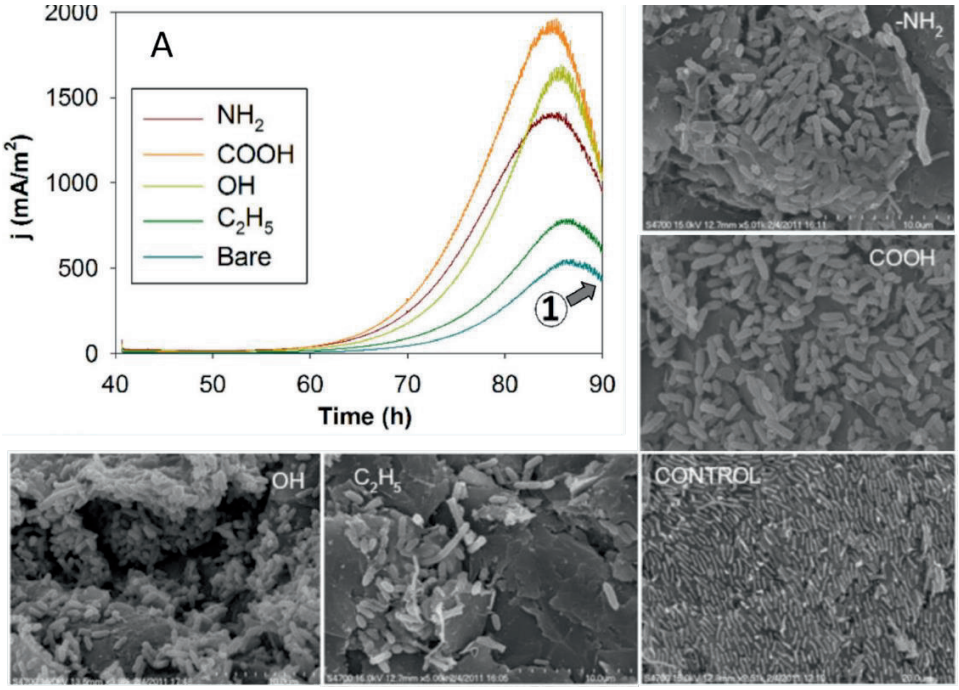

Figure 2.4. Current density as a function of time (A) and SEM comparison of the adhesion of early stage biofilms (90 hours, identified with an arrow in A) to electrode surfaces with different functional groups (adapted from Katuri et al., 2020).

2.2.5. Scanning Transmission X-ray Microscopy (STXM)

Scanning Transmission X-ray Microscopy (STXM) makes use of soft X-ray absorption to provide information on chemical bonding, charge state and magnetic state of the elements present on the analyzed samples.[35,70] Therefore, it allows to quantitatively determine the composition of biofilms in terms of proteins, polysaccharides, lipids, and nucleic acids and how they are distributed. STXM is non-invasive, has a nanometer resolution, and can be applied to hydrated samples owing to the fact that X-rays penetrate water. However, due to its low penetration depth, sectional visualization of the biofilm is very challenging (up to a maximum of around 300 nm thickness).[32]

Due to this low penetration depth, the use of STXM in the field of BESs is in a premature phase. However, the potential of this technique has been acknowledged in other studies with biofilms and there are some reports of the use of STXM in combination with other visual techniques. In these, Carrel et al., 2018, 2017 used STXM to visualize the morphology and provided biofilm volume profiles and indicated that the biofilms were exposed to shear stress, which led to non-homogeneous growth. They observed more growth in low shear stress regions, and evaluated the effect of mass transfer of nutrients and electron acceptors on the growth of the biofilm. Used here as a practical example on how to take advantage of combining different techniques, Lawrence et al., 2003

combined STXM with CLSM and Tomography Electron Microscopy (TEM) to obtain 3D structural and compositional information on biofilms. TEM was used to get structural information at high resolution, CLSM with fluorescent probes provided compositional information, and STXM was used to add information on the composition of macromolecules without probes (Figure 2.5). The mass transfer limitation and biofilm composition outcomes mentioned above are also of interest to understand the performance of EABfs. Therefore, benefits of the use of STXM and replications of this combination approach are to be expected in the field of BESs.

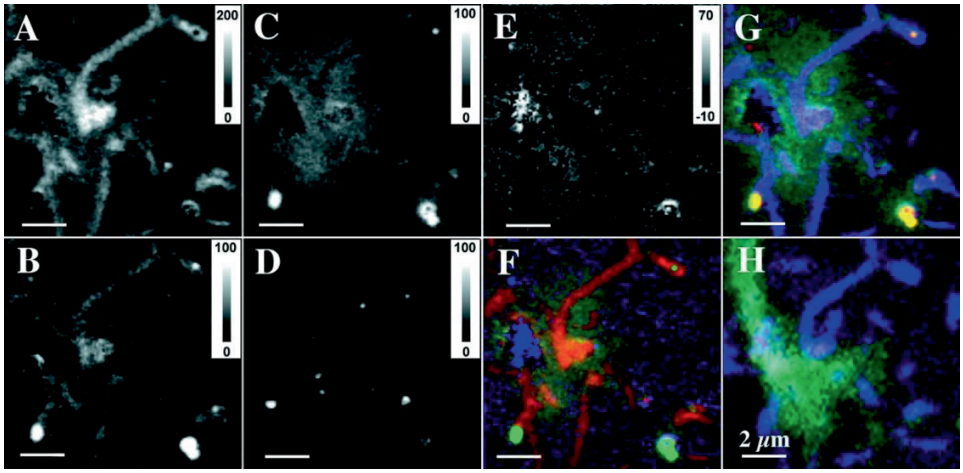

Figure 2.5. STXM imaging of A) proteins, B) lipids, C) polysaccharides, D) carbonate and E) nucleic acid in the biofilm; F) is a color mapped image showing proteins (red), polysaccharides (green), and nucleic acids (blue), whereas G) shows lipids (red), polysaccharides (green), and proteins (blue) – both F and G derived from an STXM image sequence of the biofilm. H) shows a CLSM image of the same region using probes for EPS (green) and nucleic acids (blue) (adapted from Lawrence et al., 2003).

2.2.6. Magnetic Resonance Imaging (MRI)

Many nuclei of atoms carry a quantum mechanical spin and thus a magnetic moment.[74] If a strong polarizing magnetic field is used on those nuclei they become magnetized. By irradiating the nuclei with a specific frequency, the Larmor frequency, a measurable magnetic resonance signal is created. This signal can be used to determine the structure of large molecules. Because the energy involved in this process is very low, the technique is suitable for analysis of living and hydrated objects. MRI provides information on the dynamics of water and transport properties in biofilms such as mass transport and oxygen diffusion. Therefore, this technique can be used for modelling biofilm processes and diffusion.[3] However, MRI has mainly been used in biofilm research to form a 2D or 3D image of the biofilm to show structural biofilm features.[33,35]

For biofilm imaging, magnetic field used can vary from 0.7 to 14.1 Tesla.[74] Caizán-Juanarena et al., 2019 used a magnetic field of 14.1 T to get (28 μm)^3 resolution 3D

images of EABfs (Figure 2.6) at the early stage (days 3 and 4), middle stage (days 6 and 7) and late stage (day 11 to 22). In the same study, 2D images to distinguish biofilm water from the bulk water were taken, and biofilm volume was also determined. The correlation between the total produced electric charge with the biofilm volume obtained with MRI and total nitrogen content reported in this study places MRI in an advantageous position among the techniques that allow in-situ monitoring of biofilm growth, as MRI can also be used to quantify proteins (and other nitrogen containing molecules), and it gives information on the distribution of the biofilm and on the interaction between the biofilm and the electrode surface.

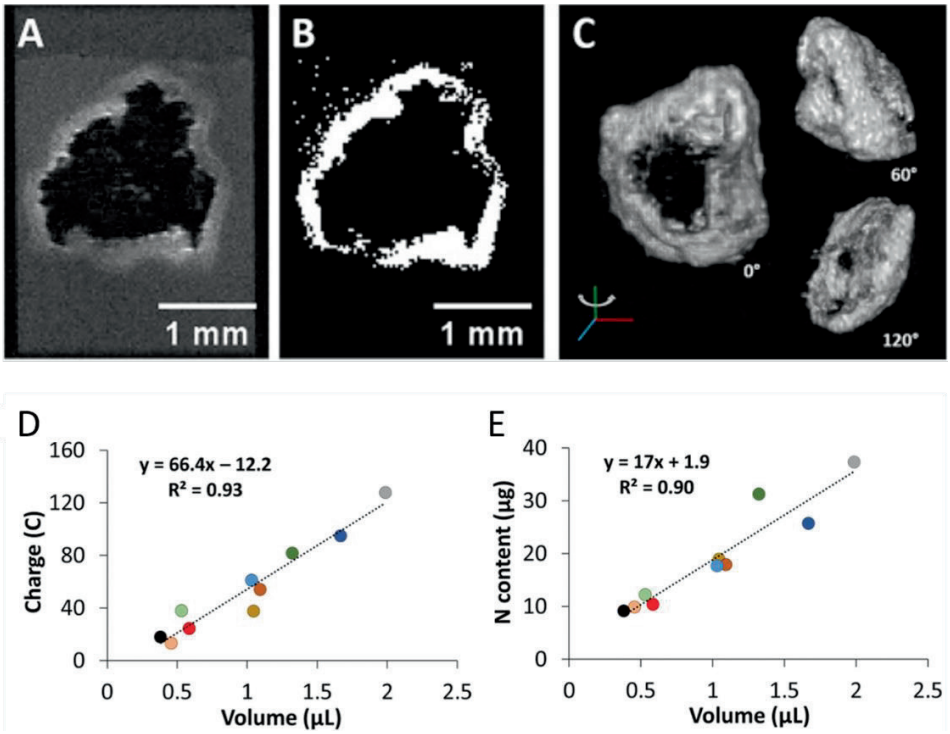

Figure 2.6. A) Cross-sectional MRI image of a granular bio-anode, B) thresholding to select voxels that contain biofilm and C) 3D reconstruction of the biofilm, D) linear relation between produced charge and biofilm volume, and E) linear relation between total nitrogen and biofilm volume (adapted from Caizán-Juanarena et al., 2019).

At the expense of the 3D image resolution, lower magnetic field of 0.7 Tesla can also be used to perform in-situ observation of the development of the biofilm.[74] With these works, MRI was used to successfully determine the biofilm distribution and its volume with the biggest advantage of not destroying the sample. In fact, MRI at low magnetic fields has been used in in-situ measurements on EABfs grown on activated carbon granules.[75,76] However, the resolution was not high enough to determine the roughness

of activated carbon granules nor to visualize bacterial growth in the inner macro-pores of the granules.

2.3. Opportunities for visual techniques to study EABfs

All visual techniques are tools to increase our understanding of the combination of biofilm and electrodes in BESs. The list of techniques used to visualize biofilms can be further expanded with techniques that have had little application in BESs. Table 2.2 describes some other visual techniques that extend the opportunities to study EABfs and the six visual techniques described above. These other visual techniques include Light Microscopy (LM), Transmission Electron Microscopy (TEM), Two Photon-Laser Scanning Microscopy (TP-LSM), Structured Illumination Microscopy (SIM), Atomic Force Microscopy (AFM), Blink Microscopy (BM), Nano-Secondary Ion Mass Spectrometry (SIMS), Scanning Electrochemical Microscopy (SECM), and Cryo Electron Microscopy (Cryo-EM). A short description of their applications in biofilm studies and pros and cons are given (Table 2.2). LM is a very basic visual technique to allow cell visualization, whereas other techniques such as TEM and AFM allow for structural investigation of the biofilm. More robust techniques, namely TP-LSM, SIM, NanoSIMS, SECM, and Cryo-EM, provide more detailed information on the biofilm structure and composition, but these are also more laborious and require image processing. Overall, this table, together with the six techniques described above, shows that the opportunities for EABfs visualization are widely available and can match several study purposes.

When a single visual technique is not enough to meet the aims of a given study, combining more than one visual technique can help overcome shortcomings and eventual incompatibilities with the experimental set-up. Besides the described example of the combination of three visual techniques provided in section 2.2.5, two more scenarios are given here. These intend to show possible approaches and the benefits of combining different visual techniques and electrochemical techniques. These should therefore not be seen as strict and defined set of techniques but rather a source of inspiration for readers to select techniques and find their own opportunities. Moreover, we encourage readers to explore other techniques to detect the electrochemical characteristics of EABfs,[77,78] alternative approaches to monitor EABfs growth,[79,80] advanced microscopy techniques,[81,82] and integrate upcoming techniques in EABfs studies.

Table 2.2. Overview of possible techniques for biofilm visualization

Technique	Application in (EA) biofilms	Advantages	Disadvantages	References
CLSM	Morphology and composition of the biofilm, and identification of species	Offers a wide range of visualization opportunities in one equipment, sub-micrometer resolution	Dyes and probes are destructive and expensive, long staining procedures can be required	[46,47]
OCT	Monitoring biofilm growth and morphology on electrode surfaces	In-situ and fast measurement of large biofilm areas (millimeters)	No information on the composition of the cells and low resolution (micrometer)	[26,55]
Raman	Target specific compounds in the biofilm structure	Non-destructive and micrometer resolution	Expensive, laborious and it requires the creation of a library to study a specie of interest	[59,62]
SEM	Visualization of cell structures on electrode surfaces	Nanometer resolution, allows elemental analysis with EDX	Not suitable for wet samples, destructive sample preparation	[66,69]
STXM	Identification and quantification of compounds present in the biofilm	Determination of a wide range of compounds of interest and high resolution (nanometer)	Low penetration depth and expensive	[71,73]
MRI	Morphology and quantification of biofilm structures	Allows for a non-destructive visualization, high resolution (micrometers)	Nanometer resolution images require destructive approach, expensive	[17,75]
LM	Bacterial growth and morphology on electrode surfaces; spot areas of interest in complex biofilms	Easily covers large biofilm surface areas, cheap and fast	Low magnification and resolution, resulting in limited information	[87]
TEM	Spatial arrangement biofilm, cellular structure; spot areas of interest in complex biofilms	Very high resolution (better than SEM)	Needs destructive sample preparation, only dehydrated samples, and time consuming	[39,73,88]

TP-LSM	Spatial distribution of active biomass and ions in biofilms (similar to CLSM)	Deep sample penetration and less fluorophores bleaching	Needs probes and a laborious procedure	[30,35]
SIM	Imaging of structural details	High resolution (up to 120 nm), allows use of conventional fluorophores	Needs probes, limited penetration depth (lower than CLSM), susceptible to errors in digital image analysis	[54]
AFM	Determination of biofilm structure, cell quantification, visualization of individual molecules	Non-destructive	Limited surface area scanned, sensitive to external physical and electrical noise	[27,89,90]
BM	Imaging cellular substructures	High resolution (nanometer scale)	Not all fluorophores can be used, imaging in z-direction is limited	[54,91]
NanoSIMS	Imaging cells, biofilm morphology and composition, and active biomass	High resolution (nanometer scale)	Destructive approach, expensive, and laborious procedure, and data interpretation	[92,93]
SECM	Detection of redox compounds and quantification of mediators involved in bacterial interactions	Microns scale resolution and in-situ measurements	Requires a suitable probe and a very precise positioning between probe and sample	[94,95]
Cryo-EM	Structural and compositional characteristics of biofilms	Macromolecular structure determination, high resolution (angstrom scale)	Destructive approach due to cryogenic temperatures	[96]

As a first example, the qualitative visualization of EABfs with SEM could be supplemented with AFM to allow for determining conductivity and mapping specific proteins. By combining these two visual techniques, the performance of EABfs could be related to their amount, distribution, and shape on an electrode (with SEM) and linked to the conductivity and activity of cytochromes (with AFM) in specific areas of the biofilm. Therefore, on a surface with several working electrodes, the activity of EABfs could be mapped and used as visual strong evidence to explain performance. As a second example, we discuss the opportunities of combining CLSM with TEM and/or cryogenic electron microscopy and flow cytometry. Operating a bio-electrochemical reactor in continuous mode on the visualization stage of an CLSM equipment and scanning EABfs on an electrode allows to monitor growth and to visualize the structure of the biofilm. Even though its versatility, allowing to assess live/dead cells and FISH analysis, CLSM would not be the most suitable visual technique to quantify and study planktonic cells in such a set-up. Here, sampling the electrolyte and using other microscopy analyses would give opportunities for a more complete characterization of planktonic cells. To this end, TEM and/or cryogenic electron microscopy could be used to provide information on cellular structure, and flow cytometry used to quantify the number of planktonic cells. By combining several visual techniques, this would allow a more complete understanding of the anode/cathode as a whole system and a higher accuracy in mass balances.

Even though this review focusses on the study of EABfs, it is relevant to highlight that the use of visual techniques to study single cells is also possible and of crucial importance. When looking at individual cells, specific characteristics can be identified and separated from the properties of the whole biofilm regarding structure, composition and/or microbial community. Therefore, the biocatalysis of single cells can be studied and insights given on the maximum performance of a single electro-active microorganism.[83] Besides the use of visual techniques, single cells present in EABfs can also be identified with microbiological techniques that target DNA and, when targeting RNA, insights on genomics and proteomics can be gained.[84,85]

Finally, the combination of any of the visual techniques with performance indicators from electrochemical measurements will lead to additional insights to better understand EABfs behavior compared to one technique on itself. The list of positive outcomes of this combination is long and important when one aims to control, characterize and scale-up a biological process: 1) quantify biofilm amounts on an electrode to calculate microbial specific activities of electro-active biofilms and biomass yields, 2) measure biofilm composition to study electron storage mechanisms and make a more accurate charge balance in EAB,[86] 3) determine biofilm density at different sheer stresses and calculate diffusion rates and identify mass transfer limitations thereof, 4) identification of active areas in the biofilm structure and determining which species are playing the key role in those, 5) chemically characterize the composition of the biofilm as a response

to different feeding and electrode potentials regimes, and 6) study the adhesion of biofilms to different electrode surfaces.

Even though electrochemical and visual techniques can stand alone, merging the advantages of these techniques creates a very solid and powerful tool for understanding and gaining more information on electro-active biofilms. At first instance, this combination of techniques is a reliable source of knowledge, but in the long run, this combination is the path that needs to be followed to provide the best operating conditions to electro-active bacteria and EABfs and to steer their catalysis towards the improvement of BESs performance.

2.4. Conclusions

The list of techniques available for biofilm visualization on an electrode is extensive. This wide range of techniques allows researchers to choose the most suitable technique to match the purpose of the study. Up until now, we have assisted a repetitive use of a limited set of techniques in the field of BESs. Despite the valuable information reported by its use, with this review we encourage researchers to refresh their approach in their coming works by showing the results and insights derived from the combination of electrochemical and visual techniques. Steps forward in the field of BESs depend on combination approaches discussed in this review and other possible combinations of the described techniques.

2.5. Acknowledgements

This work was performed in the cooperation framework of Wetsus, European Centre of Excellence for Sustainable Water Technology (www. wetsus.nl). Wetsus is co-funded by the Dutch Ministry of Economic Affairs and Ministry of Infrastructure and Environment, the European Union Regional Development Fund, the Province of Fryslân, and the Northern Netherlands Provinces. The authors thank the participants of the research theme “Resource Recovery” for the fruitful discussions and their financial support. This publication is part of the project “Understanding and controlling electron flows in electro-active biofilms” with project number 17516 of the research program Vidi which is (partly) financed by the Dutch Research Council (NWO). Thanks are extended to Leire Caizán and Casper Borsje for the conceptualization of this work, and the Wetsus Academy students Ibrahim Kathemir and Kailun Chang for their help gathering up-to date bibliography.

2.6. References

1. Borole, A. P. *et al.* Electroactive biofilms: Current status and future research needs. *Energy Environ. Sci.* **4**, 4813–4834 (2011).

2. Lahiri, D., Nag, M., Ghosh, S., Dey, A. & Ray, R. R. Electroactive biofilm and electron transfer in MES. in *Scaling Up of Microbial Electrochemical Systems* 87–101 (Elsevier, 2022). doi:10.1016/b978-0-323-90765-1.00006-x.

3. Das, D. *Microbial fuel cell: A bioelectrochemical system that converts waste to watts*. *Microbial Fuel Cell: A Bioelectrochemical System that Converts Waste to Watts* (2017). doi:10.1007/978-

3-319-66793-5.

4. Kiran, R. & Patil, S. A. Microbial Electroactive Biofilms. *ACS Symp. Ser.* **1323**, 159–186 (2019).

5. Santoro, C., Arbizzani, C., Erable, B. & Ieropoulos, I. Microbial fuel cells: From fundamentals to applications. A review. *J. Power Sources* **356**, 225–244 (2017).

6. Babauta, J., Renslow, R., Lewandowski, Z. & Beyenal, H. Electrochemically active biofilms: Facts and fiction. A review. *Biofouling* **28**, 789–812 (2012).

7. Logan, B. E. *et al.* Microbial fuel cells: Methodology and technology. *Environmental Science and Technology* vol. 40 5181–5192 (2006).

8. Logan, B. E., Rossi, R., Ragab, A. & Saikaly, P. E. Electroactive microorganisms in bioelectrochemical systems. *Nat. Rev. Microbiol.* **17**, 307–319 (2019).

9. Thapa, B. Sen *et al.* Overview of electroactive microorganisms and electron transfer mechanisms in microbial electrochemistry. *Bioresour. Technol.* **347**, 126579 (2022).

10. Erable, B., Duţeanua, N. M., Ghangrekar, M. M., Dumas, C. & Scott, K. Application of electro-active biofilms. *Biofouling* **26**, 57–71 (2010).

11. Lee, H. S. Electrokinetic analyses in biofilm anodes: Ohmic conduction of extracellular electron transfer. *Bioresour. Technol.* **256**, 509–514 (2018).

12. Jadhav, G. S. & Ghangrekar, M. M. Performance of microbial fuel cell subjected to variation in pH, temperature, external load and substrate concentration. *Bioresour. Technol.* **100**, 717–723 (2009).

13. Choi, S. & Chae, J. Optimal biofilm formation and power generation in a micro-sized microbial fuel cell (MFC). *Sensors Actuators, A Phys.* **195**, 206–212 (2013).

14. Hindatu, Y., Annuar, M. S. M. & Gumel, A. M. Mini-review: Anode modification for improved performance of microbial fuel cell. *Renew. Sustain. Energy Rev.* **73**, 236–248 (2017).

15. Chong, P., Erable, B. & Bergel, A. Effect of pore size on the current produced by 3-dimensional porous microbial anodes: A critical review. *Bioresour. Technol.* **289**, 121641 (2019).

16. Schröder, U., Harnisch, F. & Angenent, L. T. Microbial electrochemistry and technology: Terminology and classification. *Energy Environ. Sci.* **8**, 513–519 (2015).

17. Caizán-Juanarena, L. *et al.* 3D biofilm visualization and quantification on granular bioanodes with magnetic resonance imaging. *Water Res.* **167**, (2019).

18. Bartosch, S., Mansch, R., Knotzch, K. & Bock, E. CTC staining and counting of actively respiring bacteria in natural stone using confocal laser scanning microscopy. *J. Microbiol. Methods* **52**, 75–84 (2003).

19. Lusk, B. G., Parameswaran, P., Popat, S. C., Rittmann, B. E. & Torres, C. I. The effect of pH and buffer concentration on anode biofilms of Thermincola ferriacetica. *Bioelectrochemistry* **112**, 47–52 (2016).

20. Pepè Sciarria, T., Arioli, S., Gargari, G., Mora, D. & Adani, F. Monitoring microbial communities' dynamics during the start-up of microbial fuel cells by high-throughput screening techniques. *Biotechnol. Reports* **21**, e00310 (2019).

21. de Smit, S. M., Buisman, C. J. N., Bitter, J. H. & Strik, D. P. B. T. B. Cyclic Voltammetry is Invasive on Microbial Electrosynthesis. *ChemElectroChem* **8**, 3384–3396 (2021).

22. ter Heijne, A. *et al.* Analysis of bio-anode performance through electrochemical impedance spectroscopy. *Bioelectrochemistry* **106**, 64–72 (2015).

23. He, Z. & Mansfeld, F. Exploring the use of electrochemical impedance spectroscopy (EIS) in microbial fuel cell studies. *Energy Environ. Sci.* **2**, 141–240 (2009).

24. Droop, M. R. Vitamin B12 and Marine Ecology III. An experiment with a chemostat. *J. Mar. Biol. Assoc. United Kingdom* **46**, 659 (1966).

25. Strycharz, S. M. *et al.* Application of cyclic voltammetry to investigate enhanced catalytic current generation by biofilm-modified anodes of Geobacter sulfurreducens strain DL1 vs. variant strain KN400. *Energy Environ. Sci.* **4**, 896–913 (2011).

26. Pereira, J. *et al.* The effect of intermittent anode potential regimes on the morphology and extracellular matrix composition of electro-active bacteria. *Biofilm* **4**, 100064 (2021).

27. Azeredo, J. *et al.* Critical review on biofilm methods. *Crit. Rev. Microbiol.* **43**, 313–351 (2017).

28. Zhang, X., Prévoteau, A., Louro, R. O., Paquete, C. M. & Rabaey, K. Periodic polarization of electroactive biofilms increases current density and charge carriers concentration while modifying biofilm structure. *Biosens. Bioelectron.* **121**, 183–191 (2018).

29. Reguera, G. Microbial nanowires and electroactive biofilms. *FEMS Microbiol. Ecol.* **94**, 1–13 (2018).

30. Hu, Z. *et al.* Determination of spatial distributions of zinc and active biomass in microbial biofilms by two-photon laser scanning microscopy. *Appl. Environ. Microbiol.* **71**, 4014–4021 (2005).

31. Li, C., Felz, S., Wagner, M., Lackner, S. & Horn, H. Investigating biofilm structure developing on carriers from lab-scale moving bed biofilm reactors based on light microscopy and optical coherence tomography. *Bioresour. Technol.* **200**, 128–136 (2016).

32. Zhang, P., Chen, Y., Qiu, J., Dai, Y. & Feng, B. Imaging the Microprocesses in Biofilm Matrices. *Trends Biotechnol.* **37**, 214–226 (2019).

33. Franklin, M. J., Chang, C., Akiyama, T. & Bothner, B. New technologies for studying biofilms. *Microbiol Spectr.* **3**, (2015).

34. Tejedor-Sanz, S., Ortiz, J. M. & Esteve-Núñez, A. Merging microbial electrochemical systems with electrocoagulation pretreatment for achieving a complete treatment of brewery wastewater. *Chem. Eng. J.* **330**, 1068–1074 (2017).

35. Neu, T. R. *et al.* Advanced imaging techniques for assessment of structure, composition and function in biofilm systems. *FEMS Microbiol. Ecol.* **72**, 1–21 (2010).

36. Schlafer, S. & Meyer, R. L. Confocal microscopy imaging of the biofilm matrix. *J. Microbiol. Methods* **138**, 50–59 (2017).

37. Palmer, R. J., Haagensen, J. A. J., Neu, T. R. & Sternberg, C. Confocal microscopy of biofilms - Spatiotemporal approaches. in *Handbook of Biological Confocal Microscopy: Third Edition* 870–888 (2006). doi:10.1007/978-0-387-45524-2_51.

38. Nevin, K. P. *et al.* Power output and columbic efficiencies from biofilms of Geobacter sulfurreducens comparable to mixed community microbial fuel cells. *Environ. Microbiol.* **10**, 2505–2514 (2008).

39. Kim, B. H. *et al.* Enrichment of microbial community generating electricity using a fuel-cell-type electrochemical cell. *Appl. Microbiol. Biotechnol.* **63**, 672–681 (2004).

40. Yang, L. *et al.* Building electrode with three-dimensional macroporous interface from

biocompatible polypyrrole and conductive graphene nanosheets to achieve highly efficient microbial electrocatalysis. *Biosens. Bioelectron.* **141**, 111444 (2019).

41. Dong, Y. *et al.* Responses of electroactive biofilms to chronic chlorine exposure: Insights from the composition and spatial structure of extracellular polymeric substances. *Bioelectrochemistry* **142**, 107894 (2021).

42. Franks, A. E. *et al.* Novel strategy for three-dimensional real-time imaging of microbial fuel cell communities: Monitoring the inhibitory effects of proton accumulation within the anode biofilm. *Energy Environ. Sci.* **2**, 113–119 (2009).

43. Richter, H. *et al.* Cyclic voltammetry of biofilms of wild type and mutant Geobacter sulfurreducens on fuel cell anodes indicates possible roles of OmcB, OmcZ, type IV pili, and protons in extracellular electron transfer. *Energy Environ. Sci.* **2**, 506–516 (2009).

44. Takenaka, S., Iwaku, M. & Etsuro, H. Artificial Pseudomonas aeruginosa biofilms and confocal laser scanning microscopic analysis. *J Infect Chemother* **7**, 87–93 (2001).

45. Marsili, E., Rollefson, J. B., Baron, D. B., Hozalski, R. M. & Bond, D. R. Microbial biofilm voltammetry: Direct electrochemical characterization of catalytic electrode-attached biofilms. *Appl. Environ. Microbiol.* **74**, 7329–7337 (2008).

46. Reguera, G. *et al.* Biofilm and nanowire production leads to increased current in Geobacter sulfurreducens fuel cells. *Appl. Environ. Microbiol.* **72**, 7345–7348 (2006).

47. Sun, D. *et al.* The effect of biofilm thickness on electrochemical activity of Geobacter sulfurreducens. *Int. J. Hydrogen Energy* **41**, 16523–16528 (2016).

48. Cao, B. *et al.* Extracellular polymeric substances from Shewanella sp. HRCR-1 biofilms: Characterization by infrared spectroscopy and proteomics. *Environ. Microbiol.* **13**, 1018–1031 (2011).

49. Vu, B., Chen, M., Crawford, R. J. & Ivanova, E. P. Bacterial extracellular polysaccharides involved in biofilm formation. *Molecules* **14**, 2535–2554 (2009).

50. Schmidt, I. *et al.* In Situ Autofluorescence Spectroelectrochemistry for the Study of Microbial Extracellular Electron Transfer. *ChemElectroChem* **4**, 2515–2519 (2017).

51. Esteve-Núñez, A., Sosnik, J., Visconti, P. & Lovley, D. R. Fluorescent properties of c-type cytochromes reveal their potential role as an extracytoplasmic electron sink in Geobacter sulfurreducens. *Environ. Microbiol.* **10**, 497–505 (2008).

52. Aumann, S., Donner, S. & Fischer, J. Optical Coherence Tomography (OCT): Principle and Technical Realization. in *High Resolution Imaging in Microscopy and Ophthalmology* (ed. JF, B.) 59–85 (Springer, 2019). doi:10.1007/978-3-030-16638-0.

53. Weiss, N., van Leeuwen, T. G. & Kalkman, J. Simultaneous and localized measurement of diffusion and flow using optical coherence tomography. *Opt. Express* **23**, 3448 (2015).

54. Neu, T. R. & Lawrence, J. R. Innovative techniques, sensors, and approaches for imaging biofilms at different scales. *Trends Microbiol.* **23**, 233–242 (2015).

55. Molenaar, S. D. *et al.* In situ biofilm quantification in bioelectrochemical systems by using optical coherence tomography. *ChemSusChem* **11**, 2171–2178 (2018).

56. Xi, C., Marks, D., Schlachter, S., Luo, W. & Boppart, S. A. High-resolution three-dimensional imaging of biofilm development using optical coherence tomography. *J. Biomed. Opt.* **11**, 034001 (2006).

57. Pereira, J. *et al.* Real-time monitoring of biofilm thickness allows for determination of acetate limitations in bio-anodes. *Bioresour. Technol. Reports* **18**, 101028 (2022).

58. Maquelin, K. *et al.* Vibrational Spectroscopic Studies of Microorganisms. in *Handbook of Vibrational Spectroscopy* (eds. Chalmers, J. M. & Griffiths, P. R.) 3308–3334 (2002).

59. Virdis, B., Harnisch, F., Batstone, D. J., Rabaey, K. & Donose, B. C. Non-invasive characterization of electrochemically active microbial biofilms using confocal Raman microscopy. *Energy Environ. Sci.* **5**, 7017–7024 (2012).

60. Virdis, B., Millo, D., Donose, B. C. & Batstone, D. J. Real-time measurements of the redox states of c-type cytochromes in electroactive biofilms: A confocal resonance raman microscopy study. *PLoS One* **9**, (2014).

61. Lebedev, N., Strycharz-Glaven, S. M. & Tender, L. M. Spatially resolved confocal resonant Raman microscopic analysis of anode-grown Geobacter sulfurreducens biofilms. *ChemPhysChem* **15**, 320–327 (2014).

62. Krige, A., Sjöblom, M., Ramser, K., Christakopoulos, P. & Rova, U. On-line Raman spectroscopic study of cytochromes' redox state of biofilms in microbial fuel cells. *Molecules* **24**, (2019).

63. Keleştemur, S., Avci, E. & çulha, M. Raman and surface-enhanced Raman scattering for biofilm characterization. *Chemosensors* **6**, (2018).

64. Vyas, N., Sammons, R. L., Addison, O., Dehghani, H. & Walmsley, A. D. A quantitative method to measure biofilm removal efficiency from complex biomaterial surfaces using SEM and image analysis. *Sci. Rep.* **6**, 2–11 (2016).

65. Read, S. T., Dutta, P., Bond, P. L., Keller, J. & Rabaey, K. Initial development and structure of biofilms on microbial fuel cell anodes. *BMC Microbiol.* **10**, (2010).

66. Bond, D. R. & Lovley, D. R. Evidence for involvement of an electron shuttle in electricity generation by Geothrix fermentans. *Appl. Environ. Microbiol.* **71**, 2186–2189 (2005).

67. Kim, C. W. *et al.* Effect of monochromatic illumination on lipid accumulation of Nannochloropsis gaditana under continuous cultivation. *Bioresour. Technol.* **159**, 30–35 (2014).

68. Torres, C. I. *et al.* A kinetic perspective on extracellular electron transfer by anode-respiring bacteria. *FEMS Microbiol. Rev.* **34**, 3–17 (2010).

69. Katuri, K. P. *et al.* Electroactive biofilms on surface functionalized anodes: The anode respiring behavior of a novel electroactive bacterium, Desulfuromonas acetexigens. *Water Res.* **185**, 116284 (2020).

70. Santini, M. ; *et al.* Three-dimensional X-ray microcomputed tomography of carbonates and biofilm on operated cathode in single chamber microbial fuel cell. *Biointerphases* **10**, 1–9 (2015).

71. Carrel, M. *et al.* Biofilm imaging in porous media by laboratory X-Ray tomography: Combining a non-destructive contrast agent with propagation-based phase-contrast imaging tools. *PLoS One* **12**, (2017).

72. Carrel, M. *et al.* Biofilms in 3D porous media: Delineating the influence of the pore network geometry, flow and mass transfer on biofilm development. *Water Res.* **134**, 280–291 (2018).

73. Lawrence, J. R. *et al.* Scanning transmission X-ray, laser scanning, and transmission electron microscopy mapping of the exopolymeric matrix of microbial biofilms. *Appl. Environ. Microbiol.* **69**, 5543–5554 (2003).

74. Bartacek, J. *et al.* Iron, cobalt, and gadolinium transport in methanogenic granules measured by 3D magnetic resonance imaging. *Front. Environ. Sci.* **4**, 1–8 (2016).

75. Renslow, R. S. *et al.* A biofilm microreactor system for simultaneous electrochemical and nuclear magnetic resonance techniques. *Water Sci. Technol.* **69**, 966–973 (2014).

76. Renslow, R. S. *et al.* In situ effective diffusion coefficient profiles in live biofilms using pulsed-field gradient nuclear magnetic resonance. *Biotechnol. Bioeng.* **106**, 928–937 (2010).

77. Gimkiewicz, C. & Harnisch, F. Waste water derived electroactive microbial biofilms: growth, maintenance, and basic characterization. *J. Vis. Exp.* 50800 (2013) doi:10.3791/50800.

78. Harnisch, F. & Rabaey, K. The diversity of techniques to study electrochemically active biofilms highlights the need for standardization. *ChemSusChem* **5**, 1027–1038 (2012).

79. Millo, D. An Electrochemical Strategy to Measure the Thickness of Electroactive Microbial Biofilms. *ChemElectroChem* **2**, 288–291 (2015).

80. Millo, D. Spectroelectrochemical analyses of electroactive microbial biofilms. *Biochem. Soc. Trans.* **40**, 1284–1290 (2012).

81. Grohmann, E. & Vaishampayan, A. Techniques in Studying Biofilms and Their Characterization: Microscopy to Advanced Imaging System in vitro and in situ. *Biofilms Plant Soil Heal.* 215–230 (2017) doi:10.1002/9781119246329.ch12.

82. Golden, J., Yates, M. D., Halsted, M. & Tender, L. Application of electrochemical surface plasmon resonance (ESPR) to the study of electroactive microbial biofilms. *Phys. Chem. Chem. Phys.* **20**, 25648–25656 (2018).

83. Jiang, X. *et al.* Probing single- to multi-cell level charge transport in Geobacter sulfurreducens DL-1. *Nat. Commun.* **4**, 1–6 (2013).

84. Mollaei, M. *et al.* Comparative proteomics of Geobacter sulfurreducens PCAT in response to acetate, formate and/or hydrogen as electron donor. *Environ. Microbiol.* **23**, 299–315 (2021).

85. Orellana, R. *et al.* Proteome of Geobacter sulfurreducens in the presence of U(VI). *Microbiol. (United Kingdom)* **160**, 2607–2617 (2014).

86. ter Heijne, A., Pereira, M. A., Pereira, J. & Sleutels, T. Electron Storage in Electroactive Biofilms. *Trends Biotechnol.* **39**, 34–42 (2020).

87. Rabaey, K., Boon, N., Siciliano, S. D., Verhaege, M. & Verstraete, W. Biofuel cells select for microbial consortia that self-mediate electron transfer. *Appl. Environ. Microbiol.* **70**, 5373–5382 (2004).

88. Zakaria, B. S., Barua, S., Sharaf, A., Liu, Y. & Dhar, B. R. Impact of antimicrobial silver nanoparticles on anode respiring bacteria in a microbial electrolysis cell. *Chemosphere* **213**, 259–267 (2018).

89. Schechter, M., Schechter, A., Rozenfeld, S., Efrat, E. & Cahan, R. Anode Biofilm. in *Technology and Application of Microbial Fuel Cells* 57–75 (2014). doi:http://dx.doi.org/10.5772/58432.

90. Sivasankar, V., Mylsamy, P. & Omine, K. *Microbial fuel cell technology for bioelectricity*. *Microbial Fuel Cell Technology for Bioelectricity* (2018). doi:10.1007/978-3-319-92904-0.

91. Agrawal, U., Reilly, D. T. & Schroeder, C. M. Zooming in on biological processes with fluorescence nanoscopy. *Curr. Opin. Biotechnol.* **24**, 646–653 (2013).

92. He, C., Fong, L. G., Young, S. G. & Jiang, H. NanoSIMS imaging: An approach for visualizing and quantifying lipids in cells and tissues. *J. Investig. Med.* **65**, 669–672 (2017).

93. Chadwick, G. L., Otero, F. J., Gralnick, J. A., Bond, D. R. & Orphan, V. J. NanoSIMS imaging reveals metabolic stratification within current-producing biofilms. *Proc. Natl. Acad. Sci. U. S. A.* **116**, 20716–20724 (2019).

94. Caniglia, G. & Kranz, C. Scanning electrochemical microscopy and its potential for studying biofilms and antimicrobial coatings. *Anal. Bioanal. Chem.* **412**, 6133–6148 (2020).

95. Darch, S. E. & Koley, D. Quantifying microbial chatter: Scanning electrochemical microscopy as a tool to study interactions in biofilms. *Proc. R. Soc. A Math. Phys. Eng. Sci.* **474**, (2018).

96. Filman, D. J. *et al.* Cryo-EM reveals the structural basis of long-range electron transport in a cytochrome-based bacterial nanowire. *Commun. Biol.* **2**, 19–24 (2019).

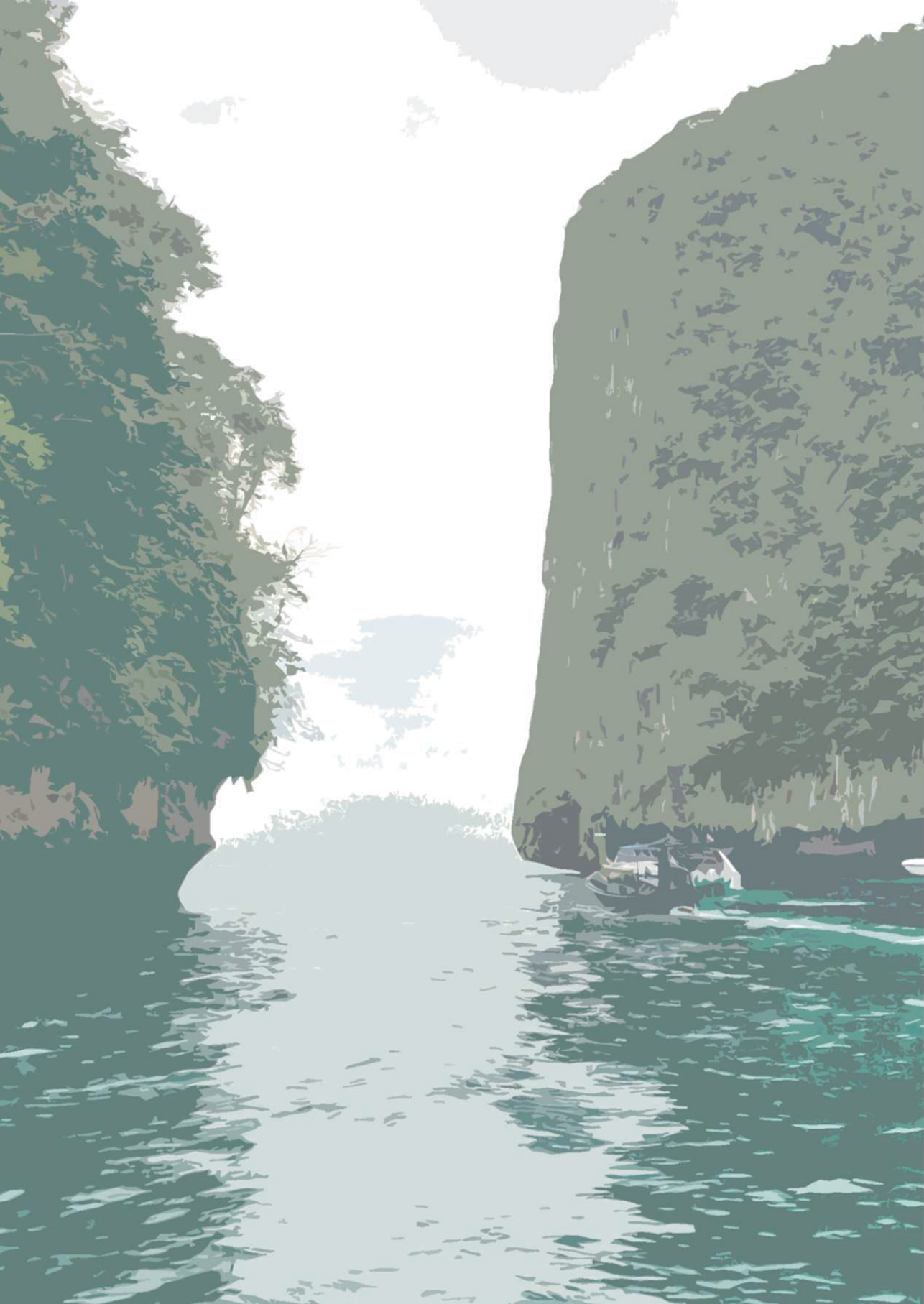

3 Real-time monitoring of biofilm thickness allows for the determination of acetate limitations in bio-anodes

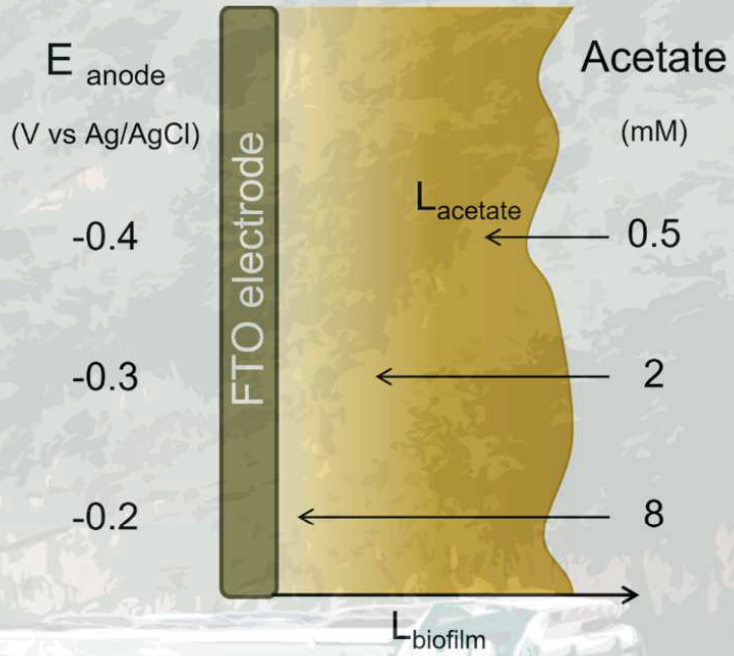

This chapter has been published as:

Pereira J, Pang S, Borsje C, Sleutels T, Hamelers B, ter Heijne A. *Real-time monitoring of biofilm thickness allows for determination of acetate limitations in bio-anodes*. Bioresour Technol Reports 2022;18:101028.

Abstract

Several studies have reported that current produced by electro-active bacteria (EAB) is dependent on anode potential and substrate concentration. However, information about the relation between biofilm growth and current density is scarce. In this study, biofilm thickness was monitored in-situ and this relation explored at three anode potentials and three acetate concentrations. The highest current densities of 3.7 $A.m^{-2}$ were obtained for biofilms thinner than 40 μm, even though thicknesses up to 88 μm were measured. Fick's law was used to estimate the acetate penetration depth in the biofilm, acetate diffusion rates in the biofilm, and specific acetate utilization rates. A maximum biofilm thickness of a non-acetate limited biofilm of 55 μm and an acetate diffusion rate of 2.68×10^{-10} $m^2.s^{-1}$ were estimated at -0.2 V vs Ag/AgCl. The results provide information on the target biofilm thickness for which no acetate limitations occur and provide data for modeling works with bio-anodes.

3.1. Introduction

Current production of bio-anodes in bio-electrochemical systems (BESs) depends on several parameters, such as reactor design, anode potential, substrate concentration and the amount of biomass present on the electrode.[1–3] Since current production is catalyzed by electro-active bacteria (EAB), it is essential to determine the optimal set of parameters that lead to high amount of these bacteria in the biofilm developed on the anode surface.

The combination of more positive anode potentials and higher acetate concentrations has often been reported to stimulate growth of electro-active biofilms and results in higher current densities.[4–6] The difference between the anode potential and the acetate oxidation potential (overpotential) is a measure of the energy available for bacterial growth and maintenance, and as a result, the anode becomes more attractive as a surface to allow biomass growth when poised at higher overpotential. Regarding the acetate concentration, at low concentrations, the current can be limited by acetate, while at higher concentrations, the current does not increase anymore as a function of concentration.[7,8] While the effect of anode potential and acetate concentration on current production has been the subject of several studies, it is not known how biofilm thickness and current are related. On top of that, in continuous systems, the current has been observed to reach a maximum value already after a couple of days, after which it starts decreasing, most likely induced by certain limitations such as accumulation of protons in the biofilm due to acetate conversion.[9,10] So far, the effect of biofilm development has not been related to current production. Understanding the effect of biofilm thickness on current is important because it can help understanding limitations of bio-anodes and how to overcome those.

Real-time monitoring of biofilm thickness on the electrode is a challenging task due to the invasive characteristics of most techniques.[11] Recently, a method has been developed to quantify the amount of electro-active biofilm, by using transparent Fluorine-doped Tin Oxide (FTO) electrodes.[12] Optical Coherence Tomography (OCT) was used to scan the biofilm on the electrode, and the biofilm volume was determined. With OCT, it is thus possible to study the development of the biofilm on the anode real-time as a function of acetate concentration and anode potential.

Even though more current is produced when thicker biofilms are present on the electrode,[12] too thick biofilms may lead to mass transfer limitations of substrate, protons, and buffer species between bulk solution and electrode surface. Ultimately, this may be reflected in decreasing current production as the biofilm grows thicker. On the one hand, being in direct contact with the electrode is an advantage since the resistance to transfer electrons is low, however, this comes at the expense of substrate availability. On the outer layers of the biofilm, facing the bulk solution, the microorganisms will have

high acetate availability. However, the generated electrons after substrate oxidation need to pass a longer distance (higher resistance) to reach the electrode.

This trade-off between resistance for electron transfer and substrate availability in the biofilm suggests that the current produced per amount of total biofilm (commonly named specific microbial activity) will decrease when the biofilm grows so thick that limitations occur. Therefore, it is of crucial importance to define maximum biofilm thickness that guarantees access to acetate and avoids limitations in electron transfer. Measurement of biofilm growth over time under different conditions (substrate concentration and anode potential) allows understanding limiting factors and optimal thickness depending on these conditions and can provide information on specific biofilm activity. Moreover, these data can also be used to determine parameters, such as acetate diffusion in biofilms that are scarce in literature and need to commonly be assumed for modelling purposes.

In this study, the development of the biofilm was investigated on the anode surface at different anode potentials and acetate concentrations. Biomass growth was monitored real-time using Optical Coherence Tomography (OCT). Based on the combination of a continuous monitoring of biofilm growth on the electrode and the produced current, a model that identifies acetate limitations in the biofilm was developed. This model was used to estimate the thickness of a biofilm through which acetate can penetrate completely, at three acetate concentrations and three anode potentials, and it was used to calculate acetate diffusion rates inside electro-active biofilms and specific acetate utilization rates of EAB.

3.2. Materials and Methods

3.2.1. Experimental setup and reactor configuration

The experiments were performed with the electrochemical cells previously described by Molenaar et al., 2018. These reactors were composed of two flow compartments: an anode and a cathode (each with a volume of 33 cm^3). Between these compartments, a bipolar membrane (Ralex PEBPM, MEGA a.s., Czech Republic) was placed with the anion side facing the anode and the cation side facing the cathode to keep the pH in the anode stable. To allow real time monitoring of the biofilm development, a transparent Fluorine-doped Tin Oxide (FTO) coated glass electrode was used as anode. Graphite sheet was placed in contact with the FTO electrode (around its operating area of 22.3 cm^2) to work as current collector. In the cathode compartment, a flat platinum/iridium coated titanium plate (Pt/IrO2 80:20, Magneto special anodes BV, Schiedam, The Netherlands) was used as counter electrode.

The anode compartment was continuously fed with influent at a rate of 0.36 $mL.min^{-1}$, while both anolyte (stream present in the anode compartment of the reactor) and catholyte (stream present in the cathode compartment of the reactor) were continuously recirculated at 60 $mL.min^{-1}$ (Masterflex L/S, Cole-Parmer, Barendrecht, The

Netherlands). The anode compartments were operated with a hydraulic retention time of 10 h (volume of anolyte of 220 mL), while the cathode compartments were operated in batch (i.e. without inflow of fresh catholyte nor outflow of catholyte). The reactors were electrically connected to a potentiostat (N-stat d-module, Ivium Technologies, Eindhoven, The Netherlands) that was used to control the anode potential. Reference electrodes were positioned in between the FTO electrode and the bipolar membrane by means of Haber–Luggin capillaries filled with 3 M KCl solution. All potentials are expressed using an Ag/AgCl electrode (+0.203V vs. Standard Hydrogen Electrode; Prosense, Oosterhout, The Netherlands), and the current produced by each bio-anode was recorded every minute. The reactors were operated at 298 K in a temperature-controlled cabinet. To avoid oxygen penetration in the reactors during sampling in the OCT, Quick-Coupler valves (Swagelok SS-QC4-D-400, USA) were used.

3.2.2. Inoculum and electrolyte composition

A mixture of acetate fed biomass from active bio-anodes was used as inoculum in all experiments. The influent was prepared according to DSMZ culture medium 141 and it constituted of ($g.L^{-1}$): 0.04, 0.17, and 0.65 $NaCH_3COO$, 3.40 KH_2PO_4, 4.36 K_2HPO_4, 0.1 $MgSO_4.7H_2O$, 0.74 KCl, 0.58 NaCl, 0.28 NH_4Cl, 0.1 $CaCl_2.2H_2O$, 1 mL of trace metals mixture and 1 mL of vitamins mixture.[13] Sodium 2-bromoethanesulfonate (1.97 $g.L^{-1}$) was added to the influent to inhibit methanogenesis. Anaerobic conditions in the reactor were maintained by continuously sparging the influent with nitrogen before and during the experiments. The catholyte consisted of 50 mM phosphate buffer solution at pH 7. Nitrogen was continuously sparged into the catholyte recirculation vessel during operation to avoid accumulation of hydrogen and possible diffusion towards the anode.

3.2.3. Experimental strategy

The influence of anode potential and different acetate concentrations on electro-active biofilm growth was studied based on 18 experimental runs. Each reactor operated for at least 10 days and each condition was tested in duplicate. All the data points of each experiment are shown. This approach was chosen as all the trends of the data are shown and it provides the most information for the modelling. Acetate concentrations of 0.5, 2 and 8 mM were used in the influent, with the aim to include limiting, average, and high acetate concentrations. The anode potential was controlled at -0.2, -0.3, and -0.4 V vs Ag/AgCl. Considering the thermodynamic acetate oxidation potential at biological standard conditions of -496 mV vs Ag/AgCl,[14] these are low overpotentials, and only up to 0.3 V will be available for cell growth and maintenance. However, this range of low anode potentials was selected to represent conditions in which reasonable voltage efficiency can be achieved in a Microbial Fuel Cell.

3.2.4. Acetate consumption and online monitoring of biofilm growth

Acetate concentration was measured using Ultra-High-Performance Liquid Chromatography (UHPLC) (300x7.8 mm Phenomenex Rezex Organic Acid H+ column,

Dionex ultimate 3000RS, Thermo Fisher Scientific, The Netherlands) after filtration of samples through a 0.45 µm pore-size filter (EMD Millipore SLFH025NS, Barendrecht, The Netherlands).[15] Consumed acetate ($Ac_{consumed}$, mol) was calculated as described in Equation 3.1, in which Ac_{in} (mM) is the acetate concentration in the influent, Ac_{out} (mM) is the acetate concentration in the anolyte, *flow* is the flowrate (mL.min^{-1}) and Δt (min) is the time between samples.

$$Ac_{consumed} = (Ac_{in} - Ac_{out}) \times flow \times \Delta t \quad \text{(Eq. 3.1)}$$

Optical Coherence Tomography (OCT) was used to monitor the biofilm growth on the anode in real time.[12] For OCT measurements, the reactors were disconnected hydraulically and electrically and placed on the OCT visualization stage. The electrode was then scanned at 54 evenly distributed spots, to allow for accurate imaging of the amount of the biofilm on the electrode within reasonable measuring duration. The OCT measurements took approximately 45 minutes, and no significant changes in acetate concentration nor produced current before and after the measurements were observed. The scans of the electrode with biofilms were run in a MATLAB script that isolated and counted the pixels corresponding to biofilm. The resulting number of pixels was converted to biomass weight (mg COD) using the calibration line reported.[12] Biofilm thickness (in µm) was determined after dividing the average volume of each biofilm by the area of the electrode. Due to the detection limit of the OCT, biofilm thicknesses thinner than 5 µm were not considered. Since different anode potentials and acetate concentrations were used in this study when compared to the operating conditions used by Molenaar et al., 2018, COD measurements of the biofilms were performed on the last day and confirmed that the calibration curve was valid. Both acetate analysis and OCT measurements were performed every two or three days throughout each experiment.

3.2.5. Basic model to identify acetate limitation in biofilms

A basic model to identify acetate limitations in the biofilms was used. This model was used to calculate the penetration depth of acetate inside the biofilm based on Fick's law (Equation 3.2), where $L_{acetate}$ is the penetration depth (m), D_s is the diffusion of acetate in the biofilm (m^2.s^{-1}), Ac_{out} is the acetate concentration in the anolyte (mol Ac.m^{-3}) and, k_0 is the specific acetate utilization rate (mol Ac.m^{-3}.s^{-1}).

$$L_{acetate} = \sqrt{[(2 \times D_s \times Ac_{out})/k_0]} \quad \text{(Eq. 3.2)}$$

Measured concentrations of acetate in the anolyte and measured biofilm thicknesses were used as input. Based on these, the model was used to estimate the penetration depth of acetate, acetate diffusion, and specific acetate utilization rate. In addition, using the specific acetate utilization rate, an estimated current density based on substrate availability was calculated and was compared with the measured current density. The estimated current density was calculated according to Equation 3.3:

$$j_{estimated} = L_{minimum} \times k_0 \quad \text{(Eq. 3.3)}$$

where $j_{estimated}$ represents the current density estimated by the model (mol Ac.m^{-2}.s^{-1}) and $L_{minimum}$ is the minimum biofilm thickness, which is the lowest thickness when comparing the estimated acetate penetration depth, or the measured biofilm thickness. The specific acetate utilization rate was used to estimate the current density (in mol Ac.m^{-2}.s^{-1}) assuming a 100 % Coulombic efficiency, which is realistic since the Coulombic efficiencies obtained for all bio-anodes were high (above 90 %).

The three parameters of interest: $L_{acetate}$, D_s, and k_0 were determined using minimization of the sum of squares between the estimated and the experimental current densities. This approach was used for the 126 experimental data points that constitute the dataset of this study. The data were grouped for anode potential and the three parameters were estimated. More details on the model can be found in Appendices.

3.3. Results and discussion

3.3.1. Higher acetate concentrations lead to higher current at the bio-anode

Figure 3.1.a shows the relation between the measured current density and the acetate concentration in the anolyte, based on the 126 measurements performed for all experiments together. Overall, an increase in acetate concentration resulted in higher current density. A maximum current density of 3.7 A.m^{-2} was obtained when the bio-anode was fed with 8 mM acetate.

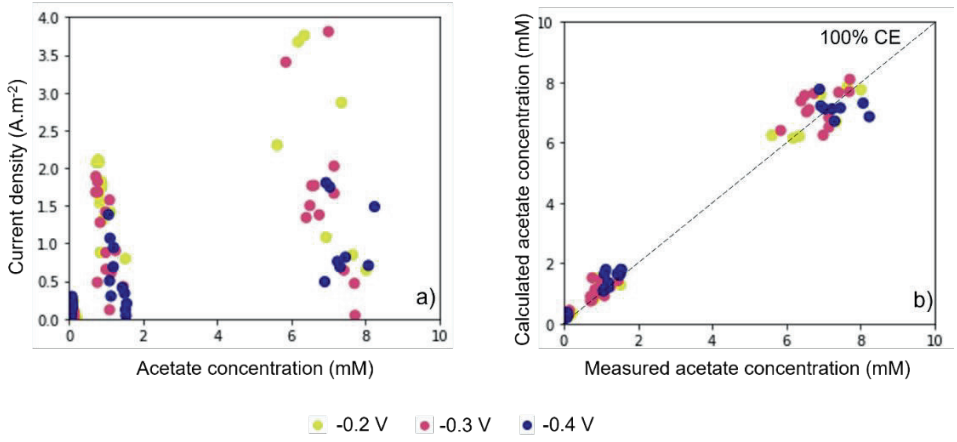

Figure 3.1. (a) Current produced as a function of the acetate concentration in the anolyte for -0.4, -0.3, and -0.2 V vs Ag/AgCl, and (b) relation between measured and calculated acetate concentration in the anolyte shows that Coulombic efficiency was close to 100 % (dashed line) for all data points.

The influence of anode potential on current produced and acetate consumed is also depicted in Figure 3.1. More acetate was consumed when the anode was controlled at -0.2 and -0.3 V, resulting in higher current densities (approximately 2 mM of acetate

was consumed at -0.2 V and 1.5 mM at -0.3 V, both determined when the anode was fed with 8 mM acetate). Overall, these results show that the current produced by EABs is mainly limited by the anode potential when controlled at -0.4 V, since similar current densities were obtained when the bio-anode was fed with 2 and 8 mM. Nevertheless, current produced is mainly limited by the acetate concentration when the anode potential is controlled at -0.2 and -0.3 V, since similar current densities at these two anode potentials were obtained when the bio-anode was fed the same acetate concentration.

The relation between the measured concentration of acetate and the calculated acetate concentration in the anolyte based on current produced shows that the Coulombic efficiency was close to 100 % in all experiments (Figure 3.1.b). Since the current produced relates to the acetate consumption, this confirms that acetate was consumed by electro-active microorganisms. Therefore, competitive processes in the anode such as the presence of methanogens and sulphur reducers are neglected, making this experimental setup suitable to study electro-active biofilms.

3.3.2. Current density reaches a maximum at biofilm thickness between 10 and 30 µm and decreases when biofilms grow thicker

The current profiles as a function of time were similar for all the bio-anodes (in Appendices): for all experiments, the current reached a peak, after which it flattened out or decreased, while the biofilm thickness increases with time, and keeps increasing also after a maximum in current is reached. Figure 3.2 shows the current density produced by the biofilm on the electrode for all the conditions applied. Generally, the maximum current density was reached at biofilm thicknesses in the range of 10-30 µm. When biofilm thickness increases beyond 30 µm, the current does not further increase and in most cases decreases. Nevertheless, a high current density was obtained when the biofilm thickness was approximately 47 µm (at -0.3 V vs Ag/AgCl). The reason for this high acetate conversion cannot be explained with the measured parameters that constitute the dataset of this study.

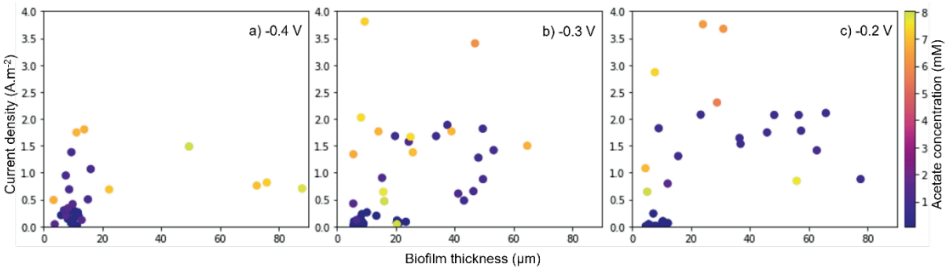

Figure 3.2. Current density profiles as a function of the biofilm thickness when the anode was poised at a) - 0.4 V, b) -0.3 V, and c) -0.2 V (vs Ag/AgCl). Current reached a maximum at biofilm thickness between 10 and 30 µm, while at higher biofilm thickness, current decreased.

When the bio-anode was fed with 0.5 mM acetate, current densities were lower than 0.5 $A.m^{-2}$ and the maximum biofilm thickness was 25 µm (at -0.3 V). At this acetate concentration, increasing the anode potential did not have an effect on current density (Figure 3.2.b and 3.2.c). This indicates that the current production was determined by acetate availability at the lowest acetate concentration. Increasing the influent acetate concentration to 2 mM resulted in current densities varying between 1.0 and 2.0 $A.m^{-2}$. The biofilm thickness ranged between 5 and 20 µm at -0.4 V (Figure 3.2.a), and thicker biofilms were found for more positive anode potentials, reaching a maximum of 55 µm at -0.3 V and 78 µm at -0.2 V. However, this increase in biofilm thickness did not result in a higher current. Feeding the bio-anode with 8 mM acetate (highest acetate concentration) resulted in the highest current densities of approximately 3.7 $A.m^{-2}$. These current densities were obtained at -0.3 V when the biofilm was 10 µm thick (Figure 3.2.b), and at -0.2 V when the biofilm was 25-30 µm thick (Figure 3.2.c). Even though increasing the anode potential from -0.4 to -0.3 V resulted in a steep increase in current density, when the potential was further increased from -0.3 to -0.2 V, there was no clear increase in current density. The thickest biofilm at -0.4 V was 88 µm, 65 µm at -0.3 V, both measured when 8 mM acetate was used whereas the thickest biofilm at -0.2 V was 78 µm when 2 mM acetate was used.

The current densities obtained are comparable to previously reported current density ranges obtained with flat and non-capacitive electrodes. With a similar reactor design, Molenaar et al., 2018 reported maximum current densities up to 2 $A.m^{-2}$ followed by a decrease to approximately 1 $A.m^{-2}$ when the anode was fed with 10 mM acetate and the anode potential controlled at -0.35 V. Under the same operating conditions and with a circular FTO electrode, Heijne et al., 2018 reported a maximum current of 0.7 $A.m^{-2}$ and 1.1 $A.m^{-2}$. These results are also in accordance with previous studies that reported higher currents when higher anode potentials and non-limiting acetate concentrations were used.[8,17]

3.3.3. Identifying acetate limitations via penetration depth in bio-anodes

The biofilm thicknesses of 18 experiments were measured in 126 measurements, and the measured biofilm thicknesses ranged between 5 and 88 µm. Generally, for biofilm thicknesses up to about 30 µm, thicker biofilms resulted in higher current density. Further growth of the biofilm resulted in stable or decreasing currents. Since the biofilm continued growing when the current leveled off and/or decreased, the specific bio-electrocatalytic activity of the bio-anodes, i.e. the current produced per amount of biofilm, decreased for thicker biofilms. At early stages of biofilm growth, the highest specific bio-electrocatalytic activity was found for the most positive anode potential of -0.2 V in combination with the highest acetate concentration of 8 mM, for biofilms thinner than 30 µm. The highest specific bio-electrocatalytic activity was 2.5 $A.g_{COD}^{-1}$. When the biofilms grew thicker, specific activities decreased to 0.2-0.5 $A.g_{COD}^{-1}$ for all anode potentials and acetate concentrations tested.

Even though biofilm growth is always linked to current produced, two different relations between growth and current can be defined. During early-stage growth, the measured increase in biofilm thickness is related to increase in current density. This relation between biofilm thickness and current is characteristic for the low range of biofilm thicknesses (up to approximately 30 μm), in which the highest specific activities are obtained as long as current is not limited by substrate availability and anode potential. When biofilms grow further, current produced flattens out or decreases, shifting the relation between biofilm thickness and current produced. In this stage, characterized by lower specific microbial activities, there is growth and accumulation of biomass that results in an overall decrease in the rate of electrons transfer to the anode. This decrease in specific bio-electrocatalytic activity could be caused by diffusion limitations in the biofilm that creates an additional resistance for the electrons to flow towards the electrode as well as mass transfer limitations of acetate and/or products.[18,19] Thus, the biofilm as a whole becomes less electro-active.

3.3.4. Ratio of electro-active biofilm on the electrode increases with higher acetate concentration and more positive anode potential

The shift in the relation between the current density and the thickness of the biofilm on the anode indicates that bacteria slow down the rate of electrons transferred to the electrode when biofilm grows thicker. The measurements obtained on real-time biofilm thickness can be used to better understand diffusion limitations in the bio-anode and to determine the optimal biofilm thickness depending on the conditions applied (anode potential and acetate concentration). The acetate penetration depth in the biofilm was selected as the most limiting factor since the availability of acetate showed to be more determinant for the current density of bio-anodes than the anode potential applied (as shown in Figure 3.2 and mentioned in the previous sections). The concentration of acetate and the biofilm thickness (distance to the electrode) are intrinsically related parameters determining the produced current. If the availability of the carbon source is not evenly distributed over the depth of the biofilm, the bacteria experiencing low acetate concentration will oxidize less acetate and, therefore, produce lower current at the electrode than bacteria experiencing higher acetate concentrations. Moreover, as the biofilm grows further away from the electrode, the losses to use the electrode as electron acceptor become bigger.

By calculating the acetate penetration depth into the biofilm at different conditions, the biofilm thickness that is non-acetate limited, and that is therefore able to contribute to the produced current, can be determined. Figure 3.3 shows the ratio between non-acetate limited biofilm and the total biofilm measured on the FTO electrode as a function of the measured biofilm thickness. Ratios of 1 are obtained when acetate penetrates the whole biofilm, i.e. the biofilm activity is not limited by acetate supply. Ratios below 1 show which part of the biofilm has access to acetate: for example, a ratio

of 0.6 means that acetate penetrates 60 % of the measured biofilm thickness and the remaining 40 % of the biofilm has no acetate.

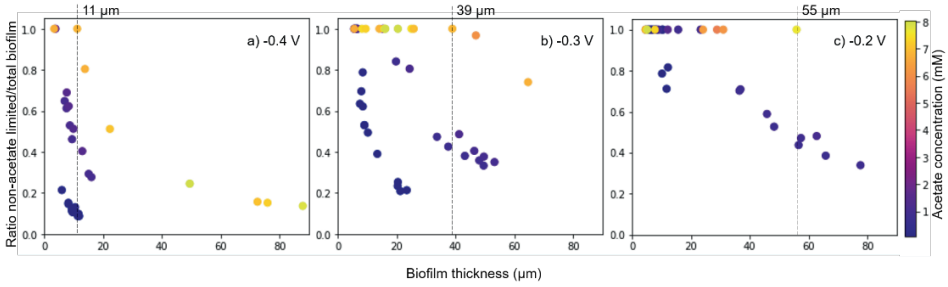

Figure 3.3. Ratio between non-acetate limited biofilm and total biofilm measured with OCT as a function of the biofilm thickness when the anode was poised at a) - 0.4 V, b) -0.3 V, and c) -0.2 V (vs Ag/AgCl).

In general, the thickness of a non-acetate limited biofilm increases with higher acetate concentrations and more positive anode potentials. At low acetate concentrations, only part of the biofilm will have access to acetate, and most of the data points show a ratio <1. For the highest acetate concentrations, a ratio of non-acetate limited biofilm over total biofilm of 1 is found, meaning that the whole biofilm has access to acetate, until a certain biofilm thickness is reached, and after that, the ratio goes down. A maximum thickness of 55 µm was calculated for biofilms fed with 8 mM acetate and with the anode potential controlled at -0.2 V. At the same concentration, the thickness of the biofilms that faced no acetate diffusion limitations decreased to 39 µm when the anode potential was poised at -0.3 V, and to 11 µm at -0.4 V. At lower acetate concentrations, the penetration depth of acetate is smaller: for 0.5 mM acetate in the influent, a maximum biofilm thickness of 10 µm was obtained, while for 2 mM acetate in the influent, a maximum biofilm thickness of 24 µm was obtained, both at -0.2 V. Particularly for the bio-anodes fed with 0.5 mM acetate (the lowest acetate concentration), a steep increase in acetate-limited biomass was observed within a few micrometers of biofilm thickness, indicating that extremely low acetate concentrations 1) do not allow an efficient penetration of acetate in the biofilm, and 2) do not result in growth of thick biofilms.

Although very limited studies have been performed, the limiting biofilm thicknesses determined based on the acetate penetration depth are in line with other findings. For example, the CLSM study on bio-anodes reported by Sun et al. (2016) reported an increasing microbial activity until a biofilm thickness of 20 µm in a bio-anode fed with 16 mM acetate. They reported a decrease in activity for a 45 µm thick biofilm that was associated with the presence of a dead layer of bacteria in direct contact with the electrode.[21] In other studies, a biofilm thickness of 50 µm has been reported to guarantee a thoroughly electro-active biofilm and limitations in produced current were encountered at biofilm thicknesses ranging from 40 and 60 µm.[22–24] Biofilm thicknesses

in the range of 4 to 58 μm have been reported in a study on the effect of shear stress on bio-anodes, and biofilms thicker than 68 μm have been measured in a study focused on the effect of pH and buffer concentration on current produced at the anode.[25,26]

Even though thicker biofilms grew on the FTO electrode with higher acetate concentrations and more positive anode potentials, it is essential to highlight that large parts of these biofilms were not accessible to acetate (60-90 %). These were the biofilms that produced the lowest current densities (Appendices). Even though these acetate limited biofilms (ratio lower than 1) produced current densities up to 2 $A.m^{-2}$, only non-acetate limited biofilms (ratios equal to 1) produced higher current densities. The analysis of the ratio of non-acetate limited biomass indicates the operating conditions and the thicknesses at which the biofilm should be controlled to guarantee and maintain high current densities. This is of crucial importance in practical applications since higher current production is related to maximum acetate conversion, which can only be obtained in non-acetate limited biofilms. Therefore, strategies to keep the biofilm thickness within the non-limiting range of thicknesses, by means of sheer stress or scraping off the top layers of the biofilm must be taken into account when developing microbial electrochemical technologies for practical applications.

In practical applications with real wastewater, the thicknesses of a non-acetate limited electro-active biofilm are expected to be slightly thinner than the thicknesses reported in this study. Given the complexity of real wastewater streams that include the presence of several microbial species and alternative electron donors and acceptors, it is likely that other species will thrive in the biofilm and competing processes for acetate will happen.[17] Nevertheless, in the research field, the reported optimal range of biofilm thicknesses and acetate limitations can give fruitful insights into bio-cathodes. Even though bio-cathodes have an opposed working principle to bio-anodes (in the sense that energy is consumed to produce chemical compounds and consumption of electrons is related to consumption of protons), limitations due to the distance to the cathode (electron donor) and the accumulation of products (acetate or other long chain fatty acids such as caproate) will also create limitations in the biofilm. The results reported here for electro-active biofilms on an anode cannot be directly extrapolated to the growth of electro-active biofilms on a cathode, given the different substrates and products and microbial community of the biofilms. However, applying a similar methodology on bio-cathodes to measure and monitor their thickness over time can reveal the optimal operating range and give insights on how to optimize their performance.

3.3.5. Practical acetate diffusion and specific acetate utilization rates in electro-active biofilms

Two parameters were derived from Fick's equation: the acetate diffusion rate, D_s, and the specific acetate utilization rate, k_0. These are essential parameters to characterize

any bioprocess as they allow for a better understanding and for a more accurate description and control of processes. In bio-anode studies, these parameters are often needed for modeling purposes and assumed values are used since no experimental data are available. With the extended dataset on biofilm thicknesses and concentrations of acetate, practical diffusion rates of acetate in biofilms and specific acetate utilization rates at three different anode potentials can be estimated (Table 3.1). Even though these parameters are not directly linked to the applied anode potential, more understanding of structural and compositional differences in the electro-active biofilms can be obtained when deriving these parameters for each anode potential tested in this study. Acetate diffusion rates are also influenced by factors other than the acetate concentration in the anolyte. These factors include structural and compositional characteristics and viability of the biofilm. When denser biofilms grow on the electrode (i.e., less porous and more cellular packed biofilm structures), lower acetate diffusions rates are expected. Acetate penetration can also be hindered by the presence of a more solid extracellular matrix composed of saturated lipids and less flexible polysaccharides and protein structures. Finally, lower acetate diffusion rates are expected to be obtained if biofilms were mainly composed of dead biomass.

Table 3.1. Acetate diffusion rate and specific acetate utilization rate in electro-active biofilms as a function of the anode potential (all anode potentials are expressed vs Ag/AgCl).

Parameters	E = - 0.4 V	E = - 0.3 V	E = - 0.2 V
D_s ($m^2.s^{-1}$)	1.02×10^{-11}	1.09×10^{-10}	2.68×10^{-10}
k_0 (mol $Ac.m^{-3}.s^{-1}$)	0.14	0.08	0.08

Acetate diffusion rates in the order of 10^{-10} $m^2.s^{-1}$ were obtained when the anode potential was -0.3 and -0.2 V, and 10^{-11} $m^2.s^{-1}$ when the anode potential was -0.4 V. These diffusion rates are slightly lower than those typically reported for diffusion rates in water (10^{-9} $m^2.s^{-1}$). Since the acetate diffusion rates are here calculated inside the biofilm structure, where mass transfer resistance is higher than when acetate diffuses in water, it is not surprising that the rates are one order of magnitude lower.

The diffusion of acetate in the biofilm increased with more positive anode potentials (1.02×10^{-11} $m^2.s^{-1}$ at -0.4 V, 1.09×10^{-10} $m^2.s^{-1}$ at -0.3 V, and 2.68×10^{-10} $m^2.s^{-1}$ at -0.2 V). For the more positive anode potentials, acetate diffusion rates similar to the values commonly assumed in literature were obtained. Korth et al., 2015 assumed an acetate diffusion rate in biofilms of 5.5×10^{-10} $m^2.s^{-1}$ after using a 0.5 correction factor from the acetate diffusion in water (1.1×10^{-9} $m^2.s^{-1}$), whereas Marcus et al., 2007 assumed 8.7×10^{-10} $m^2.s^{-1}$ after using a reduction factor of 0.8 [29] on the acetate diffusion rate in water reported in Lide, 2006. More acetate diffusion values have been assumed in other studies.[18,31] With the outcomes of the model, realistic acetate diffusion rates in biofilms

at three different anode potentials are provided and can be used for future modeling work in electro-active biofilms.

The model also predicts specific acetate utilization rates. This parameter is a measure of the maximum acetate converted (so-called maximum activity) by EAB. Specific acetate utilization rates of 0.08 mol $Ac.m^{-3}.s^{-1}$ were obtained at -0.3 and -0.2 V and a higher specific acetate utilization rate of 0.14 mol $Ac.m^{-3}.s^{-1}$ was obtained at -0.4 V. These results corroborate with data previously reported for EAB. For example, Marcus et al., 2007 used a maximum acetate utilization of 0.08 mol $Ac.m^{-3}.s^{-1}$ and Lee et al., 2009 reported a maximum acetate utilization of 0.20 mol $Ac.m^{-3}.s^{-1}$ (biomass density of 50 kg $VS.m^{-3}$ [15] was used to convert the reported activities of 0.132 mmol Ac.mg $VS^{-1}.d^{-1}$ and 22.3 kg COD.kg $VS^{-1}.d^{-1}$, respectively). When compared to anaerobic digesters that usually use as rule of thumb a conversion of 2 kg COD.kg $VS^{-1}.d^{-1}$ [32] (approximately 0.02 mol $Ac.m^{-3}.s^{-1}$ considering a biomass density of 50 kg $VS.m^{-3}$), these results show comparable specific acetate utilization rates for EAB. However, tailoring biofilm thicknesses to avoid acetate limitation and optimize acetate conversion rates by EAB is essential, especially when the higher operating rates reported in anaerobic digesters need to be achieved (5-25 kg COD.kg $VS^{-1}.d^{-1}$).[33]

3.4. Conclusion

Bio-anodes must be operated in a way that the highest current is achieved with a thin electro-active biofilm. This requires a controlled biomass development on the electrode up to a certain thickness to guarantee acetate availability inside the biofilm and to ensure high electron transfer rates to the electrode. Therefore, growing thin biofilms and managing the biomass thickness on the electrode to suit the operating conditions is essential to maintain higher current densities, and it serves as a strategy to narrow down the limiting variables towards a better understanding of other possible limiting phenomena occurring in the EAB.

3.5. Acknowledgements

This work was performed in the cooperation framework of Wetsus, European Centre of Excellence for Sustainable Water Technology (www. wetsus.nl). Wetsus is co-funded by the Dutch Ministry of Economic Affairs and Ministry of Infrastructure and Environment, the European Union Regional Development Fund, the Province of Fryslân, and the Northern Netherlands Provinces. The authors thank the participants of the research theme “Resource Recovery” for the fruitful discussions and their financial support. This publication is part of the project “Understanding and controlling electron flows in electro-active biofilms” with project number 17516 of the research program Vidi which is (partly) financed by the Dutch Research Council (NWO).

3.6. References

1. Borole, A. P. *et al.* Electroactive biofilms: Current status and future research needs. *Energy Environ. Sci.* **4**, 4813–4834 (2011).
2. Hindatu, Y., Annuar, M. S. M. & Gumel, A. M. Mini-review: Anode modification for improved performance of microbial fuel cell. *Renew. Sustain. Energy Rev.* **73**, 236–248 (2017).
3. Guo, Y., Rosa, L. F. M., Müller, S. & Harnisch, F. Monitoring stratification of anode biofilms in bioelectrochemical laminar flow reactors using flow cytometry. *Environ. Sci. Ecotechnology* **4**, 100062 (2020).
4. Zhu, X., Yates, M. D. & Logan, B. E. Set potential regulation reveals additional oxidation peaks of Geobacter sulfurreducens anodic biofilms. *Electrochem. commun.* **22**, 116–119 (2012).
5. Aelterman, P., Freguia, S., Keller, J., Verstraete, W. & Rabaey, K. The anode potential regulates bacterial activity in microbial fuel cells. *Appl. Microbiol. Biotechnol.* **78**, 409–418 (2008).
6. Villano, M., Ralo, C., Zeppilli, M., Aulenta, F. & Majone, M. Influence of the set anode potential on the performance and internal energy losses of a methane-producing microbial electrolysis cell. *Bioelectrochemistry* **107**, 1–6 (2016).
7. Dhar, B. R. & Lee, H. S. Evaluation of limiting factors for current density in microbial electrochemical cells (MXCs) treating domestic wastewater. *Biotechnol. Reports* **4**, 80–85 (2014).
8. Sleutels, T., Darus, L., Hamelers, H. V. M. & Buisman, C. J. N. Effect of operational parameters on Coulombic efficiency in bioelectrochemical systems. *Bioresour. Technol.* **102**, 11172–11176 (2011).
9. Torres, C. I. *et al.* A kinetic perspective on extracellular electron transfer by anode-respiring bacteria. *FEMS Microbiol. Rev.* **34**, 3–17 (2010).
10. De Lichtervelde, A. C. L., Ter Heijne, A., Hamelers, H. V. M., Biesheuvel, P. M. & Dykstra, J. E. Theory of Ion and Electron Transport Coupled with Biochemical Conversions in an Electroactive Biofilm. *Phys. Rev. Appl.* **12**, 1 (2019).
11. Azeredo, J. *et al.* Critical review on biofilm methods. *Crit. Rev. Microbiol.* **43**, 313–351 (2017).
12. Molenaar, S. D. *et al.* In situ biofilm quantification in bioelectrochemical systems by using optical coherence tomography. *ChemSusChem* **11**, 2171–2178 (2018).
13. DSMZ. 141. Methanogenium Medium (H2/CO2). 6–8 https://www.dsmz.de/microorgan- isms/medium/pdf/DSMZ_Medium141.pdf (2017).
14. Logan, B. E. *et al.* Microbial fuel cells: Methodology and technology. *Environmental Science and Technology* vol. 40 5181–5192 (2006).
15. Lee, H.-S., Torres, C. I. & Rittmann, B. E. Effects of substrate diffusion and anode potential on kinetic parameters for anode-respiring bacteria. *Environ. Sci. Technol.* **43**, 7571–7577 (2009).
16. Heijne, A. ter, Liu, D., Sulonen, M., Sleutels, T. & Fabregat-Santiago, F. Quantification of bio-anode capacitance in bioelectrochemical systems using Electrochemical Impedance Spectroscopy. *J. Power Sources* **400**, 533–538 (2018).
17. Sleutels, T., Molenaar, S., Heijne, A. & Buisman, C. Low Substrate Loading Limits

Methanogenesis and Leads to High Coulombic Efficiency in Bioelectrochemical Systems. *Microorganisms* **4**, 1–11 (2016).

18. Renslow, R. S., Babauta, J. T., Majors, P. D. & Beyenal, H. Diffusion in biofilms respiring on electrodes. *Energy Environ. Sci.* **6**, 595–607 (2013).

19. ter Heijne, A. *et al.* Analysis of bio-anode performance through electrochemical impedance spectroscopy. *Bioelectrochemistry* **106**, 64–72 (2015).

20. Sun, D. *et al.* The effect of biofilm thickness on electrochemical activity of Geobacter sulfurreducens. *Int. J. Hydrogen Energy* **41**, 16523–16528 (2016).

21. Sun, D., Cheng, S., Zhang, F. & Logan, B. E. Current density reversibly alters metabolic spatial structure of exoelectrogenic anode biofilms. *J. Power Sources* **356**, 566–571 (2017).

22. Franks, A. E., Nevin, K. P., Glaven, R. H. & Lovley, D. R. Microtoming coupled to microarray analysis to evaluate the spatial metabolic status of Geobacter sulfurreducens biofilms. *ISME J.* **4**, 509–519 (2010).

23. Franks, A. E., Glaven, R. H. & Lovley, D. R. Real-time spatial gene expression analysis within current-producing biofilms. *ChemSusChem* **5**, 1092–1098 (2012).

24. Ly, H. K. *et al.* Unraveling the interfacial electron transfer dynamics of electroactive microbial biofilms using surface-enhanced raman spectroscopy. *ChemSusChem* **6**, 487–492 (2013).

25. Pham, H. T. *et al.* High shear enrichment improves the performance of the anodophilic microbial consortium in a microbial fuel cell. *Microb. Biotechnol.* **1**, 487–496 (2008).

26. Lusk, B. G., Parameswaran, P., Popat, S. C., Rittmann, B. E. & Torres, C. I. The effect of pH and buffer concentration on anode biofilms of Thermincola ferriacetica. *Bioelectrochemistry* **112**, 47–52 (2016).

27. Korth, B., Rosa, L. F. M., Harnisch, F. & Picioreanu, C. A framework for modeling electroactive microbial biofilms performing direct electron transfer. *Bioelectrochemistry* **106**, 194–206 (2015).

28. Marcus, A. K., Torres, C. I. & Rittmann, B. E. Conduction-Based Modeling of the Biofilm Anode of a Microbial Fuel Cell. *Biotechnol. Bioeng.* **98**, 1171–1182 (2007).

29. Wanner, O. *et al. Mathematical Modeling of Biofilms*. (2006).

30. Lide, D. *CRC handbook of chemistry and physics*. (Cleveland: CRC Press., 2006).

31. Wanner, O. & Gujer, W. A Multispecies Biofilm Model. *Biotechnol. Bioeng.* **28**, 314–328 (1986).

32. Arends, J. B. A. & Verstraete, W. 100 years of microbial electricity production: Three concepts for the future. *Microbial Biotechnology* vol. 5 333–346 (2012).

33. Pham, T. H. *et al.* Microbial fuel cells in relation to conventional anaerobic digestion technology. *Eng. Life Sci.* **6**, 285–292 (2006).

3.7. Appendices

A. Model to identify acetate diffusion limitations

We used Python to quantify the acetate penetration depth and estimate acetate diffusion rate and specific acetate utilization rates in bio-anodes. Some lines of the script used to translate the equations mentioned in Material and Method into Python language are discriminated below. The estimated diffusion rate and specific acetate utilization rate are *par[1]* and *par[2]*, respectively.

*"data_pd['Acetate penetration depth'] = (2*np.abs(par[1])*data_pd['Acetate concentration (mM)']).apply(np.sqrt)*

data_pd[' $L_{minimum}$ ']=(data_pd[['l_sub','Biofilm thickness (µm)']].min(axis=1))

*data_pd['Estimated current density']=data_pd['$L_{minimum}$']*par[0]*

data_pd['Ratio non-acetate limited/total biofilm']=data_pd['l_min']/data_pd['Biofilm thickness (µm)']

*data_pd['i_res**2']=(data_pd['Measured current density']-data_pd['Estimated current density'])**2"*

Nelder-Mead was used as the method to minimize the variation between estimated and measured current. Equation 3.A1 was used to calculate the "*correlation factor*", in which *ssq mode* is the mode of the sum of squares and *ssq avg* is the average of the sum of squares. A correlation of approximately 0.3 was obtained for each group of data divided by the applied anode potential.

correlation factor = 1 - *ssq mode*/*ssq avg* (Eq. 3.A1)

Obviously, the variance between the estimated and measured current decreased when the number of data points was decreased. For example, "*correlation factors*" of 0.4 and 0.7 were obtained when the dataset was fragmented by small ranges of biofilm thicknesses. However, when the model was used over the different stages of the biofilm development on the anode surface, the estimated acetate diffusions and the specific acetate utilization rate were biased. This is related to the unbalance in the number of biofilm thicknesses measured for each condition tested in this study when a certain biofilm thickness range is defined. Therefore, the outcomes were mainly determined by the experimental conditions that contained the highest number of data points within a defined biofilm thickness range. This was overcome by including all the thicknesses gathered in the dataset and providing a general characterization of EAB as a function of the anode potential.

B. Current density and biofilm growth on the electrode

Figure 3.B shows the current profile (Fig. 3.B1) and biomass growth (Fig. 3.B2) for all the experiments performed in this study. We observed an initial increase in current produced that was followed by a constant and stable current produced over time (Figure

3.B1). For some runs, the current decreased after the peak and stabilized at a value lower than the peak. Data were removed when the current decreased down to zero after reaching the peak. The amount of biomass present on the electrode is shown in Figure 3.B2.

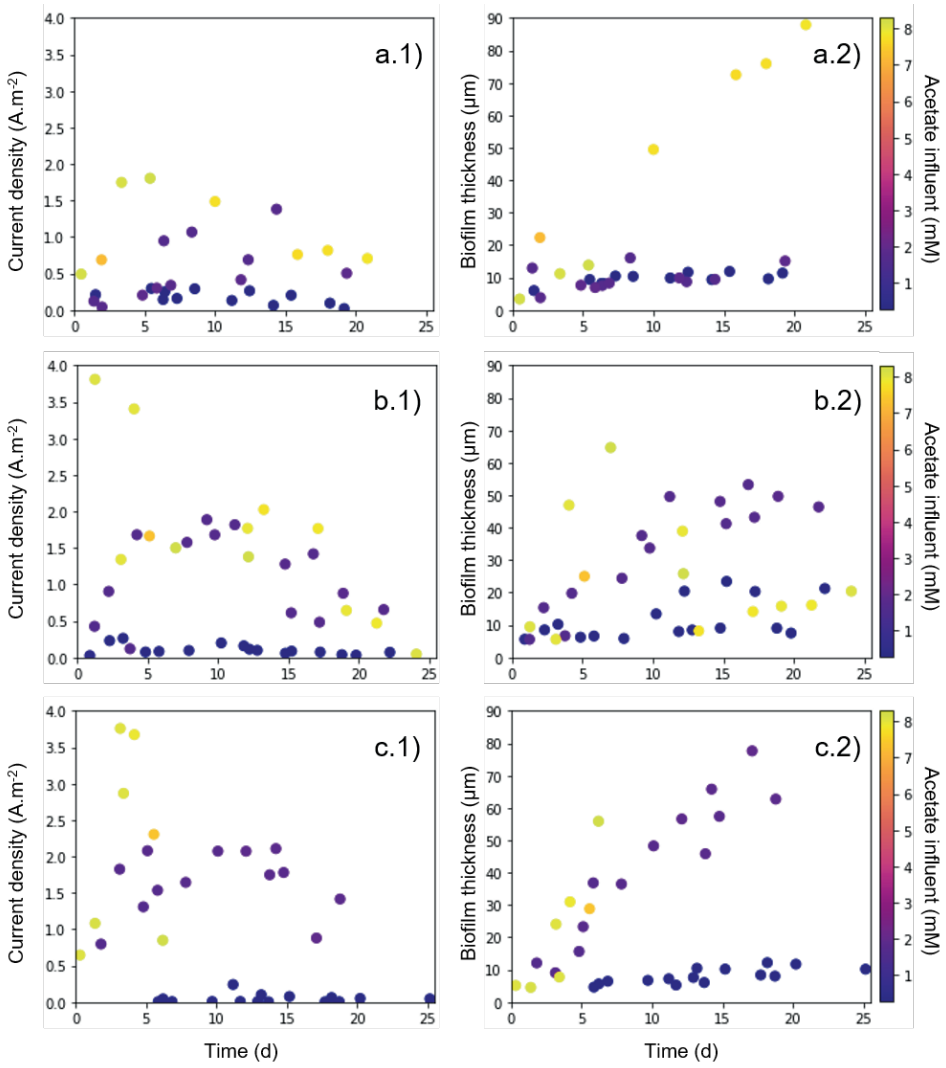

Figure 3.B. Current density (1) and biofilm growth (2) profiles over time when the anode was poised at a) - 0.4 V, b) -0.3 V, and c) -0.2 V (vs Ag/AgCl).

Even though current profiles were different for each experiment, an increase in biomass with time was observed for the period evaluated in all experiments. This shows that while current was produced, even when current decreased, biomass thickness kept increasing on the FTO electrode.

C. Calculation of the equivalent acetate concentration in the anolyte

Acetate concentration in the anolyte was calculated based on the current produced, assuming a Coulombic efficiency of 100 %. After, the concentrations were compared with the measured acetate concentrations to confirm the high range of Coulombic efficiencies of the dataset. Equation 3.C1 was used to calculate the acetate concentration in the anolyte, $Ac_{out,equi}$ (mM acetate), in which Ac_{in} is the measured acetate concentration in the influent (mM acetate), i is the measured current (C.s^{-1}), $flow$ (0.36 mL.min^{-1}) is the flowrate, F is the Faraday constant (96485 Coulombs.mol$_{electrons}$ $^{-1}$) and n (8 mol$_{electrons}$.mol$_{acetate}$$^{-1}$) is the amount of moles of electrons produced per mole of acetate consumed.

$$Ac_{out,equi} = Ac_{in} - i/flow/(F \times n) \qquad \text{(Eq. 3.C1)}$$

D. Relation between current produced and non-acetate limited biofilm

Figure 3.D1 shows the ratio between non-acetate limited biofilm and measured biofilm thickness as a function of current density. Acetate limited biofilms produced current densities lower than 2.2 A.m^{-2} whereas higher current densities were only reached by non-acetate limited biofilms.

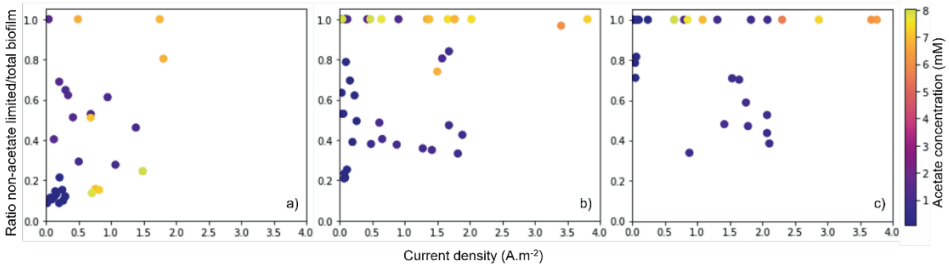

Figure 3.D. Ratio between non-acetate limited biofilm and total biofilm present on the anode as a function of the current densities when the anode was poised at a) - 0.4 V, b) -0.3 V, and c) -0.2 V (vs Ag/AgCl).

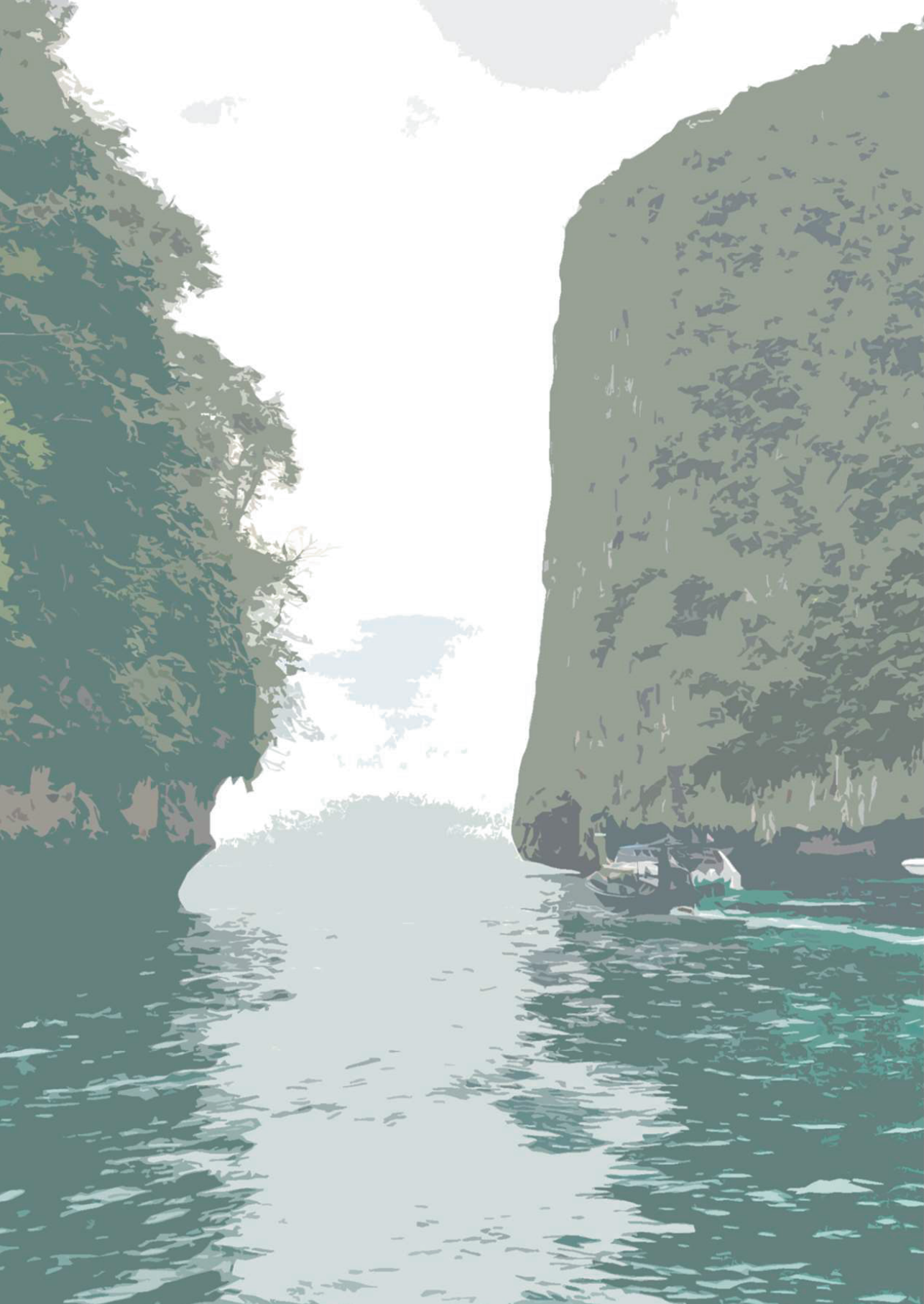

4 Maximum thickness of non-buffer limited electro-active biofilms decreases at higher anode potentials

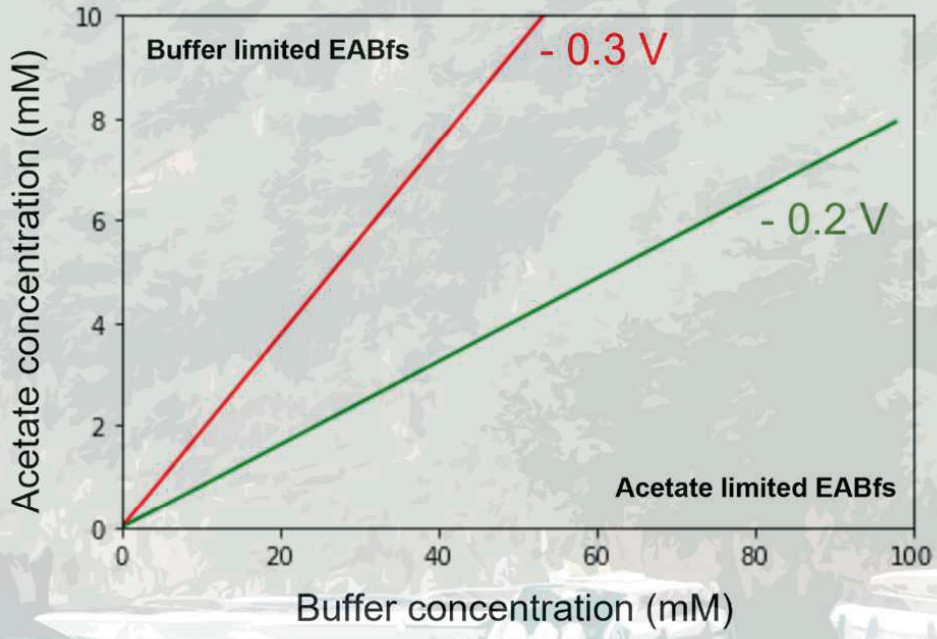

This chapter has been published as:

Pereira J, Wang G, Sleutels T, Hamelers B, ter Heijne A. Maximum *Thickness of Non-Buffer Limited Electro-Active Biofilms Decreases at Higher Anode Potentials*. Biofilm 2022;4.

Abstract

The accumulation of protons in electro-active biofilms (EABfs) has been reported as a critical parameter determining produced currents at the anode since the very beginning of the studies on Bio-electrochemical systems (BESs). Even though the knowledge gained on the influence of this parameter on the produced currents, its influence on EABfs growth is frequently overlooked. In this study, we quantified EABfs thicknesses in real-time and related them to the produced current at three buffer concentrations, two anode potentials, and two acetate concentrations. The thickest EABfs (80 μm) and higher produced currents (2.5 $A.m^{-2}$) were measured when a 50 mM buffer concentration was used. By combining the measured EABfs thicknesses with the pH in the anolyte, a simple model was developed to identify buffer limitations. Buffer limited EABfs with thicknesses of 15 and 42 μm were identified at -0.3 V vs Ag/AgCl when 10 and 50 mM buffer concentrations were used, respectively. At -0.2 V vs Ag/AgCl, the thicknesses of buffer limited EABfs decreased to 13 and 20 μm, respectively. The model also estimated buffer and acetate diffusion rates in EABfs and allowed to determine the boundary between a buffer and acetate limited EABfs. The diffusion rates reported in this study and the definition of the boundary between buffer and acetate limited EABfs provide a powerful tool to avoid limitations, leading to higher produced currents at the anode.

4.1. Introduction

Bio-electrochemical systems (BESs) combine electro-active bacteria and electrodes.[1,2] These bacteria are the catalysts and the conductive biomaterial between organic and electrical energy. When growing on an anode, these bacteria catabolize chemical compounds such as acetate molecules and generate electrical energy by using the anode as final electron acceptor.[3] Besides allowing to recover electrical energy in an external electrical circuit, the exchange of electrons with the electrode yields energy for metabolism and the growth of electro-active bacteria on the electrode surface.[4–6]

The growth of bacteria on a surface typically leads to the development of a bacterial layer, a so-called biofilm.[7] When combining electro-active bacteria and a solid electrode surface, an electro-active biofilm (EABf) is formed. The growth and thickness of EABfs on an anode depend on several parameters such as the anode material, anode potential, and substrate concentration.[8–11] EABfs being the biocatalysts between electron donor and electron acceptor, the produced current at the anode (i.e. reduction of the electron acceptor) is a measure of the activity of EABfs. However, this activity changes as thicker EABfs develop on the anode surface.[12]

When thin acetate fed EABfs grow on the anode, both a complete access to acetate (electron donor) over all the bacterial layers and a contribution of the EABf as a whole to produced current are expected.[13] However, mass transfer limitations are expected when thick EABfs develop on the anode, which results in gradients in the EABf. These gradients in the EABf can be categorized into three main parameters: 1) anode potential, 2) acetate concentration, and 3) buffer concentration.

The anode potential and the type of substrate determine the energy bacteria gain when exchanging electrons with the anode.[14] Therefore, the difference between the reduction reaction (meaning the use of the anode as final electron acceptor) and the biological oxidation of the electron donor (approximately -0.5 V vs Ag/AgCl for acetate [15]) is a measure of the available energy gain by bacteria. However, the energy gain is not homogeneous over the whole EABf thickness as the potential of the final electron acceptor decreases as the distance to the anode surface increases.[16] Therefore, due to the lower potential of the redox compounds present in the matrix of the EABfs when compared to the anode surface, the energy gain for the bacteria on the top layers of the EABf decreases. Consequently, even though the top layers of the biofilm are less likely to be deprived of electron donor, the rate of electrons transfer with the anode surface is lower, resulting in lower overall current densities. As opposed to the top layer of the EABf, bacteria present at the anode interface gain more energy by using the anode as electron acceptor but may have limited access to electron donor when the EABf grows too thick. It is therefore important to monitor and control the thickness of EABfs on the anode to circumvent the presence of these gradients and to guarantee that EABfs

activity is evenly distributed in every layer through the whole EABf thickness on an anode.

The effect of the anode potential, acetate concentration, and EABfs thickness on the produced current at the anode has recently been studied.[17] In this study, an increasing current density was observed for EABfs thicknesses up to 40 µm. For thicker EABfs, the overall produced current was constant or even decreased. In the same study, acetate limitations were identified as a reason for constant or decreasing currents, and a maximum thickness of 55 µm was found to sustain non-acetate limited EABfs when the anode potential was controlled at -0.2 V vs Ag/AgCl. Even though the relation between acetate concentration, produced current, and EABfs thickness allowed to identify maximum thicknesses that guarantee non-acetate limited EABfs at different anode potentials, the buffer concentration and eventual buffer limitations as a function of the EABfs thickness were not considered.

The effect of buffer concentration on the produced current by EABfs has thoroughly been explored, and the diffusion of protons (resulting from acetate consumption) out of EABfs has been pointed out as a bottleneck since a very early stage of the studies in BESs.[18,19] These studies emphasize the importance of buffering EABfs and repeatedly indicate that buffer limitations determine the overall activity of EABfs. However, the EABfs thicknesses at which these buffer limitations occur and how these vary as a function of other parameters such as anode potential and acetate concentrations are rarely specified.

Buffer limitation in EABfs is intrinsically related to acetate consumption. When more acetate is consumed, more electrons, as well as more protons, are generated (ratio of 1 mol of acetate to 8 mol of electrons and protons, as described in Equation 4.1).[20]

$$CH_3COO^- + 3\ H_2O \rightarrow CO_2 + HCO_3^- + 8\ H^+ + 8\ e^- \qquad \text{(Eq. 4.1)}$$

As previously explained for the acetate diffusion inside EABfs, proton accumulation in EABfs due to limited buffer diffusion inside EABfs cannot be neglected, especially when thick EABfs develop on the anode surface. As a consequence of a pour diffusion of protons out of the EABf, the local pH decreases, and an acidic environment is created. This pH drop decreases the activity of EABfs as less energy can be gained by bacteria (the potential for acetate oxidation increases about 60 mV per pH unit [21]), leading to lower produced currents. To circumvent the accumulation of protons, EABfs are typically buffered to help removing the protons out of the EABf.[22–24] In the case of phosphate buffer, the mechanism involves the penetration of hydrogen phosphate (HPO_4^{2-}) in the EABf, its reduction to phosphoric acid ($H_2PO_4^-$) taking up one proton, and the regeneration of hydrogen phosphate (the conjugate base) outside the EABf (Figure 4.1).

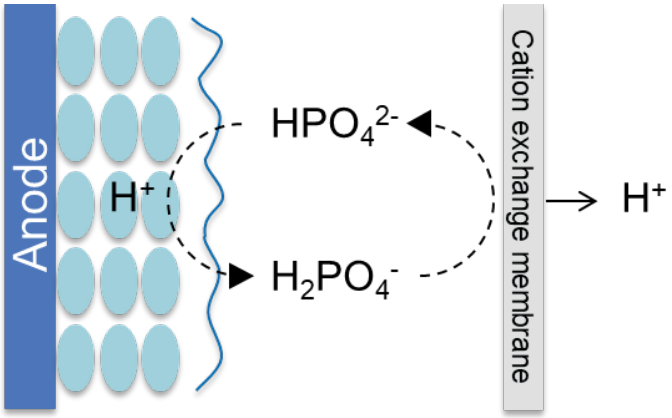

Figure 4.1. Mechanism of proton association and dissociation using phosphate buffer to remove protons out of the EABf: hydrogen phosphate diffuses in the EABf and takes up one proton forming phosphoric acid; phosphoric acid leaves the EABf and regenerates hydrogen phosphate by transporting the proton through a cation exchange membrane to the cathode.

When only considering buffer diffusion driven by concentration gradients, a higher buffering capacity (meaning more hydrogen phosphate diffusion inside the EABfs) is expected by the use of higher buffer concentrations. However, when the EABf grows thick, the rate of hydrogen phosphate diffusion inside the EABfs decreases, and protons accumulation at the bottom layers of the EABf occurs. Therefore, measuring the EABf thickness and relating it with the penetration depth of hydrogen phosphate is crucial to identify buffer limitations in EABfs. Besides, even though higher buffer gradients between the inside and outside of EABfs increase the buffer diffusion inside EABfs, the buffering needed to prevent buffer limitations in EABf also depends on the number of protons accumulated in the EABf, which is intrinsically linked to the acetate consumed. Therefore, studying the relation between buffer penetration in EABfs as a function of EABf thickness at different acetate concentrations and anode potentials allows to determine a more accurate maximum thickness of non-buffer limited EABfs and to understand how this maximum thickness changes at different conditions. Besides, integrating acetate and buffer diffusion inside EABfs at different anode potentials also allows to distinguish and define which parameter becomes limiting, and therefore, allowing to identify the boundary between acetate or buffer limited EABfs.

In this study, we aim at determining the effect of buffer concentration on the thickness and produced current by EABfs on an anode. The EABfs were buffered with three different phosphate buffer concentrations (10, 50, and 100 mM), and the EABf thickness was monitored in real-time with Optical Coherence Tomography (OCT). The occurrence of buffer limited EABfs was studied at two non-limiting acetate concentrations (5 and 10 mM) and two anode potentials (-0.2 and -0.3 V vs Ag/AgCl). By calculating the penetration depth of acetate and buffer in the EABfs, maximum

thicknesses of non-buffer limited EABfs were estimated. Besides, acetate and buffer diffusion rates in EABfs and specific acetate utilization rates were estimated at two anode potentials and used to determine the boundary between acetate and buffer limited EABfs.

4.2. Material and Methods

4.2.1. Experimental setup and reactor design

The electrochemical reactors used in this study have previously been described by Pereira et al., 2022. These reactors were assembled with two equally sized compartments (anode and cathode, each with a volume of 33 cm^3) separated with a cation exchange membrane (CEM) (Ralex CMHPP, MEGA a.s., Czech Republic). A cation exchange membrane was used to allow the regeneration of the phosphoric acid (acid conjugate of the phosphate buffer) by transporting protons to the cathode, and to avoid the diffusion of hydroxide groups from the cathode into the anode compartment. This way, the effect of the different buffer concentrations on the pH in the anode compartment could be studied. The anode electrode was built with a transparent Fluorine-doped Tin Oxide (FTO) coated glass and a layer of graphite sheet. The FTO electrode had an operating area of 22.3 cm^2, and the graphite sheet was placed in contact with the FTO electrode and used as current collector. A flat platinum/iridium coated titanium plate (Pt/IrO_2 80:20, Magneto special anodes BV, Schiedam, The Netherlands) was placed in the cathode compartment and used as counter electrode.

The anode compartment was operated in continuous mode (at a rate of 0.16 $mL.min^{-1}$ and a hydraulic retention time of 23 h) and the cathode compartment in batch mode (i.e. without inflow nor outflow). Both electrolytes, namely anolyte in the anode compartment and catholyte in the cathode compartment, were continuously recirculated at 60 $mL.min^{-1}$ (Masterflex L/S, Cole-Parmer, Barendrecht, The Netherlands). The reactors were anode potential controlled by means of a potentiostat (N-stat d-module, Ivium Technologies, Eindhoven, The Netherlands), and the current produced was recorded every minute. The anode potential was measured with an Ag/AgCl reference electrode (+0.203 V vs. Standard Hydrogen Electrode; Prosense, Oosterhout, The Netherlands) that was connected to a Haber–Luggin capillary filled with 3 M KCl and placed in the anode compartment (between the FTO electrode and the CEM). The electrochemical reactors were operated at 298 K in a temperature-controlled cabinet.

4.2.2. Inoculum and electrolyte composition

The inoculum used in these experiments was a mixed culture of active EABfs harvested from acetate-fed anodes. The influent fed into the anode compartment was adapted from the DSMZ culture medium 141 and it constituted of ($g.L^{-1}$): 0.41 and 0.82 $NaCH_3COO$, 0.1 $MgSO_4.7H_2O$, 0.74 KCl, 0.58 NaCl, 0.28 NH_4Cl, 0.1 $CaCl_2.2H_2O$, 1 mL of trace metals mixture and 1 mL of vitamins mixture.[25] This influent was buffered with

three different phosphate buffer concentrations ($g.L^{-1}$): 1) 0.68 KH_2PO_4 and 0.87 K_2HPO_4, 2) 3.40 KH_2PO_4 and 4.35 K_2HPO_4, and 3) 6.80 KH_2PO_4 and 8.70 K_2HPO_4. To guarantee the presence of an EABf on the anode, sodium 2-bromoethanesulfonate (2-BES, 1.97 $g.L^{-1}$) was added to the influent to avoid methane formation, and the influent was continuously sparged with nitrogen (before and during the experiments) to keep anaerobic conditions in the anode compartment. The cathode compartment was filled with 50 mM phosphate buffer solution at pH 7, and it was also continuously sparged with nitrogen to avoid accumulation of hydrogen and possible transport through the CEM into the anode. Even though the different phosphate buffer concentrations used in the anolyte and catholyte, no significant buffer leakages over the CEM were measured.

4.2.3. Experimental strategy

This study aimed at understanding the influence of buffer concentration on the performance and growth of EABfs on an FTO electrode. Each experimental run lasted at least 7 days and all the conditions were tested in duplicate. This dataset contains 128 data points, and all of these are presented to allow depicting trends and to provide the modelling with more information. The anode potentials (-0.2 and -0.3 V vs Ag/AgCl) were chosen based on the results previously reported by Pereira et al., 2022 and aimed at providing enough energy for the development of a wide range of EABfs thicknesses on the FTO electrode (and to be in the range of reasonable voltage efficiencies when operating the system as a Microbial Fuel Cell). The non-limiting acetate concentrations (5 and 10 mM) were chosen to allow EABf growth and to avoid acetate limited EABfs at a very thin range of thicknesses. Therefore, by allowing the growth of a wide range of EABfs thicknesses and providing non-limited acetate concentration, the study on the effect of the buffer concentration was facilitated.

In total, 12 experimental conditions were tested (two anode potentials, two acetate concentrations, and three buffer concentrations) in duplicate. All 24 experiments are grouped by anode potential in the figures presented in the Result and Discussion section. For each experiment, samples were taken every two or three days after a positive current was observed. Thus, 24 EABfs were grown, and their thicknesses were measured over time. Since the focus of the study was to understand buffer limitations in EABfs, the time variable was not included in the axis of the figures presented in the Result and Discussion section.

4.2.4. Acetate consumption, anolyte pH, and in-situ monitoring of EABfs thickness

Samples from the anolyte were taken every two or three days throughout each experiment and analyzed to monitor the acetate concentration and pH. The anolyte was initially filtered through a 0.45 μm pore-size filter (EMD Millipore SLFH025NS, Barendrecht, The Netherlands) and the acetate concentration was measured using Ultra-High-Performance Liquid Chromatography (UHPLC) (300x7.8 mm Phenomenex

Rezex Organic Acid H+ column, Dionex ultimate 3000RS, Thermo Fisher Scientific, The Netherlands). The same sample has used to measure the anolyte pH with a pH electrode (InLab Expert Pro-ISM, Mettler Toledo, USA). The acetate consumed by each EABf ($Ac_{consumed}$, mol) was calculated as expressed in Equation 4.2, in which Ac_{in} (mM) is the acetate concentration in the influent (measured as previously described), Ac_{out} (mM) is the acetate concentration in the anolyte, *flow* is the flowrate (mL.min^{-1}) and Δt (min) is the time between samples.

$$Ac_{consumed} = (Ac_{in} - Ac_{out}) \times flow \times \Delta t \quad \text{(Eq. 4.2)}$$

The monitoring of the thickness of EABfs over time was performed with OCT. For this purpose, the reactors were equipped with Quick-Coupler valves (Swagelok SS-QC4-D-400, USA) to avoid oxygen penetration in the reactors when hydraulically disconnected for the sampling in the OCT. The methodology used here to monitor the growth of EABfs in real time on the FTO electrode has previously been reported.[26] OCT is a visualization technique that allows a non-invasive measurement of biofilm thickness over time. By using near infrared light and by analysing its scattering, this technique allows imaging biofilm amount and morphology in a micrometer resolution. Briefly, a truthful imaging of the amount of the EABf was obtained by evenly scanning the FTO electrode (in 54 scanning spots) in a procedure that took approximately 45 minutes. Besides allowing an accurate imaging of EABfs, this duration resulted in no significant changes in the produced current nor acetate concentration in the anolyte before and after sampling in the OCT. The OCT scans were the input for a MATLAB script that isolated and counted the number of pixels representing EABf. These number of pixels were then converted to biomass weight (mg COD) using the calibration line reported.[26] The thickness of the EABfs was calculated by dividing the average volume of each EABf by the area of the electrode (22.3 cm^2). Given the different anode potentials and acetate concentrations tested here when compared to the conditions previously described by Molenaar et al., 2018, the applicability of the reported calibration line for these experiments was confirmed by measuring the COD of the EABfs on the last day of the experiments. The sampling in the OCT was performed after the anolyte samples to measure the acetate concentration and the anolyte pH were taken (therefore, with the same sampling frequency of two or three days).

4.2.5. Identification of buffer limited EABfs using real time monitoring of EABf thickness and anolyte pH

The accumulation of protons derived from acetate consumption results in decreasing pHs inside EABfs and decreasing produced currents at the anode. The higher the buffer concentration in the anolyte, the higher diffusion of buffer inside the EABf inner layers, and the more efficient diffusion of protons out of the EABfs. A basic model was developed to identify buffer limitations in EABfs by calculating the penetration depth of buffer in EABfs. The penetration depth was calculated using Fick's law (Equation 4.3),

where L_{buffer} is the buffer penetration depth (m), D_{buffer} is the diffusion of buffer (hydrogen phosphate) in the biofilm ($m^2.s^{-1}$), HPO_4^{2-} is the concentration of hydrogen phosphate in the anolyte (mol equivalent $Ac.m^{-3}$) and, k_0 is the specific acetate utilization rate (mol $Ac.m^{-3}.s^{-1}$).

$$L_{buffer} = \sqrt{[(2 \times D_{buffer} \times HPO_4^{2-})/k_0]} \quad \text{(Eq. 4.3)}$$

The concentration of hydrogen phosphate in the anolyte was chosen to calculate the penetration of buffer inside the EABf as this is the conjugate base that is available to take up one proton and diffuse it out of the EABf. However, the concentration of the hydrogen phosphate in the anolyte is not always equal to the initial concentration added to the influent. The decrease in the available hydrogen phosphate in the anolyte is related to an incomplete regeneration of the hydrogen phosphate (exchange of protons by the phosphoric acid at the CEM), that could be related to a favored transport of other cations through the CEM over protons, or to a pour diffusion of phosphoric acid out of the EABf (however, the diffusion of phosphoric acid is commonly reported to be higher than the diffusion of hydrogen phosphate).[18] As a consequence, the ratio between phosphoric acid and hydrogen phosphate in the anolyte increases, which leads to a decrease in the anolyte pH. Therefore, the concentration of the available hydrogen phosphate based on the anolyte pH was used for a more accurate calculation of the buffer penetration depth in the EABf. This concentration was calculated as described in Equation 4.4, in which HPO_4^{2-} is the concentration of hydrogen phosphate in the anolyte (mol equivalent $Ac.m^{-3}$), *anolyte pH* is the measured anolyte pH, *pKa* (7.2) is the pH of the proton dissociation from phosphoric acid to hydrogen phosphate, *Buffer* ($mol.m^{-3}$) is the total buffer concentration added in the influent (both the acid and base conjugates), and *8* is the number of protons generated per mol of acetate consumed.

$$HPO_4^{2-} = (10^{\,anolyte\,pH\,-\,pKa})/\,(1+10^{\,anolyte\,pH\,-\,pKa}) \times Buffer/8 \quad \text{(Eq. 4.4)}$$

Even though the acetate concentrations used in this study aimed at preventing acetate limitations, Fick's law was also used to calculate the penetration depth of acetate inside the EABfs and to compare it to the buffer penetration depth. The acetate penetration depth, $L_{acetate}$ (m) was calculated using Equation 4.5, in which $D_{acetate}$ is the diffusion of acetate in the biofilm ($m^2.s^{-1}$), and Ac_{out} is the concentration of acetate in the anolyte (mol $Ac.m^{-3}$).

$$L_{acetate} = \sqrt{[(2 \times D_{acetate} \times Ac_{out})/k_0]} \quad \text{(Eq. 4.5)}$$

Three inputs were used for the model: anolyte pH (to calculate buffer penetration depths), acetate concentration in the anolyte (to calculate acetate penetration depths), and the measured EABfs thicknesses. By using these data, the model estimated acetate and buffer diffusion rates, and specific acetate utilization rate. The specific acetate utilization rate was used to calculate an estimated current density based on the minimum non-limited EABf thickness as described in Equation 4.6. In this equation,

$j_{estimated}$ represents the estimated current density (mol Ac.m^{-2}.s^{-1}) and $L_{minimum}$ is the minimum EABf thickness, which is the lowest thickness when comparing the calculated buffer penetration depth, acetate penetration depth, and the measured EABf thickness.

$$j_{estimated} = L_{minimum} \times k_0 \quad \text{(Eq. 4.6)}$$

The calculation of the estimated current density as described above assumes the presence of a fully EABf on the FTO electrode. This is proven by the high range of Coulombic efficiencies (above 95 %) obtained in all experimental runs and supported by the inhibition of methanogenesis (with 2-BES) and the absence of H_2 oxidation in the anode (given the continuous nitrogen sparging in the cathode compartment) (Section A, Appendices).

To merge into a single and realistic estimation of acetate and buffer diffusion rates and specific acetate utilization rates, a minimizing function was chosen to decrease the sum of squares between the estimated and measured current densities. All the 128 data points were used for the modeling approach, and the data were grouped in the two anode potentials used (-0.2 and -0.3 V vs Ag/AgCl). These two anode potentials were assumed constant over the whole measured thicknesses of the EABfs, being the eventual presence of anode potential gradients neglected in the modeling approach. For each anode potential, acetate and buffer diffusion rates and a specific acetate utilization rate are described. The script and more details on the model can be found in the Appendices (Section B).

4.3. Results and discussion

4.3.1. Decreasing anolyte pH with increasing currents indicates buffer limitations

Figure 4.2 shows the decrease in the measured anolyte pH as a function of the current density for the different buffer concentrations and anode potentials tested. The decrease in the anolyte pH was steeper for EABfs buffered with 10 mM when compared to higher buffer concentrations. This acidification of the anolyte pH to approximately 6.2, indicating a decrease in the hydrogen phosphate concentration in the anolyte, was observed at a low range of current densities (up to 0.8 A.m^{-2}).

Decreasing anolyte pHs were also observed when 50 and 100 mM buffer concentrations were used. However, these decreases were obtained at a higher range of current densities. For both 50 and 100 mM buffer concentrations, the anolyte pH fluctuated between 6.6 and 6.9 with increasing current densities up to 1.5 A.m^{-2}, and anolyte pHs of approximately 6.4 were measured when the current density further increased up to 2.5 A.m^{-2}. At this higher range of current densities, the lowest anolyte pHs were measured when 50 mM buffer concentration was used. A better buffering capacity was thus obtained when 100 mM buffer concentration was used, as the pH in the anolyte kept more stable at higher current densities.

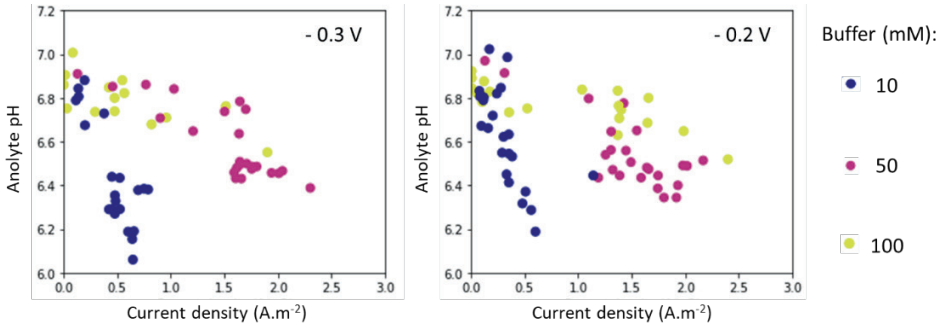

Figure 4.2. Decrease in the anolyte pH as a function of the current density for the three buffer concentrations (10 mM – blue; 50 mM – purple, 100 mM – yellow), when the anode potential was controlled at -0.3 V (left) and -0.2 V (right) vs Ag/AgCl. The steepest decrease was obtained at -0.3 V when 10 mM buffer was used, and more stable anolyte pHs were obtained when the EABfs were buffered with 50 and 100 mM.

Besides showing that current densities of 2.5 $A.m^{-2}$ were only obtained when the EABfs were buffered with 50 and 100 mM, Figure 4.2 also shows that the anode potential had very little effect on the anolyte pH. However, more positive anode potential resulted in higher current densities as it is indicated by the density of data points observed between current densities of 1.0 and 2.5 $A.m^{-2}$ at -0.2 V. The range of current densities obtained and the higher current densities with increasing anode potential are in accordance with previously reported works with EABfs on a flat FTO electrode.[17,26,27]

For all the buffer concentrations tested, the observed decrease in anolyte pH as the current density increased indicates an insufficient buffering of the EABfs. However, based on the range of current densities obtained in this study, the anolyte pH would decrease down to 3 - 4 if no buffer was present in the anolyte (Equation 4.C1, Appendices). The difference between the measured anolyte pH and the estimated anolyte pH in the absence of buffer and the decreasing anolyte pHs with increasing current densities show that EABfs were partially buffered, suggesting buffer limitations.

4.3.2. Thickest EABfs were measured when a buffer concentration of 50 mM was used

By monitoring the thickness of EABfs in real time with OCT, the effect of the buffer concentration and the anolyte pH on the growth of EABfs can be assessed. Overall, the anolyte pH decreases with increasing EABf thicknesses (Figure 4.3). A maximum EABf thickness of 78 μm was measured when 50 mM buffer concentration and an anode potential of -0.2 V were used. In fact, the widest ranges of EABfs thicknesses were obtained for both applied anode potentials when 50 mM buffer concentration was used. With this buffer concentration, the anolyte pH varied between 6.6 and 6.9 for EABfs thicknesses up to approximately 20 μm (early stages of the EABf development on the anode, with increasing current densities up to 1.5 $A.m^{-2}$), and it decreased to

approximately 6.4 when EABfs grew thicker (current densities between 1.5 – 2.5 A.m^{-2}). Some anolyte pHs in the range of 6.6 and 6.9 measured when the EABfs were thicker than 20 µm can be explained by a decrease in current density and/or due to partial EABf detachment from the FTO electrode, both resulting in a slight increase in the anolyte pH. As a consequence of EABf detachment from the FTO electrode, different measured anolyte pHs are shown at a given EABf thickness. Even though equal EABf thicknesses were measured when part of a thick EABf was washed out and when the EABf was still growing on the FTO electrode, the activity (or current produced by EABf thickness) of the EABf may differ. Therefore, for the same EABf thickness, when less (or more) current is produced, less (or more) protons have to diffuse out of the EABf, resulting in a higher (or lower) anolyte pH.

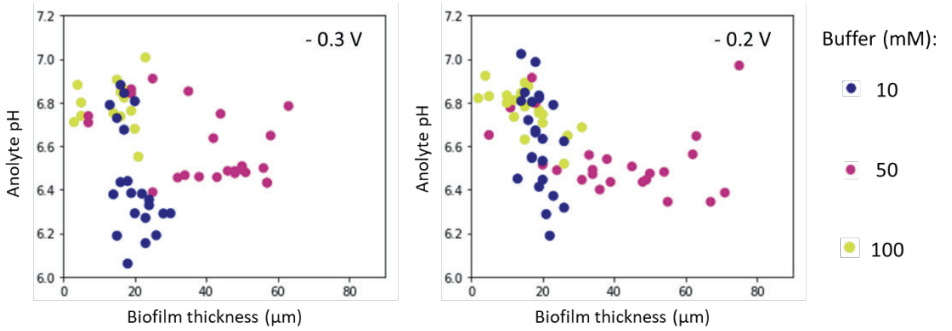

Figure 4.3. Changes in the anolyte pH as a function of the measured EABf thicknesses for the three buffer concentrations (10 mM – blue; 50 mM – purple, 100 mM – yellow), when the anode potential was controlled at -0.3 V (left) and -0.2 V (right) vs Ag/AgCl. Thickest EABfs were obtained with 50 mM buffer concentration.

The thinnest EABfs were measured when 10 and 100 mM buffer concentrations were used. For the 10 mM buffer concentration, a maximum EABf thickness of approximately 30 µm was measured at both anode potentials. The little growth of EABfs with this low buffer concentration is a consequence of the 1) low current densities (a maximum of 0.8 A.m^{-2}) and 2) steep anolyte pH decrease (insufficient buffering). For 100 mM buffer concentration, a similar range of maximum EABfs thicknesses was measured when compared to the 10 mM buffer concentration: approximately 20 µm at -0.3 V and 30 µm at -0.2 V. The thicker EABfs measured at -0.2 V corroborates with the higher current densities measured at this anode potential. Surprisingly, these EABfs did not grow thicker than the EABfs buffered with 50 mM. This little EABf growth is related to the quick decrease in current density after reaching the peak current observed for the EABfs buffered with 100 mM (Section D, Appendices). Even though this decrease to very low current densities cannot be explained with the data collected in this study, these results suggest a negative effect of high buffer concentration in the anolyte on EABfs growth. High salinity has been reported as a stressful condition that affects the physiology,

transcription, and membrane transport functions of EABf, which results in lower produced currents.[28–30] Other reasons that could explain the measured thin EABfs buffered with 100 mM are: 1) depletion of important nutrients for EABfs formation (for example calcium) due to their binding to phosphate, 2) an uneven disposition of the EABfs on the electrode that could lead to an underestimation of the EABf thickness measured with the OCT, and 3) changes in the microbial community. However, the continuous operation mode of all the reactors, the OCT scans, and the high obtained CE in this dataset exclude these other suggested reasons for the little growth of EABfs buffered with 100 mM.

Similar ranges of EABfs thicknesses have been reported in studies aiming at understating the effect of buffer on anodic EABfs. Yang et al., 2021 measured final EABfs thicknesses of 42.6, 52.2, and 60.0 μm when phosphate buffer concentrations of 5, 50, and 100 mM were used, respectively. In this study, higher buffer concentration led to an increase in extracellular polymeric substances (EPS) production and steered the microbial community of the EABf towards an EABf dominated by *Geobacter* species. In another study with *Thermincola ferriacetica* and using bicarbonate buffer, Lusk et al., 2016 reported an increase in EABfs thickness from 68 μm with 10 mM buffer concentration to EABfs thicker than 150 μm with 100 mM buffer concentration. In both works, higher current densities and thicker EABfs were reported with increasing buffer concentrations, which could be related to the more positive anode potentials (-0.08 V and +0.14 V and vs Ag/AgCl) when compared to the anode potentials used in this study (-0.3 V and -0.2 V vs Ag/AgCl).

4.3.3. Maximum thickness of a non-buffer limited EABfs decreases with increasing anode potential

Calculation of the penetration depths of acetate and buffer in EABfs enabled the determination of the ratio between the thickness of a non-limited EABfs and total measured EABf thickness. After comparing the acetate and buffer penetration depths with the measured EABf thickness with the OCT, the smallest dimension was chosen and divided by the measured EABf thickness. Thus, the ratio of non-limited EABf and total measure EABf thickness was determined, and it indicates the fraction of EABf that was not limited in acetate nor buffer and therefore, able to contribute to the produced current. Figure 4.4 depicts this ratio as a function of the measured EABf thickness on the electrode for the three buffer concentrations tested at both anode potentials.

As intended with the experimental plan, the use of non-limiting acetate concentrations resulted in the growth of EABfs that were only buffer limited (in other words, the acetate penetration depth was always bigger than the buffer penetration depth and the measured EABf thickness). Therefore, buffer limited EABfs were found when the calculated ratio was lower than 1, and when the ratio equaled 1, the buffer (and acetate) penetration depth was bigger than the measured EABf thickness. As an example, when

the ratio of non-buffer limited EABfs equals 0.6, this means that 60 % of the EABfs is non-buffer limited and the remaining 40 % of the EABfs is buffer limited. Figure 4.4 shows that buffer limitations occurred at both anode potentials when the EABfs were buffered with 10 and 50 mM buffer concentrations. Given the low range of EABfs thicknesses measured when the EABfs were buffered with 100 mM, no buffer limitations were found at this high buffer concentration (ratio of 1 for all EABfs as depicted in Fig. 4.4).

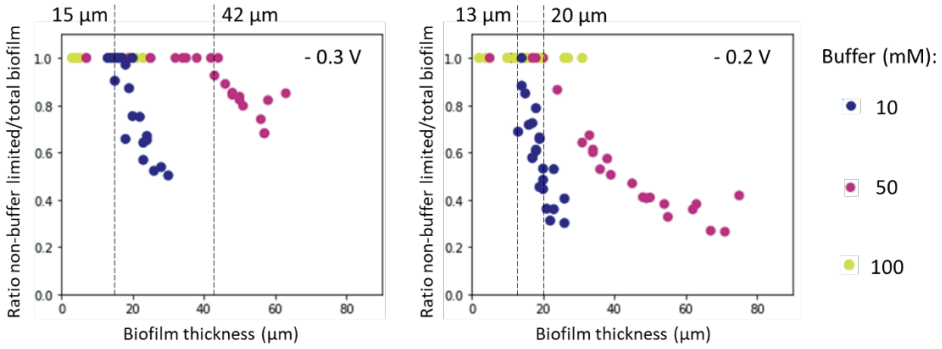

Figure 4.4. Ratio of non-buffer limited EABfs and total measured EABf on the electrode as a function of the EABf thickness measured with OCT for the three buffer concentrations (10 mM – blue; 50 mM – purple, 100 mM – yellow), when the anode potential was controlled at -0.3 V (left) and -0.2 V (right) vs Ag/AgCl.

When the buffer concentration increased from 10 to 50 mM, the thickness of non-buffer limited EABfs increased from 15 µm to 42 µm at -0.3 V and from 13 µm to 20 µm at -0.2 V. Thus, the same increase in buffer concentration resulted in a smaller increase in the maximum thickness of a non-buffer limited EABf when a more positive anode potential was used. This indicates that the buffering capacity decreases with increasing anode potential. Besides, for a given buffer concentration, the maximum thickness of a non-buffer limited EABf decreased when a more positive anode potential was used. These results are related to the higher acetate consumption (and higher produced current) at more positive anode potentials (approximately 1.4 mM of acetate were consumed at -0.3 V and 1.7 mM of acetate were consumed at -0.2 V), which makes buffer the limiting factor for thinner EABfs. When more acetate is consumed, more buffer is used to neutralize the higher concentration of generated protons in the EABf and, therefore, lower available hydrogen phosphate remains present in the anolyte. Therefore, the buffering capacity decreases (lower buffer penetration depths), resulting in ratios lower than 1 at a thinner range of EABfs thicknesses. This is further emphasized when comparing the ratios between the thickness of a non-limited EABfs and total measured EABf thickness on the FTO electrode obtained at the two anode potentials: the lowest ratio at -0.3 V is approximately 0.5 when 10 mM buffer concentration was used and 0.7 when 50 mM buffer concentration was used, whereas ratios of

approximately 0.2 were obtained at -0.2 V when both 10 and 50 mM buffer concentrations were used. This low ratio indicates that about 80 % of the measured EABf thickness on the electrode was buffer limited.

4.3.4. Determining the boundary between acetate and buffer limited EABfs

Acetate and buffer concentration in the anolyte are two intertwined parameters that can be controlled to avoid limitations in EABfs on an anode. As previously shown, higher buffer capacities are needed when the anode is poised at more positive potentials, as more acetate is consumed. This indicates that the relation between the buffer concentration needed to avoid accumulation of protons in the EABf and the acetate concentration present in the anolyte depends on the anode potential.

By estimating both the acetate and buffer diffusion rates and the specific acetate utilization rate of EABfs at two anode potentials (Table 4.1), the boundary between acetate and buffer limited EABfs can be determined.

Table 4.1. Acetate and buffer diffusion rates, and specific acetate utilization rate in EABfs when the anode potential was controlled at -0.3 V and -0.2 V vs Ag/AgCl.

Parameters	E = - 0.3 V	E = - 0.2 V
k_0 (mol Ac.m^{-3}.s^{-1})	0.05	0.08
$D_{acetate}$ (m^2.s^{-1})	2.22×10^{-10}	2.20×10^{-10}
D_{buffer} (m^2.s^{-1})	3.33×10^{-10}	1.31×10^{-10}

The estimated specific acetate utilization rate increased from 0.05 to 0.08 mol Ac.m^{-3}.s^{-1} when the anode potential increased from -0.3 to -0.2 V. The higher specific acetate utilization rate at -0.2 V confirms the higher acetate consumption and the higher buffer capacity needed at higher anode potentials. The model also estimated acetate diffusion rates of 2.22×10^{-10} m^2.s^{-1} at -0.3 V and 2.20×10^{-10} m^2.s^{-1} at -0.2 V, and buffer diffusion rates of 3.33×10^{-10} m^2.s^{-1} at -0.3 V and 1.31×10^{-10} m^2.s^{-1} at -0.2 V. The acetate diffusion rates are in the same order of magnitude as the acetate diffusion rates commonly used in modeling works with EABfs, however, these are commonly calculated based on the diffusion rate of acetate and buffer in water and adjusted to diffusion rates in EABfs using empiric coefficients.[17,19,32–34] Given the identified buffer limitations in the EABfs studied in this work, the modelling approach was reproduced with the dataset previously reported by Pereira et al., 2022, only considering the EABfs that were not buffer limited (these EABfs were buffered with 50 mM, and no buffer limitations were identified, for both experiments at -0.2 and -0.3 V, when the acetate concentration in the anolyte was lower than 6.6 mM). The estimated buffer diffusion rates with the non-buffer limited EABfs were very similar to the diffusion rates obtained in this study (2.47×10^{-10} m^2.s^{-1} at -0.3 V and 3.19×10^{-10} m^2.s^{-1} at -0.2 V), validating the use of the buffer

diffusion rates here reported to calculate the boundaries between acetate and buffer limitations in EABfs.

The boundary between acetate and buffer limitations in EABfs was calculated using Fick's law and the acetate and buffer diffusion rates estimated in this study. The acetate and buffer concentrations in the anolyte were derived from Fick's law considering a range of minimum penetration depths ($L_{minimum}$) up to 100 µm. This range was chosen to result in an acetate concentration of 10 mM and a buffer concentration of 100 mM in the anolyte, matching the conditions used in the study. Figure 4.5 shows the range of conditions under which EABfs are acetate and buffer limited when the anode potential is controlled at -0.2 and -0.3 V. The boundaries defined for -0.3 and -0.2 V divide the conditions under which EABfs are prompt to be buffer (above boundary) or acetate (below boundary) limited.

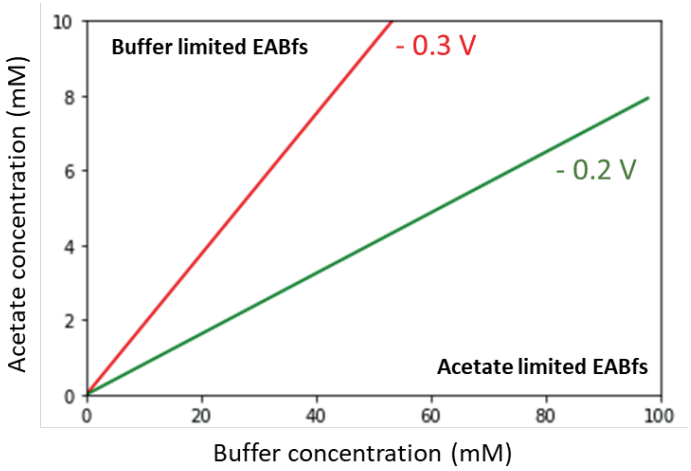

Figure 4.5. Definition of the boundaries between acetate and buffer limited EABfs when the anode potential is controlled at -0.3 V (red) and -0.2 V (green) vs Ag/AgCl. Combination of acetate and buffer concentrations above the boundary leads to buffer limited EABfs, and below the boundary leads to acetate limited EABfs.

The slopes of the two boundaries indicate that the buffer concentration should be approximately 5 times higher than the acetate concentration when the anode is controlled at -0.3 V, and approximately 12 times when the anode potential is increased to -0.2 V. These ratios of buffer and acetate emphasize that, when acetate consumption is bio-catalyzed in an EABf, the stochiometric relation between acetate and protons (Eq. 4.1) should also consider diffusion rates of acetate and buffer.

It is important to note that the defined boundaries only consider acetate and buffer limitations, leaving out EABfs thicknesses on the anode. Too little EABf growth on an electrode can also limit the current density. These "biomass" limited EABfs can occur

throughout the whole range of acetate and buffer concentrations shown in the axis of Fig. 4.5 (with their highest frequency of occurrence expected to be located at the highest range of buffer and acetate concentrations) (Section E, Appendices). Besides their thickness, other parameters such as the composition of the extracellular polymeric matrix, cell density, and the morphology of EABfs are also very important as different EABfs structures and compositions could potentially change the acetate and buffer concentrations under which limitations occur. Nevertheless, from an industrial point of view, these boundaries are an important tool to control and to increase the energy recovered with these BESs, by showing the buffer concentration required as a function of the acetate concentration present in a real wastewater stream. Finally, both from a performance and from a research point of view, considering the diffusion of substrate and products in relation to EABf thickness could also bring valuable information to increase the performance of cathodic EABfs.

4.4. Conclusion

Real-time measurement of EABfs thicknesses is of key importance to understand how EABfs respond to provided operating conditions. As shown in this study, thicker EABfs do not always produce higher currents at the anode, as thick EABfs are more prompt to run into limitations. Therefore, determining the maximum thicknesses of non-limited EABfs, and controlling the thicknesses of EABfs on the anode up to the determined maximum thicknesses, is crucial to prevent limitations and to guarantee high produced currents. Moreover, identifying the limiting factor at a wide range of conditions is also a very important tool to control limitations towards higher produced currents.

4.5. Acknowledgements

This work was performed in the cooperation framework of Wetsus, European Centre of Excellence for Sustainable Water Technology (www. wetsus.nl). Wetsus is co-funded by the Dutch Ministry of Economic Affairs and Ministry of Infrastructure and Environment, the European Union Regional Development Fund, the Province of Fryslân, and the Northern Netherlands Provinces. The authors thank the participants of the research theme “Resource Recovery” for the fruitful discussions and their financial support. This publication is part of the project “Understanding and controlling electron flows in electro-active biofilms” with project number 17516 of the research program Vidi which is (partly) financed by the Dutch Research Council (NWO).

4.6. References

1. Logan, B. E., Rossi, R., Ragab, A. & Saikaly, P. E. Electroactive microorganisms in bioelectrochemical systems. *Nat. Rev. Microbiol.* **17**, 307–319 (2019).

2. Lahiri, D., Nag, M., Ghosh, S., Dey, A. & Ray, R. R. Electroactive biofilm and electron transfer in MES. in *Scaling Up of Microbial Electrochemical Systems* 87–101 (Elsevier, 2022). doi:10.1016/b978-0-323-90765-1.00006-x.

3. Thapa, B. Sen *et al.* Overview of electroactive microorganisms and electron transfer mechanisms in microbial electrochemistry. *Bioresour. Technol.* **347**, 126579 (2022).

4. Yang, G. *et al.* Anode potentials regulate Geobacter biofilms: New insights from the composition and spatial structure of extracellular polymeric substances. *Water Res.* **159**, 294–301 (2019).

5. Aelterman, P., Freguia, S., Keller, J., Verstraete, W. & Rabaey, K. The anode potential regulates bacterial activity in microbial fuel cells. *Appl. Microbiol. Biotechnol.* **78**, 409–418 (2008).

6. Scarabotti, F., Rago, L., Bühler, K. & Harnisch, F. The electrode potential determines the yield coefficients of early-stage Geobacter sulfurreducens biofilm anodes. *Bioelectrochemistry* **140**, 107752 (2021).

7. Azeredo, J. *et al.* Critical review on biofilm methods. *Crit. Rev. Microbiol.* **43**, 313–351 (2017).

8. Pinto, D., Coradin, T. & Laberty-Robert, C. Effect of anode polarization on biofilm formation and electron transfer in Shewanella oneidensis/graphite felt microbial fuel cells. *Bioelectrochemistry* **120**, 1–9 (2018).

9. Pereira, J. *et al.* The effect of intermittent anode potential regimes on the morphology and extracellular matrix composition of electro-active bacteria. *Biofilm* **4**, 100064 (2021).

10. Hindatu, Y., Annuar, M. S. M. & Gumel, A. M. Mini-review: Anode modification for improved performance of microbial fuel cell. *Renew. Sustain. Energy Rev.* **73**, 236–248 (2017).

11. Lee, H. S., Torres, Ć. I. & Rittmann, B. E. Effects of substrate diffusion and anode potential on kinetic parameters for anode-respiring bacteria. *Environ. Sci. Technol.* **43**, 7571–7577 (2009).

12. Sun, D. *et al.* The effect of biofilm thickness on electrochemical activity of Geobacter sulfurreducens. *Int. J. Hydrogen Energy* **41**, 16523–16528 (2016).

13. Chadwick, G. L., Otero, F. J., Gralnick, J. A., Bond, D. R. & Orphan, V. J. NanoSIMS imaging reveals metabolic stratification within current-producing biofilms. *Proc. Natl. Acad. Sci. U. S. A.* **116**, 20716–20724 (2019).

14. Dennis, P. G. *et al.* Anode potential influences the structure and function of anodic electrode and electrolyte-associated microbiomes. *Sci. Rep.* **6**, 1–11 (2016).

15. Logan, B. E. *et al.* Microbial fuel cells: Methodology and technology. *Environmental Science and Technology* vol. 40 5181–5192 (2006).

16. Korth, B., Rosa, L. F. M., Harnisch, F. & Picioreanu, C. A framework for modeling electroactive microbial biofilms performing direct electron transfer. *Bioelectrochemistry* **106**, 194–206 (2015).

17. Pereira, J. *et al.* Real-time monitoring of biofilm thickness allows for determination of acetate limitations in bio-anodes. *Bioresour. Technol. Reports* **18**, 101028 (2022).

18. Torres, C. I., Marcus, A. K. & Rittmann, B. E. Proton transport inside the biofilm limits electrical current generation by anode-respiring bacteria. *Biotechnol. Bioeng.* **100**, 872–881 (2008).

19. Marcus, A. K., Torres, C. I. & Rittmann, B. E. Conduction-Based Modeling of the Biofilm Anode of a Microbial Fuel Cell. *Biotechnol. Bioeng.* **98**, 1171–1182 (2007).

20. Sleutels, T., Molenaar, S., Heijne, A. & Buisman, C. Low Substrate Loading Limits Methanogenesis and Leads to High Coulombic Efficiency in Bioelectrochemical Systems. *Microorganisms* **4**, 7 (2016).

21. Jung, S., Mench, M. M. & Regan, J. M. Impedance characteristics and polarization behavior of a microbial fuel cell in response to short-term changes in medium pH. *Environ. Sci. Technol.* **45**, 9069–9074 (2011).

22. ter Heijne, A. *et al.* Analysis of bio-anode performance through electrochemical impedance spectroscopy. *Bioelectrochemistry* **106**, 64–72 (2015).

23. Dhar, B. R. & Lee, H. S. Evaluation of limiting factors for current density in microbial electrochemical cells (MXCs) treating domestic wastewater. *Biotechnol. Reports* **4**, 80–85 (2014).

24. Lusk, B. G., Parameswaran, P., Popat, S. C., Rittmann, B. E. & Torres, C. I. The effect of pH and buffer concentration on anode biofilms of Thermincola ferriacetica. *Bioelectrochemistry* **112**, 47–52 (2016).

25. DSMZ. 141. Methanogenium Medium (H2/CO2). 6–8 https://www.dsmz.de/microorgan- isms/medium/pdf/DSMZ_Medium141.pdf (2017).

26. Molenaar, S. D. *et al.* In situ biofilm quantification in bioelectrochemical systems by using optical coherence tomography. *ChemSusChem* **11**, 2171–2178 (2018).

27. Heijne, A. ter, Liu, D., Sulonen, M., Sleutels, T. & Fabregat-Santiago, F. Quantification of bio-anode capacitance in bioelectrochemical systems using Electrochemical Impedance Spectroscopy. *J. Power Sources* **400**, 533–538 (2018).

28. Rousseau, R., Dominguez-Benetton, X., Délia, M. L. & Bergel, A. Microbial bioanodes with high salinity tolerance for microbial fuel cells and microbial electrolysis cells. *Electrochem. commun.* **33**, 1–4 (2013).

29. Lefebvre, O., Tan, Z., Kharkwal, S. & Ng, H. Y. Effect of increasing anodic NaCl concentration on microbial fuel cell performance. *Bioresour. Technol.* **112**, 336–340 (2012).

30. Wang, J. *et al.* Effect of salinity on mature wastewater treatment biofilm microbial community assembly and metabolite characteristics. *Sci. Total Environ.* **711**, 134437 (2020).

31. Yang, G., Mai, Q., Zhuang, Z. & Zhuang, L. Buffer capacity regulates the stratification of anode-respiring biofilm during brewery wastewater treatment. *Environ. Res.* **201**, 111572 (2021).

32. Babauta, J. T. & Beyenal, H. Mass transfer studies of Geobacter sulfurreducens biofilms on rotating disk electrodes. *Biotechnol. Bioeng.* **111**, 285–294 (2014).

33. Renslow, R. S., Babauta, J. T., Majors, P. D. & Beyenal, H. Diffusion in biofilms respiring on electrodes. *Energy Environ. Sci.* **6**, 595–607 (2013).

34. Bonanni, P. S., Bradley, D. F., Schrott, G. D. & Busalmen, J. P. Limitations for current production in Geobacter sulfurreducens biofilms. *ChemSusChem* **6**, 711–720 (2013).

4.7. Appendices

A. High Coulombic efficiencies proving the presence of a EABfs on the anode

To calculate the Coulombic efficiency of the EABfs, acetate concentration in the anolyte was calculated based on the produced current. Equation 4.A1 was used to calculate the acetate concentration in the anolyte, $Ac_{out,equi}$ (mM acetate), in which Ac_{in} is the measured acetate concentration in the influent (mM acetate), i is the measured current (C.s^{-1}), $flow$ (0.16 mL.min^{-1}) is the flowrate, F is the Faraday constant (96485 Coulombs.mol$_{electrons}^{-1}$) and n (8 mol$_{electrons}$.mol$_{acetate}^{-1}$) is the number of moles of electrons produced per mole of acetate consumed.

$$Ac_{out,equi} = Ac_{in} - i/flow/(F \times n) \quad \text{(Eq. 4.A1)}$$

The Coulombic efficiency (CE) can be determined by the ratio between the calculated concentration of acetate in the anolyte based on current produced, $Ac_{out,equi}$ (meaning the difference between the acetate concentration in the influent and the consumed acetate based on produced current) and the measured acetate concentration in the anolyte, Ac_{out} (Equation 4.A2). Figure 4.A1 shows that the Coulombic efficiency was close to 100 % in all experiments.

$$CE = Ac_{out,equi} / Ac_{out} \quad \text{(Eq. 4.A2)}$$

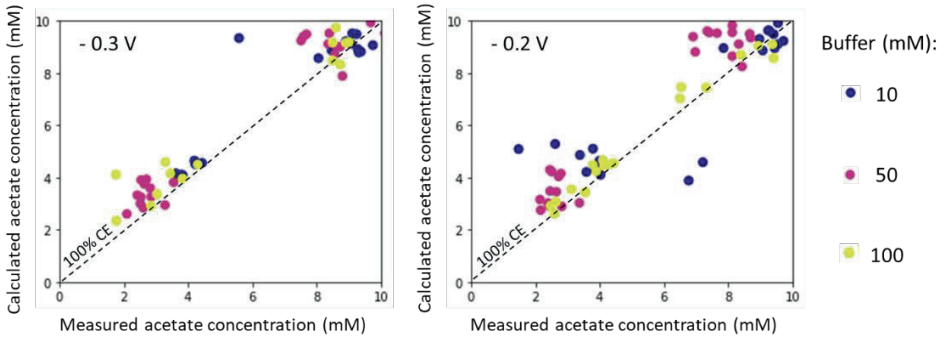

Figure 4.A1. Relation between measured and calculated acetate concentration in the anolyte for the three buffer concentrations (10 mM – blue; 50 mM – purple, 100 mM – yellow), when the anode potential was controlled at -0.3 V (left) and -0.2 V (right) vs Ag/AgCl.

Therefore, competitive processes in the anode such as the presence of methanogens and sulphur reducers are neglected, making this experimental setup suitable to study EABfs.

B. Script used for the modelling approach

Python was used to quantify buffer and acetate penetration depths and to estimate buffer and acetate diffusion rates and specific acetate utilization rates in EABfs. Some lines of the script used to translate the equations mentioned in the Material and Method section into Python language are discriminated below. The estimated specific acetate

utilization rate, acetate diffusion, and buffer diffusion are coded as par[0], par[1], and par[2], respectively.

*"data_pd[HPO_4^{2-} concentration']=10**(data_pd['anolyte pH']-7.2)/(1+10**(data_pd['anolyte pH']-7.2))*data_pd['Buffer concentration (mM)']/8*

*data_pd['Buffer penetration depth'] = (2*np.abs(par[2])*data_pd[' HPO_4^{2-} concentration"]).apply(np.sqrt)*

*data_pd['Acetate penetration depth'] = (2*np.abs(par[1])*data_pd['Acetate concentration (mM)']).apply(np.sqrt)*

data_pd['$L_{minimum}$']=(data_pd[['Buffer penetration depth','Biofilm thickness (μm)', 'Acetate penetration depth']].min(axis=1))

*data_pd['Estimated current density']=data_pd['$L_{minimum}$']*par[0]*

data_pd['Ratio non-buffer limited/total biofilm']=data_pd[' $L_{minimum}$ ']/data_pd['Biofilm thickness (μm)']

*data_pd['calculation of squares']=(data_pd['Measured current density']-data_pd['Estimated current density'])**2"*

return data_pd['calculation of squares'].sum()"

Nelder-Mead was used as the method to minimize the variation between estimated and measured current. Equation 4.B1 was used to calculate the "*correlation factor*", in which *ssq mode* is the mode of the sum of squares and *ssq avg* is the average of the sum of squares. A correlation of approximately 0.4 was obtained for each group of data divided by the applied anode potential.

$$correlation\ factor = 1 - ssq\ mode / ssq\ avg \quad \text{(Eq. 4.B1)}$$

C. Determining the anolyte pH based on produced current in a non-buffered anode

Eq. 4.C1 shows the calculation of the anolyte pH based on the current produced (electrons produced from acetate oxidation, which equals the number of protons produced) in case no buffer was present in the influent. $pH_{no\ buffer}$ is the expected anolyte pH in the absence of buffer in the influent, j is the measured current density ($A.m^{-2}$), *electrode area* is the operating area of the electrode (0.0023 m^2), *flow* is the flowrate (0.16 $mL.min^{-1}$ × 0.001 $L.mL^{-1}$ × 1/60 $min.s^{-1}$), and F is the Faraday constant (96485 $Coulombs.mol_{electrons}^{-1}$).

$$pH_{no\ buffer} = -\log_{10}(j \times electrode\ area / flow / F) \quad \text{(Eq. 4.C1)}$$

D. The effect of buffer concentration on the produced current profiles

Figure 4.D1 shows the produced current profile and the EABfs growth for all the experiments performed in this study. We observed an initial increase in produced current that was followed by a constant and stable current produced over time (Figure 4.D1.a). For experiments with 100 mM buffer concentration, the produced current decreased after the peak and stabilized at a value lower than the peak. The amount of biomass present on the electrode is shown in Figure 4.D1.b.

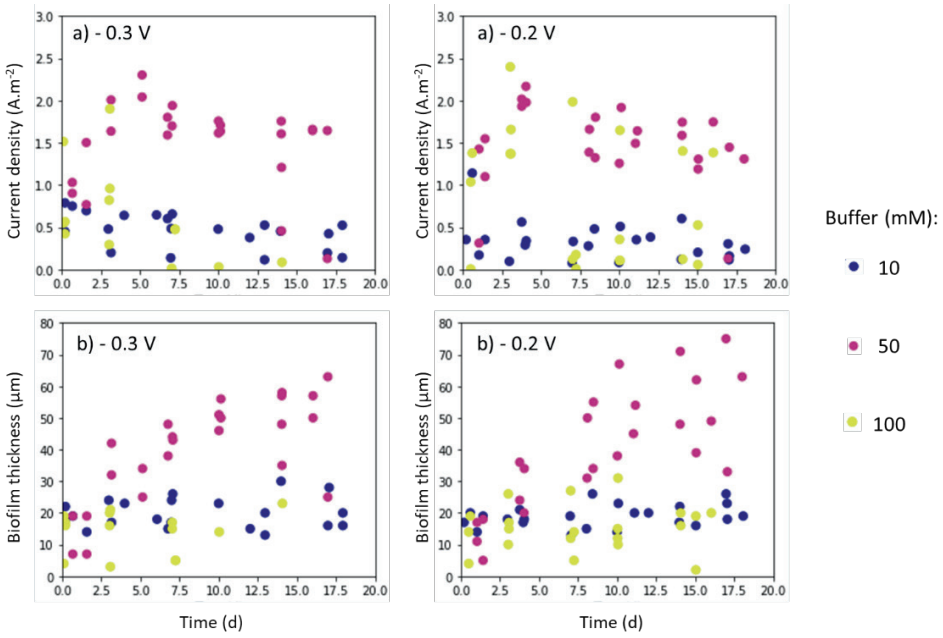

Figure 4.D1. a) Current density and b) measured EABf thickness on the FTO electrode as a function of time for the three buffer concentrations (10 mM – blue; 50 mM – purple, 100 mM – yellow), when the anode potential was controlled at -0.3 V (left) and -0.2 V (right) vs Ag/AgCl.

Even though current profiles were different for each experiment, an increase in biomass with time was observed for the period evaluated in all experiments. This shows that while current was produced, even when current decreased, biomass thickness kept increasing on the FTO electrode.

E. Determining the boundary between acetate and buffer limited EABfs

Figure 4.E1 shows the boundaries between buffer and acetate limited EABfs and the distribution of the experimental data. In this Figure, "biomass" limited EABfs obtained in the experiments performed in this study are also discriminated (in purple).

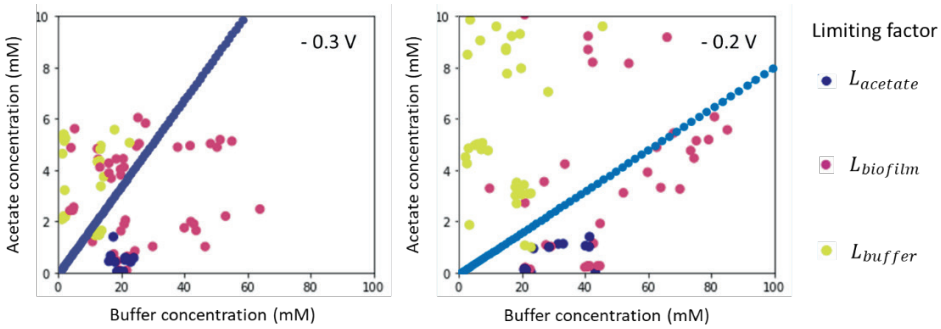

Figure 4.E1. Boundary between acetate and buffer limited EABfs and distribution of the experimental data when the anode potential was controlled at -0.3 V (left) and -0.2 V (right) vs Ag/AgCl. Acetate limited EABfs are colored in blue, buffer limited EABfs are colored in yellow, and "biomass" limited EABfs are colored in purple.

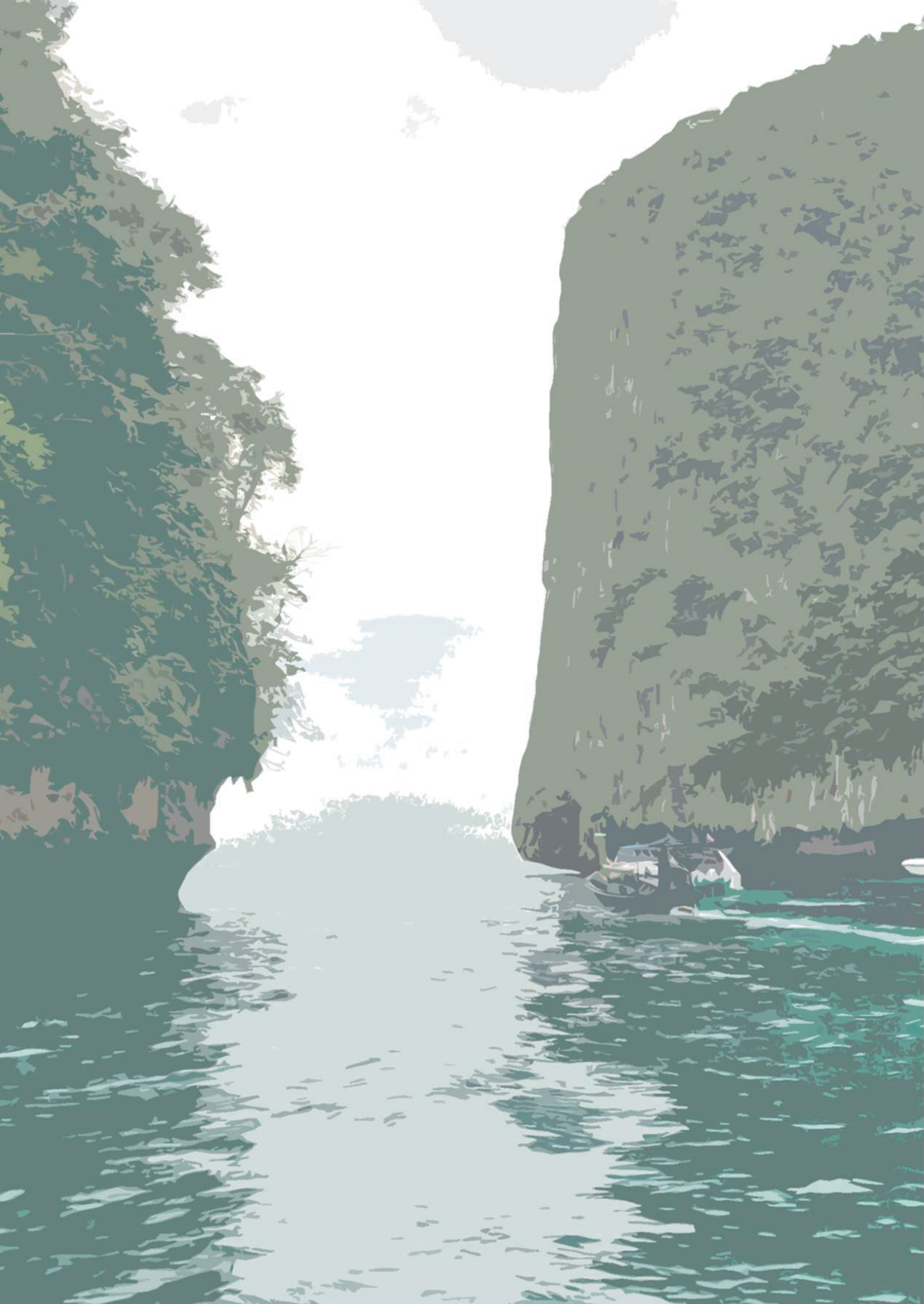

5 The effect of intermittent anode potential regimes on the morphology and extracellular matrix composition of electro-active bacteria

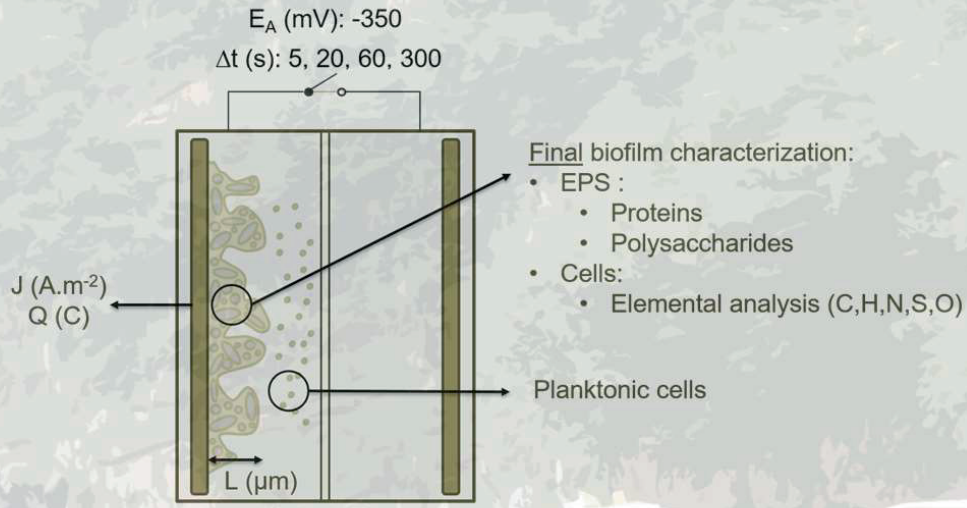

This chapter has been published as:

Pereira J, Mediayati Y, van Veelen HPJ, Temmink H, Sleutels T, Hamelers B, et al. *The effect of intermittent anode potential regimes on the morphology and extracellular matrix composition of electro-active bacteria*. Biofilm 2021;4:100064.

Abstract

Electro-active bacteria (EAB) can form biofilms on an anode (so-called bioanodes), and use the electrode as electron acceptor for oxidation of organics in wastewater. So far, bioanodes have mainly been investigated under a continuous anode potential, but intermittent anode potential has resulted in higher currents and different biofilm morphologies. However, little is known about how intermittent potential influences the electron balance in the anode compartment. In this study, we investigated electron balances of bioanodes at intermittent anode potential regimes. We used a transparent non-capacitive electrode that also allowed for in-situ quantification of the EAB using Optical Coherence Tomography (OCT). We observed comparable current densities between continuous and intermittent bioanodes, and stored charge was similar for all the applied intermittent times (5 mC). Electron balances were further investigated by quantifying Extracellular Polymeric Substances (EPS), by analyzing the elemental composition of biomass, and by quantifying biofilm and planktonic cells. For all tested conditions, a charge balance of the anode compartment showed that more electrons were diverted to planktonic cells than biofilm. Besides, 27 to 43 % of the total charge was detected as soluble EPS in intermittent bioanodes, whereas only 15 % was found as soluble EPS in continuous bioanodes. The amount of proteins in the EPS of biofilms was higher for intermittently operated bioanodes (0.21 mg COD proteins.mg COD biofilm^{-1}) than for continuous operated bioanodes (0.05 mg COD proteins.mg COD biofilm^{-1}). OCT revealed patchy morphologies for biofilms under intermittent anode potential. Overall, this study helped understanding that the use of a non-capacitive electrode and intermittent anode potential deviated electrons to other processes other than electric current at the electrode by identifying electron sinks in the anolyte and quantifying the accumulation of electrons in the form of EPS.

5.1. Introduction

Bio-electrochemical systems (BESs) are environmental biotechnologies with a wide range of applications such as wastewater treatment, nutrient recovery, chemicals synthesis, and biosensors.[1–3] The functioning of these systems relies on electro-active bacteria (EAB) that grow on an electrode and planktonic cells. The first performs direct electron transfer with the anode surface whereas the formed may contribute to electron transfer using soluble redox mediators. These microorganisms in the biofilm catalyze the degradation of organic compounds using the electrode as electron acceptor (at the anode), or they catalyze the synthesis of chemical compounds using the electrode as electron donor (at the cathode).

Bioanodes are the combination of EABs and anodes. Given their ability to combine the oxidation of organic matter with energy recovery, bioanodes form the basis for sustainable wastewater treatment technologies.[4] A key performance parameter of bioanodes is the produced current, which depends on the activity of the electro-active bacteria. The current represents the electron transfer rate to the electrode catalyzed by these EAB and depends, amongst others, on the anode potential.[5,6]

A common approach to study EAB is by poising the electrode at a continuous anode potential.[7,8] Instead of continuous anode potential, EABs can also be cultured and studied under intermittent anode potential. Intermittent anode potential regimes consist of alternating the anode potential between open cell potential (OCP) and a controlled potential (also called charge-discharge regime). Higher current densities have been reported when electro-active bacteria are grown under intermittent anode potential regimes[9,10] compared to continuous potential. Until now, studies have focused on the EAB adaptation to this intermittent anode potential regime aiming at linking biofilm composition and morphology to bioanode performance (current, charge recovered, and Coulombic efficiency).[11,12] It has been observed that the biofilm morphology on the electrode changes to a more porous structure when an intermittent potential regime is applied.[10,13] This porous structure has been suggested to result in higher current production in thick biofilms by reducing mass transfer resistances and increasing substrate availability inside the biofilm. The application of intermittent anode potential regimes has also been shown to upregulate the production of extracellular structural components present in the biofilm matrix (for example, *pili* structures and cytochromes) that are important for electron transfer within the biofilm and current production.[14–16]

The higher current and the higher recovered charge when bioanodes are operated at intermittent anode potential have also been associated with a continued oxidation of the substrate during charging periods (open cell potential).[17] During these periods, due to the absence of the electrode as final electron acceptor, it is likely that the electrons generated from substrate oxidation are stored inside the cell.[18]

Ter Heijne et al., 2020 have suggested two different storage mechanisms for these electrons that are generated at open circuit: (a) electrons are temporarily stored in redox proteins present in the cell membrane (cytochromes and flavins) and released to the electrode after repolarization and (b) electrons are taken up by the cells and accumulated in the form of intracellular storage compounds (for example in the form of polyhydroxyalkanoates) that can later be used as electron donor for bacterial growth.[19] From previous work, it is expected that longer intermittent anode potential times stimulate the formation of intracellular storage compounds.[10,19,20] Some of the compounds formed by bacteria can also be released into the extracellular matrix of the EABs.[21,22] When outside the cell membrane, these compounds are commonly called Extracellular Polymeric Substances (EPS). The synthesis of these EPS also consumes electrons, and their amount and composition typically change as a function of the conditions provided to the biofilms.[23] For example, large EPS production is commonly found in bioprocesses in which bacteria are grown at low nitrogen concentrations but non-limiting carbon concentrations (high C/N ratios).[24]

These storage processes and formation of EPS influence the electron balance in bioanodes. Determining the electron balances at bioanodes is of pivotal importance to tackle electron losses and to divert the majority of the electrons towards the electrode. Thus, electron balances are essential to identify and quantify electron consuming processes other than the desired one. Since the performance of BES relies on the EAB, including their storage processes and planktonic growth in the electron balance is key to understand their adaptation to intermittent anode potential conditions.

In this study, we aim to elucidate the effect of intermittent anode potential on bioanode performance, EAB morphology, and electron balances in the anode compartment. The EAB were grown on a Fluorine Tin Oxide (FTO) electrode and its structure and quantity were monitored in-situ using Optical Coherence Tomography (OCT). Electron balances were made based on the total charge, EPS, amount of biofilm, and number of planktonic cells. Finally, the elemental composition of the biomass was assessed.

5.2. Material and Methods

5.2.1. Experimental setup and reactor configuration

The bio-electrochemical reactor used in these experiments has previously been described by Molenaar et al. 2018. The anode compartment was composed of an anode flow channel (33 cm^3), and the anode was a transparent Fluorine-doped Tin Oxide (FTO) coated glass electrode. The flat and transparent electrode surface with an operating area of 22.3 cm^2 allowed the real-time monitoring of biofilm growth.[25] Besides, the low capacitance of this electrode allowed the study of electron storage mechanics in the biofilm rather than in the electrode. The current collector (graphite sheet) was placed in contact with the FTO electrode and was surrounding the operating area of the anode flow channel. A bipolar membrane (Ralex PEBPM, MEGA a.s., Czech Republic)

was placed between the anode and cathode compartment with the anion side oriented towards the anode and the cation side oriented towards the cathode. A bipolar membrane was used to allow migration of protons to the cathode compartment and hydroxyl groups to the anode compartment. The cathode compartment was composed of a flow channel with the same volume as the anode, and a flat platinum/iridium coated titanium plate (Pt/IrO_2 80:20, Magneto special anodes BV, Schiedam, The Netherlands) was used as counter electrode. The projected area of membrane and cathode was 22.3 cm^2.

Each anode chamber was connected to a feed and recirculation peristaltic pump (Masterflex L/S, Cole-Parmer, Barendrecht, The Netherlands). The feed was pumped at 0.16 mL/min and both anolyte and catholyte were recirculated at a rate of 60 mL/min. Considering the total volume of anolyte (220 mL), a 23 h hydraulic retention time was obtained. A potentiostat (N-stat d-module, Ivium Technologies, Eindhoven, The Netherlands) was used to poise the anode at -0.35 V vs Ag/AgCl electrode (+0.203 V vs. standard hydrogen electrode; Prosense, Oosterhout, The Netherlands). The reference electrodes were connected to the anode flow channel using Haber–Luggin capillary filled with 3 M KCl solution and positioned in between the FTO electrode and the bipolar membrane. Quick-Coupler valves (Swagelok SS-QC4-D-400, USA) were connected to the tubing of each reactor to avoid oxygen penetration into the system while reactors were disconnected for sampling in the OCT (as described in Molenaar et al. 2018). Reactor temperature was controlled in a climate chamber at 298 K.

5.2.2. Inoculum and electrolyte composition

Reactors were inoculated with a mixture of biomass collected from previous bioanodes operated with acetate as substrate. The anolyte constituted of ($g.L^{-1}$): 0.82 $NaCH_3COO$, 3.40 KH_2PO_4, 4.35 K_2HPO_4, 0.1 $MgSO_4.7H_2O$, 0.74 KCl, 0.58 NaCl, 0.28 NH_4Cl, 0.1 $CaCl_2.2H_2O$, 1 mL of trace metals mixture and 1 mL of vitamins mixture according to DSMZ culture medium 141.[26] In order to inhibit methanogenesis and only evaluate the effect of intermittent anode potential on the EAB, 1.97 $g.L^{-1}$ of $BrCH_2CH_2SO_3Na$ was also added to the medium. The anolyte inflow was continuously sparged with nitrogen before and during the experiments to maintain anaerobic conditions before being pumped into the reactor. The catholyte consisted of a 50 mM phosphate buffer solution at pH 7. Nitrogen was continuously sparged into the catholyte recirculation vessel during reactors operation to remove hydrogen.

5.2.3. Experimental design

We tested the effect of intermittent anode potential on electro-active bacteria activity, morphology, and composition. The anode potential was controlled at -0.35 V vs Ag/AgCl and open circuits were applied with a duration of 5, 20, 60, and 300 seconds. The open circuit and close circuit durations were equal, meaning that all intermittently operated reactors were operated with a duty cycle of 0.5. As a control experiment,

continuous polarization of the anode at a potential of -0.35 V vs Ag/AgCl was used. An acetate concentration of 0.82 $g.L^{-1}$ was used in the influent to feed the microorganisms with non-limiting substrate conditions. All the reactors were operated for approximately 30 days (maximum of 41 days), and each condition was tested in duplicate.

5.2.4. Analysis of the effect of intermittent potential on bioanodes

5.2.4.1. Acetate consumption

Acetate consumption was determined as the difference between the influent and effluent concentrations. After filtration through 0.45 µm pore-size filter (EMD Millipore SLFH025NS, Barendrecht, The Netherlands), acetate concentration was measured using Ultra-High-Performance Liquid Chromatography (UHPLC) (300x7.8 mm Phenomenex Rezex Organic Acid H+ column, Dionex ultimate 3000RS, Thermo Fisher Scientific, The Netherlands).[27] Samples were taken every 2 or 3 days.

5.2.4.2. Recovered charge

The recovered charge from each bioanode was calculated by the integration of the current produced over the time the anode was poised at -0.35 V vs Ag/AgCl. For the intermittent experiments, the total recovered charge from the bioanodes was calculated by adding the cumulative charge obtained at the end of a polarization cycle to the first charge data point of the following cycle. Data were recorded every second for the intermittent bioanodes in order to quantify the peak current, and every minute for the continuous bioanodes. The storage charge in the intermittent bioanodes was calculated as a difference between all the charge recovered in a discharging cycle and the charge recovered integrating the last measured current density of that cycle over the whole discharging time.

5.2.5. Bioanode growth and morphology

5.2.5.1. Visualization of biofilm growth and morphology

Biofilm growth on the bioanode was measured using Optical Coherence Tomography (OCT). The use of this visualization technique as a non-invasive method to quantify the biofilm on an electrode in real time was previously reported by Molenaar et al. 2018. After disconnecting the reactors from the system, both hydraulically and electrically, the OCT was used to scan the FTO electrode at 54 evenly distributed spots. The resulting images were processed using a MATLAB script that isolates and counts the biofilm pixels. The number of pixels was converted to biomass weight (mg COD) using the calibration line reported.[25] Given the use of different operating conditions as the ones used by Molenaar et al. 2018, COD measurements of bioanodes grown at continuous and intermittent anode potential were performed to validate the use of the reported calibration line for biofilm quantification. The data obtained fitted the calibration line. Besides the total amount of biofilm used to monitor the growth, OCT was also used to investigate the effect of intermittent anode potential on the biofilm morphology. Thus, 3D pictures (Field of View (mm) – x=2; y=2; z=0.52 and Pixel size

(μm) – x=80.00; y=7.78; z=2.05) of the biofilm structure developed on the electrode were taken throughout the experiment for each condition.

5.2.5.2. Quantification of cells in the anolyte

The amount of biomass in the anolyte was quantified using flow cytometry. Cells were stained with Sybr Green and Propidium Iodide (SGPI) (Invitrogen, Thermo Scientific, The Netherlands), and the fluorescence intensity was measured with Flow Cytometer (EasyCyte HT, Guava, The Netherlands). Phosphate buffer solution was used as negative control.

5.2.6. Final bioanode chemical characterization

5.2.6.1. Separation of cells and EPS

At the end of the experiment, the biofilm was scraped off the FTO electrode. To separate the biomass from the EPS in the biofilm, an ultrasound-based extraction was used as previously described by Yang et al. 2019. This methodology was reported as the most appropriate to perform a rigorous analysis of the EPS because of its high extraction efficiently and minimal cell lysis. Small modifications to the volumes and centrifugation forces used in the original protocol were included. Briefly, biomass was resuspended in 6 mL of 0.9 % NaCl solution and sonicated at 20 kHz for 2 min. Then, samples were horizontally shaken at 150 rpm for 10 min and sonicated again for 2 min. After centrifugation at 10000 g for 15 min, the supernatant was filtered through a 0.22 μm membrane filter (Nalgene syringe filter, Thermo Scientific, The Netherlands) and labeled as loosely bound EPS (LB EPS). The pellet was subsequently resuspended in 4 mL of 0.9 % NaCl solution, sonicated for 10 min, and centrifuged at 10000 g for 20 min. Next, the pellet was washed twice with 1 mL of 0.9 % NaCl solution. These supernatants were filtered and labelled as tightly bound EPS (TB EPS). The anolyte was also harvested at the end of the experiment, centrifuged at 10000 g for 15 min and the obtained supernatant was filtered through a 0.22 μm membrane filter. This fraction was finally labelled as soluble EPS (S EPS).

5.2.6.2. Total protein and polysaccharides content present in EPS

The EPS was further investigated for protein and polysaccharide composition. Both proteins and polysaccharides concentration were assessed using colorimetric techniques. Total protein content was quantified with the Pierce BCA protein Assay Kit (ThermoFisher) using bovine serum albumin (BSA) as standard protein. The polysaccharides content was quantified by means of the phenol-sulphuric acid method and by using glucose as standard sugar.[29] The absorbance of the protein samples was measured at 560 nm whereas the absorbance of the polysaccharides samples was measured at 490 nm (spectrophotometer Victor3 1420 Multilabel Counter, Perkin Elmer).

5.2.6.3. Elemental analysis of dry cells

The biomass component of the biofilm was assessed for the relative percentage of the main biomass building elements: C, H, N, S, and O. For an effective quantification of the relative percentage of each element in the microorganisms, the pellet obtained after EPS extraction was washed with mili-Q water to remove the salts from the EPS extraction solution. Cells were afterwards freeze dried, and, after this heat treatment, the elemental composition of the cells grown in each bioanode was assessed with the elemental analyzer (Flash Smart, Thermo Scientific, The Netherlands).

5.2.6.4. Microbial community analysis

Samples of the EABs and planktonic cells were taken at the end of the experiment, as well as the starting culture used to inoculate these reactors. DNA was extracted at the end of the experiment following the method described elsewhere.[30] Briefly, the FastDNA SPIN Kit for Soil (MP Biomedicals, Irvine, CA, USA) was used to disrupt the cell membranes and extract DNA using a binding matrix of silica. Subsequently, DNA purity was verified with Nanodrop (NanoDrop 1000 Spectrophotometer, Thermo Scientific, The Netherlands). Normalized DNA extracts (20 $ng.mL^{-1}$) and a negative extraction control were afterwards sent to MrDNA (Shallowater, TX, USA) for library preparation and amplicon sequencing. Briefly, the V4-V5 region of the 16S rRNA gene was amplified in a PCR using primers 515F[31] and 926R[32] and PCR products were pooled in equimolar proportions. Prepared libraries were then sequenced with V3 chemistry to generate 300 bp paired-end reads with an Illumina MiSeq (San Diego, Ca, USA) (detailed information can be found in Appendices). The microbial community was analyzed for the reactor operated with an intermittent time of 300 seconds and continuous anode potential. All experiments were performed in duplicate.

5.2.7. Calculations

5.2.7.1. Current density and biomass yield of intermittent and continuous bioanodes

The current produced by the bioanodes over time was recorded for each experiment. Since the shape of the current density curves was not always similar for all experiments, and given the peak currents obtained for the intermittent bioanode, a current density was calculated to allow comparison between the different operating conditions. The current density ($A.m^{-2}$) was determined by dividing the total charge recovered by the time the anode was controlled at -0.35 V vs Ag/AgCl (in seconds) and the area of the anode. Normalizing to the closed-circuit time, instead of the total time, allows a straightforward comparison between the current of intermittent and continuous anode potential regimes.

Monitoring the amount of biomass over time with OCT also allowed the calculation of biofilm yields. The biofilm yield measures the fraction of electrons derived from acetate

oxidation that was used for biomass formation in the bioanode (maintenance and overall anabolic processes). Therefore, this is expressed as the ratio between the amount of biofilm measured on the anode, *biofilm on anode (C)*, and the cumulative acetate converted, *Σ Acetate consumed (C)* (Equation 5.1).

Biofilm yield = Biofilm on anode (C) / Σ Acetate consumed (C) (Eq. 5.1)

We compared the amount of biofilm on the anode with the current density since we assume that the contribution of planktonic cells for the overall charge recovery is negligible (no direct electron transfer possible between cells and the anode). We used the biomass yields to study the effect of the anode potential regime as the growth of the biofilm on the electrode is time, current, and acetate dependent. Experimentally, we measured different biofilm thicknesses and acetate consumptions for each experiment. However, the measured thickness for biofilms under continuous and intermittent anode potentials were in the same range (for example, 16.0 μm for continuous and 16.4 μm for 20 s intermittent) and slightly more acetate was consumed by biofilms under a continuous anode potential.

5.2.7.2. Charge balance

A charge balance was calculated to identify the effect of intermittent anode potential on the distribution of charge among the electron sinks measured in the reactor. In this simplified charge balance (Equation 5.2), we assume that the electrons generated after acetate oxidation can have four different sinks: (i) the anode, measured as charge (Q), (ii) biomass growth on the electrode, $X_{biofilm}$, (iii) biomass growth/biofilm detachment as planktonic cells, $X_{planktonic}$, and (iv) soluble EPS (S, EPS) in the anolyte.

Total charge = $Q + X_{biofilm} + X_{planktonic} + S,EPS$ (Eq. 5.2)

Methane formation was not included in the balance given the addition of methanogens inhibitor in the medium, and sulphate reduction was assumed negligible since we used low sulphate concentration (0.1 mM). Oxygen penetration in the system was also monitored with an O_2 probe (Memosens COS81D, Endress+Hauser, Switzerland). A negligible rate of approximately 1 $C.day^{-1}$ (<1 % of the total charge) was lost in oxygen reduction, and no significant O_2 leakages were registered while sampling the reactors.

In order to get insight on the charge distribution in the anode, each of the electron sinks was represented as a fraction of total charge. These fractions were calculated by dividing the cumulative charge measured for each process by the total charge of all four processes. The amount of charge of planktonic cells and soluble EPS were calculated after converting these data to COD. For the planktonic growth, a factor of 2×10^{-10} mg COD.planktonic $cell^{-1}$ was used[33] and to convert the mass of polysaccharides and proteins to COD, a calculated value of 1.07 g COD.g $glucose^{-1}$ and 1.47 g COD.g BSA^{-1} were used, respectively. The COD results were later converted to Coulombs (C) using the molecular weight of O_2 (32 $g.mol^{-1}$), the moles of electrons per mole of O_2 (4), and

Faraday constant (96485 $C.mol^{-1}$). The LB and TB EPS fractions were not included in the charge balance since these are quantified in the $X_{biofilm}$ parcel. Detailed information about the calculations performed can be found in Appendices.

5.3. Results and Discussion

5.3.1. Intermittent anode potential decreased the specific activity and increased the biomass yields compared to continuous anode potential

Table 5.1 shows the current densities calculated for each condition. The current densities for the continuous bioanodes were similar to the current densities for the intermittent anode potential (1.4 ± 0.1 $A.m^{-2}$ for continuous and 1.2 ± 0.1 $A.m^{-2}$ for 20 and 60 seconds). Slightly lower current densities (≈0.7 ± 0.1 $A.m^{-2}$) were observed for 5 and 300 seconds intermittent times. At these intermittent times, after reaching a peak, the current dropped faster and stabilized at a lower value compared to 20 and 60 seconds (examples of current profiles and peak currents can be found in Figure 5.C1 and 5.C2). The presented current densities are in the same range as previously reported for studies on bioanodes using FTO as anode.[25,34]

Table 5.1. Performance analysis of the bioanodes: current density and biomass yield (results expressed as average ± standard deviation).

Anode potential regime	Current density ($A.m^{-2}$)	Biomass yield ($C_{biofilm}.C_{acetate}^{-1}$)
cont	1.4 ± 0.1	0.012 ± 0.000
5s	0.5 ± 0.2	0.009 ± 0.004
20s	1.2 ± 0.0	0.020 ± 0.001
60s	1.5 ± 0.2	0.014 ± 0.001
300s	0.9 ± 0.0	0.025 ± 0.003

In contrast to what has previously been reported,[35] we did not observe more recovered charge for intermittent operation compared to continuous operation. This may be related to the use of FTO electrodes that have a low capacitance and, therefore, do not allow electron storage in the electrode. Instead, electrons can only be stored in the biofilm or used to form EPS. This electron storage in the biofilm can be quantified from the peak currents observed in the current profiles of intermittent bioanodes. These peaks reflect the accumulation of electrons during OCP that are released to the electrode after repolarization (capacitive current). The duration of these peaks was approximately 3 seconds for all intermittent bioanodes, and the stored charge calculated from these peaks was around 5 mC for all the applied intermittent times. Even though EAB operated in intermittent mode acted as a capacitor and electrons were stored, the small amount of charge stored did not increase the overall recovered charge when compared to the EAB operated in continuous mode, as no clear differences in current density were observed.

Analysis of electron balances in the anodic compartment is crucial to understand how most electrons can be diverted towards electric current. The first electron sink that we analyzed was biofilm growth, and the combination of biofilm quantification from OCT measurements and consumed acetate allowed us to determine biofilm yields. Biofilm yields of the bioanodes at intermittent anode potential were higher compared to the continuous bioanode, except for the 5 seconds intermittent bioanode (Table 5.1). An average biomass yield of 0.02 $C_{biofilm}.C_{acetate}^{-1}$ was found for biofilms grown with intermittent times longer than 20 seconds, whereas 0.01 $C_{biofilm}.C_{acetate}^{-1}$ was found in biofilms grown with continuous anode potential. This higher yield for intermittent operation suggests that intermittent anode potential increases anabolic processes of electroactive bacteria for non-capacitive electrodes. The biomass yields are lower, but in the same order of magnitude as the yields of 0.05 and 0.02 g biomass-C per substrate-C reported by Aelterman et al. 2008 (at -0.2 V vs Ag/AgCl) and 0.04 g biomass COD per g acetate COD reported by Molenaar et al. 2018 (at the same potential used in this study).

5.3.2. More planktonic cells and more soluble EPS in bioanodes operated with intermittent anode potential

Electron balances in the anode compartment allow for analysis of the different electron sinks and designating which of these electron sinks has the largest contribution under the operational regimes. Some studies have focused on and quantified the Coulombic losses due to the presence of alternative electron acceptors on the performance of bioanodes.[36,37] In our experiments, a range in Coulombic efficiency of 30-70 % was obtained for all the bioanodes (cumulative charge recovered divided by cumulative charge generated out of acetate consumption), and no clear relation between Coulombic efficiency and operational regimes could be discerned.

To compare the electron sinks between operational regimes, we made electron balances by calculating the total charge for the four electron sinks: (i) charge recovered as electric current at the anode, (ii) biofilm, (iii) planktonic cells, and (iv) soluble EPS, and calculated the share of each sink compared to the total charge. Figure 5.1 shows the share of each process and how these shares change with the anode potential regime.

Of the four electron sinks, the charge recovered at the anode was the largest fraction for all conditions: higher than 60 % for all the bioanodes, except for 5 seconds of intermittent time. This bioanode at 5 seconds intermittent time showed lower reproducibility due to partial biofilm detachment from the anode registered in one of the replicates, introducing additional variability in current as well as the quantification of planktonic cells.

EPS produced by the bacteria partly remains part of the biofilm and was measured with OCT as biofilm volume (LB and TB EPS are measured as $X_{biofilm}$ in the charge balance). A fraction of these polymers, however, detaches from the biofilm, ending up in solution,

referred to as soluble EPS. Interestingly, the second largest electron sink was this soluble EPS: between 27 to 43 % of the charge was found as soluble EPS in reactors operated with intermittent anode potential whereas only about 15 % of the charge was found as soluble EPS for continuous potential (Figure 5.1).

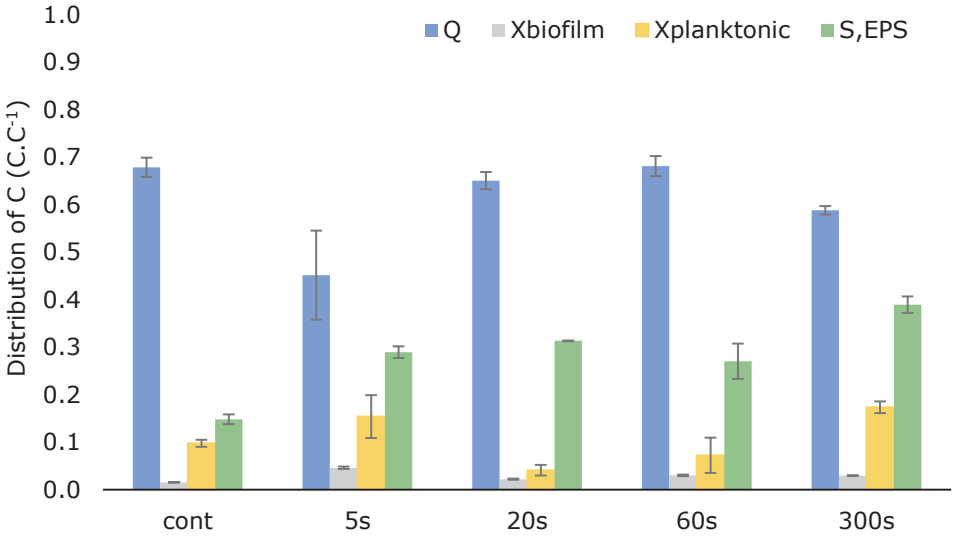

Figure 5.1. Distribution of charge in the anode compartment: each bar represents the fraction of charge measured in a process normalized by the total charge calculated in the four processes presented.

Planktonic cells were the third largest electron sink for all bioanodes, ranging from 5 to 20 % of the total charge. Even though there is not a clear trend and effect of intermittent anode potential on the growth of planktonic cells, it is evident that planktonic cells did contribute to the charge balance more than growth of cells in the biofilm for all bioanodes, since the biofilm represented only 2 to 5 % of the total charge. At all operating conditions, the growth of planktonic bacteria that are not involved in direct electron transfer with the electrode appears favored over the growth of bacteria in the biofilm. However, since the presence of alternative electron acceptors in the anolyte is negligible, the presence of planktonic cells is likely a result of detachment of bacteria from the biofilm.

5.3.3. Biofilm and planktonic cells consist of different microbial communities

Microbial community analysis for the continuous and 300 seconds reactors revealed a predominance of *Geobacter* in the biofilm communities (approximately 75 % of the taxa) and a more diverse microbial composition was found for planktonic bacteria, even though *Geobacter* was still present (less than 10 % of *Geobacter*) (Figure 5.2; Figure 5.B1). Nevertheless, the intermittent (300 seconds) and continuous anode potential did not

affect the microbial community of the biofilm nor the planktonic cells (Figure 5.2; Figure 5.B1).

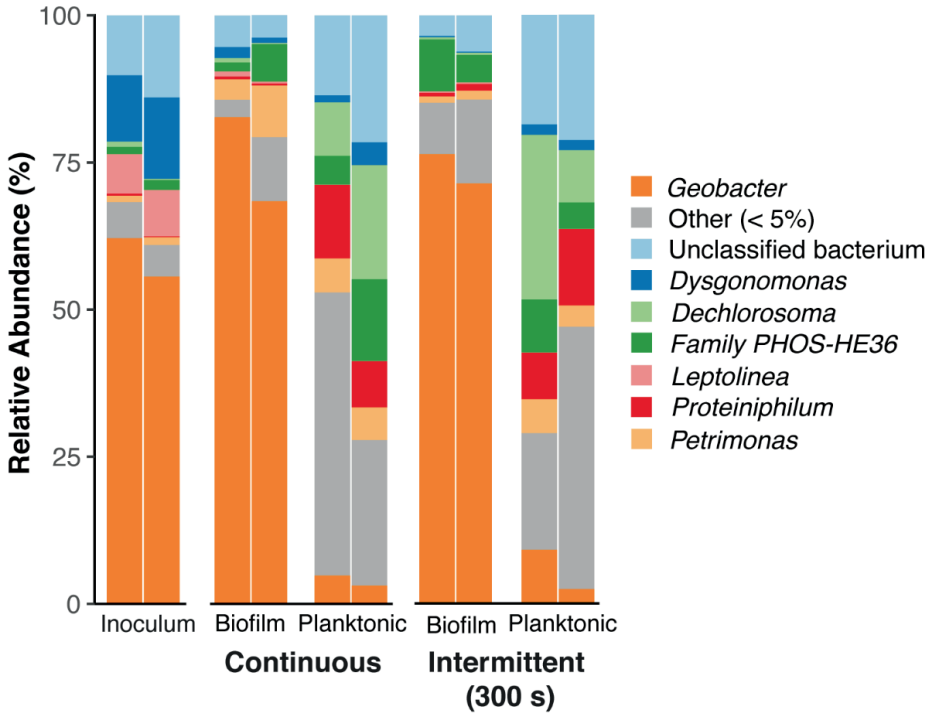

Figure 5.2. Barplot showing the relative abundances of dominant bacterial genera (> 5 % on average) in the inoculum, biofilm, and planktonic samples.

The compositions of the biofilm communities were similar to the composition of the inoculum. The low abundance of *Geobacter* and the diverse community found as planktonic cells suggest that *Geobacter* grows mainly in direct contact with the electrode surface, and that the top layers of the biofilm, that are more likely to detach, are composed of a more diverse and non-electroactive microbial community. The microbial composition of planktonic cells includes only anaerobic bacteria, indicating that no oxygen leakage occurred in the anode compartment. Among the genera identified, some bacteria may have thriven using alternative electron acceptors other than the electrode (for example, species from de genus *Dechlorosoma* are known to reduce (per) chlorate[38] whereas the growth of some species of *Petrimonas* is stimulated by the presence of sulphur[39]). Regarding the electron donor, proteolytic bacteria from the genus *Proteiniphilum* are known to use proteins as energy source for growth.[40,41] None of the genera identified contains species well-known for EPS production. More

information about the microbial community of the EAB and the planktonic cells can be found in Appendices.

5.3.4. Continuous acetate feeding and intermittent control of the anode potential led to more EPS formation

Anabolic processes include, for example, the synthesis of biomolecules such as proteins and polysaccharides. When under certain conditions, cells tend to produce and release more biomolecules to the extracellular biofilm matrix. The biofilm matrix consists, in addition to microorganisms, of loosely-bound (LB) and tightly-bound (TB) EPS. Here, we quantified the total amount of LB and TB EPS in the electro-active biofilm by adding up the amount of proteins and polysaccharides in each EPS fraction. Since the amount of biofilm on the electrode was different for each experiment, we normalized the EPS produced by the final amount of biofilm measured at the end of each experiment. Figure 5.3 demonstrates that the amount of LB-EPS per amount of electro-active biofilms increased when intermittent times longer than 20 seconds were applied, whereas the EPS fraction tightly bound to the cells was not affected by the polarization regime.

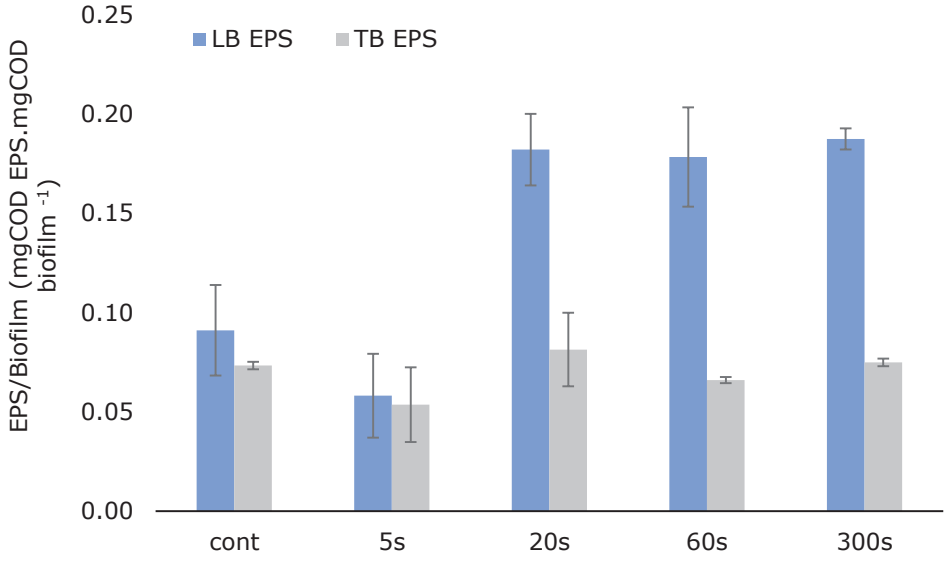

Figure 5.3. Fraction of LB and TB EPS in the biofilm. The total EPS amount (mg COD) was calculated as a sum of the COD of proteins and polysaccharides measured in the LB and TB EPS. This amount was normalized by the COD of biofilm measured with the OCT. The fraction of EPS is expressed in mg COD protein+polysaccharides.mg COD biofilm^{-1}.

The highest amount of LB EPS of 0.19 mg COD protein+polysaccharides.mg COD biofilm^{-1} was found for the biofilm with an intermittent time of 300 seconds, while the continuous and 5 seconds intermittent time had the lowest amount of LB EPS of 0.06 mg COD protein+polysaccharides.mg COD biofilm^{-1}. The results suggest that longer intermittent times favor the use of electrons to synthesize EPS, a metabolic process that

is less evident in the biofilms grown under continuous anode potential and in the biofilm grown with an intermittent time of 5 seconds.

5.3.5. Morphological adaptation of biofilms to anode potential regime

OCT was used not only to quantify the biofilm but also to evaluate the morphological and structural adaptation of the biofilm to the anode potential regime. The OCT images taken of EAB with intermittent anode potential showed irregular shapes whereas more flat and thicker structures were observed in EAB with continuous anode potential. Acknowledging the studies that propose mushroom-like structures as strategies to maximize the biofilm surface area and therefore increase the substrate availably,[10,42] these similar structures that we observe in our OCT images in combination with the higher production of LB-EPS suggest that these irregular and loose structures may be clusters of polymers excreted to the extracellular matrix (Figure 5.4). The biofilms included in Figure 5.4 were scanned at different stages of development.

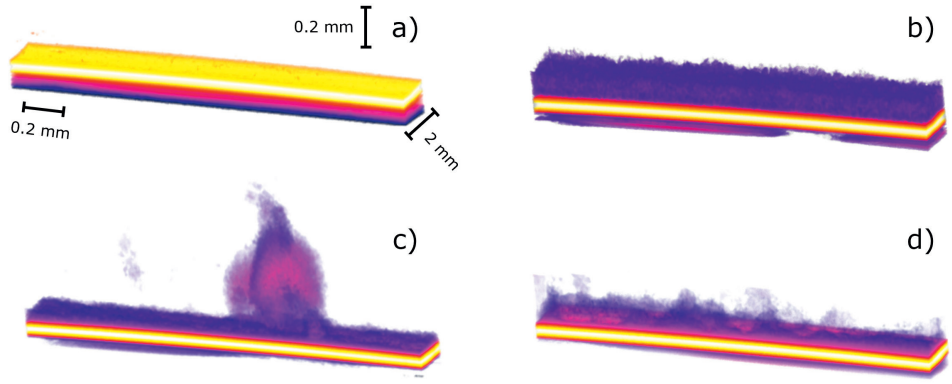

Figure 5.4. Volume Viewer function in ImageJ was used to visualize the 3D morphology of the biofilm on the electrode: (a) bare electrode, (b) continuous bioanode, (c) 5s intermittent bioanode, and (d) 300s intermittent bioanode. The yellow structure illustrates the FTO electrode, and the surface where the biofilm grew is depicted on top of this layer. The color underneath the electrode (outside the reactor) is a consequence of partial light reflection on the glass electrode. The scans aim at illustrating exclusively the morphology of the biofilm, and not total amounts.

5.3.6. The amount of proteins in the EPS of biofilms increased in the bioanodes operated intermittently

To study the effect of intermittent time on the EPS composition of each EAB, the amount of proteins and polysaccharides was measured and normalized to the total amount of biofilm on the anode. Since not all biofilms were grown for the same time nor reached the same thickness, the normalization by the amount of biofilm was used. Figure 5.5 shows that more proteins were found in the EPS of EAB that grew under an intermittent anode potential longer than 20 seconds, while the polysaccharides in the EPS were similar for each condition. The amount of proteins was approximately four

times higher when compared with the biofilms under continuous anode potential (≈0.21 and 0.05 mg COD proteins.mg COD biofilm^{-1}, respectively). Overall, the production of proteins was favored over the production of polysaccharides at intermittent times >20 seconds.

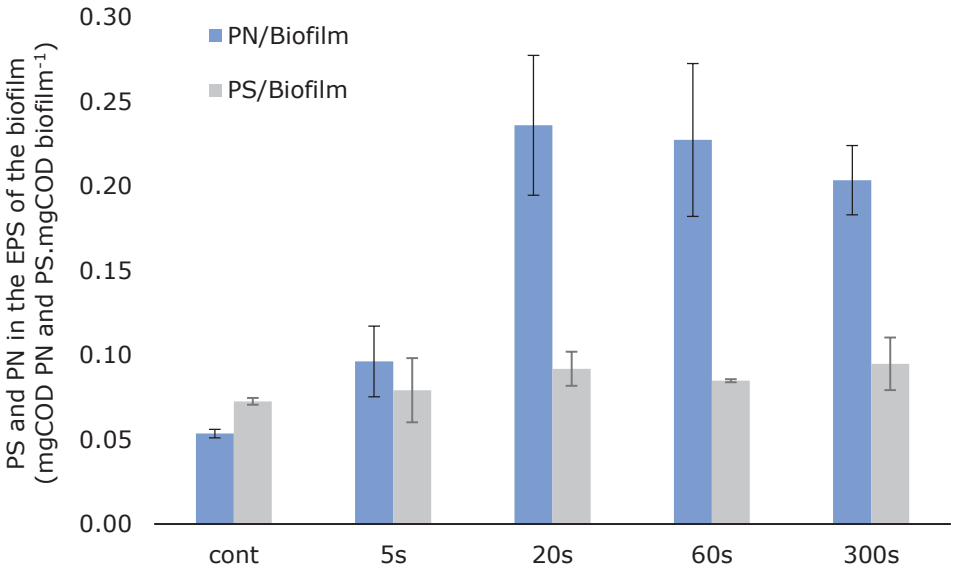

Figure 5.5. Amount of proteins (PN) and polysaccharides (PS) in the EPS per total amount of biofilm: calculated by dividing the total COD of proteins in the EPS by the total COD of biofilm, and the total COD of polysaccharides in the EPS by the total COD of biofilm (mg COD proteins.mg COD biofilm^{-1} and mg COD polysaccharides.mg COD biofilm^{-1}).

5.3.7. Production of EPS in EABs and the effect of intermittent anode control

EPS production is often related to protection mechanisms in response to unbalanced operating conditions.[43,44] In this study, the stressful condition imposed to the bioanodes was the intermittent availability of the electrode as electron acceptor and the continuous feeding of acetate. The combination of these two parameters challenged the bacteria on finding alternative metabolisms to use the electrons generated after acetate oxidation.

In EABs, a higher amount of proteins is commonly associated with redox-active proteins used in the extracellular electron transfer chain.[10] Yang et al. 2019 studied the EPS composition of electro-active biofilms grown at different continuous anode potentials and reported more proteins when biofilms adapt towards the improvement of electron transfer and more polysaccharides as protection mechanism to assure biofilm structure stability. There is thus a balance between protection and electron transfer, reflected in the polysaccharides and protein composition of the EPS.

Since EPS formation facilitates the adhesion of biofilms to surfaces,[45–48] the increasing EPS amount with longer intermittent times may have been the strategy adopted by biofilms under intermittent anode potentials to keep their structure attached to the electrode (the electron acceptor). The higher production of EPS in these biofilms to adapt to the anode potential regime corroborates with the higher S EPS concentration in the anolyte of intermittent bioanodes (charge balance in Figure 5.1) as the S EPS is a consequence of the release of LB and TB EPS from the biofilm into solution, as well as the washout of cells from the biofilm structure. We neglected the production of EPS from planktonic cells due to the low presence of soluble electron acceptors and, therefore, lack of energy source. However, the composition of the S EPS is slightly different from the composition of the LB and TB EPS. For example, the ratios PN/PS in continuous bioanode and in the 300 seconds intermittent bioanode are higher than the ratios PN/PS obtained in the anolyte (≈0.4 for the biofilms under continuous anode potential and ≈1.6 for the biofilms under intermittent anode potential whereas ≈0.02 was found in the S EPS for both experiments). The higher concentration of polysaccharides than proteins in the anolyte indicates that more polysaccharides are released to the anolyte and is also likely to be related to the presence of proteolytic bacteria.

Besides their potential role in extracellular electron transfer, proteins are generally more reduced than polysaccharides. The higher amount of proteins in the EPS of biofilms under intermittent anode potential could be related to the fact that the synthesis of proteins is a more efficient use of electrons in anabolic processes than synthesis of polysaccharides, since more electrons are used to synthesize proteins. Protein synthesis could thus be the strategy adopted by EAB to efficiently use the excess electrons derived from acetate oxidation in periods when the electrode was not available as electron acceptor.

Finally, intermittent bioanodes found the production of EPS an electron consuming mechanism and, at the same time, a strategy to stay attached to the electrode surface.

5.3.8. No effect of the anode potential regime on elemental composition of EAB (dry cells)

Differences in the elemental composition of dry cells could indicate intracellular accumulation of components other than EPS, which may occur as a function of intermittent anode potential control. We used elemental analysis to determine the elemental coefficients of C, H, O, N, and S and compared the results to the general biomass formula $C_1H_{1.8}O_{0.5}N_{0.2}S_{0.02}$.[48] No difference in elemental composition was observed between the conditions, and coefficients were close to the general biomass formula, which means that the intermittent anode potential does not seem to lead to intracellular accumulation of specific elements (Table 5.D1, in Appendices).

5.4. Outlook

EPS production in BES is an unexplored field and its production mechanisms are still to be further understood. Here, we pioneered the study of EPS production in electro-active biofilms as a response to intermittent anode potential regimes by quantifying their production and characterizing their composition in proteins and polysaccharides. The combination of continuous acetate feeding (and no other nutrient limitations) with an intermittent availability of the electron acceptor (non-capacitive FTO electrode), led to more electrons being diverted to EPS production. The production of EPS is an energy consuming process that is often observed in aerobic processes.[50–52] In bioanodes, only the electrode acts as electron acceptor. The only energy yielding process is acetate oxidation and transfer of electrons through the electron transfer chain towards the electrode. The use of intracellular storage compounds as energy source was not considered, since there was no substrate limitation nor other stress factors (such as nutrient limitation) in the system and thus no trigger to form intracellular storage compounds. Thus, more studies are needed to decipher the energy source used for EPS production. Although there are some potential sources of error in the EPS measurements, it is clear that intermittent anode potential led to more EPS production. As an alternative to high ratios C/N required to stimulate EPS production,[24] we observed relevant EPS production yields by controlling the anode potential regime intermittently: ≈30 % EPS in the biofilm and an average of 20 % of total EPS recovered from the acetate consumed. In addition to a duty cycle of 0.5, it would be of interest to explore the effects of varying duty cycles on EPS production. Besides, follow-up research is needed for further characterization of the EPS constituents.

Even though the formation of EPS is not the priority application of BES, the results shown here, and the potential practical application of the produced EPS, show the versatility of BES and the value of electro-active bacteria. In the scope of current density enhancement, this study helped understanding that the use of a non-capacitive electrode and intermittent anode potential deviated electrons to other processes other than electric current at the electrode. This knowledge is of key importance to predict electro-active bacteria dynamics in a real wastewater treatment plant where waste streams are continuously fed into the reactor. Testing the influence of intermittent anode potential in the electro-active biofilm morphology and composition using capacitive electrodes is part of the recommended follow-ups for this study. Besides, in a more fundamental study on the effect of intermittent anode potential in EAB, more steps should be taken towards investigating the equilibrium between storage compound formation and the current production from these compounds. This would unravel the reversibility between formed storage compounds and their use to produce current. More information on these electron consuming processes will allow a more complete and detailed charge balance.

5.5. Conclusion

We studied the effect of intermittent anode potential on the electron balances in the anodic compartment. The composition of the extracellular matrix in which cells are embedded reflected the adaptation of EABs to the applied conditions and provided insights into the fate of electrons in the biofilm. We identified EPS as a major electron sink. In the biofilm, more EPS and more proteins were formed per biomass at intermittent periods > 20 seconds. Besides the biofilm itself, soluble EPS and planktonic growth in the anode compartment represented a considerable fraction of electron sinks. The identification and quantification of these electron sinks are key to tackle losses in the systems and to aim at providing optimum growth operating conditions to increase Coulombic efficiencies of bioanodes.

5.6. Acknowledgment

This work was performed in the cooperation framework of Wetsus, European Centre of Excellence for Sustainable Water Technology (www.wetsus.nl). Wetsus is co-funded by the Dutch Ministry of Economic Affairs and Ministry of Infrastructure and Environment, the European Union Regional Development Fund, the Province of Fryslân, and the Northern Netherlands Provinces. The authors thank the participants of the research theme “Resource Recovery” for the fruitful discussions.

5.7. References

1. Borole, A. P. *et al.* Electroactive biofilms: Current status and future research needs. *Energy Environ. Sci.* **4**, 4813–4834 (2011).
2. Logan, B. E. *et al.* Microbial fuel cells: Methodology and technology. *Environmental Science and Technology* vol. 40 5181–5192 (2006).
3. Hamelers, H. V. M. *et al.* New applications and performance of bioelectrochemical systems. *Appl. Microbiol. Biotechnol.* **85**, 1673–1685 (2010).
4. Bajracharya, S. *et al.* An overview on emerging bioelectrochemical systems (BESs): Technology for sustainable electricity , waste remediation , resource recovery , chemical production and beyond. *Renew. Energy* **98**, 153–170 (2016).
5. Sleutels, T. H. J. A., Darus, L., Hamelers, H. V. M. & Buisman, C. J. N. Effect of operational parameters on Coulombic efficiency in bioelectrochemical systems. *Bioresour. Technol.* **102**, 11172–11176 (2011).
6. Commault, A. S., Lear, G., Packer, M. A. & Weld, R. J. Influence of anode potentials on selection of Geobacter strains in microbial electrolysis cells. *Bioresour. Technol.* **139**, 226–234 (2013).
7. Zhu, X., Yates, M. D. & Logan, B. E. Set potential regulation reveals additional oxidation peaks of Geobacter sulfurreducens anodic biofilms. *Electrochem. commun.* **22**, 116–119 (2012).
8. Dennis, P. G. *et al.* Anode potential influences the structure and function of anodic electrode and electrolyte-associated microbiomes. *Sci. Rep.* **6**, 1–11 (2016).
9. Deeke, A., Sleutels, T. H. J. A., Heijne, A. Ter, Hamelers, H. V. M. & Buisman, C. J. N. Influence of the thickness of the capacitive layer on the performance of bioanodes in Microbial Fuel Cells. *Journal of Power Sources* vol. 243 611–616 (2013).

10. Zhang, X., Prévoteau, A., Louro, R. O., Paquete, C. M. & Rabaey, K. Periodic polarization of electroactive biofilms increases current density and charge carriers concentration while modifying biofilm structure. *Biosens. Bioelectron.* **121**, 183–191 (2018).

11. Guo, F., Babauta, J. T. & Beyenal, H. Impact of intermittent polarization on electrode-respiring Geobacter sulfurreducens biofilms. *Journal of Power Sources* vol. 406 96–101 (2018).

12. Zhang, E., Yu, Q., Zhang, Y., Scott, K. & Diao, G. The Effect of Intermittent Limiting Anodic Current Stimulation on the Electro Activity of Anodic Biofilms. *J. Adv. Chem. Eng.* **7**, 1–7 (2017).

13. Renslow, R. S., Babauta, J. T., Majors, P. D. & Beyenal, H. Diffusion in biofilms respiring on electrodes. *Energy Environ. Sci.* **6**, 595–607 (2013).

14. Richter, H. *et al.* Cyclic voltammetry of biofilms of wild type and mutant Geobacter sulfurreducens on fuel cell anodes indicates possible roles of OmcB, OmcZ, type IV pili, and protons in extracellular electron transfer. *Energy Environ. Sci.* **2**, 506–516 (2009).

15. Reguera, G. *et al.* Biofilm and nanowire production leads to increased current in Geobacter sulfurreducens fuel cells. *Appl. Environ. Microbiol.* **72**, 7345–7348 (2006).

16. Zhang, X., Rabaey, K. & Prévoteau, A. Reversible effects of periodic polarization on anodic electroactive biofilms. *ChemElectroChem* **6**, 1921–1925 (2019).

17. Kubannek, F., Schröder, U. & Krewer, U. Revealing metabolic storage processes in electrode respiring bacteria by differential electrochemical mass spectrometry. *Bioelectrochemistry* **121**, 160–168 (2018).

18. ter Heijne, A., Pereira, M. A., Pereira, J. & Sleutels, T. Electron Storage in Electroactive Biofilms. *Trends Biotechnol.* **39**, 34–42 (2020).

19. Freguia, S., Rabaey, K., Yuan, Z. & Keller, J. Electron and carbon balances in microbial fuel cells reveal temporary bacterial storage behavior during electricity generation. *Environ. Sci. Technol.* **41**, 2915–2921 (2007).

20. Aelterman, P., Freguia, S., Keller, J., Verstraete, W. & Rabaey, K. The anode potential regulates bacterial activity in microbial fuel cells. *Appl. Microbiol. Biotechnol.* **78**, 409–418 (2008).

21. Cao, B. *et al.* Extracellular polymeric substances from Shewanella sp. HRCR-1 biofilms: Characterization by infrared spectroscopy and proteomics. *Environ. Microbiol.* **13**, 1018–1031 (2011).

22. Rollefson, J. B., Stephen, C. S., Tien, M. & Bond, D. R. Identification of an extracellular polysaccharide network essential for cytochrome anchoring and biofilm formation in Geobacter sulfurreducens. *J. Bacteriol.* **193**, 1023–1033 (2011).

23. Voběrková, S., Hermanová, S., Hrubanová, K., & Krzyžánek, V. Biofilm formation and extracellular polymeric substances (EPS) production by Bacillus subtilis depending on nutritional conditions in the presence of polyester film. *Folia Microbiol* 91–100 (2016) doi:10.1007/s12223-015-0406-y.

24. Ajao, V. *et al.* Valorization of glycerol/ethanol-rich wastewater to bioflocculants recovery, properties, and performance. *J. Hazard. Mater.* **375**, 273–208 (2019).

25. Molenaar, S. D. *et al.* In situ biofilm quantification in bioelectrochemical systems by using optical coherence tomography. *ChemSusChem* **11**, 2171–2178 (2018).

26. Deutsche Sammlung von Mikroorganismen und Zellkulturen. 141. Methanogenium Medium (H2/CO2).

https://www.dsmz.de/microorganisms/medium/pdf/DSMZ_Medium141.pdf.

27. Lee, H.-S., Torres, C. I. & Rittmann, B. E. Effects of substrate diffusion and anode potential on kinetic parameters for anode-respiring bacteria. *Environ. Sci. Technol.* **43**, 7571–7577 (2009).

28. Yang, G., Lin, J., Zeng, E. Y. & Zhuang, L. Extraction and characterization of stratified extracellular polymeric substances in Geobacter biofilms. *Bioresour. Technol.* **276**, 119–126 (2019).

29. Dubois, M., Gilles, K., Hamilton, J. K., Rebers, P. A. & Smith, F. A colorimetric method for the determination of sugars. *Nature* **168**, 167 (1951).

30. Virdis, B., Harnisch, F., Batstone, D. J., Rabaey, K. & Donose, B. C. Non-invasive characterization of electrochemically active microbial biofilms using confocal Raman microscopy. *Energy Environ. Sci.* **5**, 7017–7024 (2012).

31. Parada, A. E., Needham, D. M. & Fuhrman, J. A. Every base matters: Assessing small subunit rRNA primers for marine microbiomes with mock communities, time series and global field samples. *Environ. Microbiol.* **18**, 1403–1414 (2016).

32. Quince, C., Lanzen, A., Davenport, R. J. & Turnbaugh, P. J. Removing Noise From Pyrosequenced Amplicons. *BMC Bioinformatics* **12**, (2011).

33. Münch, E. V. & Pollard, P. C. Measuring bacterial biomass-COD in wastewater containing particulate matter. *Water Res.* **31**, 2550–2556 (1997).

34. Heijne, A. ter, Liu, D., Sulonen, M., Sleutels, T. & Fabregat-Santiago, F. Quantification of bio-anode capacitance in bioelectrochemical systems using Electrochemical Impedance Spectroscopy. *J. Power Sources* **400**, 533–538 (2018).

35. Deeke, A., Sleutels, T. H. J. A., Hamelers, H. V. M. & Buisman, C. J. N. Capacitive bioanodes enable renewable energy storage in microbial fuel cells. *Environ. Sci. Technol.* **46**, 3554–3560 (2012).

36. Sleutels, T., Darus, L., Hamelers, H. V. M. & Buisman, C. J. N. Effect of operational parameters on Coulombic efficiency in bioelectrochemical systems. *Bioresour. Technol.* **102**, 11172–11176 (2011).

37. Sleutels, T., Molenaar, S., Heijne, A. & Buisman, C. Low Substrate Loading Limits Methanogenesis and Leads to High Coulombic Efficiency in Bioelectrochemical Systems. *Microorganisms* **4**, 7 (2016).

38. Achenbach, L. A., Michaelidou, U., Bruce, R. A., Fryman, J. & Coates, J. D. Dechloromonas agitata gen. nov., sp. nov. and Dechlorosoma suillum gen. nov., sp. nov., two novel environmentally dominant (per)chlorate-reducing bacteria and their phylogenetic position. *Int. J. Syst. Evol. Microbiol.* **51**, 527–533 (2001).

39. Grabowski, A., Tindall, B. J., Bardin, V., Blanchet, D. & Jeanthon, C. Petrimonas sulfuriphila gen. nov., sp. nov., a mesophilic fermentative bacterium isolated from a biodegraded oil reservoir. *Int. J. Syst. Evol. Microbiol.* **55**, 1113–1121 (2005).

40. Hahnke, S., Langer, T., Koeck, D. E. & Klocke, M. Description of Proteiniphilum saccharofermentans sp. nov., Petrimonas mucosa sp. nov. and Fermentimonas caenicola gen. nov., sp. nov., isolated from mesophilic laboratory-scale biogas reactors, and emended description of the genus Proteiniphilum. *Int. J. Syst. Evol. Microbiol.* **66**, 1466–1475 (2016).

41. Chen, S. & Dong, X. Proteiniphilum acetatigenes gen. nov., sp. nov., from a UASB reactor treating brewery wastewater. *Int. J. Syst. Evol. Microbiol.* **55**, 2257–2261 (2005).

42. Sun, D. *et al.* The effect of biofilm thickness on electrochemical activity of Geobacter sulfurreducens. *Int. J. Hydrogen Energy* **41**, 16523–16528 (2016).

43. Jayathilake, P. G. *et al.* Extracellular polymeric substance production and aggregated bacteria colonization influence the competition of microbes in biofilms. *Front. Microbiol.* **8**, (2017).

44. Szumigaj, J., Zakowska, Z. & Klimek, L. Exopolysaccharide production by Bacillus strains colonizing packaging foils. *Polish J. Microbiol.* **57**, 281–287 (2008).

45. Vu, B., Chen, M., Crawford, R. J. & Ivanova, E. P. Bacterial extracellular polysaccharides involved in biofilm formation. *Molecules* **14**, 2535–2554 (2009).

46. Mayer, C. *et al.* The role of intermolecular interactions: Studies on model systems for bacterial biofilms. *Int. J. Biol. Macromol.* **26**, 3–16 (1999).

47. Lazarova, V. & Manem, J. Biofilm characterization and activity analysis in water and wastewater treatment. *Water Res.* **29**, 2227–2245 (1995).

48. Christensen, B. E. The role of extracellular polysaccharides in biofilms. *J. Biotechnol.* **10**, 181–202 (1989).

49. Heijnen, J. J. & Robbert, K. Bioenergetics of Microbial Growth. in *Encyclopedia of Industrial Microbiology: Bioprocess, Bioseparation and Cell Technology*. (2010). doi:10.1002/0471250589.ebt026.

50. Chen, Z., Zhang, W., Wang, D., Ma, T. & Bai, R. Enhancement of activated sludge dewatering performance by combined composite enzymatic lysis and chemical re-flocculation with inorganic coagulants: Kinetics of enzymatic reaction and re-flocculation morphology. *Water Res.* **83**, 367–376 (2015).

51. Habermacher, J., Benetti, A. D., Derlon, N. & Morgenroth, E. The effect of different aeration conditions in activated sludge - Side-stream system on sludge production, sludge degradation rates, active biomass and extracellular polymeric substances. *Water Res.* **85**, 46–56 (2015).

52. Adav, S. S., Lee, D. J. & Tay, J. H. Extracellular polymeric substances and structural stability of aerobic granule. *Water Res.* **42**, 1644–1650 (2008).

53. Bolyen, E. *et al.* Reproducible, interactive, scalable and extensible microbiome data science using QIIME 2. *Nat. Biotechnol.* **37**, 852–857 (2019).

54. Callahan, B. J. *et al.* DADA2 : High-resolution sample inference from Illumina amplicon data. *Nat. Methods* **13**, 581–583 (2016).

55. Katoh, K. & Standley, D. M. MAFFT multiple sequence alignment software version 7: Improvements in performance and usability. *Mol. Biol. Evol.* **30**, 772–780 (2013).

56. Price, M. N., Dehal, P. S. & Arkin, A. P. FastTree 2 - Approximately maximum-likelihood trees for large alignments. *PLoS One* **5**, (2010).

57. Quast, C. *et al.* The SILVA ribosomal RNA gene database project: Improved data processing and web-based tools. *Nucleic Acids Res.* **41**, 590–596 (2013).

58. McMurdie, P. J. & Holmes, S. Phyloseq: An R Package for Reproducible Interactive Analysis and Graphics of Microbiome Census Data. *PLoS One* **8**, e61217 (2013).

59. Bisanz, J. E. qiime2R: Importing QIIME2 artifacts and associated data into R sessions. (2018).

60. R Core Team. R: A language and environment for statistical computing. (2020).

61. Oksanen, A. J. *et al.* Community Ecology Package. … *Ecol. Packag.* … 263 (2012).

5.8. Appendices

A. Charge balance

The charge balance was calculated using the total recovered charge at the anode, the amount of biofilm measured at the end of the experiment, the total amount of planktonic cells as well as the total soluble EPS. The fraction of charge used for each process was calculated by dividing the charge of each process by the total charge measured in four electron consuming processes. Equation 5.A1 describes the calculation for the fraction of charge recovered at the anode (Q). This was considered the most suitable approach to analyse the data since it directly points out the influence of intermittent potential in the share of each parameter.

$$\text{Fraction Q} = Q / (Q + X_{biofilm} + X_{planktonic} + S,EPS) \quad \text{(Eq. 5.A1)}$$

For the soluble EPS and the planktonic cells, additional steps were taken to convert these data to Coulombs. For the planktonic cells, a factor of $2x10^{-10}$ mg COD.planktonic cell^{-1} was used to convert the number of cells to COD units,[33] and the COD of glucose ($C_6H_{12}O_6$) and BSA ($C_{123}H_{193}N_{35}O_{37}$) were calculated to convert the mass of polysaccharides and proteins to COD units, respectively. The oxidation reactions of glucose and BSA are represented in Equations 5.A2 and 5.A3.

$$C_6H_{12}O_6 + x\ O_2 \rightarrow 6\ CO_2 + 6\ H_2O \quad \text{(Eq. 5.A2)}$$

$$C_{123}H_{193}N_{35}O_{37} + x\ O_2 \rightarrow 123\ CO_2 + ((193\text{-}3\times35)/2)\ H_2O + 35\ NH_3 \quad \text{(Eq. 5.A3)}$$

We acknowledge that the use of standard composition of sugars and proteins for calculating the charge balance may lead to inaccuracies, since in reality, there may be different sugars and proteins present. Besides, the presence of decay material and other compounds in the EPS may have contributed to interferences in the standard methods used to quantify EPS.

The oxidation coefficient, x, represents the moles of O_2 needed to oxidase the reactant. This parameter was calculated and converted to mass units using the molecular weight of O_2 (MW_{O2} = 32 g.mol^{-1}), glucose ($MW_{glucose}$ = 180 g.mol^{-1}), and BSA (MW_{BSA} = 2751 g.mol^{-1}). Equation 5.A4 explains the calculation for the glucose and Equation 5.A5 for the BSA.

$$x = (4\times6+12\text{-}2\times6)/4 = 6\ mol_{O2}.mol_{glucose}^{-1} \cong 1.07\ g_{COD}.g_{glucose}^{-1} \quad \text{(Eq. 5.A4)}$$

$$x = (4\times123+193\text{-}2\times37\text{-}3\times35)/4 = 126\ mol_{O2}.mol_{BSA}^{-1} \cong 1.47\ g_{COD}.g_{BSA}^{-1} \quad \text{(Eq. 5.A5)}$$

The COD ($mgO_2.mL^{-1}$) data were converted to charge (C) using the molecular weight of O_2 (MW_{O2} = 32 g.mol^{-1}), the moles of electrons per mole of O_2 (n=4) and Faraday constant (F = 96485 C.mol^{-1}). Since the reactors were operated continuously, the charge used in planktonic cells growth and soluble EPS (Equation 5.A6) were calculated considering the operating flowrate (Flow = 0.16 mL.min^{-1}) and time between sampling points (Δt = time (d) × 1440).

$$\text{Charge} = COD \times (n \times F \times Flow \times \Delta t) / MW_{O2} \quad \text{(Eq. 5.A6)}$$

The total amount of planktonic cells used in the cumulative charge balance was calculated by summing the growth of planktonic cells calculated for every sampling point, whereas the cumulative soluble EPS was calculated assuming a constant concentration of proteins and polysaccharides over the whole experiment time.

B. Bioinformatics and microbial community analysis (bioanode and planktonic)

We processed raw 16S rRNA gene sequence data with QIIME2 (v. 2019.10).[53] Briefly, DADA2[54] was applied to denoise the data and infer exact amplicon sequence variants (ASVs) from error-corrected sequences. We performed quality filtering as follows: primers were removed, sequence length was trimmed first at a median quality score of 30, and then for forward and reverse sequences at 240 and 200 bp, respectively. After that, reads were merged, assembled into representative sequences, and dereplicated. We then used MAFFT[55] to align representative sequences, and we applied FastTree2[56] to construct a bacterial phylogeny. Taxonomic affiliations of representative sequences were predicted using a naïve-Bayesian classification model trained on the SILVA database (v. 132).[57]

The ASV frequency table, phylogeny and taxonomic information were imported into phyloseq using qiime2R[58,59] in R (v. 4.0.3).[60] Sequencing of the negative extraction control sample yielded only 479 reads, which was far outside the range of samples (63198 - 152883 reads per sample). No potential contaminant taxa were thus removed from the data prior to downstream analyses. Differences in bacterial community composition (i.e. beta diversity) between inoculum, biofilm, and planktonic samples under continuous and intermittent experiments were visualized with principal coordinates analysis (PCoA) from the vegan package.[61] The Bray-Curtis dissimilarity metric was used for this PCoA and was calculated on a feature table containing relative abundances. No rarefaction was applied because all samples leveled off in rarefaction curves (data not shown). Alpha diversity within the communities was assessed using the Shannon diversity index. Bacterial community structure was calculated and visualized at the genus level, highlighting the most dominant genera (average in each set of duplicate samples > 5 %). Co-occurrence of genera (> 5 % abundance) between biofilm and planktonic samples under continuous and intermittent experiments was visualized using Venn diagrams.

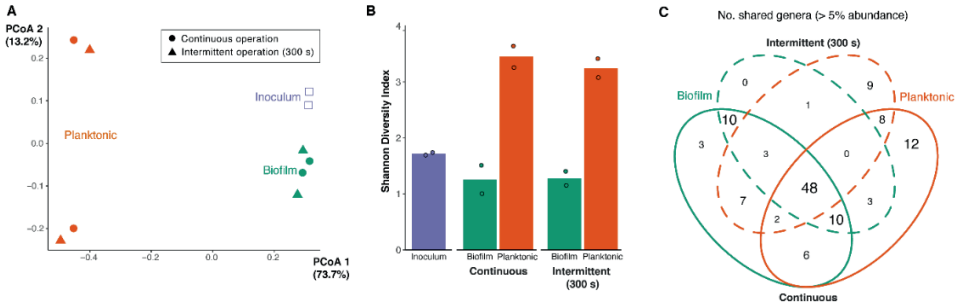

Figure 5.B1. A) Ordination plot showing the variation in bacterial community composition among electrode biofilm and planktonic samples from bioreactors operated in continuous and intermittent modes. Ordination was based on principal coordinates analysis (PCoA) of Bray-Curtis dissimilarities among samples, where each point represents a community and the proximity between points depicts their compositional similarity. B) Barplot showing the median Shannon diversity of two duplicate samples (points) across sample types and operation conditions. Shannon diversity denotes the bacterial diversity within a community and becomes lower when the proportion of rare taxa increases. C) Venn diagram showing the number of co-occurring dominant bacterial genera among sample types and operation conditions. Duplicate runs of the reactors have been inoculated with biofilm (inoculum) formed on an electrode in a previous run. *Geobacter* was the dominant bacterium in the biofilms. Note that bacterial biomass in planktonic communities is low, and that the presented bacterial community structure represents that low biomass with a minor fraction of *Geobacter*.

C. Examples of current densities and demonstrations of peak currents

Figure 5.C1 shows examples of the current profiles of both continuous and intermittent bioanodes. The current profiles of the intermittent bioanodes were filtered in order to remove the data points recorded during open circuit (no current). Besides, an average of the currents measured during closed circuits was calculated and used to show the current profile of intermittent experiments over time. An illustration of the peak currents is shown in Figure 5.C2 (experiment at 60 s intermittent time). A peak current followed by a decreasing current (until a stable current was reached) was the current profile observed during closed circuit for all the intermittent times tested.

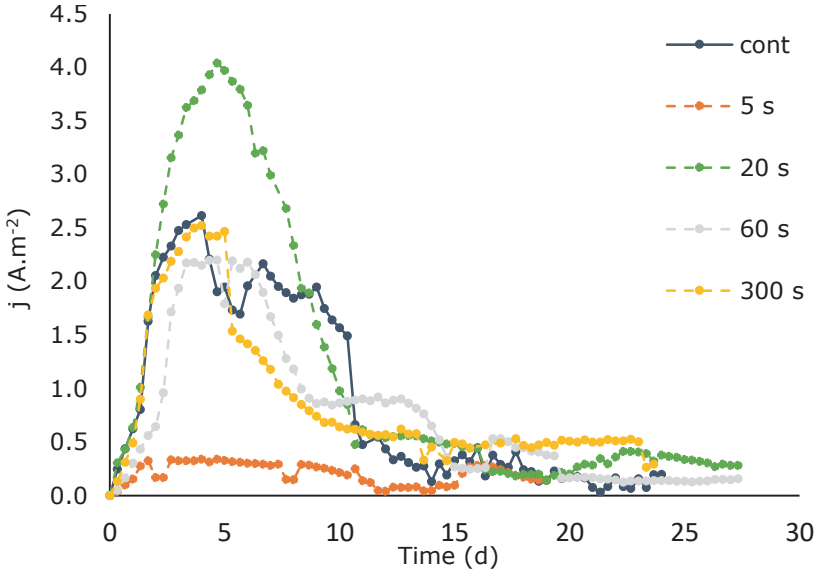

Figure 5.C1. Examples of the current profiles of the bioanodes operated at continuous and intermittent anode potentials.

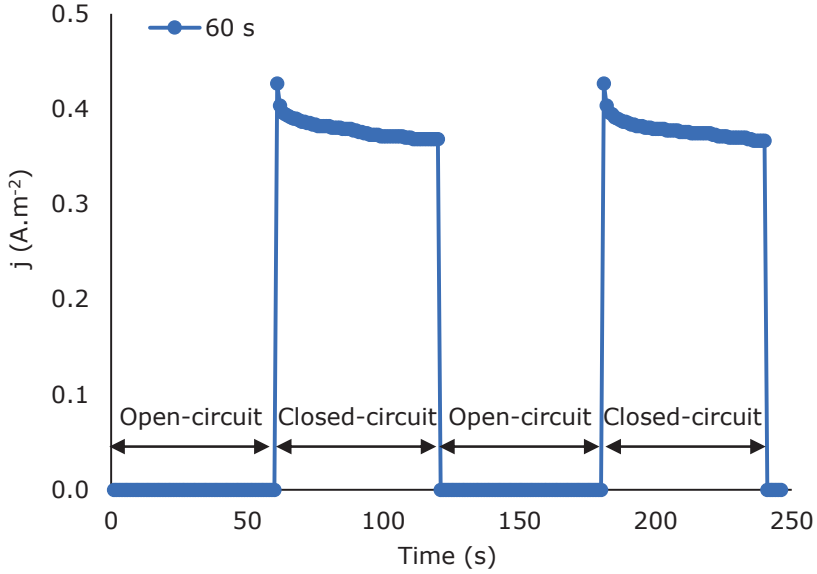

Figure 5.C2. Representation of current profiles during closed circuit (discharging time): two consecutive peak currents measured for the bioanode operated at 60 s intermittent time.

D. Elemental coefficient of the dry cells present in the biofilms of intermittent and continuous bioanodes

Intracellular accumulation of electrons was studied by performing elemental analysis on the dry cells harvested at the end of each experiment (after EPS extraction). Table 5.D1 shows the calculated elemental coefficients of the biomass grown under each condition tested.

Table 5.D1. Elemental coefficients of the dry cells present in the biofilms of intermittent and continuous bioanodes (results expressed as average ± standard deviation).

Anode regime	C	H	O	N	S
cont	1	1.69 ± 0.05	0.30 ± 0.07	0.18 ± 0.01	0.01 ± 0.00
5s	1	1.59 ± 0.06	-*	0.20 ± 0.01	0.01 ± 0.00
20s	1	1.64 ± 0.02	0.31 ± 0.02	0.19 ± 0.01	0.01 ± 0.00
60s	1	1.71 ± 0.01	0.31 ± 0.03	0.20 ± 0.00	0.01 ± 0.00
300s	1	1.70 ± 0.04	0.33 ± 0.02	0.20 ± 0.00	0.01 ± 0.00

*Not enough biomass to analyze the O_2 content of the cells grown with an intermittent time of 5 seconds.

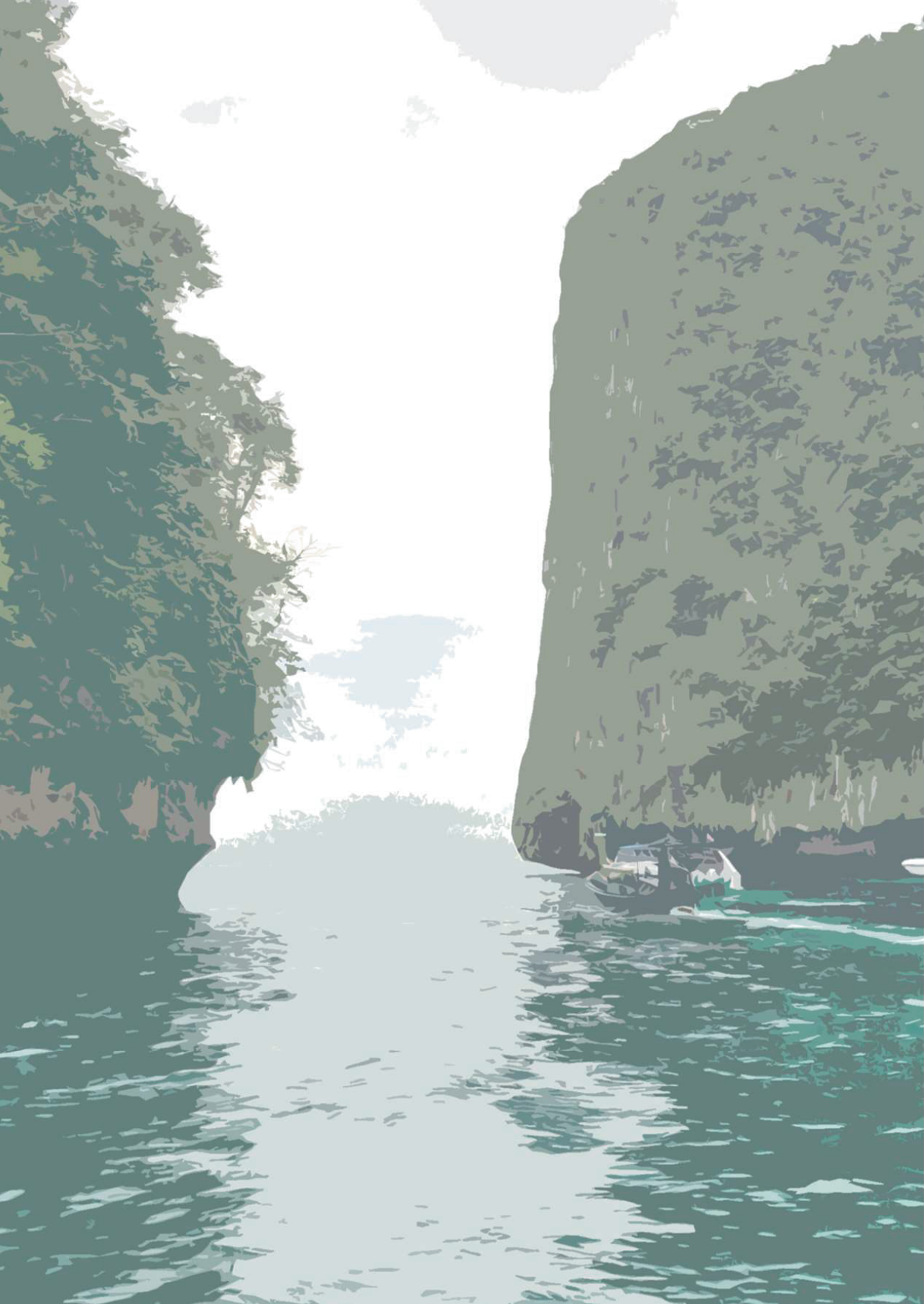

6 Starvation combined with continuous anode potential triggers intracellular electron storage in *Geobacter* dominated electro-active biofilms

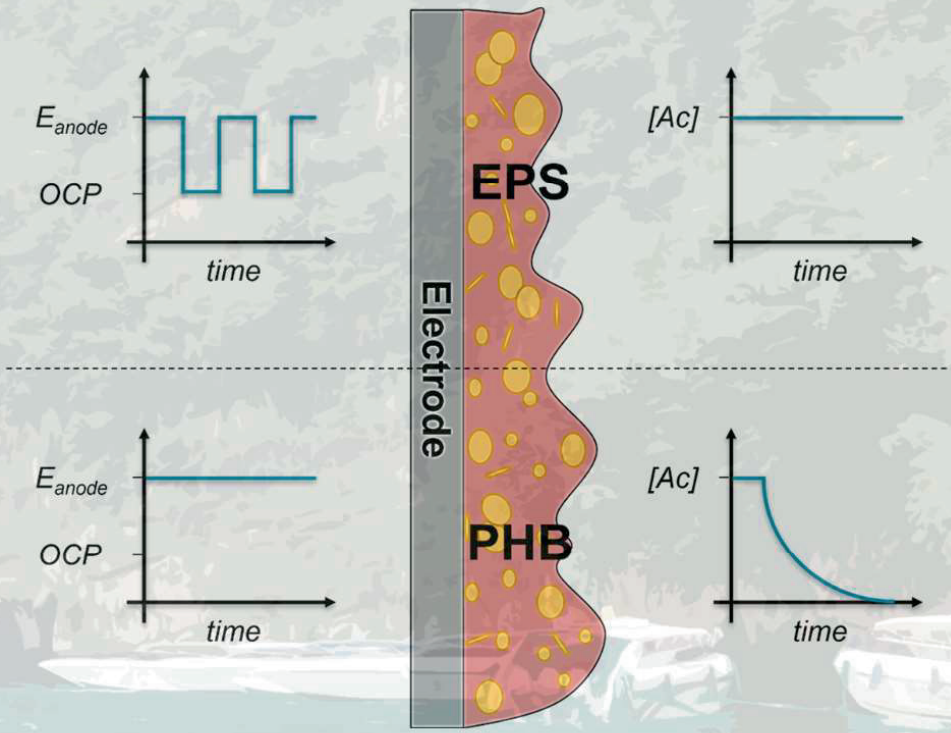

An updated version of this chapter has been published as:

Pereira J, Neves P, Nemanic V, Pereira M A, Sleutels T, Hamelers B, ter Heijne A. *Starvation combined with constant anode potential triggers intracellular electron storage in electro-active biofilms*. Water Research 2023;242, 120278.

Abstract

The accumulation of electrons in the form of Extracellular Polymeric Substances (EPS) and poly-hydroxyalkanoates (PHA) has been studied in anaerobic processes by adjusting the access of microorganisms to the electron donor and final electron acceptor. In Bio-electrochemical systems (BESs), intermittent anode potential regimes have also recently been used to study electron storage in anodic electro-active biofilms (EABfs), but the effect of electron donor feeding mode on electron storage has not been explored. Therefore, in this study, the accumulation of electrons in the form of EPS and PHA was studied as a function of the operating conditions. EABfs were grown under both continuous and intermittent anode potential regimes and fed with acetate (electron donor) continuously or in batch. Confocal Laser Scanning Microscopy (CLSM) and Fourier-Transform Infrared Spectroscopy (FTIR) were used to assess electron storage. The range of Coulombic efficiencies, from 25 to 82 %, and the biomass yields, between 10 and 16 %, indicate that storage could have been an alternative electron consuming process. From image processing, a 0.92 pixel ratio of poly-hydroxybutyrate (PHB) and amount of cells was found in the batch fed EABf grown under a continuous anode potential. This storage was linked to the presence of living *Geobacter* and shows that energy gain and carbon source starvation were the triggers for intracellular electron storage. The highest EPS content (extracellular storage) was observed in the continuously fed EABf under an intermittent anode potential, showing that continuous access to electron donor and intermittent access to the electron acceptor leads to the formation of EPS from the excess energy gained. Tailoring operating conditions can thus steer the microbial community and result in a trained EABf to perform a desired biological conversion, which can be beneficial for a more efficient and optimized BES.

6.1. Introduction

The ability of electro-active microorganisms to exchange electrons with an electrode is the core mechanism of Bio-electrochemical systems (BESs) and a unique feature for their potential applications.[1–3] By combining these bacteria with an electrode (so-called bio-anode), an electro-active biofilm (EABf) is typically formed that catalyses the conversion between electrical and chemical energy. In an anode, anodic EABfs can oxidize organic compounds and exchange the electrons derived from this biological oxidation reaction with the electrode, whereas in the cathode, cathodic EABfs take up electrons provided by the cathode and use them in metabolic processes in which high value compounds can be synthesized.[4,5] Besides these two directions of electron flows from and towards EABfs, electrons can also flow towards alternative electron sinks inside EABfs such as biomass growth, maintenance, protein synthesis, and other anabolic processes.

For anodic EABfs, the electrons derived from the oxidation of a carbon source can be used for different pathways as illustrated in Figure 6.1. The electrons can be used to reduce the anode to generate energy for biological conversions by flowing via (membrane) electron carriers and being directly exchanged with the electrode (so-called direct electron transfer) (pathway 1),[6] or via external redox mediators towards the electrode (so-called mediated electron transfer) (pathway 2). Besides, electrons can also remain inside the electro-active microorganisms and be used to reduce intracellular electron carriers such as NAD+/NADH and flavines (pathway 3),[7,8] a regenerative process that leads to a proton gradient inside the microorganism and allows for the formation of ATP, and therefore energy generation. This energy can be used for cell growth (pathway 4) and maintenance,[9,10] and for anabolic processes: for example the synthesis of proteins and polysaccharides that can be excreted to the extracellular matrix (extracellular polymeric substances, EPS) (pathway 5) to promote the formation of an EABf on the anode, increasing the cohesion and adherence of the EABf to the electrode,[11–13] or the synthesis of lipophilic inclusions such as poly-hydroxyalkanoates (PHA) that remain stored inside the cells (pathway 6).[14] Even though efforts have been made to improve the exchange of electrons with the electrode and to understand how this electron exchange is affected by the growth of EABfs on an electrode,[15,16] little is known about the electrons that end up intracellularly stored in anodic EABfs and how this storage depends on the operating conditions.

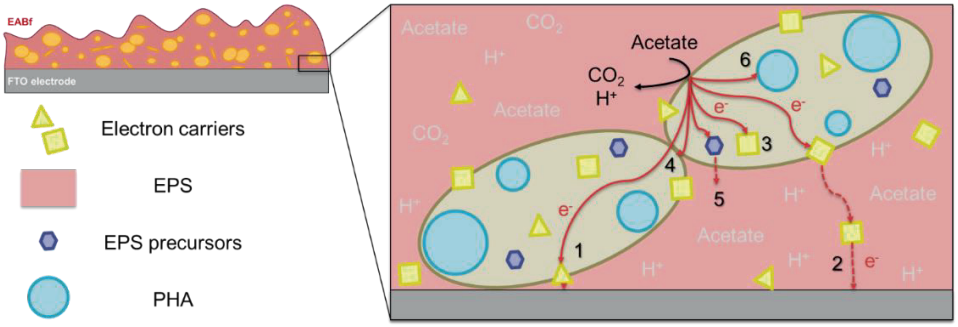

Figure 6.1. Scheme of the different electron flow pathways from acetate oxidation in anodic EABfs: 1) direct electron transfer between the redox carriers on the extracellular membrane and the anode, 2) extracellular electron transfer chain towards the anode mediated by electron carries, 3) reduction of intracellular electron carriers (such as NAD+/NADH and flavines), 4) cell duplication 5) synthesis of extracellular polymeric substances (EPS), and 6) intracellular storage in the form of poly-hydroxyalkanoates (PHA).

Electron storage is typically reported as a strategy used by cells to cope with unfavourable conditions related to the lack of organic donors.[17,18] When carbon sources deplete, cells can still thrive when they have stored compounds such as lipophilic inclusions that can be oxidized to be used as energy source. This is a competitive advantage in comparison to other cells that are not capable of storing electrons intracellularly. However, even though the operating conditions that favour storage and steer a microbial community to be enriched in cells that have a high storage capacity are well defined under anaerobic conditions,[19,20] the operating conditions that favour storage in anaerobic systems combined with electrodes (BESs) are poorly investigated. For example, famine and feast cycles are commonly related to high electron storage in the form of PHA,[21] and different carbon sources are known to lead to the formation of different storage polymers (PHA and/or EPS) in anaerobic systems without electrodes.[22,23] So far, little is known about the operating conditions to stimulate PHA production in EABfs.

One of the few studies on electron storage in anode EABfs has explored the use of intermittent anode potential regimes.[24,25] This intermittency - alternation between closed circuit and open circuit - has gained increasing attention as more electrons were recovered as current at the anode as a result of changes in the composition and morphology of anodic EABfs. Higher production of c-type cytochromes and matrices enriched in EPS have been reported in *Geobacter* dominated EABfs when an intermittent anode regime was imposed.[24,25] A temporary electron storage in electron carriers (reduction of the membrane redox carriers, pathway 1 or 2 in Figure 6.1) has also been proven possible with the intermittent anode regime, however, intracellular electron storage as a result of an intermittent anode potential regime has not yet been reported.

Besides alternating the availability of the anode as final electron acceptor, it is known from other biological processes, e.g. PHA accumulating bacteria under anaerobic conditions, that intracellular electron storage can be determined by the feeding mode.[26] Pereira et al., 2021 have shown that continuously feeding acetate did not trigger evident intracellular electron storage as long as the substrate was available as carbon source in a continuously acetate fed anodic EABf. Instead, EPS was formed to be able to use the excess of ATP accumulated in the EABfs (due to the continuous acetate feeding and the intermittent availability of the anode as final electron acceptor). In another study, Freguia et al., 2007 studied electrons and carbon balances in anodic EABfs and highlighted the existence and contribution of stored compounds on the produced current in an anode operated in a batch feeding mode. Here, poly-hydroxybutyrate (PHB) was identified as storage compound and its use as carbon source was shown by both a shift in the Open Cell Potential (OCP) towards more reducing potentials (more negative) and visualisation using Confocal Laser Scanning Microscopy (CLSM). This work showed the contribution of electron storage to understand electron flows in anodic EABfs and framed electron storage as an important parcel to close electron balances. Besides these efforts to close electron and carbon balances, it is important to know how storage can be influenced by the operating conditions as accumulating electrons can represent a competitive advantage for some species to deal with the surrounding environment, making them more resilient. To make the link between operating conditions and electron storage, information is still missing regarding electron storage quantification and the identification of the dominant species responsible for storing mechanisms.

This study aimed at understanding the influence of anode potential regime and acetate feeding mode on the performance and electron storage in EABfs. Anodic EABfs were grown under continuous and intermittent anode potential regimes and continuous and batch acetate feeding modes and their intracellular electron storage compounds were measured. During the experiments, the thickness of the EABfs was monitored in real-time with Optical Coherence Tomography (OCT) to assess the electrons used for growth, and at the end of the experiments, EABfs were stained to evaluate the effect of the operating conditions on cells viability and intracellular storage with CLSM. The effect of the operating conditions on the microbial community present in the EABfs was determined, and combining this DNA analysis with image processing provided insights on the species responsible for intracellular electron storage.

6.2. Materials and Methods

6.2.1. Experimental setup and reactor design

The design of the electrochemical reactors used in this study has previously been described in Pereira et al., 2022. Briefly, these electrochemical reactors consisted of anode and cathode flow compartments separated by a cation exchange membrane (CEM) (Ralex CMHPP, MEGA a.s., Czech Republic). Each compartment had an inner

volume of 33 mL and the total hydraulic system including piping and recirculation glass vessels had a total volume of 220 mL. A transparent and flat glass electrode coated with Fluorinated Tin Oxide (FTO) was used as anode (operating area of 22.3 cm^2 surrounded by a layer of graphite sheet used as current collector) whereas platinum/iridium coated titanium plate (Pt/IrO_2 80:20, Magneto special anodes BV, Schiedam, The Netherlands) was used as counter electrode.

Both the anolyte (electrolyte in the anode compartment) and catholyte (electrolyte in the cathode compartment) were continuously recirculated at 60 $mL.min^{-1}$ (Masterflex L/S, Cole-Parmer, Barendrecht, The Netherlands). A potentiostat (N-stat d-module, Ivium Technologies, Eindhoven, The Netherlands) was used to perform chronoamperometric measurements to the electrochemical reactors, and an Ag/AgCl reference electrode (+0.203V vs. Standard Hydrogen Electrode; Prosense, Oosterhout, The Netherlands), that was connected to a Haber–Luggin capillary filled with 3 M KCl and placed between the FTO electrode and the CEM, was used to measure and control the anode potential. The electrochemical reactors were operated at 298 K in a temperature controlled cabinet.

6.2.2. Inoculum and electrolytes composition

A mixture of acetate-fed biomass from previous experiments with anodic EABfs was used as inoculum in these experiments. The anode compartment was fed with an adapted culture medium from DSMZ and it constituted of ($g.L^{-1}$): 1.64 $NaCH_3COO$, 3.40 KH_2PO_4 and 4.35 K_2HPO_4, 0.1 $MgSO_4.7H_2O$, 0.74 KCl, 0.58 NaCl, 0.28 NH_4Cl, 0.1 $CaCl_2.2H_2O$, 1 mL of trace metals mixture and 1 mL of vitamins mixture.[28] Sodium 2-bromoethanesulfonate (2-BES, 1.97 $g.L^{-1}$) was added to the medium to avoid methane formation and to guarantee the presence of an EABf on the anode surface. The medium was sparged with nitrogen before and during the experiments to guarantee anaerobic conditions in the anode compartment. The cathode compartment was filled with a 50 mM phosphate buffer solution (same concentration as in the anolyte) at pH 7, and it was also continuously sparged with nitrogen to avoid accumulation of hydrogen and possible transport through the CEM into the anode.

6.2.3. Experimental strategy

A non-limiting acetate concentration (20 mM) was used to guarantee enough supply of carbon and electrons and fed in two different feeding modes into the anode: 1) continuous acetate feeding at a rate of 0.16 $mL.min^{-1}$ (hydraulic retention time of 23 h) and 2) a batch feeding mode (no inflow of fresh medium nor outflow). The recirculation pump was kept on during both feeding modes experiments to guarantee homogeneity in the anode compartment. The batch experiments had a pre-phase of 5 to 7 days in which the anodic EABfs were initially grown in continuous acetate feeding mode before the batch feeding mode started. This pre-phase aimed at allowing more EABf growth on the FTO surface and thus more biomass for chemical, visual and microbial analyses

at the end of the batch experiments. The batch feeding experiments ended when the measured produced current was zero and when acetate was no longer detected in the anolyte. For both acetate feeding modes experiments, the anode potential was controlled at -0.35 V vs Ag/AgCl and operated under 1) a continuous and 2) an intermittent regime. During the continuous anode potential control, the anode was controlled at the set potential during the whole experiment whereas in the intermittent anode potential regime, the anode potential was consecutively switched on and off (i.e., closed circuit and open circuit, respectively) in ten-minute intervals. The same ten-minute interval was used for the on and off time (duty cycle of 0.5), meaning that one whole intermittent cycle took twenty minutes. All the aforementioned conditions were tested in duplicate (Figure 6.2) and the experimental runs lasted for approximately twelve days for the continuously fed EABfs and from five to twenty days for the batch fed EABfs (not accounting for the pre-phase).

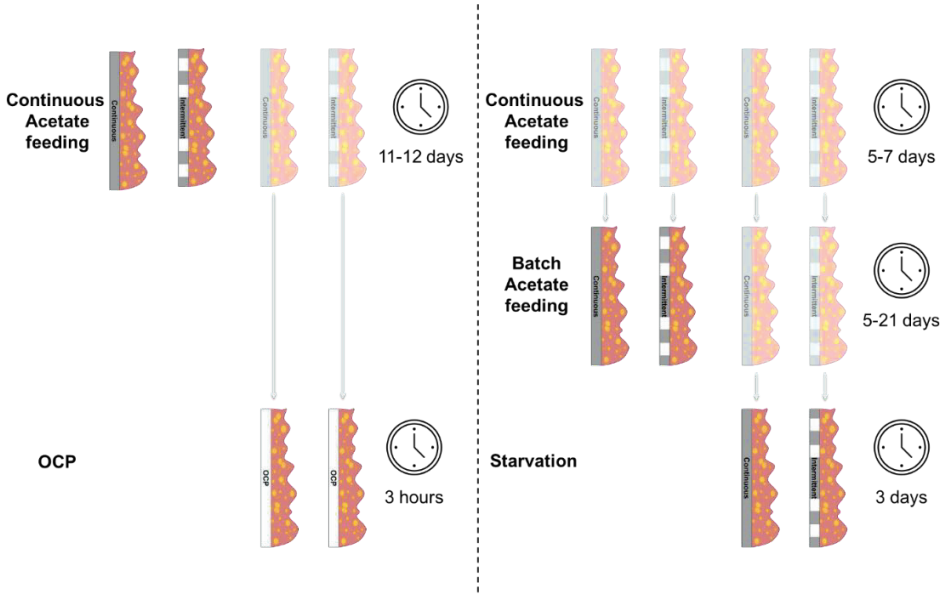

Figure 6.2. Scheme of the experimental strategy to study electron storage in EABfs: (left) EABfs were grown on an FTO electrode with continuous (solid electrode) and intermittent anode potential (dashed electrode), and (right) EABfs were initially grown on an FTO electrode with continuous and intermittent anode potential and continuously fed with acetate (pre-phase) and later switched to a batch feeding mode with the same anode potential regimes as during the pre-phase. Finally, a three-hour OCP was imposed to the continuously acetate fed EABfs (blank electrode), and a starvation of three days combined with a continuous and an intermittent anode potential was imposed to the batch fed EABfs. Electron storage was assessed in the highlighted EABfs.

At the end of the experiments as described above, the effect of two additional operating conditions on electron storage in EABfs was tested. For the EABfs grown under a

continuous acetate feeding, the anode potential regime was stopped, and the Open Cell Potential (OCP) was measured for a duration of three hours while the continuous acetate feeding was maintained. This strategy aimed at providing the EABfs with enough acetate while the anode was not available as final electron acceptor (therefore, no electron transfer with the anode) and evaluate whether the acetate would then be stored inside the cells instead of being used to gain energy and for EABf growth. For the EABfs grown under a batch feeding mode, a starvation of three days long was applied after acetate was no longer detected in the anolyte while the anode regime was maintained. This strategy aimed at giving the EABfs the possibility to exchange electrons derived from storage compounds with the anode to get energy when acetate was no longer available as carbon source. By tailoring the anode potential regime and the acetate feeding modes, understanding of intracellular electron storage and on the effect of the operating conditions in electron storage in anodic EABfs were facilitated.

6.2.4. Chemical analyses and calculations

The acetate concentrations were measured using Ultra-High-Performance Liquid Chromatography (UHPLC) (300x7.8 mm Phenomenex Rezex Organic Acid H+ column, Dionex ultimate 3000RS, Thermo Fisher Scientific, The Netherlands), after samples filtration through a 0.45 µm pore-size filter (EMD Millipore SLFH025NS, Barendrecht, The Netherlands). The acetate concentration in the anolyte and influent were measured every two or three days throughout the continuous feeding mode experiments whereas the acetate concentration in the anolyte was measured twice a day for the batch feeding mode experiments. The acetate consumed by each EABf ($Ac_{consumed}$, mol) was calculated as expressed in Equation 6.1 for the continuous feeding mode experiments, and Equation 6.2 for the batch feeding mode experiments. In Equation 6.1, $[Ac]_{in}$ (mM) is the acetate concentration in the influent (measured as previously described), $[Ac]_{anolyte}$ (mM) is the acetate concentration in the anolyte, V_{anode} (mL) is the volume of the anode compartment, V_{total} (mL) is the total volume of the anolyte , *flow* is the flowrate ($mL.min^{-1}$) and Δt (min) is the time between sampling, whereas in Equation 6.2, $[Ac]_{anolyte}$ and $[Ac]_{anolyte+t}$ (mM) are the acetate concentrations in the anolyte of two consecutive sampling points (taken with a time difference of *t*).

$$Ac_{consumed} = \left([Ac]_{in} - [Ac]_{anolyte}\right) \times \frac{V_{anode}}{V_{total}} \times flow \times \Delta t \quad \text{(Eq. 6.1)}$$

$$Ac_{consumed} = \left([Ac]_{anolyte} - [Ac]_{anolyte+t}\right) \times V_{anode} \quad \text{(Eq. 6.2)}$$

The produced current was measured every minute for the experiments with a continuous anode potential regime and every second for the experiments with an intermittent anode potential regime for a more accurate quantification of the charge recovered during the peak currents (i.e., when the circuit was closed after an OCP period). The Coulombic efficiency (CE) was calculated based on the total charge recovered at the anode and the total charge generated from acetate consumption in

each experiment, as formulated in Equation 6.3. Here, current is represented by i (A), the total time of the experiment is given by t (s), and the integration of the current over time results in the total recovered charge. The time was halved for the experiments in which the anode potential was intermittently controlled to remove the OCP period, in which no current was measured. The conversion from acetate molarity to Coulombs (in the denominator) is calculated with n (8 mol e^-/mol Ac) and Faraday's constant (96485 C/mol e^-).

$$CE = \frac{\int_0^t i\, dt}{Ac_{consumed} \times n \times F} \qquad \text{(Eq. 6.3)}$$

To compare the current profiles over time between the two anode potential regimes, and also to compare the results obtained in this study with literature, current densities were calculated (j, A/m^2) by normalizing the produced current (i, A) to the anode surface area (22.3 cm^2). More detailed information on the current profiles over time can be found in Appendices (Figure 6.A1).

6.2.5. Assessing growth and electron storage using OCT, CLSM, and FTIR

After acetate consumption, electrons follow using different pathways within the EABf. To better understand the fate of these electrons, EABf growth was monitored during the experiments with Optical Coherence Tomography (OCT) and intracellular electron storage was assessed at the end of the experiments using Confocal Laser Scanning Microscopy (CLSM) and Fourier-Transform Infrared Spectroscopy (FTIR).

During the experiments, the anode was scanned using OCT (Thorlabs Ganymede SDOCT System, Germany) in 54 evenly spaced spots and the scans were further processed with MATLAB to calculate the thickness of the EABfs over time. This non-destructive methodology has previously been described by Molenaar et al., 2018 and more details can be found elsewhere.[16,27] EABf thickness was measured at least three times for each experiment.

At the end of the experiments, the EABfs were scraped off from the anode surface and stained with Boron dipyrromethene (BODIPY 493/503®) and 4',6-diamidine-2-phenylindole (DAPI) (Thermo Fisher Scientific, MA, USA) to visualize the storage content in relation to the total amount of cells present in the EABf sample, respectively. BODIPY is a bright, green-fluorescent dye that binds with non-specific lipids (peak excitation wavelength at 488 nm and emission at 503 nm) whereas DAPI is a DNA-specific dye that forms a blue-fluorescent complex when attached to non-specific AT regions of double stranded DNA, allowing the observation of any cell with a DNA sequence containing AT (excited at a wavelength of 405 nm and a maximum emission at 461 nm). The staining methodology was adapted from Pei et al., 2022 and, in short, it initially consisted of fixing the EABfs samples with 4 % paraformaldehyde for 3 hours at 4 °C and preparing 3-5 µL of the fixed EABfs samples on a Teflon-coated glass slide by dehydration in an ethanol series (3 min in 30, 70, and 90 %, sequentially). A 10 µL

hybridization buffer with 20 % formamide was added to the EABfs samples, followed by 0.5 µL of BODIPY and DAPI at a working concentration of 50 ng/µL. The hybridization occurred at 46 °C for 3 h, and the EABfs samples were after kept at 48 °C for 15 min in a pre-heated washing buffer solution with 2150 µL of 5 M NaCl, and finally washed with cold Milli-Q water. Compressed air was used to dry the slides before being mounted and sealed with Vectashield (VECTASHIELD® HardSet™ Antifade Mounting Medium H-1400-10, Vector Laboratories, CA, USA). Besides the amount of storage compounds in the EABfs samples, the viability of the cells at the end of the experiment was also assessed in a separate sample of each EABf. This aimed at understanding whether the cells in the EABf were alive or dead and how their viability related to electron storage. For this purpose, the Live/Dead BacLight method (Thermo Fisher Scientific, MA, USA) was used with dye SYTO™ 9 and propidium-iodide. Syto9 can penetrate all cell membranes, allowing to visualize all living cells (excitation at 488 nm and emission at 498 nm), whereas propidium iodide only penetrates damaged cell membranes (excitation at 561 nm and emission at 617 nm). Briefly, EABfs samples were washed with 1 mL of Milli-Q water and centrifuged at 10000 x g for 3 min. The EABf pellets were stained with 1.5 µL of a mixture containing 1.67 mM Syto9 and 18.3 mM propidium iodide, followed by an incubation period of 20 min. The EABf pellets were washed two times with 1 mL of Milli-Q, and the pellet was mounted and sealed with Vectashield on a glass slide. In another fraction of each EABf sample, the amount of polysaccharides present in the EPS was stained with Calcofluor White (Calcofluor White Stain 18909-100ML-F, Sigma-Aldrich, USA). This blue-fluorescent dye binds to β-1,3 and β-1,4 glucans (excitation and emission wavelengths of 405 and 430 nm, respectively) and it allows for the quantification of the extracellular polysaccharidic storage. A similar stepwise methodology and slide preparation were used for the CW staining as for the live/dead staining, being a 1 mL of a staining solution with 0.2 g/L Calcofluor White M2R added to the EABfs samples and allowing for an incubation time of 60 minutes. Due to the overlapping emission signals of DAPI and CW, the ratio of polysaccharides/cells for a given EABf was calculated by combining the signals of two different samples of the same EABf. This procedure assumes a homogeneous cell density over all the samples of a given EABf.

After the staining procedures, the EABfs samples were visualized with the Confocal Laser Scanning Microscope 880 equipped with Plan-Apochromat 10X/0.45 M27, 20X/0.8 M27 and 63X/1.4 Oil DIC objectives (Carl Zeiss, Germany). The dyes were excited with the lasers Diode 405-30 laser at 405 nm, Argon laser at 488 nm, and DPSS 561-10 laser at 561 nm coupled to the confocal microscope. The imaging routine included a screening of the EABf sample on the well towards a focus spot on which a high quality of the emission signals of the dyes could be obtained. With the 40X objective, a sequence of at least 3 (up to 5) pictures per EABf sample was taken with a digital resolution of 1584 by 1584 pixels, averaged from 8 scans, and saved to separate

file channels at 12-bit depth. The used settings for the laser power and gain were kept constant for the different EABfs samples. The saved images were further processed with Fiji Image J (ImageJ2, Ver 1.52P), in which a threshold level intensity was chosen without overexposing pixel data, and a binary format of each image was created. With this binary format, the pixels were counted to allow comparison of the ratios between BODIPY and DAPI (indicating the amount of stored compounds per amount of cells), Live/Dead cells (indicating the viability of the cells), and CW and DAPI (indicating the extracellular polysaccharidic content per amount of cells) for each of the operating conditions tested. As the ratios differ at different spots of a single EABf sample due to the different local composition in the EABf and/or due to uneven staining efficiency, the median of the calculated ratios between dyes for the three (or five) images taken to each EABf sample was chosen as the representative ratio.

A fraction of each continuously fed EABf was freeze dried at the end of the experiment and used for FTIR analysis (FTIR was not performed on batch fed EABfs due to the insufficient amount of biomass). The dried EABfs samples were placed on top of a diamond crystal for attenuated total reflection FTIR (ATR-FTIR) measurements with ALPHA II Bruker equipped with OPUS version 8.5 (Leiderdorp, The Netherlands) (Section C, in Appendices). FTIR measurements were also performed to acetate, 2-BES, and a 90 % pure PHB powder (Figure 6.C2, in Appendices) to investigate the presence of these medium components in the EABf matrices and to identify the presence of PHB in the EABfs samples.

6.2.6. Microbial community of the EABfs

The effect of the operating conditions on the microbial community of the EABfs on the FTO electrode was analyzed with Next Generation Sequencing (NGS). This technique allowed to study the microbial diversity present in the EABfs and, in combination with the CLSM and FTIR, provided insights on the species responsible for electron storage. Briefly, DNA was extracted from the EABfs using FastDNA SPIN Kit for Soil (MP Biomedicals, Irvine, CA, USA), purity checked with Nanodrop (NanoDrop 1000 Spectrophotometer, Thermo Scientific, The Netherlands), and the normalized DNA extracts (20 ng/mL) were afterward sent to MrDNA (Shallowater, TX, USA) for library preparation and amplicon sequencing. The V4–V5 region of the 16S rRNA gene was amplified in a PCR using primers 515F[31] and 926R[32] and PCR products were pooled in equimolar proportions. Prepared libraries were then sequenced with V3 chemistry to generate 300 bp paired-end reads with an Illumina MiSeq (San Diego, Ca, USA). Detailed information on the NGS analysis can be found elsewhere,[11] with the following adjustments: lengths of forward and reverse reads were trimmed at 200 and 190 bp, respectively, and rarefying was applied to 20865 reads per sample. Silva database v.138 was used for taxonomic classification.

6.3. Results and discussion

6.3.1. Coulombic efficiencies and biomass yields showed a potential 25 to 50 % charge storage for all conditions tested

Figure 6.3 shows the total charge recovered and the amount of EABf on the anode surface as a function of the charge generated from acetate consumption. More acetate was consumed by the continuously fed EABfs grown under a continuous anode potential (approximately 950 C, or 1.2 mmol Ac, Figure 6.3.a) when compared to the EABfs grown under an intermittent anode potential (approximately 600 C, or 0.8 mmol Ac, Figure 6.3.b), even though both experiments ran for the same 11-12 days. This showed that an intermittent anode potential regime combined with a continuous acetate feeding decreased acetate consumption by EABfs when compared to a continuous anode potential regime, as previously reported in Pereira et al., 2021.

For the batch fed EABfs, approximately 400-500 C (0.5-0.6 mmol Ac fed at the beginning of the experiment) were generated from acetate consumption. However, the acetate consumption rate of the intermittent EABfs was lower than the acetate consumption rate of the continuous EABfs (approximately 20 days for the intermittent EABfs and 5 days for the continuous EABfs until acetate was depleted in the anolyte).

The CEs in the continuous experiments were 62-82 % for the EABfs grown under a continuous anode potential and 26-47 % for the EABfs grown under an intermittent anode potential. A low range of thickness from 15 to 20 μm was measured for EABfs grown under both the anode potential regimes tested, without a clear increase or decrease in thickness as a function of recovered charge or acetate consumption. Assuming a conversion factor of 0.154 $g_{(COD\ EABf)}/mL_{(EABf)}$ [29] and excluding eventual detachment and reattachment of cells to the EABf nor cell maintenance, EABfs growth on the anode surface accounted for about 10 % of the electrons derived from acetate oxidation in the continuous anode potential experiments and 16 % in the intermittent anode potential experiments. For the batch fed EABfs, the CEs were 56-65 % for the EABfs grown under a continuous anode potential and 25-43 % for the EABfs grown under an intermittent anode potential. EABf thicknesses of 10-15 μm were measured for the EABfs grown under a continuous anode potential and 11-17 μm for the EABfs grown under an intermittent anode potential. The percentage of electrons used for EABfs growth on the anode surface was not considered as an electron sink in the batch experiments as the EABfs were already formed on the anode when the batch experiments started. However, it is important to mention that 1 to 2 μm of the EABfs grown under a continuous anode potential detached from the anode surface in the last days of the experiment, which could be related to the age of the EABfs,[33,34] and could thus explain the lower CE when compared to the continuously fed EABf grown under the same anode potential regime.

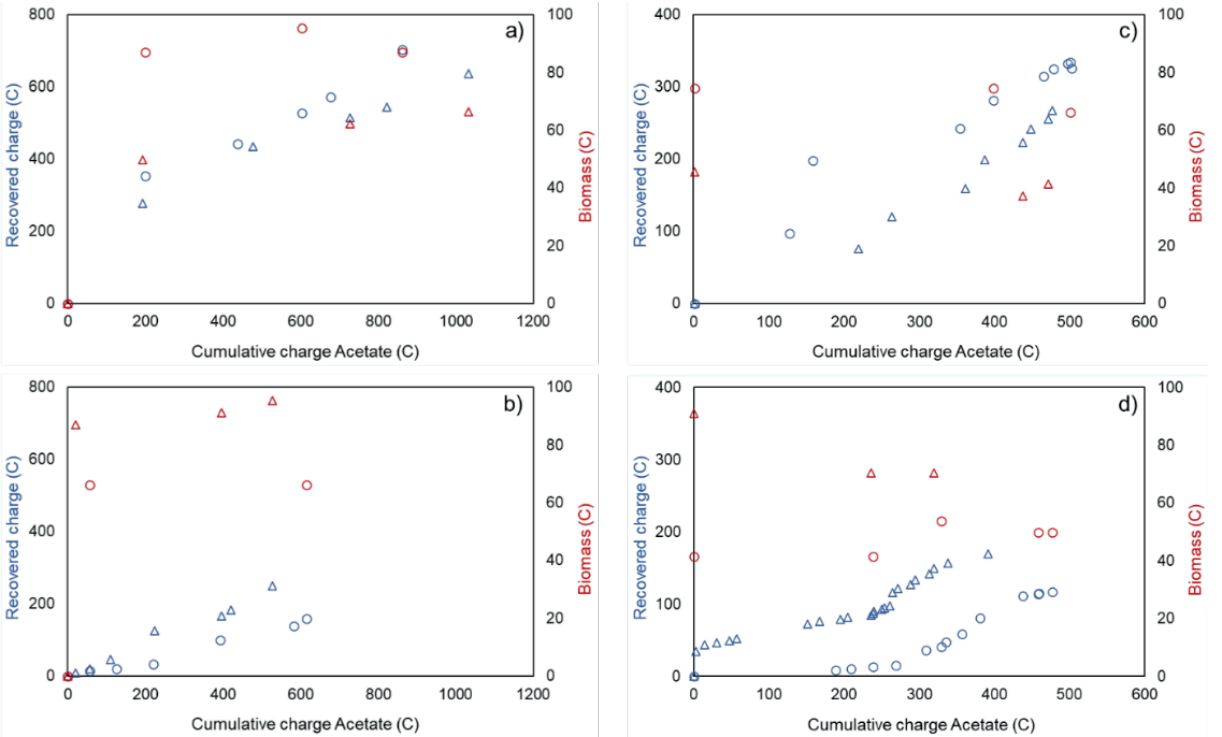

Figure 6.3. Recovered charge (blue) and amount of EABf on the anode (red) as a function of the acetate consumed for the continuously fed EABfs under a a) continuous and an b) intermittent anode potential regime and for the batch fed EABfs under a c) continuous and an d) intermittent anode potential regime (duplicates for each experiment are represented in triangles and circles). For all experiments, storage could have accounted for approximately 25 to 50 % of the available charge after acetate consumption.

Slightly higher CEs and up to ten times thicker EABfs have been reported in comparable studies on anodic EABfs with non-limiting acetate concentrations.[35,36] Other processes that can lead to lower CEs are: 1) planktonic growth, 2) formation and excretion of EPS to the anolyte, 3) the use of alternative final electron acceptors (like sulphate) or the formation of methane, and 4) electron storage in the EABfs. In another study with a similar reactor design and with a continuous acetate feeding mode, both planktonic growth and soluble EPS in the anolyte constituted between 30 to 60 % of the electron sinks for both EABfs grown under a continuous and under an intermittent anode potential.[11] The low sulphate concentration in the anolyte (0.1 mM) and the undetected methane in the headspace of the reactors, combined with the low range of EABf thicknesses (neglecting mass transfer limitations), suggest that electron storage happened and could have been the sink to the remaining fraction of electrons generated from acetate consumption, and the explanation for the remaining 25-50 % not recovered as charge at the anode (CEs) nor measured as EABf growth.

6.3.2. Measured OCPs and produced current during starvation were inconclusive about intracellular electron storage

At the end of the continuous acetate feeding mode, OCP was measured for a three-hour period while the EABfs were continuously fed acetate. This strategy aimed at providing non-limiting carbon source and therefore enhancing electron storage. A rather stable OCP of -0.43 V vs Ag/AgCl was measured in the anode of the EABfs that were previously grown under a continuous anode potential whereas an oscillating OCP between -0.42 and -0.44 V vs Ag/AgCl was measured in the anode of the EABfs that were previously grown under an intermittent anode potential (Figures 6.B1.a and 6.B1.b, in Appendices). These OCPs were 20 to 40 mV more reduced than the expected OCP based on the acetate concentration measured in the anolyte (-0.40 V vs Ag/AgCl, detailed calculation in section B, in Appendices), which means that the EABfs were charged during this three-hour period, as the OCP measures the more reduced charge carrier in the EABfs.[37]

For the batch experiments, a starvation phase of three days was tested with the same anode potential regimes as during the batch experiment. No positive current was produced during this starvation phase, as it was initially expected as no acetate was measured in the anolyte at the end of the batch experiments. However, other carbon sources could have been used as electron donor in the absence of acetate. The fact that no current was measured only meant that the anode was not used as electron acceptor to provide EABfs with energy, however, storage compounds could have been formed and remained unused inside the EABfs. The measured OCPs in the batch fed EABf grown under an intermittent anode potential were approximately -0.2 V vs Ag/AgCl when the electric circuit was opened, which also suggests that EABfs were charged during OCP.

6.3.3. Combination of continuous anode potential and batch feeding showed high PHB/cells ratio after acetate starvation

At the end of the experiments, EABfs samples were stained and visualized under the CLSM to evaluate their viability and electron storage. In Figure 6.4, representative examples of the Live/Dead staining, BODIPY and DAPI, and CW staining are shown.

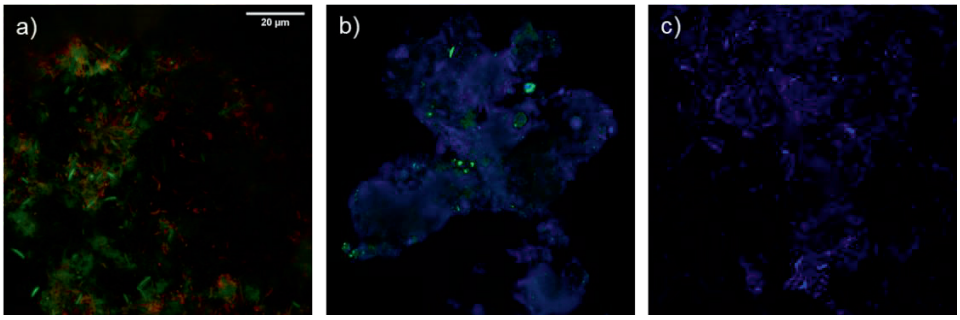

Figure 6.4. Examples of EABfs imaged with CLSM: a) live/dead staining (green and red, respectively) to visualize the viability of the cells, b) BODIPY and DAPI staining (green and blue, respectively) to visualize PHB and the amount of cells, and c) CW (blue) to visualize the polysaccharidic content in the EPS of the EABfs. EABfs samples from a) batch feeding and continuous anode potential, b) batch feeding and intermittent anode potential, and c) continuous feeding and intermittent anode potential.

For the live/dead image, a prevalence of living cells (green) as well as the different cell shapes can be observed – in Figure 6.4.a the elongated bacterial shapes in green suggest the presence of living *Geobacter* cells in the EABf. For the image with BODIPY and DAPI (Figure 6.4.b), storage (green) was observed in some regions of the EABf samples, and the overlapping with the DNA staining (blue) confirmed intracellular electron storage. Finally, the CW staining in Figure 6.4.c shows the polysaccharides distribution in the overall shape of an EABf cluster, in which cells were embedded.

Coloured pixel counting and calculation of the live/dead, PHB/cells, and polysaccharides/cells ratios allows to understand the effect of the tested conditions on the viability of the cells in the EABfs and on the amount of intracellular and extracellular storage compounds, respectively (Figure 6.5).

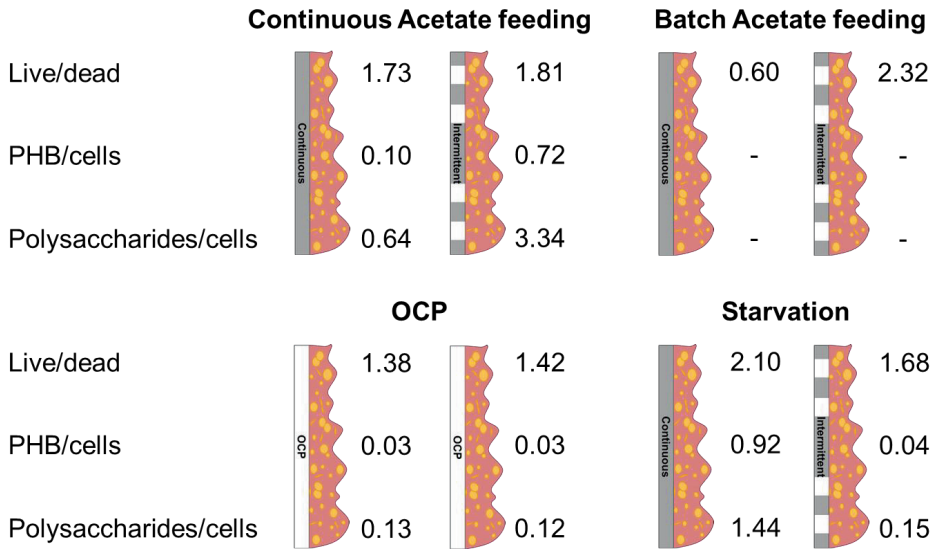

Figure 6.5. Schematic overview of the live/dead, PHB/cells, and polysaccharides/cells ratios for all the conditions tested. The highest live/dead ratio was found in the batch fed EABf grown under an intermittent anode potential, the highest PHB/cells ratio was found after the starvation in the EABf previously grown under a continuous anode potential, and the highest polysaccharides/cell ratio was found in the continuously fed EABf under an intermittent anode potential.

The ratios of live/dead showed that the EABfs were composed of more living cells when compared to dead cells, indicating that even though cell lysis happened, none of the tested conditions led to a dominance of dead cells, proving thus the resilience of EABfs to the absence of electron donor (starvation experiments) and to the absence of the electron acceptor (OCP experiments). An exception to this predominance of living cells was observed in the batch fed EABf grown under a continuous anode potential. As will later be discussed, this was a result of the low amount of EABf sample and highly diverse microbial community present in this EABf.

Regarding intracellular storage, the highest amount of storage for the continuously fed EABfs was measured when the anode potential was controlled intermittently (PHB/cells ratio of 0.72). This ratio suggests intracellular storage, which was not reported in a similar study under comparable operating conditions.[11] Besides the different methodologies used to assess storage (elemental composition of the EABfs was analyzed instead of CLSM imaging), the CEs reported here are slightly lower, which could indicate higher intracellular electron storage. The combination of a continuous acetate feeding and an OCP period of three hours did not increase the amount of storage compounds inside the EABfs. In fact, the amount of storage compounds at the end of the OCP period was lower for both EABfs previously grown under continuous and

intermittent anode potential (final PHB/cells ratio after OCP period of 0.03). The FTIR spectra of the EABfs grown under a continuous anode potential before and after the OCP period showed a decrease in the absorbance peak at the wavenumber of 2921 cm^{-1}, which is characteristic of the CH_2 asymmetric stretch present in lipophilic inclusions (Figure 6.C1, in Appendices).[38–40] This decrease in absorbance, combined with the absence of the characteristic absorbance peak for acetate in the EABf sample, suggests that the consumption of lipidic content in the EABf was preferred over acetate consumption when the anode was not available as electron acceptor, justifying the lower amount of storage compounds obtained at the end of the three-hour OCP periods. Besides, the characteristic PHB absorbance peak was also not found in the FTIR spectra of any of these continuously acetate fed EABfs for both anode potential regimes before and after the OCP periods, which indicates that storage happened in a lipidic form before the OCP period and not in the form of PHB. These low PHB/cells ratios after the OCP period can also be related to the continuous acetate availability in the anolyte, meaning that the electro-active microorganisms were not triggered to start storage mechanisms.

Interestingly, the highest PHB/cells ratio was obtained for the batch fed EABf grown under a continuous anode potential, after a starvation period of three days. The ratio of 0.92 suggested that the majority of the microorganisms present in the sampled EABf contained PHB, even after acetate was depleted in the anolyte. In a batch operating anode, both the depletion of acetate and the saturation of the buffer are likely to become important factors to determine the fate of the electrons in the EABf.[41,42] The high PHB/cells ratio showed that intracellular storage, in the form of PHB, was the anabolic metabolism chosen by the microorganisms to cope with the decreasing concentration of acetate in the anolyte and the accumulation of protons derived by the oxidation of acetate. The lower acetate consumption rate and decrease in produced current measured when acetate was still available in the anolyte indicated this shift in the metabolism of the cells inside the EABfs from acetate oxidation to produce current when buffer was still non-limiting to acetate oxidation to produce PHB when the buffer became limiting, that would otherwise result in a more acidic environment in the EABfs. Therefore, to cope with the excess amount of protons, and to keep a neutral environment, batch fed EABfs grown under a continuous anode potential slowed the acetate consumption rate and deviated more electrons (and protons) to PHB formation while maintaining a low produced current. The high amount of stored PHB was only observed in the EABfs grown under a continuous anode potential. This showed the importance of a continuous availability of the electron acceptor to provide energy for anabolic processes such as the synthesis of PHB. When the electrode was intermittently available as final electron acceptor, little intracellular electron storage was found (PHB/cells ratio of 0.04) suggesting that eventually stored compounds were used for other purposes such as building up an extracellular matrix that optimizes EABf adhesion

to the electrode.[43–45] Besides, it has also been suggested that the mushroom like structures observed in intermittent EABfs is used as a biological strategy to overcome mass transfer limitations, suggesting that less protons were accumulated and that the need to consume the extra amount of protons was reduced in intermittent EABfs when compared to continuous EABfs that typically have a flat and less patchy morphology.[11,25] Due to the low amounts of EABf developed on the anode surface, no ratios of PHB/cells (and therefore no polysaccharides/cells) could be calculated at the end of the batch experiment, nor FTIR analysis could be performed for the batch fed EABf at both the moment no acetate was detected in the anolyte and after the starvation. However, the fact that no current was measured during the starvation (meaning that PHB was not used as carbon source) combined with the depletion of acetate, and the absence of alternative electron acceptors (only the electrode could be reduced for electro-active microorganisms to obtain energy) suggest that the PHB/cells ratios obtained after the starvation were comparable to the ratios at the end of the batch experiments.

Even though EPS is a complex matrix composed of proteins, polysaccharides, DNA, and humic acids, among others,[46] the ratio between the polysaccharidic content in the EPS normalized by the total DNA allows to compare the extracellular storage of EABfs under the different operating conditions tested. The highest polysaccharides/cells ratio was obtained for the continuously fed EABfs under an intermittent anode potential. This is in agreement with the higher amount of EPS found in the intermittent EABfs reported by Pereira et al., 2021, and it reinforces that an intermittent anode potential stimulates the formation of EPS to improve the adhesion of anodic EABf to the anode surface. For the continuously fed EABfs, low polysaccharides/cells ratios were found at the end of the OCP period. This suggests that 1) the EPS got detached from the EABfs and ended up in the anolyte or 2) EPS was consumed by the EABf as energy source. Even though the OCT measurements did not show a decrease in EABf thickness after the OCP periods for either of the EABfs, a decrease in the characteristic absorbance peak in the polysaccharides' region (at 1055 cm^{-1} wavenumber) and the shift of the highest peak absorbances towards the proteins' region (at 1539 and 1643 cm^{-1} wavenumbers) observed in the spectra of the EABfs grown under an intermittent anode potential before and after the OCP period indicates that the polysaccharides content decreased and that protein content in the EABf increased (Figure 6.C1, in Appendices).[38–40] For the batch fed EABfs, more polysaccharides were found per amount of cells in the EABf grown under a continuous anode potential when compared to the EABf grown under an intermittent anode potential. As opposed to the continuously fed EABf after the OCP period, OCT measurements did show a decrease in EABf thickness after the starvation for the EABf grown under an intermittent anode potential (from 22 to 17 μm) suggesting that the polysaccharides and cells were either lost into the anolyte or that the polysaccharides were consumed in the EABf.

Finally, comparing the live/dead ratios to the PHB/cells and the polysaccharides/cells, it is clear that the highest ratios of storage compounds, both intracellular and extracellular, were related to the higher ratio of living cells in the EABfs. Therefore, even though the link between living cells and PHB could not be made due to the green signal overlap, these ratios correlation proved that storing mechanisms were determined and mainly influenced by living cells. This emphasizes that storage compounds boosted cells' resilience and adaptability, even though some storage compounds could also have been accumulated in dead cells present in the EABfs.

6.3.4. DNA sequencing showed that *Geobacter* was storing electrons in the form of PHB

Figure 6.6 shows the relative abundance of the genera present in the EABfs for all the conditions tested in this study. *Geobacter* was the most dominant genus for all the tested conditions (when only considering classified bacterium and not accounting the total abundance of bacteria that were present in relative abundances lower than 5 %), with the exception being the batch fed EABf grown under a continuous anode potential.

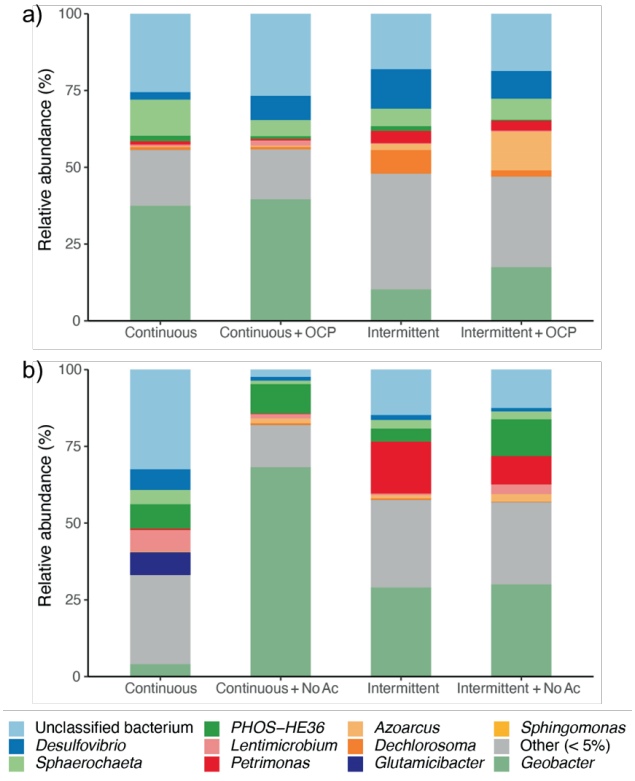

Figure 6.6. Bar plot showing the relative abundances of dominant bacterial genera (>5% on average) in the a) continuously and b) batch fed EABfs, for all the different anode potential regimes tested.

In this EABf, the relative abundance of *Geobacter* was only slightly higher than 5 %. This could be related to the higher accumulation of cells and DNA in a batch system, when compared to a continuous system in which cells and DNA are likely to be washed out, leaving the EABf and the reactor. This accumulation increases the probability that DNA from dead cells was amplified and detected in the microbial community analysis, which could explain the low live/dead ratio obtained in this EABf (0.60, in Figure 6.5). Given the microbial community of the continuously fed EABf grown under a continuous anode potential (first bar in Figure 6.6.a) and the microbial community of the batch fed EABf after starvation grown under a continuous anode potential (second bar in Figure 6.6.b), these conditions alone are not likely to explain the low amount of *Geobacter* in the EABf obtained at the end of the batch experiment. Finally, another possible explanation for the low amount of *Geobacter* present in this EABf was the low amount of sample used for the DNA sequencing, that could result in the amplification of contaminations.[47] The highest relative abundance of *Geobacter* was found in the batch fed EABf grown under a continuous anode potential, after the starvation period. This coincided with the EABfs in which the highest PHB/cells ratio was found, indicating that *Geobacter* was the genera accumulating PHB. PHB accumulation in anodic EABfs has already been suggested,[14,48] but the ratios of live/dead and PHB/cells indicate that living *Geobacter* in a fed batch EABf grown under a continuous anode potential was essential to trigger PHB formation.

The intermittent anode regime decreased the relative abundance of *Geobacter* present in the microbial community of the EABfs by approximately 50 %, for both the continuous and batch acetate fed EABfs (assuming that the microbial community of the batch fed EABf grown under a continuous anode potential is similar before and after starvation). This is coherent with the lower produced currents measured in the EABfs grown under an intermittent anode potential (in Appendices). However, the decrease in relative abundance of *Geobacter* in the microbial community present in the EABf has never previously been reported, for example in Pereira et al., 2021 in a similar work when an intermittent time of five minutes was used. The decrease in the relative abundance of *Geobacter* observed here suggests that a ten-minute intermittent time without the electrode available as final electron acceptor (nor alternative electron acceptors in the anolyte) was too long to still guarantee the dominance of *Geobacter*, and other genera such as *Desulfovibrio* in the continuously fed EABfs and *Petrimonas* in the batch fed EABfs throve in the EABfs. As opposed to the decrease in the relative abundance of *Geobacter* caused by the anode potential regime, the three-hour OCP and the three-day starvation periods did not seem to change the relative abundance of *Geobacter* in the microbial community of the EABfs, which supports that *Geobacter* did not grow during these periods. More information about the other anaerobic genera found in the EABfs can be found in Appendices (in Section D).

6.4. Conclusions and outlook

Electrodes and EABfs are a powerful tool to steer biological conversions. Besides the exchange of electrons between EABfs and the electrode, parallel electron flows take place in electro-active microorganisms that can play a very important role in biological processes. One of these parallel processes is the electron storage which allows EABfs to adapt to the operating conditions and strengthen their resilience once under unfavourable conditions, which is frequently neglected. Studying storage is required for a better understanding of the EABfs composition which in turn is key towards better performing BES. This pioneering study to understand intracellular storage showed that an available electron acceptor and the depletion of carbon source were the triggers to promote intracellular storage in anodic EABfs. This showed that feeding mode and anode potential regime are two parameters that can be tailored to steer biological conversions in anodic EABfs. The different settings for the electron donor and acceptor also affected the viability of the cells present in the anodic EABfs, being both intracellular and extracellular storage proven to be strictly linked to the presence of living cells. In line with the changes in the biological conversions and cells viability, the microbial community was also shifted and the EABf community became dominated by the genera that can better cope with the provided operating conditions. Here, close to 90 % of the EABf dominated by *Geobacter* contained intracellular products when acetate was depleted and the anode was continuously available as final electron acceptor. This elucidated that substrate starvation is a trigger for electron storage and that energy (electrode continuously available as final electron acceptor) is essential for anabolism and thus electron storage. Besides elucidating storage, it is important to highlight that biological conversions can be steered by combining EABfs and electrodes. Exploring a wider range of intermittent times and anode potentials could be of interest for future research, as well as implementing starvation cycles to stimulate even more storage and increase the abundance of *Geobacter* in the EABf. In addition, identifying the storage compounds and how their relative quantities change as a function of the acetate feeding mode and anode potential regime would allow to steer biological conversions, by regulating the energy available and its regime as well as altering the access to a carbon source, and thus to a better control of anodic EABfs. To conclude, this ensemble electrode and EABfs can be used not only to study a wide range of biological responses but also to grow trained and highly efficient EABfs in which composition and microbial community match the targeted conversions of a given biological system.

6.5. Acknowledgements

This work was performed in the cooperation framework of Wetsus, European Centre of Excellence for Sustainable Water Technology (www. wetsus.nl). Wetsus is co-funded by the Dutch Ministry of Economic Affairs and Ministry of Infrastructure and Environment, the European Union Regional Development Fund, the Province of Fryslân, and the Northern Netherlands Provinces. The authors thank the participants of

the research theme “Resource Recovery” for the fruitful discussions and their financial support. This publication is part of the project “Understanding and controlling electron flows in electro-active biofilms” with project number 17516 of the research program Vidi which is (partly) financed by the Dutch Research Council (NWO). The acknowledgments are extended to Marta Cardoso and Pieter van Veelen for their help with CLSM visualization and DNA analysis, Carlos Davila for the nice discussions about fermentations and EPS/PHA formation, and finally to Alan Werker for the explanation and interpretation of the FTIR spectra.

6.6. References

1. Logan, B. E., Rossi, R., Ragab, A. & Saikaly, P. E. Electroactive microorganisms in bioelectrochemical systems. *Nat. Rev. Microbiol.* **17**, 307–319 (2019).
2. Lahiri, D., Nag, M., Ghosh, S., Dey, A. & Ray, R. R. Electroactive biofilm and electron transfer in MES. in *Scaling Up of Microbial Electrochemical Systems* 87–101 (Elsevier, 2022). doi:10.1016/b978-0-323-90765-1.00006-x.
3. Erable, B., Duţeanua, N. M., Ghangrekar, M. M., Dumas, C. & Scott, K. Application of electro-active biofilms. *Biofouling* **26**, 57–71 (2010).
4. Santoro, C., Arbizzani, C., Erable, B. & Ieropoulos, I. Microbial fuel cells: From fundamentals to applications. A review. *J. Power Sources* **356**, 225–244 (2017).
5. Kracke, F., Vassilev, I. & Krömer, J. O. Microbial electron transport and energy conservation - The foundation for optimizing bioelectrochemical systems. *Front. Microbiol.* **6**, 1–18 (2015).
6. Kiran, R. & Patil, S. A. Microbial Electroactive Biofilms. *ACS Symp. Ser.* **1323**, 159–186 (2019).
7. Korth, B., Rosa, L. F. M., Harnisch, F. & Picioreanu, C. A framework for modeling electroactive microbial biofilms performing direct electron transfer. *Bioelectrochemistry* **106**, 194–206 (2015).
8. Korth, B. & Harnisch, F. Spotlight on the energy harvest of electroactive microorganisms: The impact of the applied anode potential. *Front. Microbiol.* **10**, 1–9 (2019).
9. Borole, A. P. *et al.* Electroactive biofilms: Current status and future research needs. *Energy Environ. Sci.* **4**, 4813–4834 (2011).
10. Sun, D. *et al.* The effect of biofilm thickness on electrochemical activity of Geobacter sulfurreducens. *Int. J. Hydrogen Energy* **41**, 16523–16528 (2016).
11. Pereira, J. *et al.* The effect of intermittent anode potential regimes on the morphology and extracellular matrix composition of electro-active bacteria. *Biofilm* **4**, 100064 (2021).
12. Cao, B. *et al.* Extracellular polymeric substances from Shewanella sp. HRCR-1 biofilms: Characterization by infrared spectroscopy and proteomics. *Environ. Microbiol.* **13**, 1018–1031 (2011).
13. Dong, Y. *et al.* Responses of electroactive biofilms to chronic chlorine exposure: Insights from the composition and spatial structure of extracellular polymeric substances. *Bioelectrochemistry* **142**, 107894 (2021).
14. Freguia, S., Rabaey, K., Yuan, Z. & Keller, J. Electron and carbon balances in microbial fuel cells reveal temporary bacterial storage behavior during electricity generation. *Environ. Sci. Technol.* **41**, 2915–2921 (2007).

15. Millo, D. An Electrochemical Strategy to Measure the Thickness of Electroactive Microbial Biofilms. *ChemElectroChem* **2**, 288–291 (2015).

16. Pereira, J. *et al.* Real-time monitoring of biofilm thickness allows for determination of acetate limitations in bio-anodes. *Bioresour. Technol. Reports* **18**, 101028 (2022).

17. Ruiz, Y., Ribot-Llobet, E., Baeza, J. A. & Guisasola, A. Conditions for high resistance to starvation periods in bioelectrochemical systems. *Bioelectrochemistry* **106**, 328–334 (2015).

18. Yang, G., Mai, Q., Zhuang, Z. & Zhuang, L. Buffer capacity regulates the stratification of anode-respiring biofilm during brewery wastewater treatment. *Environ. Res.* **201**, 111572 (2021).

19. Mino, T., Van Loosdrecht, M. C. M. & Heijnen, J. J. Microbiology and biochemistry of the enhanced biological phosphate removal process. *Water Research* vol. 32 3193–3207 (1998).

20. van Loosdrecht, M. C. M., Pot, M. A. & Heijnen, J. J. Importance of bacterial storage polymers in bioprocesses. *Water Sci. Technol.* **35**, 41–47 (1997).

21. Pei, R. *et al.* Exploring the Limits of Polyhydroxyalkanoate Production by Municipal Activated Sludge. *Environ. Sci. Technol.* **56**, 11729–11738 (2022).

22. Szenk, M., Dill, K. A. & de Graff, A. M. R. Why Do Fast-Growing Bacteria Enter Overflow Metabolism? Testing the Membrane Real Estate Hypothesis. *Cell Syst.* **5**, 95–104 (2017).

23. Prados, E. & Maicas, S. Bacterial Production of Hydroxyalkanoates (PHA). *Univers. J. Microbiol. Res.* **4**, 23–30 (2016).

24. ter Heijne, A., Pereira, M. A., Pereira, J. & Sleutels, T. Electron Storage in Electroactive Biofilms. *Trends Biotechnol.* **39**, 34–42 (2020).

25. Zhang, X., Prévoteau, A., Louro, R. O., Paquete, C. M. & Rabaey, K. Periodic polarization of electroactive biofilms increases current density and charge carriers concentration while modifying biofilm structure. *Biosens. Bioelectron.* **121**, 183–191 (2018).

26. Estévez-Alonso, Á., Pei, R., van Loosdrecht, M. C. M., Kleerebezem, R. & Werker, A. Scaling-up microbial community-based polyhydroxyalkanoate production: status and challenges. *Bioresour. Technol.* **327**, (2021).

27. Pereira, J., Wang, G., Sleutels, T., Hamelers, B. & ter Heijne, A. Maximum Thickness of Non-Buffer Limited Electro-Active Biofilms Decreases at Higher Anode Potentials. *Biofilm* **4**, (2022).

28. DSMZ. 141. Methanogenium Medium (H2/CO2). 6–8 https://www.dsmz.de/microorgan- isms/medium/pdf/DSMZ_Medium141.pdf (2017).

29. Molenaar, S. D. *et al.* In situ biofilm quantification in bioelectrochemical systems by using optical coherence tomography. *ChemSusChem* **11**, 2171–2178 (2018).

30. Pei, R., Vicente-Venegas, G., Van Loosdrecht, M. C. M., Kleerebezem, R. & Werker, A. Quantification of polyhydroxyalkanoate accumulated in waste activated sludge. *Water Res.* **221**, 118795 (2022).

31. Parada, A. E., Needham, D. M. & Fuhrman, J. A. Every base matters: Assessing small subunit rRNA primers for marine microbiomes with mock communities, time series and global field samples. *Environ. Microbiol.* **18**, 1403–1414 (2016).

32. Quince, C., Lanzen, A., Davenport, R. J. & Turnbaugh, P. J. Removing Noise From Pyrosequenced Amplicons. *BMC Bioinformatics* **12**, (2011).

33. Katuri, K. P. *et al.* Electroactive biofilms on surface functionalized anodes: The anode respiring behavior of a novel electroactive bacterium, Desulfuromonas acetexigens. *Water Res.* **185**, 116284 (2020).

34. Korth, B., Kretzschmar, J., Bartz, M., Kuchenbuch, A. & Harnisch, F. Determining incremental coulombic efficiency and physiological parameters of early stage Geobacter spp. enrichment biofilms. *PLoS One* **15**, 1–19 (2020).

35. Lusk, B. G., Parameswaran, P., Popat, S. C., Rittmann, B. E. & Torres, C. I. The effect of pH and buffer concentration on anode biofilms of Thermincola ferriacetica. *Bioelectrochemistry* **112**, 47–52 (2016).

36. Lee, H. S. Electrokinetic analyses in biofilm anodes: Ohmic conduction of extracellular electron transfer. *Bioresour. Technol.* **256**, 509–514 (2018).

37. Hamelers, H. V. M., ter Heijne, A., Stein, N., Rozendal, R. A. & Buisman, C. J. N. Butler-Volmer-Monod model for describing bio-anode polarization curves. *Bioresour. Technol.* **102**, 381–387 (2011).

38. Schmitt, J. & Flemming, H. C. FTIR-spectroscopy in microbial and material analysis. *Int. Biodeterior. Biodegrad.* **41**, 1–11 (1998).

39. Arcos-Hernandez, M. V. *et al.* Rapid quantification of intracellular PHA using infrared spectroscopy: An application in mixed cultures. *J. Biotechnol.* **150**, 372–379 (2010).

40. Chan, C. M. *et al.* Mixed culture polyhydroxyalkanoate-rich biomass assessment and quality control using thermogravimetric measurement methods. *Polym. Degrad. Stab.* **144**, 110–120 (2017).

41. Torres, C. I., Marcus, A. K. & Rittmann, B. E. Proton transport inside the biofilm limits electrical current generation by anode-respiring bacteria. *Biotechnol. Bioeng.* **100**, 872–881 (2008).

42. Rozendal, R. A., Hamelers, H. V. M., Molenkamp, R. J. & Buisman, C. J. N. Performance of single chamber biocatalyzed electrolysis with different types of ion exchange membranes. *Water Res.* **41**, 1984–1994 (2007).

43. Laspidou, C. S. & Rittmann, B. E. Modeling the development of biofilm density including active bacteria, inert biomass, and extracellular polymeric substances. *Water Res.* **38**, 3349–3361 (2004).

44. Jayathilake, P. G. *et al.* Extracellular polymeric substance production and aggregated bacteria colonization influence the competition of microbes in biofilms. *Front. Microbiol.* **8**, (2017).

45. Caudan, C., Filali, A., Spérandio, M. & Girbal-Neuhauser, E. Multiple EPS interactions involved in the cohesion and structure of aerobic granules. *Chemosphere* **117**, 262–270 (2014).

46. Seviour, T. *et al.* Extracellular polymeric substances of biofilms: Suffering from an identity crisis. *Water Res.* **151**, 1–7 (2019).

47. Cologgi, D. L., Otwell, A. E., Speers, A. M., Rotondo, J. A. & Reguera, G. Genetic analysis of electroactive biofilms. *Int. Microbiol.* (2021) doi:10.1007/s10123-021-00176-y.

48. Howley, E., Ki, D., Krajmalnik-Brown, R. & Torres, C. I. Geobacter sulfurreducens' Unique Metabolism Results in Cells with a High Iron and Lipid Content. *Microbiol. Spectr.* **10**, (2022).

49. Babauta, J. T. & Beyenal, H. Mass transfer studies of Geobacter sulfurreducens biofilms on rotating disk electrodes. *Biotechnol. Bioeng.* **111**, 285–294 (2014).

50. Chadwick, G. L., Otero, F. J., Gralnick, J. A., Bond, D. R. & Orphan, V. J. NanoSIMS imaging reveals metabolic stratification within current-producing biofilms. *Proc. Natl. Acad. Sci. U. S. A.* **116**, 20716–20724 (2019).

51. ter Heijne, A. *et al.* Analysis of bio-anode performance through electrochemical impedance spectroscopy. *Bioelectrochemistry* **106**, 64–72 (2015).

52. Pereira, J., Wang, G., Sleutels, T., Hamelers, B. & ter Heijne, A. Maximum thickness of non-buffer limited electro-active biofilms decreases at higher anode potentials. *Biofilm* **4**, 100092 (2022).

53. Matias, P. M., Pereira, I. A. C., Soares, C. M. & Carrondo, M. A. Sulphate respiration from hydrogen in Desulfovibrio bacteria: A structural biology overview. *Prog. Biophys. Mol. Biol.* **89**, 292–329 (2005).

54. Philippon, T. *et al.* Denitrifying bio-cathodes developed from constructed wetland sediments exhibit electroactive nitrate reducing biofilms dominated by the genera Azoarcus and Pontibacter. *Bioelectrochemistry* **140**, (2021).

55. Qiao, S. *et al.* Comparison of Anammox Treatment Performances Using Different Kinds of Biomass Carriers. *Japanese J. Water Treat. Biol.* **45**, 1–11 (2009).

56. Koenig, A., Zhang, T., Liu, L. H. & Fang, H. H. P. Microbial community and biochemistry process in autosulfurotrophic denitrifying biofilm. *Chemosphere* **58**, 1041–1047 (2005).

57. Grabowski, A., Tindall, B. J., Bardin, V., Blanchet, D. & Jeanthon, C. Petrimonas sulfuriphila gen. nov., sp. nov., a mesophilic fermentative bacterium isolated from a biodegraded oil reservoir. *Int. J. Syst. Evol. Microbiol.* **55**, 1113–1121 (2005).

58. Hahnke, S., Langer, T., Koeck, D. E. & Klocke, M. Description of Proteiniphilum saccharofermentans sp. nov., Petrimonas mucosa sp. nov. and Fermentimonas caenicola gen. nov., sp. nov., isolated from mesophilic laboratory-scale biogas reactors, and emended description of the genus Proteiniphilum. *Int. J. Syst. Evol. Microbiol.* **66**, 1466–1475 (2016).

59. Bidzhieva, S. K., Sokolova, D. S., Tourova, T. P. & Nazina, T. N. Bacteria of the Genus Sphaerochaeta from Low-Temperature Heavy Oil Reservoirs (Russia). *Microbiol. (Russian Fed.* **87**, 757–765 (2018).

60. Sun, L. *et al.* Lentimicrobium saccharophilum gen. nov., sp. nov., a strictly anaerobic bacterium representing a new family in the phylum bacteroidetes, and proposal of lentimicrobiaceae fam. nov. *Int. J. Syst. Evol. Microbiol.* **66**, 2635–2642 (2016).

61. Santos, R. G. *et al.* Complete genome analysis of Glutamicibacter creatinolyticus from mare abscess and comparative genomics provide insight of diversity and adaptation for Glutamicibacter. *Gene* **741**, 144566 (2020).

62. Ni'matuzahroh, Gilewicz, M., Guiliano, M. & Bertrand, J. C. In-vitro study of interaction between photooxidation and biodegradation of 2-methylphenanthrene by Sphingomonas sp. 2MPII. *Chemosphere* **38**, 2501–2507 (1999).

6.7. Appendices

A. Current density and acetate concentration in the anolyte as a function of the time for all feeding modes and anode potential regimes

Figure 6.A1 shows the current profile and the acetate concentration in the anolyte for all the conditions tested. For the intermittent anode potential experiments (Figure 6.A1.b and 6.A1.d), the peak currents observed once the electrical circuit was closed after OCP periods were removed for a clearer visualization of the current density over time, without shortening the experimental time. These peaks accounted for the first 100 seconds the electrical circuit was closed after each OCP period. Therefore, the current density profiles over time for the intermittent EABfs only include the currents measured between 100 and 600 seconds of the total ten-minute closed-circuit time. The charge measured in the first 100 seconds of the closed-circuit time, that included the peak current representing the discharge of the electrons temporarily stored in the EABf and the time until a stable produced current was reached, were though considered for the calculation of the CE in the intermittent anode potential experiments.

Figures 6.A1.a and 6.A1.b show the current density and the concentration of acetate present in the anolyte as a function of time for the EABfs grown in a continuous acetate feeding mode. Under this feeding mode, an increase in current was observed after a short lag phase, representing the attachment of cells to the anode surface, followed by an exponential current increase linked to the growth and formation of an EABf on the anode surface, and finally, a steady phase with low produced current that can be a consequence of different local conditions in the EABf, associated to mass transfer limitations.[49,50] The peak current densities for the continuous anode potential experiments were approximately 0.7 and 1.5 A/m^2 whereas the peak current densities for the intermittent anode potential experiments (EABf discharge after OCP period) were approximately 1.0 A/m^2 (not included in Figure 6.A1, as explained in Material and Methods). For both anode potential regimes, the current densities at the steady phase ranged between 0.2 and 0.3 A/m^2. These current densities are in the low range of current densities typically reported for anodic EABfs studied on flat electrodes.[29,51,52]

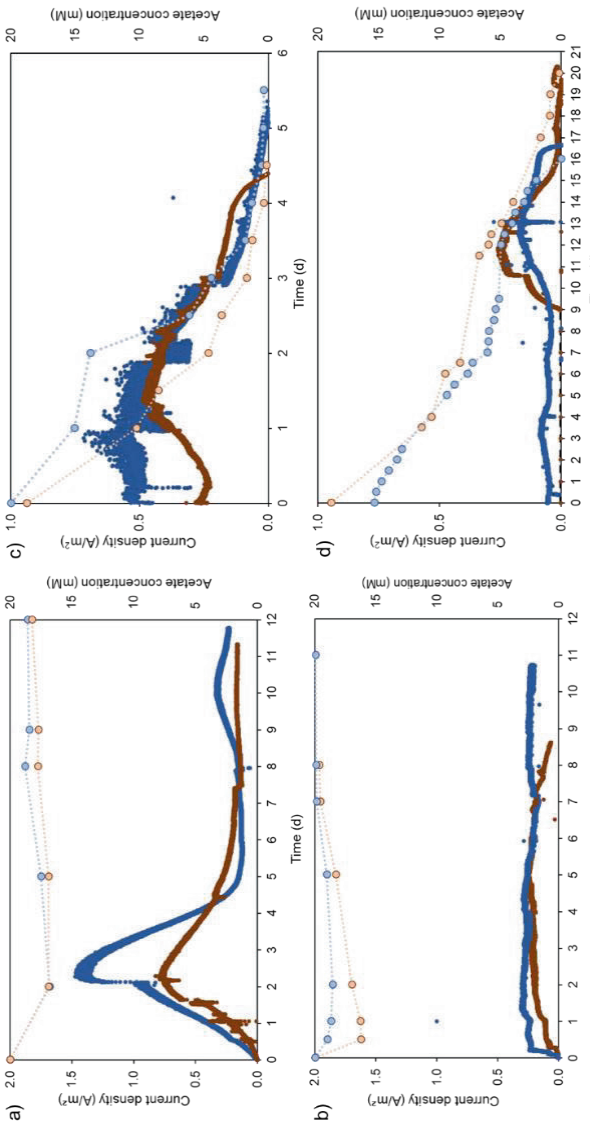

Figure 6.A1. Current density and acetate concentration in the anolyte as a function of the time for the continuously acetate fed EABfs grown under a a) continuous and an b) intermittent anode potential and for the batch fed EABfs grown under a c) continuous and an d) intermittent anode potential (duplicates represented in blue and brown). The highest current peak was obtained for the continuously fed EABfs under a continuous anode potential and the continuously fed EABfs under an intermittent anode potential produced slightly lower current densities and consumed less acetate. For the batch fed EABfs, EABfs under a continuous anode potential showed a decrease in current as the concentration of acetate in the anolyte decreased whereas the EABfs under an intermittent anode potential showed a lower acetate consumption rate and an increase in produced current when the lowest acetate consumption was measured.

The consumption of acetate over time (secondary vertical axis in Figure 6.A1) showed a very coherent trend with the produced current profile: a peak acetate consumption in the first days was linked to a peak in produced current (approximately 4 mM of acetate were consumed), followed by a decrease in acetate consumption linked to a decrease and stabilization in produced current, resulting in higher measured acetate concentrations in the anolyte. These acetate consumptions are in the same order of magnitude as previously reported for chronoamperometric growth of EABf with a similar set anode potential.[16] Even though the steady produced current can be linked to a steady acetate consumption by the EABfs grown under a continuous anode potential, a steady produced current was measured for EABfs grown under an intermittent anode potential while less acetate was consumed. This indicates that under intermittent anode potential 1) more electrons from acetate oxidation were used to produce current, meaning that less electrons were used for alternative processes such as EABf growth, resulting in higher CEs, 2) the cells in the EABf did not have access to fresh acetate and therefore less acetate consumption was observed, and/or 3) electrons from residual acetate present in the EABfs matrices or from the oxidation of an alternative carbon source were used to produce current at the anode.

After a pre-phase in which acetate was continuously fed into the anode compartment to allow EABfs growth on the anode surface, EABfs were further studied under a batch acetate feeding mode. The current density and the concentration of acetate present in the anolyte as a function of time for the EABfs grown in a batch acetate feeding mode are shown in Figure 6.A1.c and 6.A1.d. As thin EABfs were already developed on the anode surface, positive and stable currents were measured at the start of the batch experiments. Within two days of the batch experiment, the current density decreased from 0.5 A/m^2 until no more positive current was measured on the fifth day for the EABfs grown under a continuous anode potential. For the EABfs grown under an intermittent anode potential, the initially produced current was lower than for the EABfs grown under a continuous anode potential (approximately 0.1 A/m^2, with peak currents of around 0.5 A/m^2 after OCP periods) and increased up to 0.3 A/m^2 on the ninth day and slowly decreased afterward to zero on the seventeenth and twentieth days.

The decreasing acetate concentration in the anolyte over time was similar for both the EABfs grown under a continuous and an intermittent anode potential, however, the acetate consumption rate was more than three times higher for the EABfs grown under a continuous anode potential when compared to the EABfs grown under an intermittent anode potential (3.9 and 0.9 mM/d for the EABfs grown under a continuous and under an intermittent anode potential, respectively). These rates, and the difference between continuous and intermittent anode potential regimes, were similar to the acetate consumption rates for the continuously fed EABfs. For the EABfs grown under a continuous anode potential, a decrease in the produced current was observed when an acetate concentration of 5 mM was measured in the anolyte. Also at this acetate

concentration range in the anolyte, a small increase in produced current was observed for the EABfs grown under an intermittent anode potential (between days 9 and 12). Even though this current increase coincided with the lowest acetate consumption rate measured in these batch experiments (lowest slope in the dashed trend line in Figure 6.A1.d) – which could indicate the use of an alternative electron donor – enough electrons were derived from the consumed acetate to generate the measured produced current. For both anode potential regimes, the acetate consumption rate was higher at the beginning of the batch and became slower when the acetate concentration in the anolyte was ranging from 2 to 5 mM. Even though acetate was still detected in the anolyte, the produced current slowly decreased from 0.25 A/m^2 to zero within two days for the EABfs grown under a continuous anode potential and started to decrease and remained at lower than 0.1 A/m^2 for the EABfs grown under an intermittent anode potential. This slow acetate consumption and little range of produced currents when a low acetate concentration was measured in the anolyte could indicate that acetate was not homogeneously available in the EABfs (being the produced current only associated with the also decreasing number of EABf layers that were not acetate limited), or that the exchange of electrons with the anode became a less favourable electron flow pathway.

B. Measured OCPs for the EABfs grown under a continuous acetate feeding and during the prolonged starvation for the EABfs grown under an intermittent anode potential

The produced current and measured anode potential over time during the OCP periods and prolonged starvation period are shown in Figure 6.B1. No current was measured during the three-hour OCP period and the OCP was approximately -0.43 and -0.44 V vs Ag/AgCl for the EABfs that were previously grown under a continuous and intermittent anode potential, respectively. Also, no produced current was measured for the EABfs that underwent the three day prolonged starvation period. The initial produced current measured for the EABf grown under a continuous anode potential (Figure 6.B1.c) was likely due to the presence of residual acetate in the anolyte (not detected with UHPLC), and in the EABf matrix. During the prolonged starvation, the equilibrium OCP was approximately -0.22 V vs Ag/AgCl during the open cell circuit times of the intermittent anode potential regime experiment.

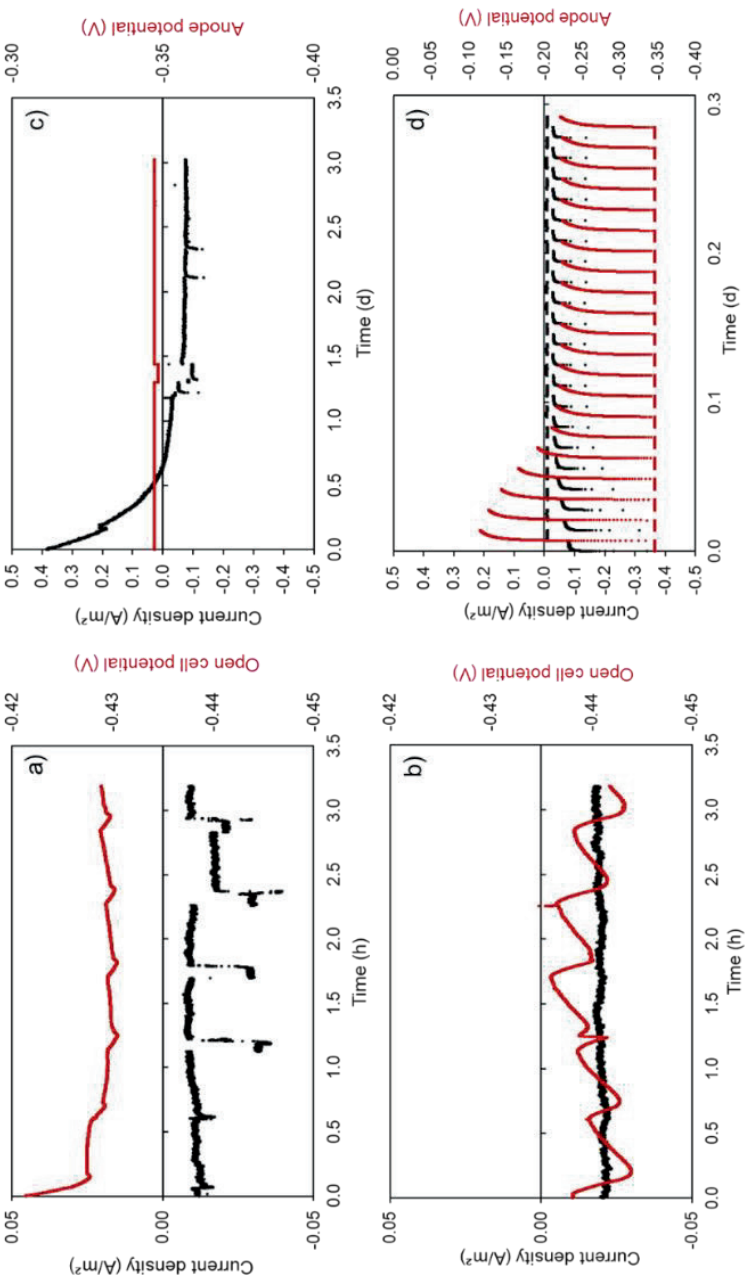

Figure 6.B1. Measured OCP (red) over time for the continuously fed EABfs that were previously grown under a) continuous and an b) intermittent anode potential regimes, and measured current density (black) during the prolonged starvation period for the batch fed EABfs grown under a c) continuous and an d) intermittent anode potential regimes (only the first 0.3 days are shown here to allow a more detailed visualization of the current and OCP, however the same pattern was kept until the end of the three day prolonged starvation).

To understand the measured OCP values, an expected OCP was calculated based on the Nernst equation and based on the acetate concentration present in the anolyte. Equation 6.B1 shows the acetate (CH_3COO^-) oxidation reaction and Equation 6.B2 shows the Nernst equation adapted for the acetate oxidation reaction, in which $E_{acetate}^{0}$ is the redox potential for the biological oxidation of acetate under standard conditions (0.187 V vs NHE), R is the ideal gas constant (8.314 J/mol/K), T is the temperature (298 K), n is the number of electrons generated per mol of acetate consumed (8 mol e^-/mol Ac), and F is the Faraday's constant (96485 C/mol e^-).

$$2\ HCO_3^- + 9\ H^+ + 8\ e^- \rightarrow CH_3COO^- + 4\ H_2O \qquad \text{(Eq. 6.B1)}$$

$$OCP = E_{acetate}^{0} - (RT / nF) \times \ln([CH_3COO^-] / ([HCO_3^-]^2 \times [H^+]^9)) \qquad \text{(Eq. 6.B2)}$$

The calculated OCP was -0.40 V vs Ag/AgCl for an acetate concentration of 18 mM in the anolyte (higher than the measured OCPs), and the measured OCP of -0.22 V vs Ag/AgCl during the prolonged starvation experiments for the EABfs grown under an intermittent anode potential suggested a very low anolyte pH (approximately 3).

C. FTIR spectra for the continuously acetate fed EABfs under both continuous and intermittent anode potentials

The FTIR spectra with the absorbance peaks are shown in Figure 6.C1 and 6.C2. The FTIR measurements were performed before and after the OCP periods for both the EABfs grown under a continuous and an intermittent anode potential (Figure 6.C1). The spectra provided information on the composition of the EABfs, including intracellular and extracellular storage compounds. In microbial analysis, polysaccharides are observed between the wavenumbers 1100 and 700 cm^{-1}, phosphates between the wavenumbers 1400 and 1100 cm^{-1}, proteins between the wavenumbers 1800 and 1400 cm^{-1}, and fatty acids between the wavenumbers 3100 and 2750 cm^{-1}. Within these ranges, there are typic peaks associated with ring vibrations (1085 cm^{-1}) and C-O and C-O-C bounds (1052 cm^{-1}) in the polysaccharidic spectrum region, amide I (C=O) (1652 and 1648 cm^{-1}), amide II, N-H, C-N and structure of proteins (1550 and 1548 cm^{-1}) in the protein spectrum region, and CH_2 asymmetric stretch (2920 cm^{-1}) in the fatty acids spectrum region.[38]

FTIR measurements were also performed on acetate, 2-BES and a 90 % pure PHB powders (Figure 6.C2) to discriminate the presence of acetate and 2-BES in the EABf matrices and to identify the presence of PHB in the EABf samples.

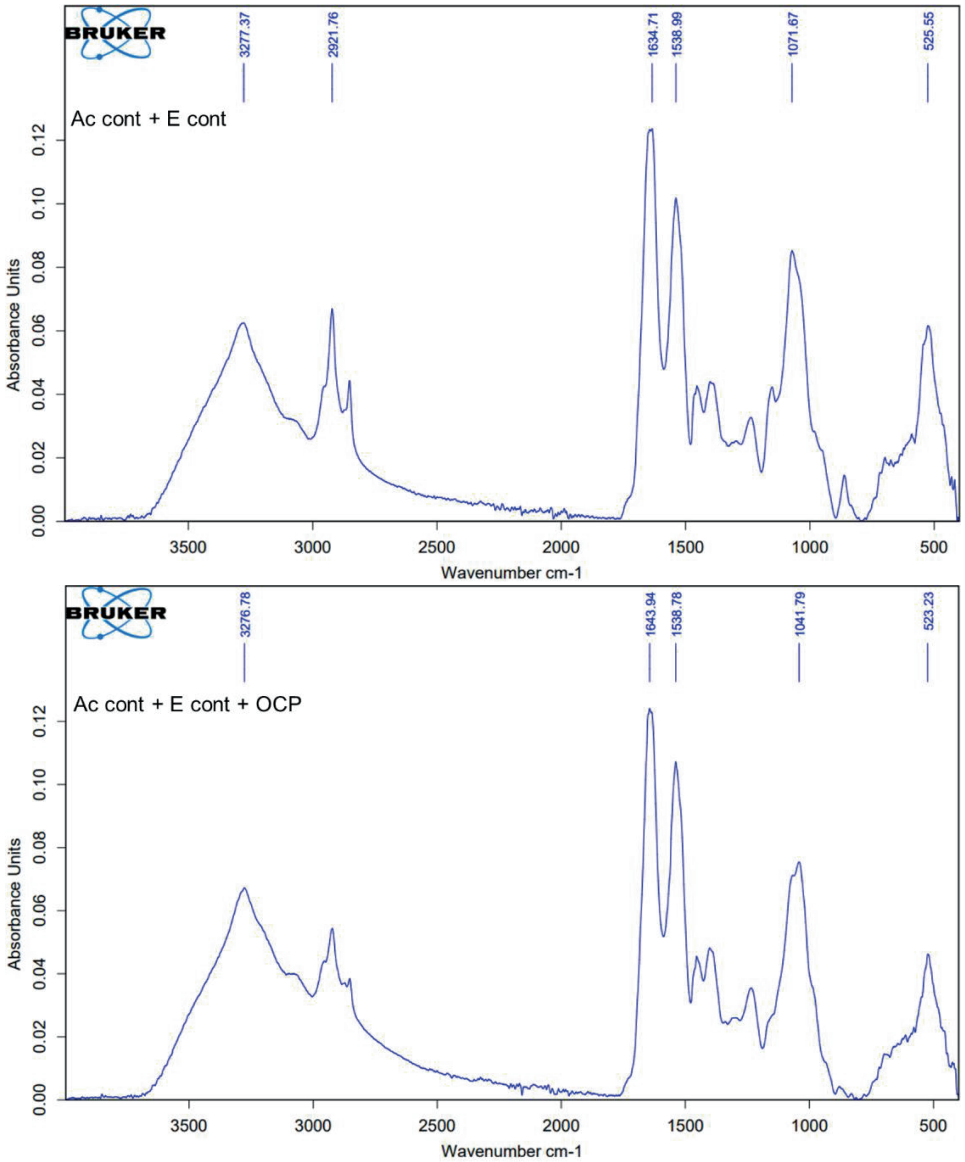
BRUKER
3277.37
2921.76
1634.71
1538.99
1071.67
525.55
Ac cont + E cont
Absorbance Units
0.00
0.02
0.04
0.06
0.08
0.10
0.12
3500
3000
2500
2000
1500
1000
500
Wavenumber cm-1
BRUKER
3276.78
1643.94
1538.78
1041.79
523.23
Ac cont + E cont + OCP
Absorbance Units
0.00
0.02
0.04
0.06
0.08
0.10
0.12
3500
3000
2500
2000
1500
1000
500
Wavenumber cm-1

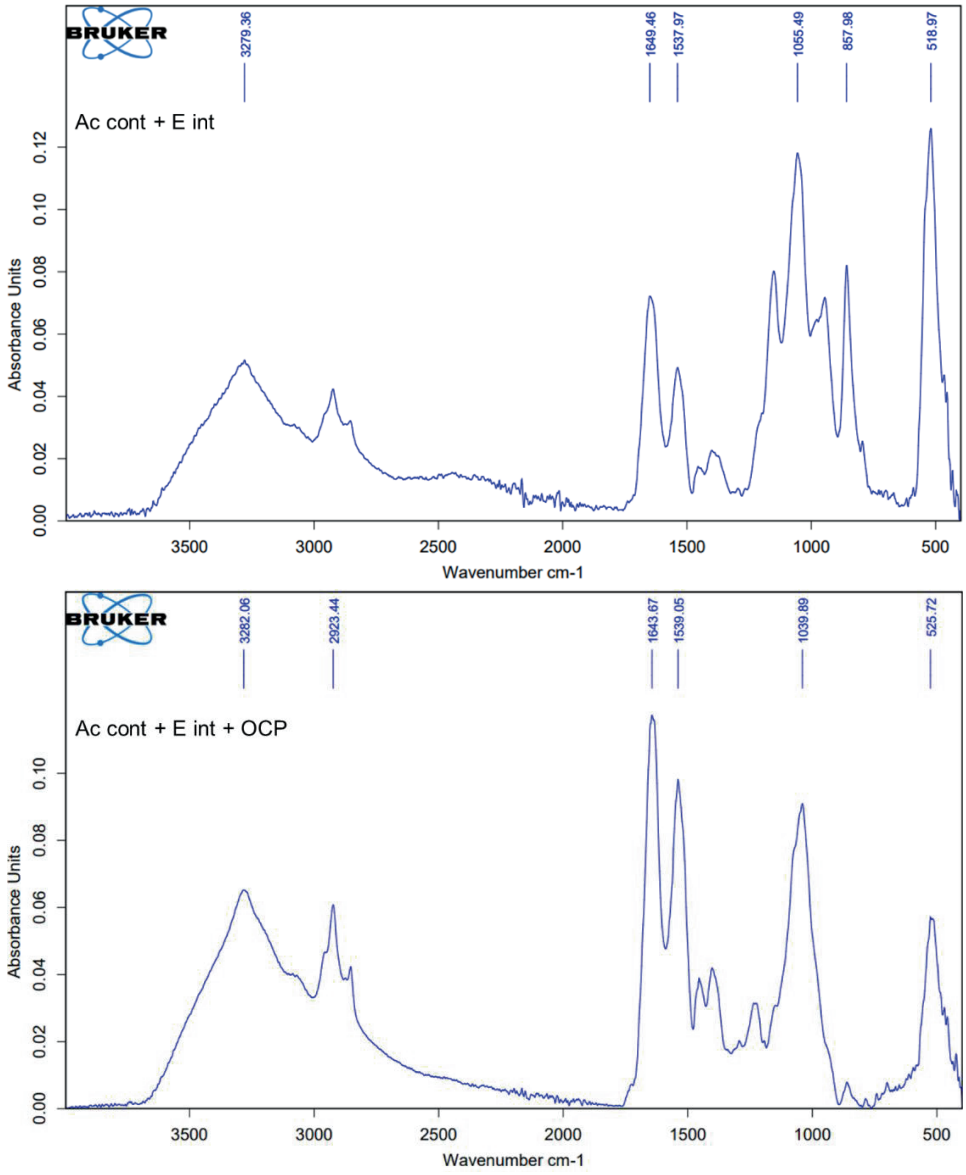

Figure 6.C1. Absorbance spectra for the continuously fed EABfs (Ac cont) grown under both a continuous (E cont) and an intermittent (E int) anode potential, before and after the three-hour OCP periods. All spectra underwent a baseline correction (Rubberband correction method), vector normalization, and finally an offset correction – a sensitivity of 20 % was used for the peak picking (OPUS 8.5).

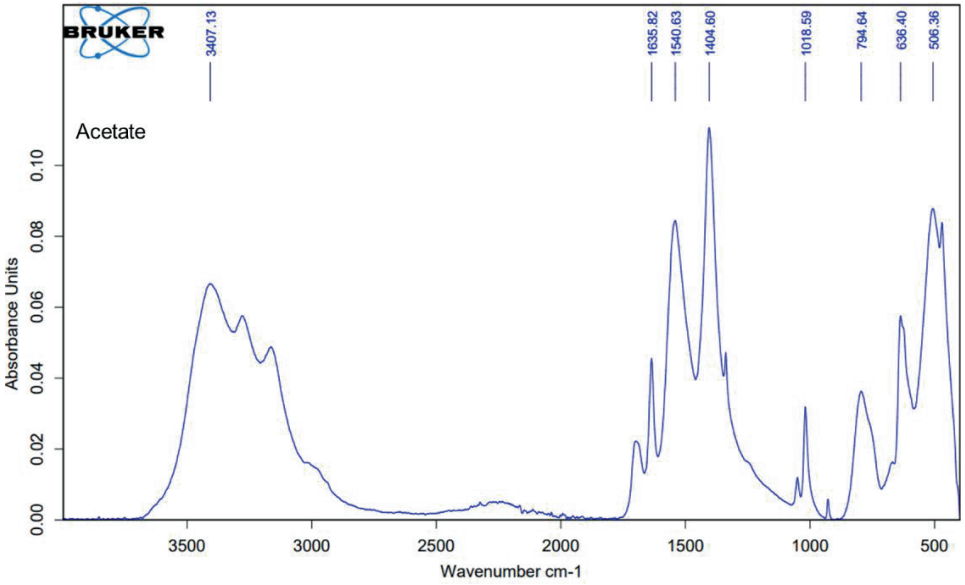
BRUKER
Acetate
3407.13
1635.82
1540.63
1404.60
1018.59
794.64
636.40
506.36
Absorbance Units
0.00
0.02
0.04
0.06
0.08
0.10
3500
3000
2500
2000
1500
1000
500
Wavenumber cm-1

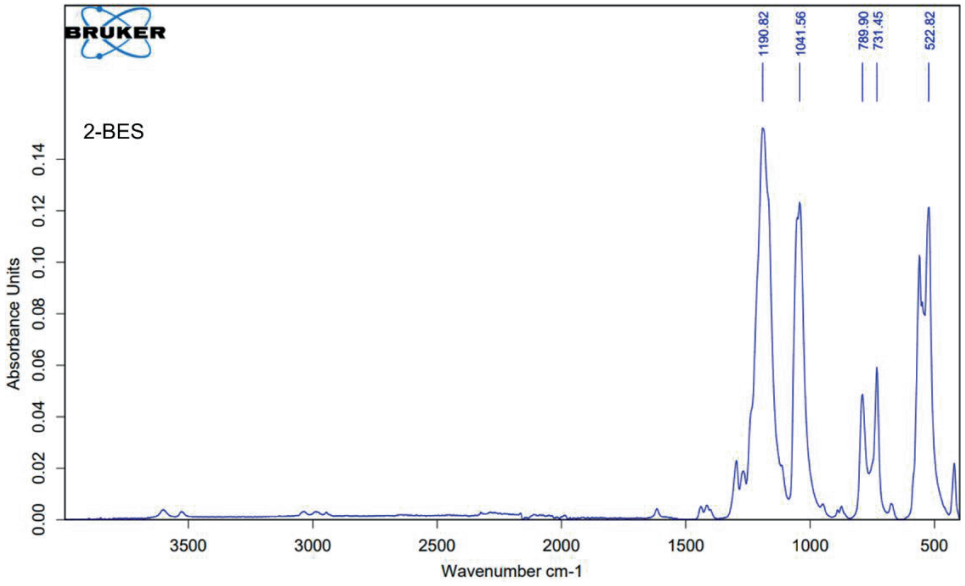
BRUKER
2-BES
1190.82
1041.56
789.90
731.45
522.82
Absorbance Units
0.00
0.02
0.04
0.06
0.08
0.10
0.12
0.14
3500
3000
2500
2000
1500
1000
500
Wavenumber cm-1

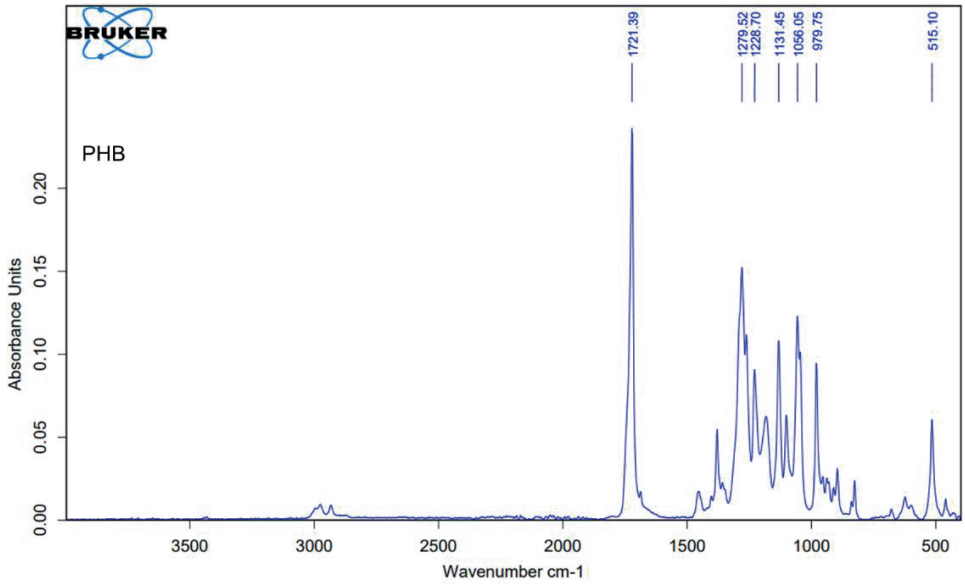

Figure 6.C2. Absorbance spectra for acetate, 2-BES, and PHB powders. All spectra underwent a baseline correction (Rubberband correction method), vector normalization, and finally an offset correction – a sensitivity of 20 % was used for the peak picking (OPUS 8.5).

D. The effect of anode potential regimes and acetate feeding mode on the microbial community in the EABfs

Besides *Geobacter*, other anaerobic genera were found in the mixed culture of EABfs for the different operating conditions tested. For the continuously fed EABfs, an increase in *Desulfovibrio* was observed after the OCP period for the EABf grown under a continuous anode potential, as well as more *Azoarcus* was observed after the OCP period for the EABf grown under an intermittent anode potential. The presence of *Desulfovibrio* could be related to the reduction of residual sulphate present in the anolyte[53] whereas the presence of *Azoarcus* (as well as *Dechlorosoma*) could be related to the reduction of nitrate present in the anolyte.[54] Due to the use of alternative electron acceptors, the relative abundance of these two genera increased in the EABfs that grew with the anode available as final electron acceptor for shorter times (OCP and intermittent anode regime). For the batch fed EABfs, more *PHOS-HE36* was found after the starvation period for both anode potential regimes, and *Petrimonas* was mainly found in the EABfs grown under an intermittent anode potential. Similar to *Desulfovibrio*, *Azoarcus*, and *Dechlorosoma*, these genera may also have thriven due to the presence of residual sulphate in the anolyte when the anode was not available as final electron acceptor.[55–58] Finally, some other genera such as *Sphaerochaeta* and *Lentimicrobium* are composed of fermenters that could have used the polysaccharides present in the EPS to grow and remain part of the microbial community of the EABfs.[59–62]

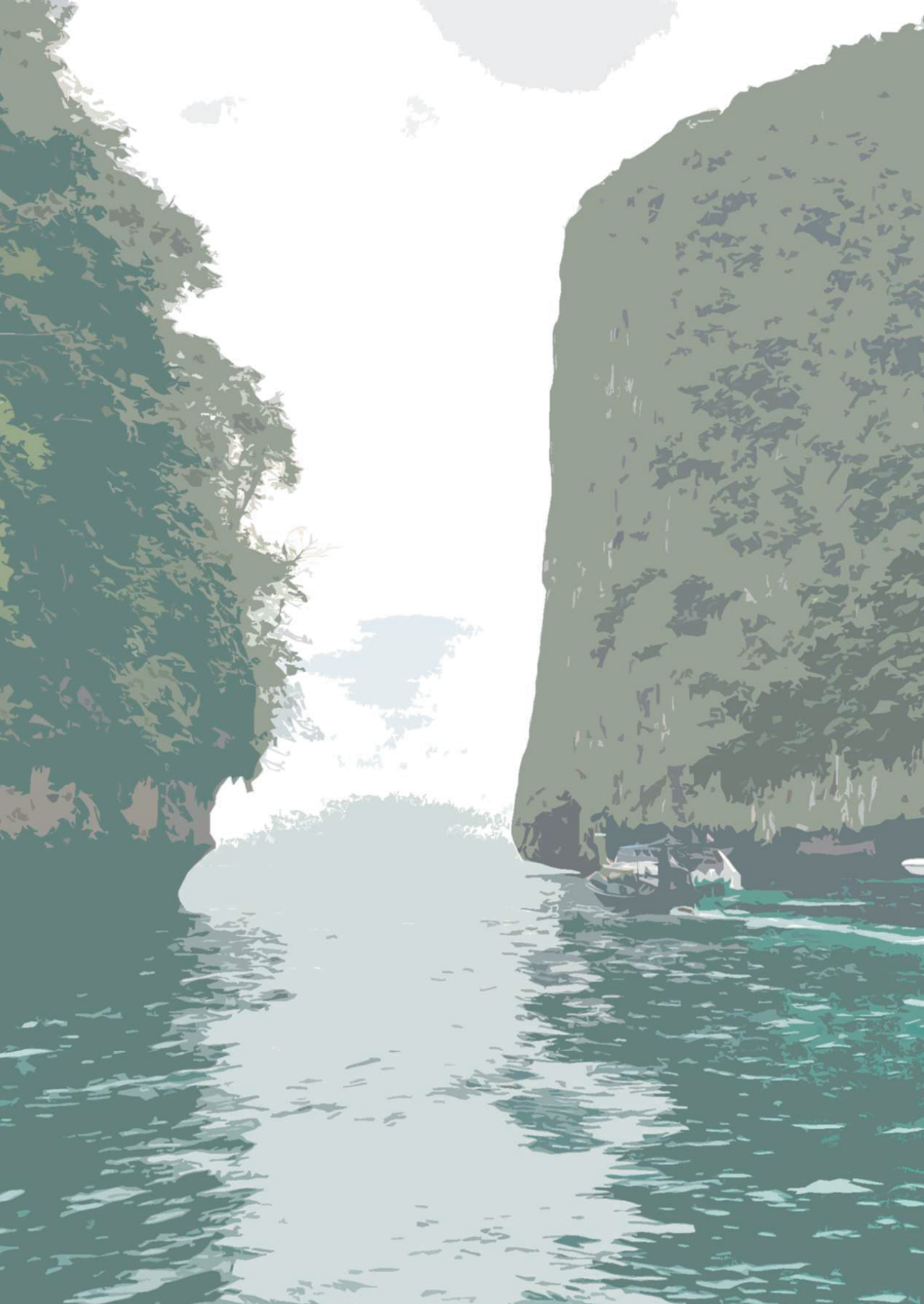

7 General discussion and outlook

In this final chapter, a general discussion on visual techniques and possible applications of anodic EABfs will be given. Firstly, the visual techniques used in this thesis and how these can be applied in future studies on anodic EABfs will be discussed. Secondly, the growth of the EABf and strategies to manage the thickness of EABfs will be addressed, and a case study in which an anodic EABf is used to recover energy from real acetate-containing waste streams will be shown. Finally, a brief reflection on possible metabolic pathways to form EPS and PHA and future applications for low current producing anodes will be discussed.

In this thesis, the importance of measuring the thickness and quantifying electron storage in anodic EABfs to better understand their performance and produced current has been reported. It has been shown that the combination of different types of measuring techniques to characterize EABf growth and composition can provide a more complete insight into the performance of anodic EABfs. With OCT and CLSM, the effect of EABf thicknesses, and associated acetate and buffer diffusion limitations, on produced currents was studied, as well as how the electron donor and acceptor conditions can influence electron storage in anodic EABfs.

7.1. Visual techniques and prospects for future research

In this thesis, OCT and CLSM were frequently used to measure the thickness of EABfs on the anode and to gain more insights into the relationship between operating conditions and electron storage in anodic EABfs. Table 7.1 shows a summary of the techniques and their use to characterize EABfs.

Table 7.1. List of visual techniques used in this thesis and their application to characterize anodic EABfs.

Chapter	Technique	EABfs characterization
3 and 4	OCT	Amount of EABf and mass transfer limitations
5	OCT	Amount and morphology of EABfs
6	CLSM	Cells viability and quantification of electron storage

The non-invasive use of OCT provides a unique advantage to study mass transfer limitations as the produced current can be related to the amount of EABf on the anode. This allows to distinguish the phase in which EABf growth leads to increasing currents from the phase in which EABf growth does not result in increasing currents – indicating mass transfer limitations. While quantification and morphology can be performed with OCT, a more targeted visualization of the composition of EABfs requires another visual technique such as CLSM. This technique allows to identify, for example, storage compounds present in the EABfs and to study the viability of microorganisms.

Even though both visual techniques provided relevant information about the development and shape of the anodic EABfs, more research can be done to further understand the relation between anodic growth and composition and the produced currents at the anode. In the following, two different approaches using CLSM will be discussed to: 1) understand changes in EABf density as a function of time and 2) quantify and identify species responsible for electron storage. Even though being specific for anodic EABfs in this context, these approaches can also provide relative information for other biotechnologies without electrodes, such as aerobic granules sludge, to better understand the effect of biofilm growth, density, and storage, on biological conversions.

7.1.1. EABfs density and its relation to produced current at anodes

The validity of using OCT as a tool to quantify the amount of EABf on the anode was confirmed by calculating the density of the EABf (using COD measurements of the EABf

and relating it to the volume measured with OCT) when other conditions were used rather than the ones previously reported in the method development described in Molenaar et al., 2018. Even though these densities were always similar to the density previously reported (0.154 $g_{COD\ EABf}/mL_{EABf}$), these expressed the overall EABf density and not the density over the height of an EABf (i.e., over the layers of microorganisms present in one EABf). Monitoring the density of the EABfs as a function of their distance to the anode can also provide valuable information that can be used to further understand mass transfer and electron transfer limitations. It is expected that denser EABfs have a better electron transfer due to the lower distance between microorganisms, but, as these have less porous matrices, this can result in higher mass transfer resistances.

As microorganisms start to attach to the anode and developing an EABf, the initial density is high at the interphase between the anode and the EABf. This high density is also linked to the typical exponential current increase and peak current obtained during the first few days when anodic EABfs are grown under chronoamperometric control. As more microorganisms grow and when the anode surface is fully covered, microorganisms will accumulate on top of the first microorganisms' layer. This process will be repeated until the access to the electron donor by the first layers of microorganisms become limited. As reported in Chapter 3, the EABf at this point can range from 10-30 μm depending on the acetate and anode potential. As the EABf keeps growing and acetate becomes limiting, an unequal growth over the height of the EABf is expected, and thus a shift in density inside the EABf. The bottom layers that are acetate limited are likely to stop growing, as opposed to the top microorganisms' layers where acetate is available. Consequently, the initial high EABf density in the bottom layers of the EABf shifts to the upper layers, which adds up resistance for acetate to diffuse towards the inside of the EABf, affecting thus the viability of the microorganisms close to the anode. When these microorganisms become depleted in acetate, and do not have any stored compounds that can be used as carbon source, they will die, and their membranes are likely to lyse. This decreases the number of living microorganisms close to the interphase between the anode and the EABf, decreasing EABf density at the interphase electrode-EABf due to both the absence of growth and the spreading of microbial material in the EABf matrix. On the contrary, the microorganisms in the top layers of the EABfs are likely to remain alive and growing, as these microorganisms have access to acetate and can still use the anode as final electron acceptor via nanowires or via the redox compounds of the underneath conductive layers of microorganisms. As the distance between the dense EABf layers and the anode increases, and as direct electron transfer between the top layers of the microorganism and the anode is not feasible, the electron transfer rate decreases, causing lower current densities at the anode. This decrease in current as the thicker EABf were measured on the anode is in line with the results reported in Chapter 3. This hypothesis on the

dynamic of EABf growth focussed on the access to the anode as final electron acceptor and acetate as electron donor. However, this is consistent with what was reported in Chapter 4 on the importance of buffer to diffuse protons out of the EABf. Higher protons concentrations are present in the layers in which more acetate is converted, and thus an efficient buffering is needed to guarantee that the use of the anode as final electron acceptor is still energetically favourable for the living microorganisms on the top layers of the EABf.

Surprisingly, even though BESs and their EABfs have been studied for a few decades, there is no consensus on the occurrence of cell viability on the anode and the reasoning for low current outputs. This knowledge on EABfs is crucial, as reaching an agreement on the viability of the bio-catalyser can help properly designed reactors that can thus lead to better performing BESs. A viable methodology to further investigate changes in the viability and density of EABf on an anode using visual techniques is here suggested. To this end, live/dead staining could be used to characterize the viability of the microorganisms over time and extrapolate the EABf density as a function of the distance between the anode surface and as a function of the total EABf thickness on the anode. To elaborate on this approach, when working with mixed cultures containing *Geobacter* species, a probe could be designed to track the positioning of *Geobacter* in the EABf matrix. With this, not only the positioning of *Geobacter* could be related to the measured current at the anode, but also related to the thickness of the EABf on the anode.

7.1.2. Improving electron storage quantification and mapping of species on an anode

In Chapter 6, a pixel ratio of 90 % PHB/cells was found in the anodic EABf in which the relative abundance of *Geobacter* was the highest. Even though this indicates that *Geobacter* was responsible for electron storage in the form of PHB, this cannot be concluded just from the combination of the CSLM and NGS analyses. In order to do so, an overlap between the emission signals of *Geobacter* and PHB using CLSM would be preferable to provide more conclusive results.

The autofluorescence signal of *Geobacter* is very weak, which makes the use of Genetically Modified Organisms (GMO) a more convenient approach for visualisation. With this microbial engineering approach, a fluorescence probe (for instance, Green Fluorescence Protein – GFP) could be added to the plasmid of the *Geobacter* species. Combining the GFP signal with the signal of the dye used to stain PHB (for instance, Nile Red; BOPIDY could not be used as both GFP and BODYPY emit in the green range of the light spectrum) this would allow to prove that PHB was intracellularly stored in *Geobacter* species. However, as intracellular lipophilic inclusions are not the only form of electron storage, targeting heme groups could be an approach to map cytochromes, and using dyes to bind to both proteins and polysaccharides would reveal the presence of storage in the form of EPS. These two last approaches could provide insights into the

concentration of cytochromes in the EABf and where these are located in the EABf, as well as allow to better quantify the total amount of electron storage normalized by *Geobacter* species. Even though this would provide a more complete insight into electron storage in relation to produced current, the choice of the dyes and performing this visualization over time is very challenging.

As a final note on the use of GMOs, this can also be used to more fundamental studies and to increase the current productions by anodic EABfs. When microorganisms are genetically manipulated, genes that are not needed can be silenced, and the desired genes can be engineered to be overexpressed.[2,3] For example, when higher currents are wanted, undesired electron flows and parallel reactions could be silenced, making the system more efficient. Besides, studies with GMOs can also provide more information on the electron transfer mechanism in electro-active microorganisms. Even though this provides fundamental knowledge, constraints are expected when transferring GMOs into real-life applications. An alternative approach towards the same direction, though less efficient than engineering microorganisms, would be to manipulate electrode potentials to grow EABf whose microbial community is dominated by electro-active microorganisms that are enriched in redox carriers and with high performance at exchanging electrons with the anode. This will be explained in section 7.4.

7.2. The growth of anodic EABfs and diffusion limited current production: what are the practical challenges?

In practice, when anodic EABfs are used to recover energy from acetate, it is desired that 1) the electron exchange between the EABf and the anode is fast (high anodic currents), 2) the growth of the EABf on the anode consumes a low fraction of electrons, so that a bigger fraction of electrons can be recorded at the anode, and 3) minimal energy is lost at the anode.

It has been reported in this thesis that even though more positive anode potentials and higher acetate concentrations lead to increasing current densities, current production is limited by the diffusion of acetate and buffer towards the anode when thick EABfs developed on the anode (Chapters 3 and 4). Thus, to guarantee high produced currents, acetate must be homogeneously available throughout all the microorganisms' layers so that the EABf can oxidize and produce current as a whole. When all the microorganisms present in the EABf are actively converting acetate and exchanging the generated electrons with the anode, higher acetate consumption rates can be obtained which can be translated into higher current densities. As opposed, when only a fraction of the EABf has access to acetate, acetate oxidation rates decrease and so does the current.

Besides creating diffusion limitations, the overgrowth of EABf is not wanted as this means that electrons are used for growth, instead of being exchanged with the anode. As such, this decreases the energy efficiency as consequently less energy can be recovered in the form of current or H_2. Thick EABfs generate concentration gradients

but also potential gradients. When direct electron transfer with the anode is not feasible, there are additional resistances that lead to energy losses (in the form of heat for example), decreasing the energy gained by the microorganisms when using the anode as final electron acceptor. Furthermore, when protons are accumulated in the EABf, the oxidation potential of acetate increases (approximately 60 mV per pH unit), leading to even lower overpotentials. Therefore, to still make the anode energetically attractive for the microorganisms, more positive potentials must be applied. However, more positive anode potentials mean more energy input is required.

To conclude, there is a trade-off between produced current and EABfs growth because when more microorganisms grow on the anode, more acerate is consumed and therefore more energy can be recovered at the anode. However, it is thus crucial to control the thickness of EABfs on the anode to avoid diffusion limitations which decrease currents and require higher energy input.

In the next section, strategies to control the EABf thickness on the anode will be discussed. Afterwards, a case study is presented in which the biomass yields reported in this thesis are used to calculate the COD from a wastewater treatment plant that needs to be invested in the growth of EABf, and what is available to be recovered as energy. Finally, the challenges in the application of anodic EABf in real wastewater treatment plants are discussed.

7.2.1. The importance of monitoring and managing EABf thicknesses on electrodes

As shown in Chapters 3 and 4, EABf can grow more than desired leading to mass transfer limitations. This means that the thickness of EABfs needs to be controlled to guarantee that all the layers of microorganisms are active and exchanging the electron from the oxidation of the substrate with the anode. This requires monitoring and controlling the thickness of the EABfs within non limiting ranges, and, in the case of overgrowth, removing the excess layers of microorganisms from the top of the EABf.

Several strategies can be used to keep a thin and fully active EABf (approximately 10-20 μm) on the anode to avoid mass transfer limitations.[4,5] These can be electrochemical – by changing the electrode potential, chemical – by means of chemical compounds that will slow down or impede microbial growth, and mechanical – by scraping off the top layers of the EABf. Electrochemical control of the amount of EABf on the anode can be done by controlling the anode potential at set potential that favour biomass formation, followed by a shift to an anode potential that favours the flow of electrons to the anode (minimizing growth rates).[6–9] With such an approach, biomass yields could be controlled, and the excess amounts of EABf on the anode could be minimized. When desired, the electrode potential could also be changed to cathodic conditions (more negative potentials, i.e., reducing conditions) to allow hydrogen evolution at the electrode, which can lead to the detachment of EABfs from the anode. Even though this

approach would not target the top layers of the EABf, this could be used to remove the mass transfer limited EABfs from the electrode and allow for the regrowth of a new EABf.

The use of toxic chemicals is a common approach to deal with unwanted biofilms.[10] However, toxic chemicals are not a green choice and can also lead to decreasing performances of anodic EABfs, which is not intended. Therefore, biocompatible chemicals are ideal as these would allow the EABfs to keep converting organic energy into electric energy, while avoiding overpopulating the anode surface. One example of such an approach is to use quorum sensing equivalent compounds.[11] Quorum sensing is proposed to be a way microorganisms communicate with each other, and thus, perturbing this communication can affect their interaction and reproduction. When microorganisms are surrounded by a high amount of quorum sensing molecules, an indication of a densely populated area is perceived, meaning that microorganisms will not grow as much as when embedded in a low concentration of quorum sensing molecules. Therefore, the addition of these chemicals could be used to prevent the overgrowth of microorganisms in EABfs, preventing mass transfer limitations. In fact, this strategy has been tested and it has been suggested to stimulate defensive mechanisms of EABfs towards unfavourable external conditions (for example, high salinities) that lead to more resilient EABfs and high performing bio-anodes.[12,13]

A less costly approach would be the regular removal of the top layers of the EABf by means of a scraper. This has not only the advantage of avoiding mass transfer limitations, but it can also play a role in the microbial community present in the EABf.[14] It has recently been reported that by repeatedly removing the top layers of an anodic EABfs, *Geobacter* became more and more dominant in the microbial community. Controlling the thickness of the EABf is thus a way to steer the microbial community in anodic EABf. Alternatively, and also using a mechanical/hydraulic approach, the shear force due to the flow of the anolyte can also be used to control the thickness of the EABf on the anode. Higher shear forces will limit EABf growth, keeping a thin and a theoretically more dense EABf on the anode. As previously discussed, a thin and dense EABf can bring advantages regarding current output. However, it should be taken into account that managing the shear force as an EABf develops on the anode is required, because high shear stress can hinder growth and lead to detachment.

Even though this thesis focussed on anodic EABf, monitoring and managing EABf thicknesses can also be applied to cathodic EABfs (Figure 7.1). In a bio-cathode (EABfs on a cathode), energy is used to synthesize compounds of interest ranging from acetate, that can be used as raw materials for synthesis of bioplastics and food, to long chain fatty acids or methane that can be used as biofuel.[15] For this, CO_2 and protons need to be available for the microorganisms that will take up the electrons from the electrode (or from soluble hydrogen in case hydrogen evolution happens at the cathode and/or

is externally provided to the microorganisms) and will use them in anabolic metabolisms towards the formation of the desired compounds.

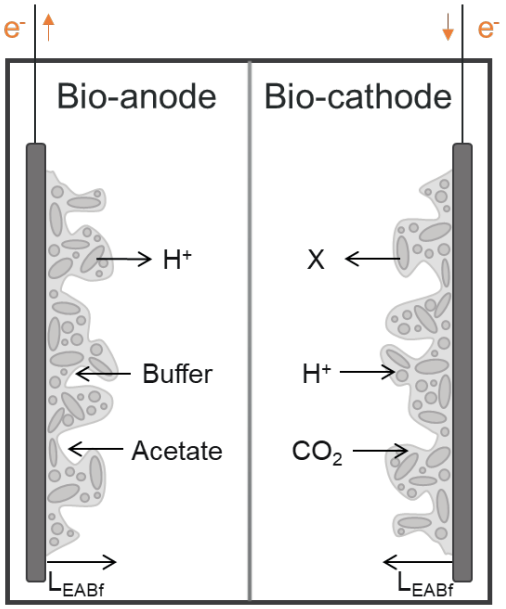

Figure 7.1. Schematics of the diffusion of reactants and products in and out of EABfs. In anodic EABfs, acetate needs to get in the EABf to be oxidized and buffer is needed to diffuse the protons out of the EABf. In cathodic EABfs, CO_2 and protons need to diffuse in the EABf to be reduced to X (for example, acetate, butyrate, methane), that should then diffuse out of the EABfs to be recovered as desired product.

In cathodic EABfs, just like in anodic EABfs, it is important to consider concentration gradients through the thickness of the EABfs, as well as the diffusion of CO_2, protons, and desired products in and out of the cathodic EABf. Therefore, measuring EABf amounts in real-time can be beneficial to study mass transfer limitations in cathodic EABfs, and also to determine product yields.

In summary, by controlling the thickness of the EABfs on electrodes, mass transfer limitations can be minimized, and the output of the system would thus be optimized. This relies on creating a more homogeneous environment in the EABfs, that favours the desired biological conversions to take place, resulting in higher Coulombic efficiencies and energy efficiencies in both anodic and cathodic EABfs.

7.2.2. Case study – anodic EABfs and their application in wastewater treatment plants

The application of anodic EABfs in wastewater treatment plants (WWTPs) was chosen as a case study to be discussed in this chapter due to ability of generating energy from waste streams. This is the case for MFC in which energy is generated in the form of

current, but also the case for MECs in which H_2 is produced at the cathode. Either technology relies on the EABf that grows on the anode and can be applied in wastewater treatment plants to recover energy from waste streams, and thus having a very important impact on the environment by stimulating a circular economy.

7.2.2.1. Biomass yields and (organic) energy used for biomass growth

In the experiments performed in the scope of this thesis, EABfs were grown at low anode potentials to guarantee relatively high cell voltages when translated to an MFC and to require lower energy input when using MECs for H_2 production. In these experiments, a maximum thickness of approximately 80 µm was obtained. Even though a synthetic growth medium was used, this will be considered as a maximum EABf thickness (L_{bio}) on the anode surface in this case study. Using the conversion factor of ρ_{EABf}=0.154 $g_{COD\ EABf}/mL_{EABf}$ and assuming the lowest biomass yield reported in this thesis (approximately $Y_{X/S}$=2 %, in Chapter 5), this would mean that approximately X=616 $g_{COD}/m^2_{anode\ area}$ from a wastewater treatment plant would be required to grow such an EABf (Equation 7.1).

$$X\left(\frac{g_{COD}}{m^2}\right) = \frac{L_{bio}\,(cm) \times \rho_{EABf}\left(\frac{g_{COD\ EABf}}{cm^3}\right)}{Y_{X/S}} = \frac{80\times10^{-4}\times0.154}{0.02} = 616\ \frac{g_{COD}}{m^2} \qquad \text{(Eq. 7.1)}$$

Considering a wastewater treatment plant with an average organic concentration of C=0.4 g_{COD}/L (equivalent to roughly 372 $mg_{acetate}/L$ or 6.3 mM) [16] and a MFC prototype as described in Hiegemann et al., 2019 (anode area, A_{anode}=4.2 m^2, processing F=114 L/day), only 16 % of the COD content in the waste stream would be used for the growth of a 80 µm EABf (Equation 7.2).

$$\frac{COD_{EABf}}{COD_{total}} = \frac{X\left(\frac{g_{COD}}{m^2}\right)\times A_{anode}\,(m^2)}{C\left(\frac{g_{COD}}{L}\right)\times F\left(\frac{L}{day}\right)\times 365\,(day)} \times 100 = \frac{616\times4.2}{0.4\times114\times365}\times 100 = 15.5\ \% \qquad \text{(Eq. 7.2)}$$

This percentage is intentionally overestimated, as in ideal cases only roughly 20 µm thick EABfs are wanted on the anode surfaces to avoid mass transfer limitations, and higher biomass yields can be obtained depending on the operating conditions (roughly 10 %, in this thesis), which both would decrease the percentage of COD need to growth an EABf to approximately 3-4 %. This estimation shows that a little fraction of the available COD is required for EABf growth, and that a bigger fraction could be recovered as energy. It is here made clear that the electrons spent in the growth of EABf are not the limiting process for the application of anodic EABfs in wastewater treatment plants. Other factors such as the treatment capacity (a small plant would need to treat approximately 8000 $m^3/L/d$ [16]), the reactor design towards optimal power densities, the prevention of excess growth of biomass (to avoid acetate and buffer limitations, as discussed in chapters 3 and 4), and the presence of other species (competition with methanogenesis) and oxygen also need to be considered to turn MFCs and/or MECs into a more competitive energy producing technology.[18,19]

7.2.2.2. Complexity of real wastewater streams

In this thesis, all the experiments were performed under controlled conditions and with a synthetic growth medium. However, in real wastewater treatment plants, more complex streams are present, which will affect the growth and performance of anodic EABfs.[20]

Firstly, the presence of other microorganisms in real waste streams may lead to competing processes and may ultimately decrease the current recovered at the anode. The presence and proliferation of other microorganisms may be stimulated by the different local conditions present in the EABf matrix (as a consequence of overgrowth) and also in solution (as planktonic cells). For example, when present, methanogens will consume acetate (thus competing for substrate) and produce methane (decreasing the current recovered at the anode by producing biogas). Methanogens can though be outcompeted by electro-active microorganisms at low acetate concentrations and higher overpotentials.[21] However, methanogens have the advantage of growing as planktonic cells since, as opposed to electro-active microorganisms, these microorganisms do not use the electrode surface as electron acceptor. Therefore, to circumvent this advantage, it is important that a very low amount of planktonic cells are present. To outcompete planktonic cells, continuous operating modes are preferred, and hydraulic retention times (HRTs) should be shortened. Nevertheless, not all microorganisms will negatively affect the performance of anodic EABfs. The presence of microorganisms that are capable of breaking down complex organic matter (such as glucose) and making acetate available through fermentation will be beneficial to electro-active microorganisms.[22] This synergetic effect has previously been reported as a way to improve power output in MFCs and to increase the hydrogen production efficiency from organic matter, which would otherwise remain as acetate in the sludge.[23–25]

Secondly, the presence of toxic compounds will also affect the growth and activity of EABfs. Even though anodic EABfs have also been proposed to operate as biosensors (being fluctuations in monitored current an indication of the presence of toxic compounds [26,27]), when toxic compounds are already present in the waste stream, EABf will have more difficulties growing and thus recovering acetate into energy.

Finally, the presence of oxygen and other oxidizing compounds (for example sulphates or nitrates) in waste streams will decrease the electron transfer with the anode, as these, when more easily available, can be used as alternative final electron acceptors.[28]

7.2.3. Changing approaches towards more practical applications of anodic EABfs

Some efforts have been made to bring anodic EABfs into practice, while overcoming the known limitations as described before. A good example to circumvent some limitations is the use of selected waste streams, that are more biocompatible and have a more controlled composition (e.g., effluents from food and beverage companies),

instead of their application in diverse and complex effluents in WWTPs. Besides, to meet larger volumes of effluents that need to be treated, a modular approach by using cassettes (or so-called modules) can help increasing the treatment capacity of these systems while saving land area.[29] This is the approach that Aquacycl (in the USA) is using together with an adjusted value proposition that targets reducing costs for waste management, even though the practical efficiencies are far from meeting the ambitions of the researchers in the field of BESs. In fact, it has been reported that CEs between 10-30 % are enough for a MFC operating at an industrial scale.[30] Therefore, this suggests that MFCs do not need to convert all the remaining energy in waste streams into electric energy, but these systems can play a role in reducing the costs related to the operation of waste treatment plants and thus valorising waste towards circularity. This has also already been suggested by other researchers that critically analyzed the integration of MFCs and anaerobic digestors.[19] Without underestimating the relevant engineering efforts to increase the produced currents at the anode, other biotechnological applications, that do not require high current outputs, can be thought and benefit from anodic EABfs. This will be addressed later in this discussion, in section 7.4.

7.3. Reflection on electron storage compounds and thoughts on their application

In chapters 5 and 6, it has been shown that electrons are stored in EABfs as a response to the applied anode potential regimes and feeding modes. This storage was found in the form of EPS and PHA, which are products of interest due to their properties as discussed below.[31–34] Briefly, EPS is characterized as a mix of polysaccharides and proteins that can be used as flocculants or applied as a biopolymer in agriculture (to increase binding capacity and plant growth) or as a component material in the building industries. On the other hand, PHA is a form of energy reservoir in some microorganism, that can be extracted and used to produce (bio)plastics. Due to their microbial production and as these can be produced in wastewater treatment plants, these are biodegradable and sustainable compounds. Therefore, the interest in EPS and PHA is increasing, and recent research is focused on ways of producing, characterizing, optimizing extraction methods and finding applications for these products.[35–37] However, what is not yet fully understood is the metabolic pathway for their microbial production. By combining suggested metabolisms for the production of EPS and PHA,[38,39] a simple schematic of the metabolic pathways was drawn and is presented in Figure 7.2. In this scheme, only the pathway used for the formation of polysaccharides that are part of the EPS is included. It should thus be noted that the synthesis of proteins, the formation of humic acids, and the presence of DNA are not described in Figure 7.2.

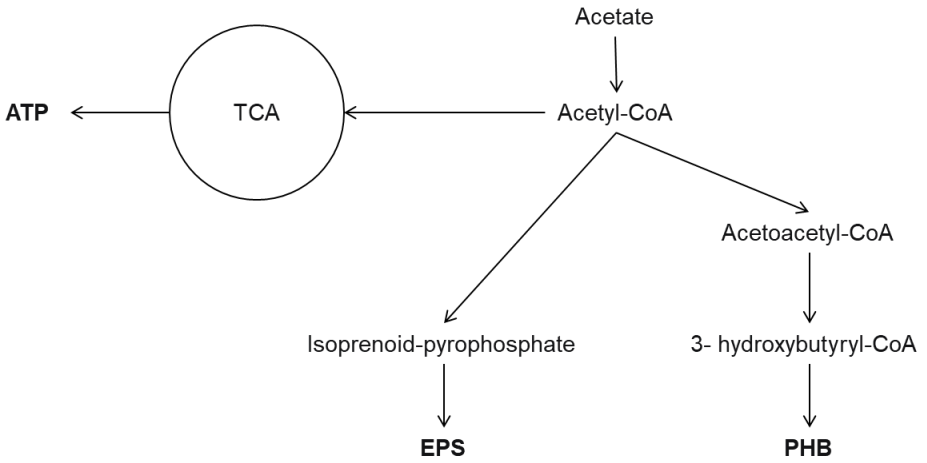

Figure 7.2. Simplistic overview of the metabolic pathways to generate ATP via the TCA cycle, and for EPS and PHB formation from acetate.

From acetate, acetyl-CoA can be formed which can then follow three different pathways: 1) the TCA cycle in which redox compounds are reduced and generate a proton gradient that leads to the production of ATP, 2) towards the formation of isoprenoid-pyrophosphate intermediates to be polymerized to polysaccharidic EPS (or via gluconeogenesis to produce glucose), and 3) combination with another acetyl-CoA and reduced (with NADH) to form 3- hydroxybutyryl-CoA to produce PHB.

Analysing these pathways and due to the presence of phosphate containing intermediates, it seems that EPS production is favoured over PHB production when phosphate is non limiting. In fact, the stimulation of PHB has been reported to the linked to low phosphate availability.[40] However, this is not the only criterium determining the pathway chosen by electro-active microorganisms. Further research is needed to understand how these storage processes are affected, and what role they have in the microorganisms as a response to external environmental conditions.

Besides the external conditions, such as phosphate concentration or nutrient limitations, internal factors also determine whether the production of ATP is more favourable than the production of storage compounds. This is related to the intracellular ratio between oxidized and reduced redox compounds. It has been reported that microorganisms use the production of storage compounds as a way to regulate the ratio of reduced and oxidized redox compounds like NADH/NAD+. When in the presence of more reduced compounds in comparison to oxidized compounds, the synthesis of ATP is stopped as there is a limited amount of oxidized redox compounds available for the deprotonation that happens in the TCA cycle. Besides, this unbalance between reduced and oxidized redox carriers is also hypothesized to be related to the growth rates of microorganisms, as fast growers have less membrane surface available for ATP synthesis, as these grow

bigger (reducing the specific area of the membrane). Therefore, the excess of reduced redox compounds is used to synthesize PHB or EPS,[41–43] and to re-equilibrate the ratio between reduced and oxidized redox compounds. Even though more research is needed to better understand the stimulus behind EPS and PHB production, as well as a more concrete and better defined composition of EPS – which makes it too premature to predict under which conditions their production would be optimal and therefore, how the conditions and results described in this thesis can be transferred to other EPS and PHA producing technologies – it is clear that these metabolisms are affected by the ratio between the electron donor and electron acceptor.[44]

Regardless of the market and desired application, EPS and PHA are not pharmaceutical molecules. These polymers can serve several applications and therefore large amounts are typically preferred. This reflects in microorganisms that need to be filled up with PHA and have high productivities of both PHA and EPS (eventually higher than 20 % of EPS from the acetate converted, as reported in Chapter 5, and 25 % of PHB from the acetate converted, considering that all the acetate that was not used for current production and EABf growth could end up in the form of PHB, estimated from Chapter 6). Besides productivities, and equally relevant to achieve acceptable industrial scale productions of EPS and PHA, the amount of biomass enriched in PHA and producing EPS should be massive. As previously discussed, anodic EABfs (and BESs in general) are not massive biomass producers and, in fact, their performance is sensible to excessive amounts of biomass in the anode. Therefore, there is a low chance BES (here referring to anodic EABfs and extrapolating to the production of these compounds by a cathodic EABf), will significantly contribute to an industrial scale production of EPS and PHA towards applications. However, BESs can be used to further understand production pathways and to study product characteristics as a function of a wide range of operating conditions.

7.4. Future biotechnology with microorganisms that grow on anodes

The low current output from anodic EABfs is a drawback for application. In this thesis, a maximum current density of approximately 4 A/m^2 was obtained. In literature, reported current densities have been increasing from a few A/m^2 up to 400 A/m^2.[45] Wide ranges of reported current densities are often a result of the different ways used to normalize the current recovered at the anode (for example, total or projected area of the electrode), but also a result of the optimization of reactor designs, the use of different substrates and composition of the anolyte, the electrode materials, and the microorganisms used.[46–48] As the electro-active microorganisms are the bio-catalysers, it is thus important to understand how much current one single microorganism can produce to estimate the maximum current density that can be expected. In a study with a single *Geobacter sulfurreducens* microorganism, a maximum current of roughly 90 fA was reported.[49] Assuming a 2×0.5 µm size for *Geobacter sulfurreducens* microorganisms (volume in the order of the $\sim 10^{-19}$ m^3), [50] this yields a volumetric current density of 2.3

A/m^3. When considering a 20 µm thick EABf on the anode – a thickness that was shown in this thesis to lead to the highest current density, as at this thickness current was not limited by mass transfer limitations – a maximum current density of 4.6 A/m^2 is expected. This theoretical current is higher but very similar to the maximum current measured for a 20 µm thick EABf as reported in Chapter 3. As previously discussed, the growth of thicker EABfs causes mass transfer limitations that negatively affect the current density.[51,52] However, when circumventing mass transfer limitations, the thicker the EABf the higher the current density.

Besides mass transfer limitations, other parameters not investigated in this thesis such as internal resistances that decrease the power output in MFCs and require more energy input in MECs, shrink the range of realistic applications for anodic EABfs for energy recovery. However, there are other products/markets of great value that could result in a better fit between the demands and intrinsic features of anodic EABfs. The low current output can be used to meet the requirements of low energy demand sensors such as by the use of sediment MFCs to power sensors for environmental monitoring.[53,54] Besides, low current outputs would have a less negative connotation if anodic EABfs energy could be coupled with the recovery of metals such as copper.[55] Another interesting alternative that can contribute to a circular economy and be more appealing for scaling up is the production of added value compounds.

In the next section, the use of anodic EABf for applications other than energy recovery will be discussed. The use of anodic EABfs for bioremediation and the production of added value compounds with electrofermentation will be covered. Finally, a brief discussion on ways to steer and enrich the composition of EABfs and possible applications thereof will be given.

7.4.1. Applications for low current producing anodes

The application of low current producing electro-active microorganisms may be an obstacle for bigger scale implementation of MFCs. However, there are other biotechnological applications in which these microorganisms can still play an important role. These include bioremediation and bio-electrofermentation.[56]

Bioremediation consists of the biological removal of pollutants from the environment. The pollutants can be present in groundwater and their removal, or neutralization into non-toxic compounds, is essential to keep groundwater as a viable source of freshwater. Microorganisms present in groundwater can degrade pollutants, for example by reducing heavy metals.[54] This degradation is dependent on several factors including temperature, pH, and redox potential. Bioremediation is usually more efficient under aerobic conditions when oxygen is used as final electron acceptor. However, in groundwater, access to oxygen can be limited, decreasing degradation rates. The use of electrodes to interfere in bioremediation is gaining momentum as electrodes can be used to control the redox conditions, and therefore, favour the biological degradation

of pollutants. Here, the main purpose is the removal of pollutants by providing optimal conditions for biological conversions. Therefore, the electrons exchanged with the anode (when used as final electron acceptor after the biological oxidation of pollutants, but also with the cathode in case of biological reduction of pollutants) are less relevant. Besides this potential application for bioremediation, electrodes can also be used to better understand the effect of the redox conditions on microorganism growth and the removal mechanisms (whether via biological degradation and/or absorption).

Bio-electrochemical driven fermentations are another application in which the use of low current producing microorganisms can be beneficial. Fermentation typically leads to less biomass growth as less energy is generated (for example, two mols of ATP per mol of glucose), but it helps microorganisms to regulate their redox state by yielding reduced products such as succinate, formate, acetate, lactate, and ethanol. These have added value and can be used as feedstocks for chemical industries.[57] However, the desired productivity and chemical composition of fermentation products can sometimes be limited by the redox conditions present in the fermenter.[58] In the light of the previous example, also in bio-electrofermentations, the current output is not the most important system performance parameter but rather the steering of the fermentative process towards higher carbon efficiencies between substrate and desired product. Some recent research has been focussed on discovering the suitable combination of fermentative microorganisms and their synergic behaviour in mixed cultures with low current producing microorganisms, and how the productivities and produced products are affected by the anodic conditions.[59]

7.4.2. Tailoring biomass and microbial composition with electrodes and possible applications thereof

As shown in Chapters 5 and 6, the interaction between electro-active microorganisms and electrodes can be manipulated by controlling the set electrode potential and the electrode potential regimes. As EABfs respond to the provided conditions, electrodes can be used to “train” microorganisms to perform a desired conversion and/or to be enriched in wanted components. For example, intermittent anode potential has been shown to increase the concentration of charge carriers in the matrix of the EABfs.[60] Theoretically, this EABf should thus have better electron transfer from the microorganisms to the electrode when compared to an equivalent amount of EABf containing less charge carriers. Besides their composition, controlling electrode conditions can also steer the microbial community present in the EABf, which can be used as a selective process to promote the dominance of a given genus in the EABfs (when no limitations occur, meaning that the electrode conditions are homogeneous in all EABf layers). After growing such a “customized” EABf, its biomass could then be integrated into another process to perform desired biological conversions the biomass “was trained for”. The same light of thinking applies to EABfs enriched in components of interest such as charge carriers (here not considered PHB and EPS due to the

discussed biomass limitations), or microorganisms of interest (such as EABfs enriched in *Geobacter*).

Finally, the biomass of EABfs has intrinsic properties that are independent of the type of microorganisms, their viability, and, to a certain extent, their composition. EABfs have electrical properties, meaning that their biomass is conductive. As such, this biomass could be applied as a conductive material. Even though this is still in an embryonic stage, the conductive biomass of EABfs has been proven to be able to power wearables.[61] The advantage of such an application is that only the biomass of the EABfs is used, easing the requirement of keeping EABfs active and viable by feeding and providing suitable electrode conditions.

7.5. References

1. Molenaar, S. D. *et al.* In situ biofilm quantification in bioelectrochemical systems by using optical coherence tomography. *ChemSusChem* **11**, 2171–2178 (2018).
2. Lovley, D. R. & Walker, D. J. F. Geobacter Protein Nanowires. *Front. Microbiol.* **10**, (2019).
3. Jiménez Otero, F. *et al.* Evidence of a Streamlined Extracellular Electron Transfer Pathway from Biofilm Structure, Metabolic Stratification, and Long-Range Electron Transfer Parameters. *Appl. Environ. Microbiol.* **87**, (2021).
4. Renslow, R. S., Babauta, J. T., Majors, P. D. & Beyenal, H. Diffusion in biofilms respiring on electrodes. *Energy Environ. Sci.* **6**, 595–607 (2013).
5. Picioreanu, C., van Loosdrecht, M. C. M. & Heijnen, J. J. Modelling and predicting biofilm structure. *Cell* **35**, 1–57 (2000).
6. Aelterman, P., Freguia, S., Keller, J., Verstraete, W. & Rabaey, K. The anode potential regulates bacterial activity in microbial fuel cells. *Appl. Microbiol. Biotechnol.* **78**, 409–418 (2008).
7. Picioreanu, C., Head, I. M., Katuri, K. P., van Loosdrecht, M. C. M. & Scott, K. A computational model for biofilm-based microbial fuel cells. *Water Res.* **41**, 2921–2940 (2007).
8. Scarabotti, F., Rago, L., Bühler, K. & Harnisch, F. The electrode potential determines the yield coefficients of early-stage Geobacter sulfurreducens biofilm anodes. *Bioelectrochemistry* **140**, 107752 (2021).
9. Brožková, I. *et al.* Electrochemical Control of Biofilm Formation and Approaches to Biofilm Removal. *Appl. Sci.* **12**, (2022).
10. Azeredo, J. *et al.* Critical review on biofilm methods. *Crit. Rev. Microbiol.* **43**, 313–351 (2017).
11. González-Rivas, F., Ripolles-Avila, C., Fontecha-Umaña, F., Ríos-Castillo, A. G. & Rodríguez-Jerez, J. J. Biofilms in the Spotlight: Detection, Quantification, and Removal Methods. *Compr. Rev. Food Sci. Food Saf.* **17**, 1261–1276 (2018).
12. Chen, S., Jing, X., Tang, J., Fang, Y. & Zhou, S. Quorum sensing signals enhance the electrochemical activity and energy recovery of mixed-culture electroactive biofilms. *Biosens. Bioelectron.* **97**, 369–376 (2017).
13. Zhou, S. *et al.* Protection of electroactive biofilms against hypersaline shock by quorum sensing. *Water Res.* **233**, 119823 (2023).

14. Yan, X. *et al.* Long-Term Succession Shows Interspecies Competition ofGeobacterin Exoelectrogenic Biofilms. *Environ. Sci. Technol.* **55**, 14928–14937 (2021).

15. Kracke, F., Vassilev, I. & Krömer, J. O. Microbial electron transport and energy conservation - The foundation for optimizing bioelectrochemical systems. *Front. Microbiol.* **6**, 1–18 (2015).

16. Korth, B., Heber, C., Normant-Saremba, M., Maskow, T. & Harnisch, F. Precious Data from Tiny Samples: Revealing the Correlation Between Energy Content and the Chemical Oxygen Demand of Municipal Wastewater by Micro-Bomb Combustion Calorimetry. *Front. Energy Res.* **9**, 1–8 (2021).

17. Hiegemann, H. *et al.* Performance and inorganic fouling of a submergible 255 L prototype microbial fuel cell module during continuous long-term operation with real municipal wastewater under practical conditions. *Bioresour. Technol.* **294**, (2019).

18. Tharali, A. D., Sain, N. & Osborne, W. J. Microbial fuel cells in bioelectricity production. *Front. Life Sci.* **9**, 252–266 (2016).

19. Pham, T. H. *et al.* Microbial fuel cells in relation to conventional anaerobic digestion technology. *Engineering in Life Sciences* vol. 6 285–292 (2006).

20. Lazarova, V. & Manem, J. Biofilm characterization and activity analysis in water and wastewater treatment. *Water Res.* **29**, 2227–2245 (1995).

21. Sleutels, T., Molenaar, S., Heijne, A. & Buisman, C. Low Substrate Loading Limits Methanogenesis and Leads to High Coulombic Efficiency in Bioelectrochemical Systems. *Microorganisms* **4**, 1–11 (2016).

22. Dhar, B. R. & Lee, H. S. Evaluation of limiting factors for current density in microbial electrochemical cells (MXCs) treating domestic wastewater. *Biotechnol. Reports* **4**, 80–85 (2014).

23. Rabaey, K., Boon, N., Höfte, M. & Verstraete, W. Microbial phenazine production enhances electron transfer in biofuel cells. *Environ. Sci. Technol.* **39**, 3401–3408 (2005).

24. Guo, X., Zhan, Y., Chen, C., Zhao, L. & Guo, S. The influence of microbial synergistic and antagonistic effects on the performance of refinery wastewater microbial fuel cells. *J. Power Sources* **251**, 229–236 (2014).

25. Logan, B. E. *et al.* Microbial Electrolysis Cells for High Yield Hydrogen Gas Production from Organic Matter. *Environ. Sci. Technol.* **42**, 8630–8640 (2008).

26. Bonadonna, L., Briancesco, R. & La Rosa, G. Innovative analytical methods for monitoring microbiological and virological water quality. *Microchem. J.* **150**, 104160 (2019).

27. Qi, X. *et al.* An electroactive biofilm-based biosensor for water safety: Pollutants detection and early-warning. *Biosens. Bioelectron.* **173**, 112822 (2021).

28. Logan, B. E., Rossi, R., Ragab, A. & Saikaly, P. E. Electroactive microorganisms in bioelectrochemical systems. *Nat. Rev. Microbiol.* **17**, 307–319 (2019).

29. Sivasankar, V., Mylsamy, P. & Omine, K. *Microbial fuel cell technology for bioelectricity*. *Microbial Fuel Cell Technology for Bioelectricity* (2018). doi:10.1007/978-3-319-92904-0.

30. AlSayed, A., Soliman, M. & Eldyasti, A. Microbial fuel cells for municipal wastewater treatment: From technology fundamentals to full-scale development. *Renew. Sustain. Energy Rev.* **134**, 110367 (2020).

31. Shi, L. L., Da, Y. Y., Zheng, W. T., Chen, G. Q. & Li, Z. J. Production of

polyhydroxyalkanoate from acetate by metabolically engineered Aeromonas hydrophilia. *J. Biosci. Bioeng.* **130**, 290–294 (2020).

32. Oshiki, M., Onuki, M., Satoh, H. & Mino, T. PHA-accumulating microorganisms in full-scale wastewater treatment plants. *Water Sci. Technol.* **58**, 13–20 (2008).

33. Seviour, T. *et al.* Extracellular polymeric substances of biofilms: Suffering from an identity crisis. *Water Res.* **151**, 1–7 (2019).

34. Nouha, K., Kumar, R. S., Balasubramanian, S. & Tyagi, R. D. Critical review of EPS production, synthesis and composition for sludge flocculation. *J. Environ. Sci. (China)* **66**, 225–245 (2018).

35. Jayathilake, P. G. *et al.* Extracellular polymeric substance production and aggregated bacteria colonization influence the competition of microbes in biofilms. *Front. Microbiol.* **8**, (2017).

36. Pei, R. *et al.* Exploring the Limits of Polyhydroxyalkanoate Production by Municipal Activated Sludge. *Environ. Sci. Technol.* **56**, 11729–11738 (2022).

37. Godbole, S. Methods for identification, quantification and charaterization of Polyhydroxyalkanoates - A review. *Res. J. Biotechnol.* **5**, 4977–4983 (2016).

38. Pirog, T. P., Kovalenko, M. A. & Kuz'minskaya, Y. V. Intensification of exopolysaccharide synthesis by Acinetobacter sp. on an ethanol-glucose mixture: Aspects related to biochemistry and bioenergetics. *Microbiology* **72**, 305–312 (2003).

39. Prados, E. & Maicas, S. Bacterial Production of Hydroxyalkanoates (PHA). *Univers. J. Microbiol. Res.* **4**, 23–30 (2016).

40. Haaksman, V. A., Schouteren, M., van Loosdrecht, M. C. M. & Pronk, M. Impact of the anaerobic feeding mode on substrate distribution in aerobic granular sludge. *Water Res.* **233**, 119803 (2023).

41. Sasaki, D., Sasaki, K., Tsuge, Y. & Kondo, A. Less biomass and intracellular glutamate in anodic biofilms lead to efficient electricity generation by microbial fuel cells. *Biotechnol. Biofuels* **12**, 1–11 (2019).

42. Rose, N. D. & Regan, J. M. Changes in phosphorylation of adenosine phosphate and redox state of nicotinamide-adenine dinucleotide (phosphate) in Geobacter sulfurreducens in response to electron acceptor and anode potential variation. *Bioelectrochemistry* **106**, 213–220 (2015).

43. Song, J. *et al.* Comprehensive metabolomic analyses of anode-respiring Geobacter sulfurreducens cells: The impact of anode-respiration activity on intracellular metabolite levels. *Process Biochem.* **51**, 34–38 (2016).

44. Frühauf-Wyllie, H. M. & Holtmann, D. Geobacter sulfurreducens metabolism at different donor/acceptor ratios. *Microbiologyopen* **11**, (2022).

45. Chen, S. *et al.* Layered corrugated electrode macrostructures boost microbial bioelectrocatalysis. *Energy Environ. Sci.* **5**, 9769–9772 (2012).

46. Slate, A. J., Whitehead, K. A., Brownson, D. A. C. & Banks, C. E. Microbial fuel cells: An overview of current technology. *Renew. Sustain. Energy Rev.* **101**, 60–81 (2019).

47. Bird, H., Heidrich, E. S., Leicester, D. D. & Theodosiou, P. Pilot-scale Microbial Fuel Cells (MFCs): A meta-analysis study to inform full-scale design principles for optimum wastewater treatment. *J. Clean. Prod.* **346**, 131227 (2022).

48. Sleutels, T. H. J. A., Ter Heijne, A., Buisman, C. J. N. & Hamelers, H. V. M.

Bioelectrochemical systems: An outlook for practical applications. *ChemSusChem* **5**, 1012–1019 (2012).

49. Jiang, X. *et al.* Probing single- to multi-cell level charge transport in Geobacter sulfurreducens DL-1. *Nat. Commun.* **4**, 1–6 (2013).

50. Caccavo, F. *et al.* Geobacter sulfurreducens sp. nov., a Hydrogen and Acetate Oxidizing dissimilatory metal reducing microorganism. *Appl. Environ. Microbiol.* **60**, 3752–3759 (1994).

51. Pereira, J. *et al.* Real-time monitoring of biofilm thickness allows for determination of acetate limitations in bio-anodes. *Bioresour. Technol. Reports* **18**, 101028 (2022).

52. Pereira, J., Wang, G., Sleutels, T., Hamelers, B. & ter Heijne, A. Maximum thickness of non-buffer limited electro-active biofilms decreases at higher anode potentials. *Biofilm* **4**, 100092 (2022).

53. Ewing, T., Ha, P. T. & Beyenal, H. Evaluation of long-term performance of sediment microbial fuel cells and the role of natural resources. *Appl. Energy* **192**, 490–497 (2017).

54. Erable, B., Duţeanua, N. M., Ghangrekar, M. M., Dumas, C. & Scott, K. Application of electro-active biofilms. *Biofouling* **26**, 57–71 (2010).

55. Heijne, A. Ter *et al.* Copper recovery combined with electricity production in a microbial fuel cell. *Environ. Sci. Technol.* **44**, 4376–4381 (2010).

56. Doyle, L. E. & Marsili, E. Weak electricigens: A new avenue for bioelectrochemical research. *Bioresource Technology* vol. 258 354–364 (2018).

57. Vassilev, I., Averesch, N. J. H., Ledezma, P. & Kokko, M. Anodic electro-fermentation: Empowering anaerobic production processes via anodic respiration. *Biotechnol. Adv.* **48**, 107728 (2021).

58. Schievano, A. *et al.* Electro-Fermentation – Merging Electrochemistry with Fermentation in Industrial Applications. *Trends Biotechnol.* **34**, 866–878 (2016).

59. Virdis, B. *et al.* Electro-fermentation: Sustainable bioproductions steered by electricity. *Biotechnol. Adv.* **59**, (2022).

60. Zhang, X., Prévoteau, A., Louro, R. O., Paquete, C. M. & Rabaey, K. Periodic polarization of electroactive biofilms increases current density and charge carriers concentration while modifying biofilm structure. *Biosens. Bioelectron.* **121**, 183–191 (2018).

61. Liu, X. *et al.* Microbial biofilms for electricity generation from water evaporation and power to wearables. *Nat. Commun.* **13**, 1–8 (2022).

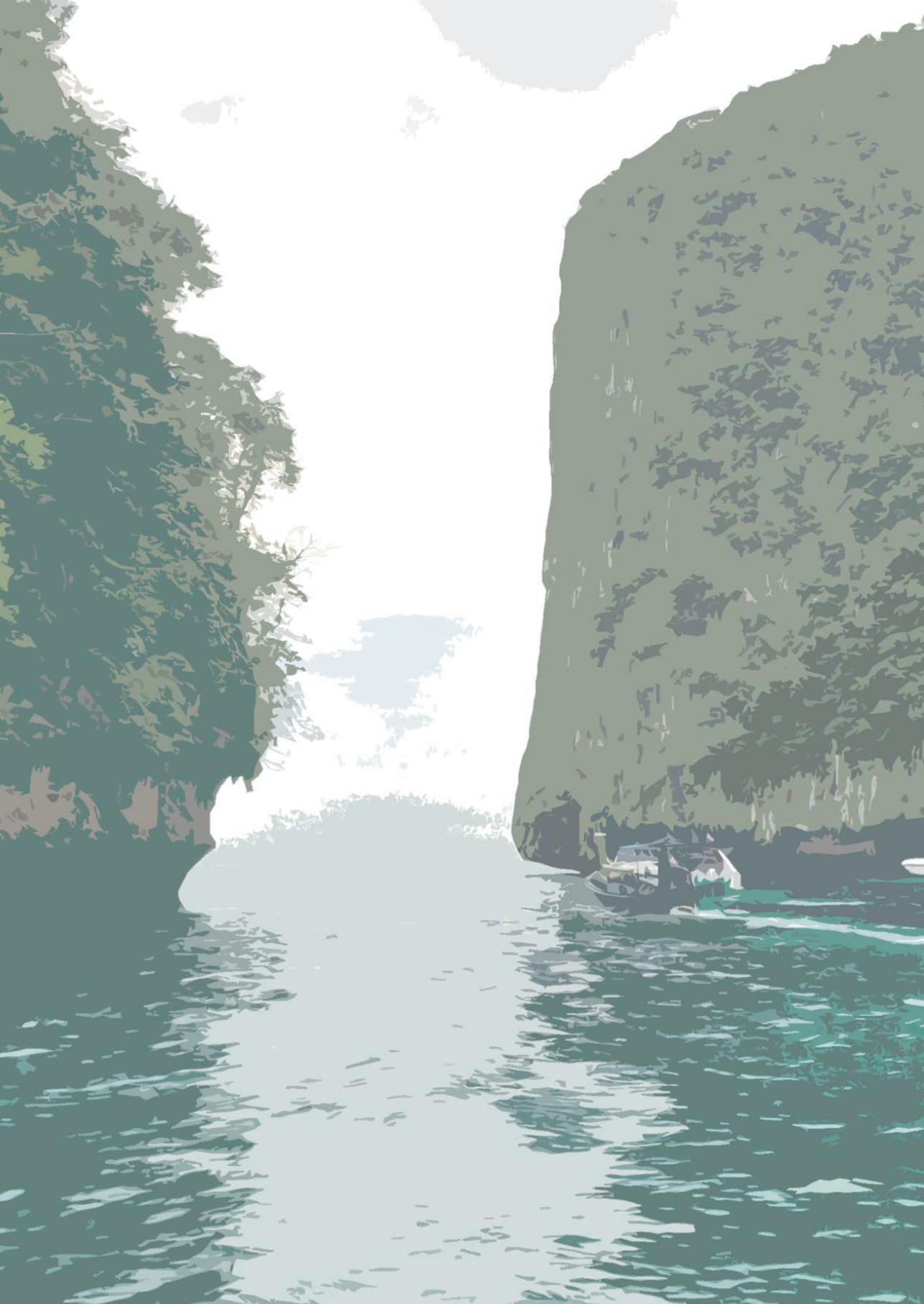

Summary

Bio-electrochemical systems (BESs) have been suggested as a promising technology to help deal with current environmental issues. With these systems, energy and resources can be recovered from waste streams and compounds can be synthesized that can be used as raw materials or as energy storage, thus contributing to a circular economy. The biocatalysts in these systems are named electro-active microorganisms due to their ability to interact with electrodes. Among other factors, the growth and interaction of the microorganisms with the electrode play a crucial role in the performance of BESs.

When growing on an electrode, these microorganisms typically form an electro-active biofilm (EABf). In the anode, EABfs degrade soluble organics and exchange the derived electrons with the anode, which are thus recovered as current. Besides this electron flow, electrons can flow towards different pathways: for example, being used for growth, being stored in the form of biopolymers, and/or end up in alternative electron acceptors rather than the anode. These electron flows can be influenced by the provided operation conditions, which makes measuring electron flows an important assessment to better understand EABf and their performances (details are given in Chapter 1). The aims of this thesis were to understand this interplay between the growth of anodic EABfs and the produced current at the anode, as well as their ability to store electrons.

Several techniques can be used to study EABfs. Due to their electrical features, the use of electrochemical techniques is the most common approach. However, to understand the response of EABfs to operating conditions and their characteristics in relation to performance, more types of techniques are needed. In Chapter 2, visual techniques are introduced as tools to add to the information obtained with electrochemical techniques. With visual techniques, both the amount of EABf on the anode can be quantified and their morphology and composition can be studied. This review chapter stresses the benefits of combining electrochemical and non-destructive visual techniques and highlights the importance of having a closer look at the microorganisms and the EABfs they are embedded in to build more knowledge towards the optimization of BESs.

In Chapter 3, the growth of EABfs was monitored with Optical Coherence Tomography (OCT), and the relation between the current density and the measured thickness of the EABf on the anode was studied under different anode potentials and acetate concentrations. A correlation between increasing current densities (maximum of roughly 4 A/m^2) and EABf thicknesses up to a range between 10-30 μm was found. When thicker EABfs develop on the anode, the current density was limited by the diffusion of acetate inside the EABfs, meaning that not all the microorganisms had access to acetate nor could contribute to current production, resulting in stable or decreasing current. The thickness of EABfs that had access to acetate increased when higher acetate concentrations and when higher anode potentials were used, resulting in higher current densities.

Another important parameter determining produced current is the concentration of protons inside the EABfs. These are generated when acetate is oxidized, and when their concentration increases in the EABfs, the oxidation potential of acetate increases, resulting in lower overpotentials and thus making the use of the anode as the final electron acceptor less energetically favorable. Therefore, protons are diffused out of the EABfs typically by using a buffer. In Chapter 4, the penetration depths of buffer were calculated and related to the thickness of the EABf on the anode at different buffer concentrations. These penetration depths were smaller at higher anode potentials, meaning that the thickness of EABf that contributed to current production became smaller. This was caused by a higher acetate consumption rate obtained at higher anode potentials. In both Chapters 3 and 4, acetate and buffer diffusion rates (in the order of 10^{-10} m^2/s) and acetate consumption rates (between 0.05 and 0.08 $mol_{acetate}/m^3/s$) at different anode potentials were reported that can be used for modeling works in anodic EABfs. Besides, these can be extrapolated to cathodic EABfs and be used as a tool to better understand BESs.

In Chapters 5 and 6, the ability of EABfs to store electrons was explored. In Chapter 5, EABfs were grown under different intermittent anode potential regimes while being continuously fed with acetate. To understand electron storage, an electron balance including electrons recovered at the anode, electrons used for EABf growth (and planktonic cells), and electrons used to produce Extracellular Polymeric Substances (EPS) was set. Even though the current produced by intermittent EABf was comparable to the one produced by continuous EABfs, the intermittent anode potential times longer than 20 seconds led to higher amounts of microorganisms in the planktonic form and increased the amount of EPS in both the anolyte (up to 40 %) and in the EABfs matrices (~0.25 g_{EPS}/g_{EABf}). The produced EPS was enriched in proteins and was used as extracellular electron storage to respond to the intermittent availability of the anode as the final electron acceptor.

In Chapter 6, the effect of the acetate feeding mode on electron storage was studied. To this end, EABfs were grown under continuous and batch feeding modes, while the anode potential was controlled under continuous and intermittent regimes. Electron storage was assessed with Confocal Laser Scanning Microscopy (CLSM) using dyes to visualize EPS and intracellular electron storage compounds (poly-hydroxyalkanoates) in the EABfs. After image processing, a 92 % pixel ratio of poly-hydroxybutyrate (PHB) and microorganisms was found in the EABfs grown under a continuous anode potential after starvation. This intracellular electron storage was linked to the presence of *Geobacter* in the EABfs, and suggested that acetate starvation combined with a constant availability of the anode as the final electron acceptor triggered intracellular electron storage. The two aforementioned chapters open the door to new niches and possible applications of BESs towards the production of EPS and bioplastics.

Finally, after identifying mass transfer limitations and the synthesis of electron storage compounds, Chapter 7 includes a discussion and reflections on the potential applications for anodic EABfs. As high current densities are desired, strategies to overcome diffusion limited currents are discussed and a case study is presented elaborating on EABf growth and foreseen challenges when applying anodic EABfs to real wastewater streams to recover energy and resources. The electron storage mechanisms and the potential application of EPS and PHB produced by anodic EABfs are covered, and some thoughts on future research combining the use of electrodes and visual techniques are shared.

Sumário

Sistemas bio-electroquímicos (SBEs) são uma tecnologia com grande potencial para ajudar a combater problemas ambientais. Com estes sistemas, energia e recursos podem ser recuperados de efluentes, assim como compostos podem ser sintetizados e ser usados como matéria-prima e armazenamento de energia, contribuindo desta forma para uma economia circular. Os biocatalisadores nestes sistemas são chamados microrganismos electro-activos devido á sua capacidade de interagir com elétrodos. Entre outros fatores, o crescimento e interação destes microrganismos com o elétrodo é de extrema importância para a performance dos SBEs.

Quando estes microrganismos crescem num elétrodo, eles tipicamente formam um biofilme electro-activo (BEA). No ânodo, BEAs degradam matéria orgânica e transferem os eletrões derivados desta reação de oxidação com o ânodo, sendo assim recuperados na forma de corrente elétrica. Para além deste fluxo de eletrões para o ânodo, eletrões podem seguir diferentes caminhos: por exemplo, os eletrões podem ser usados para o crescimento dos microrganismos, ser armazenados na forma de bio polímeros, e/ou ser usados por outros aceitadores finais de eletrões que não o ânodo. Estes diferentes fluxos de eletrões podem ser influenciados pelas condições de operação, o que faz com que quantificação e monitorização destes fluxos seja essencial para estudar BEAs e perceber as suas performances. Estes fluxos de eletrões são explicados com mais detalhe no 1° Capítulo. Os objetivos desta tese pretendem perceber a relação entre o crescimento de BEAs e a corrente elétrica produzida, e também explorar a capacidade dos BEAs para armazenar eletrões.

Várias técnicas podem ser usadas para estudar BEAs. Devido às suas propriedades elétricas, o uso de técnicas eletroquímicas é uma abordagem recorrente. Contudo, para perceber a resposta dos BEAs às condições de operação e as suas características em relação á performance, outras técnicas são necessárias. No 2° Capítulo, técnicas de visualização são introduzidas como recursos para adicionar á informação obtida com técnicas eletroquímicas. Com técnicas de visualização, ambas a quantidade de BEAs no ânodo poder ser quantificada e a sua morfologia e composição podem ser estudadas. Este capítulo destaca os benefícios da combinação de técnicas eletroquímicas e técnicas de visualização não destrutivas e realça a importância de prestar mais atenção aos microrganismos e aos BEAs onde eles estão inseridos para criar mais conhecimento para a otimização dos SBEs.

No 3° Capítulo, o crescimento de BEAs foi monitorizado com Tomografia de Coerência Ótica (TCO), e a relação entre a densidade da corrente e a espessura dos BEAs no ânodo foi estudada a diferentes potenciais dos ânodos e concentrações de acetato. Uma correlação entre densidades de corrente crescentes (até aproximadamente 4 A/m^2) e espessura dos BEAs até 10-30 μm foi encontrada. Quando BEAs mais espessos cresceram no ânodo, a densidade da corrente foi limitada pela difusão de acetato para o interior do BEAs, o que significa que nem todo o BEA tinha acesso a acetato e assim

nem todo o BEA pôde contribuir para produzir corrente, o que resultou numa corrente constante ou numa diminuição da corrente. A espessura do BEA com acesso a acetato aumentou quando potenciais de ânodo mais positivos e concentrações de acetato mais altas foram usadas, resultando em maiores densidades de correntes.

Outro parâmetro que determina a densidade da corrente é a concentração de protões dentro dos BEAs. Estes são libertados quando acetato é oxidado, e quando a sua concentração aumenta dentro dos BEAs, o potencial da oxidação de acetato aumenta, resultando em "sobre-potenciais" mais baixos e, consequentemente, tornando o uso do ânodo como aceitador final de eletrões menos energeticamente favorável. Por isso, os protões são tipicamente movidos para o exterior dos BEAs com o auxílio de soluções tampão. No 4° Capítulo, as profundidades de penetração do tampão nos BEAs foram calculadas e relacionadas com a espessura dos BEAs no ânodo a diferentes concentrações de tampão. Estas profundidades de penetração foram mais pequenas quando potenciais de ânodo mais altos foram usados, significando que a espessura do BEAs que contribuiu para a produção de corrente diminuiu. Isto foi causado pelas maiores taxas de consumo de acetato quando potenciais de ânodo mais altos foram usados. Em ambos os 3° e 4° Capítulos, coeficientes de difusão (na ordem dos 10^{-10} m^2/s) e taxas de consumo de acetato (entre 0.05 e 0.08 $mol_{acetato}/m^3/s$) a diferentes potenciais de ânodo foram reportados, e podem ser usados para trabalhos de modelação em BEAs. Para além disso, estes parâmetros podem ser extrapolados para BEAs em cátodos e usados como uma ferramenta para estudar BESs.

Nos 5° e 6° Capítulos, a habilidade dos BEAs para armazenar eletrões foi explorada. No 5° Capítulo, BEAs foram crescidos em vários regimes de potenciais de ânodo enquanto continuamente alimentados com acetato. Para perceber o armazenamento de eletrões, um balanço de eletrões foi estabelecido incluindo os eletrões recuperados no ânodo, os eletrões usados para o crescimento dos BEAs (e células planctónicas), e eletrões usados para produzir Substâncias Poliméricas Extracelulares (SPEs). Apesar a corrente produzida pelos BEAs intermitentes ter sido comparável com a corrente produzida pelo BEAs contínuos, os regimes de potencial de ânodo intermitente mais longos do que 20 segundos resultaram em mais células planctónicas e aumentaram a quantidade de SPEs em solução (até 40 %) e nas matrizes dos BEAs (~0.25 g_{SPE}/g_{BEA}). As SPEs produzidas, ricas em proteínas, foram usadas como um processo de armazenamento de eletrões extracelular como resposta á disponibilidade intermitente do ânodo como aceitador final de eletrões.

No 6° Capítulo, o efeito do modo de alimentação no armazenamento de eletrões foi estudado. Para isto, BEAs foram crescidos em modos de alimentação contínua e batch, enquanto o potencial do ânodo foi controlado em regimes continuo e intermitente. O armazenamento de eletrões foi medido com Microscópio de Varrimento a Laser Confocal (MVLC) usando corantes para colorar e visualizar SPEs e compostos de

armazenamento de eletrões intracelulares (Polihidroxialcanoatos) em BEAs. Depois de processar as imagens obtidas com o MVLC, um rácio de pixéis de 92 % entre polihidroxibutirato (PHB) e microrganismos foi encontrado nos BEAs que foram crescidos com um potencial de ânodo contínuo depois de um período de fome causado pela falta de acetato. Este armazenamento de eletrões intracelular foi relacionado com a presença de *Geobacter* nos BEAs, e sugeriu que a falta de acetato combinada com a constante disponibilidade do ânodo como aceitador final de eletrões estimulou o armazenamento intracelular de eletrões. Os dois últimos capítulos abrem a porta para novas oportunidades e possíveis mercados para a aplicação de SBEs para a produção de SPEs e bioplásticos.

Para concluir, depois de identificar limitações na transferência de massa e a síntese de compostos de armazenamento de eletrões, o 7° Capítulo inclui uma discussão e reflexões nas potenciais aplicações de BEAs em ânodos. Uma vez que altas densidades de corrente são preferidas, estratégias para ultrapassar a produção de corrente limitada por difusão são discutidas, e um "case-study" é apresentado no qual o crescimento dos BEAs e desafios na aplicação de BEAs em ânodos para a recuperação de energia e recursos em efluentes reais são abordados. Os mecanismos para o armazenamento de eletrões e as potenciais aplicações das SPEs e PHB produzidos em BEAs em ânodos são discutidos, e pensamentos para futura investigação combinando elétrodos e técnicas visuais são partilhados.

Samenvatting

Bio-elektrochemische systemen (BES) zijn gesuggereerd als een veelbelovende techniek voor het omgaan met de huidige klimaatproblemen. Met deze systemen kunnen energie en grondstoffen worden teruggewonnen uit afvalstromen en stoffen kunnen worden gesynthetiseerd die kunnen worden gebruikt als ruwe grondstoffen of energie opslag, hierdoor bijdragend aan de circulaire economie. De biokatalysatoren in deze systemen worden elektro-actieve micro-organismen genoemd, vanwege hun capaciteit om met elektrodes te interacteren. Onder andere factoren, spelen de groei en interacties van de micro-organismen met de elektrode een cruciale rol in de werking van BES.

Als de micro-organismen op een elektrode groeien, vormen ze normaliter een elektro-actief biofilm (EABf). In de anode breken EABfs oplosbare organische stoffen af en wisselen hierbij elektronen met de anode uit, welke dan worden teruggewonnen als elektrische stroom. Naast deze elektronenstroom kunnen elektronen naar verschillende routes stromen: bijvoorbeeld, worden gebruikt voor groei, opgeslagen als biopolymeren, en/of worden gebruikt door alternatieve elektron acceptoren in plaats van de anode. Deze elektronenstromen kunnen worden beïnvloed door de operatiecondities, waardoor het meten van elektronenstromen een belangrijke toetsing is om EABfs en hun werking te begrijpen (details worden gegeven in Hoofdstuk 1). Het doel van deze scriptie was om de relatie tussen de groei van anodische EABfs en de geproduceerde stroom beter te begrijpen en ook hun vermogen om elektronen op te slaan.

Om EABfs te bestuderen kunnen verschillende technieken worden gebruikt. Vanwege hun elektrische eigenschappen is het gebruik van elektrochemische technieken de meest gebruikte manier. Desalniettemin, om de reactie van EABfs op werkcondities en hun karakteristieken ten opzichte van werking te begrijpen zijn meer types van technieken nodig. In Hoofdstuk 2 worden visuele technieken geïntroduceerd als manier om de informatie vanuit elektrochemische technieken aan te vullen. Met visuele technieken kunnen zowel de hoeveelheid EABfs als hun morfologie en compositie worden gekwantificeerd. Dit overzicht hoofdstuk benadrukt de voordelen van het combineren van elektrochemische en non-destructieve visuele technieken en licht het belang van het goed bestuderen van de micro-organismen en de EABfs waar ze in zitten uit om meer kennis op te bouwen richting het optimaliseren van BES.

In Hoofdstuk 3 werd de groei van EABfs bijgehouden met Optische Coherentie Tomografie (OCT) en de relatie tussen de stroomdichtheid en de gemeten dikte van de EABfs op de anodes was bestudeerd met verschillende anode potentialen en acetaat concentraties. Een correlatie tussen toenemende stroomdichtheden (maximaal ongeveer 4 A/m^2) en EABfs diktes tot een bereik tussen 10-30 µm was gevonden. Als dikkere EABfs ontwikkelen op de anode was de stroomdichtheid gelimiteerd door de diffusie van acetaat in de EABfs, wat betekent dat niet alle micro-organismen toegang hadden tot de acetaat en dus ook niet konden bijdragen aan de stroomproductie, resulterend in een stabiele of afnemende stroom. De dikte van EABfs die toegang

hadden tot acetaat nam toe wanneer hogere acetaatconcentraties en hogere anode potentialen werden gebruikt, resulterend in hogere stroomdichtheden.

Een andere belangrijke parameter die de geproduceerde stroom bepaalt is de concentratie van protonen in de EABfs. Deze protonen worden gevormd bij de oxidatie van acetaat, en als de proton concentratie toeneemt, neemt het oxidatie potentiaal van de anode toe, resulterend in lagere overpotentialen, waardoor het gebruik van de anode als eind elektron acceptor minder gunstig maakt. Daarom worden protonen normaal gesproken uit de EABfs verspreid met behulp van een buffer. In Hoofdstuk 4 werden de penetratie dieptes van de buffer berekend en gerelateerd aan de dikte van de EABfs op de anode bij verschillende buffer concentraties. Deze penetratie dieptes waren kleiner bij hogere anode potentialen, wat betekent dat de dikte van EABfs die bijdraagt aan de stroomproductie kleiner werden. Dit werd veroorzaakt door een hogere acetaat consumptie snelheid bij hogere anode potentialen. Zowel in Hoofdstuk 3 en 4 werden acetaat en buffer diffusie snelheden (in orde grootte 10^{-10} m^2/s) en acetaat consumptie snelheden (tussen 0.05 en 0.08 $mol_{acetaat}/m^3/s$) bij verschillende anode potentialen gerapporteerd die kunnen worden gebruikt voor modelleerwerken in anodische EABfs. Daarnaast kunnen deze modellen worden geëxtrapoleerd naar kathodische EABfs en worden gebruikt als hulpmiddel om BES beter te begrijpen.

In Hoofdstuk 5 en 6 was het vermogen van EABfs om elektronen op te slaan onderzocht. In Hoofdstuk 5 werden EABfs gegroeid onder verschillende onderbroken anode potentiaal regimes, terwijl ze continu werden gevoerd met acetaat. Om elektronen opslag te begrijpen werd een elektronenbalans opgezet met de elektronen die aan de anode werden gemeten, de elektronen die werden gebruikt voor de groei van EABf (en planktonische cellen) en de elektronen gebruikt om Extracellulaire Polymere Substanties (EPS). Hoewel de stroom geproduceerd door onderbroken geopereerde EABf hetzelfde was als voor continu geopereerde EABfs, leidden onderbroken anode potentiaal tijden langer dan 20 seconden tot hogere hoeveelheden van micro-organismen in planktonische vorm en vermeerderden de hoeveelheid EPS in zowel de anoliet (tot 40 %) en in de EABfs matrixen (~0.25 g_{EPS}/g_{EABf}). De geproduceerde EPS was rijk aan eiwitten en gebruikt als extracellulaire elektronenopslag om de onderbroken beschikbaarheid van de anode als elektron acceptor op te vangen.

In Hoofdstuk 6 was het effect van acetaat voedingsmodus op elektronen opslag bestudeerd. Om dit te bereiken werden EABfs onder continue en batch voedingsmodi gegroeid, terwijl de anode potentiaal onder continue en onderbroken regimes werd gecontroleerd. Elektronen opslag was gemeten met Confocale Laser Scan Microscopie (CLSM) met kleurstoffen om EPS en intracellulaire elektron opslag verbindingen (poly-hydroxyalkanoaten) te visualiseren in de EABfs. Na het verwerken van de beelden werd een 92 % pixel ratio gevonden tussen poly-hydroxybutyraat (PHB) en micro-organismen in de EABfs die waren gegroeid onder continue anode potentialen na het stoppen van

de voeding. Deze intracellulaire elektronen opslag was gelinkt aan de aanwezigheid van *Geobacter* in de EABfs en er is gesuggereerd dat acetaat tekorten, gecombineerd met constante beschikbaarheid van de anode als eind acceptor voor elektronen, intracellulaire elektronen opslag veroorzaakte. De twee eerder genoemde hoofdstukken openen deuren naar nieuwe niches en mogelijke toepassingen van BES voor de productie van EPS en bioplastics.

Tot slot, na het identificeren van massa overdrachts limitaties en de synthese van elektron opslag verbindingen, vormt Hoofdstuk 7 een discussie en reflectie op de potentiële toepassingen voor anodische EABfs. Omdat hoge stroomdichtheden gewenst zijn, worden strategieën bediscussieerd voor het voorkomen van diffusie gelimiteerde stroomdichtheden en een voorbeeld studie wordt gepresenteerd die uitweidt over EABf groei en verwachte uitdagingen voor het toepassen van anodische EABfs in echte afvalwater stromen en het terugwinnen van energie en grondstoffen. De elektron opslag mechanismen en de potentiële toepassingen van EPS en PHB geproduceerd door anodische EABfs worden besproken, en verder enkele ideeën over toekomstig onderzoek over het gebruik van elektrodes en visuele technieken worden gedeeld.

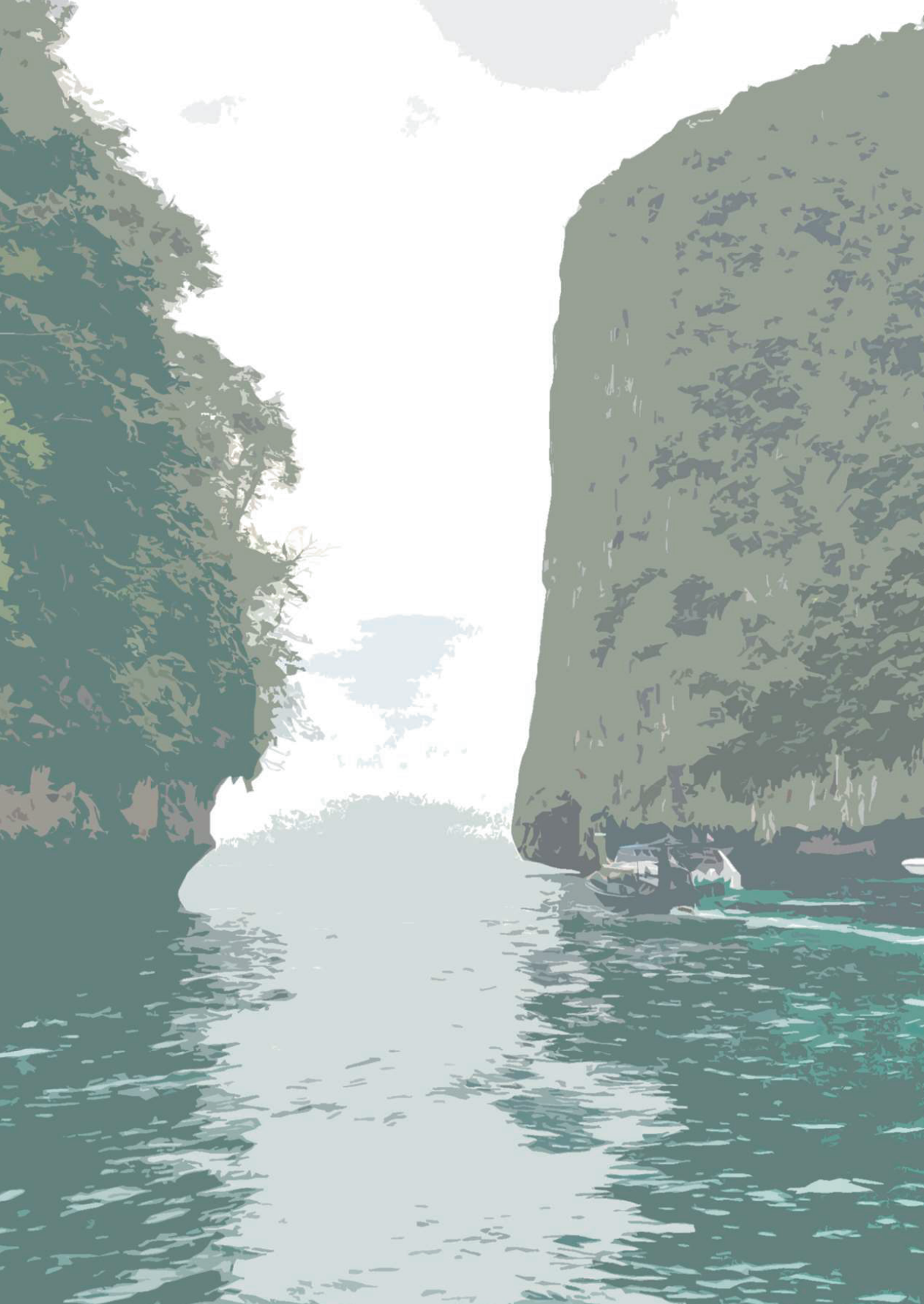

Acknowledgments

Nobody finishes a PhD without the help of others. It may not be obvious and some of us do not immediately realise that doing a PhD is not a lonely adventure. In this academic journey, friends, family, supervisors, students, lab teams, and all kinds of human resources highly contribute to the making of this book. In this section, I would like to thank all the people I met and run into (and that were thus, in different ways, involved in my PhD journey) by sharing with you a narrative of one working day including some moments my PhD was composed of.

7:30h: I would typically arrive at Wetsus a couple of minutes after 7:30h, and my day would not be the same if I did not hear the "Goedemorgen" from Gerben while getting my morning coffee. I really value the fact that Wetsus has a canteen that serves all employees soup for lunch and snacks. Gerben, I really liked your homemade sambal, and Catherina, thanks for allowing me to practice Dutch and teaching me some nice words in exchange for some Portuguese sentences. Karen, thank you very much for always being so happy in the canteen.

8:00h – 9:30h: During a PhD, and especially when working with living microorganisms, the relationship with your experiments can get deep. Therefore, I would always like to check the reactors and talk to my students in the lab. Yes, my students were really a leverage for personal growth and I'm grateful for our work together. Yuniki, you were my first student and I remember being very careful and (over)helping you in the lab when we first start assembling reactors. Looking back, I have to admit that you were more extroverted than I expected and that definitely contributed to have fun working together and to kick off the exploration of electron storage in biofilms. Vivian, I'm really thankful for your work on the development of a methodology to stain the biofilms we worked with. Without your efficiency, we would never have done it. Thanks also for being so open and for sharing personal issues, it really helped us become a stronger team. Guanxiong, we had a bumpy start due to our two completely different routines and working styles. I'm really thankful for your tremendous effort to make many experiments and analyses, and I'm proud that I could witness your learning process and personal development during your thesis. Patrícia, you were my first and only Portuguese student and I must admit that coming back to my roots was not easy. I still remember how much effort I had to put in to talk to you in our native language. But I also remember how much effort you put into your very challenging thesis, and that you kept goal-oriented until the end while working in so many places and bringing together so many research fields. Stan and Bellenod, even though your work has not been included in this book, I would like to thank you for performing risky experiments that will definitely be followed up in the future.

9:30h – 10:00h: A great part of a PhD journey is spent behind the computer answering e-mails, reading literature, analysing data, writing papers, preparing presentations, or just looking for conferences in nice places. These can be wonderful but sometimes

annoying tasks. Therefore, it is important to be part of an office that can deal with different emotions. Luckily, and due to Covid, I sat in three different offices – all of them with different vibes. My pre-covid office was a very happy one because of a nice balance between new and older colleagues. Even though I had a short stay there, I want to thank Dinis, Barbara, Jolanda, Emad, Rose, Diego, and Gosia for the jokes and for helping me start this journey by sharing some scientific knowledge and gossip. Only with such a team we could manage to still have an office dinner before Covid started. Obviously, my Covid office was way more cautious. I want to thank Chris, Ragne, Wokke, Erik, Rouél, Thomas, and Amanda for all the efforts in keeping mental sanity and trying to socialize in this difficult period. The after-covid office was more dynamic: with people coming and going. Starting with the oldest, I would like to thank Shuyana for always being so talkative and positive and connecting so nicely with people. I really liked your proactivity in organizing many events and our meetings about writing. Ruizhe, thank you very much for all the time invested in teaching me how to work with CLSM. Climbing with you was always super nice and I will never forget that I tried to belay you once. Catarina, thank you for bringing some chilling voices to the office and nice food. I really appreciated all the barbecues at your place. Chineelllloooo, I think our relationship should become standard between officemates. I really liked talking to you and being there to listen to your complaints and life experiences, and I also had a lot of fun being PhD representative together with you. Shih-Hsuan, thanks for not accepting to work with me during your internship, if that was the only way we could end up sitting in the same office. Xiao and Dhyana, thank you very much for the nice talks, Lester thank you for being so mysterious but, in your way, giving a bit of yourself to others and Berke thank you for sharing your experiences getting integrated into Dutch culture and your partner's family.

10:00h – 12:00h: Weeks without meetings only happen when one is on holiday. Meetings are a constant during PhD journeys, and for these to take place (after the Covid period) one needs a room. Therefore, I would like to start by thanking Jannie and Anita for always being available to help book rooms, help ship samples to the USA, and rent cars. Besides meetings with students, PV meetings, PhD meetings, etc., I would like to thank the Theme Resource Recovery. Particularly, the PureWater Group for the financial support, and Pieter Hack, Sam Molenaar, Paula, Michel Saakes, Alexandra Deeke, Carolina Plugge, Philip Kuntke, Casper, Sebastian, Simona, Steffen for the fruitful discussions on the presented results and thoughts toward applications. In the NWO meetings, I would like to extend the acknowledgments to Jan Klok for his creative and insightful thoughts.

12:00h – 13:00h: At the end of the morning, all different disciplines typically gather for lunch. This is the time and the opportunity to get to talk about something other than work, to look at each others' plates and discuss origins and cultures, and to plan activities outside work. Sebastian, thank you very much for introducing me to the

CrossFit world and always impressing me with your dancing skills. It was nice to team up with you for the lunch presentations. Carlos, thanks for teaching me how to add coriander to tacos when we had dinner at that tasty Mexican restaurant in Sweden (also thanks for the nice discussion on EPS and storage compounds in general). Rodrigo, it was a pleasure welcoming you at Wetsus, and I find it very funny how you are bringing Portuguese influences on Wetsus and smoked ham to your home in Leeuwarden. Olga, thank you very much for the funny lunches and thoughts about human behaviours and for always sharing your serious/not-serious opinion on e.g., big companies. And to all the other people I had the chance to talk to (not only during lunch but on other occasions) e.g., Sam, Alicia, Talie, Rutger, Kevin, Nouran, Antony, Vania, Carlo, Ángel, Asala, Mu, Barbara, Sophie, Ruben, Keestral, Pamela, Jessica, Edward, Steffen, Ha, Elfy, Edwin, Shuoguang, Sara, Raquel, Gonçalo, Maarten, Loes, Simona, Asala, Suyash, Evelyn, Xiaoxia, Nandini, Prashanth, Hakan, Yizhou, Kecen, Lucía, Ana, Marija, Lourens, Joris, and many others, thank you very much for being part of my PhD.

13:00h – 14:00h: Some days it would not be easy to finish tasks behind the computer because you would always receive messages from your students asking for help, or they would come to your office when things were very bad. Sometimes this really required the help of others, and here is where the staff working in the lab needs a very big round of applause. I want to start by thanking the team of lab technicians: JJ, John, Harm, Ernst, Jan, Johan, Wiebe, and Wim for the collaboration and for helping solve leakages, electrical problems in the set-up, and always being available to think of solutions. Special thanks go to JJ for the work with SolidWorks to design new reactors and for introducing me to Pinguin Radio! I extend the acknowledgments to the lab team: Mieke, Marianne, Lisette, Jelmer, and JW for your readiness to help, running samples and exporting the results, and for educating on the use of equipment such as freeze drier, elemental analyzer, FTIR and SEM. Also, to the microlab team: Agnieszka, Marta, Denise, Bert, Pieter, Bianca, and Cristina thank you for your help with DNA extraction, sending samples for NGS, data interpretation, biofilm staining and biofilm visualization with CLSM and epi-fluorescent microscope.

14:00h – 15:00h: Working at Wetsus and being affiliated with Wageningen UR means that some time needs to be spent at the university. At this timeslot, I would like to thank the Environmental Technology department (ETE). This includes the people I talk to for the very first time online in the ETE trip during Covid, colloquia, and group meetings, and I, fortunately, got to know a little better in the last stage of my PhD. I would like to thank Rikke for the nice chats about our research. Even though our research is slightly different, we had fun and nice scientific discussions that contributed to the shared goals of the project. In the bio-electrochemistry group, I would like to extend my thanks to Margo, Micaela, Yue, Marten, and Xiaofang for the nice brainstorming and troubleshooting meetings. Thanks for making our trip to Leipzig so cool. Another moment that I'm very grateful for is the ETE trip, and many people were involved to

make this happen. I want to thank Alessia, Marko, Jill, Yujun, and Chang for organizing the trip, and extend my thanks to Milan, Sha, Pim, Nora, Dainis, Hooman, Anran, Claudia, Silvana, Thomas, Miriam, and others for making this a super funny and successful trip. Finally, I would also like to thank Yme, Ivonne, Yi, Bi, and Mark for the nice talks at lunch.

15:00h – 16:00h: Another kind of meeting, and typically a very useful one, is the meeting with the supervision team. I would typically have a monthly meeting with all my supervisors to share some progress, interpret and discuss data. This was scheduled on Thursdays at 15:00h, but today we will start it later as Bert needs to get his coffee first. This gives me time to walk on the 2nd floor and thank people that I would see less regularly at Wetsus. First, I would like to thank Johannes and Cees for having created an inspiring research institute that I'm sure it will have brilliant outcomes in the future. I'm also very grateful I could join the meeting with you (the board) to discuss improvement strategies for PhDs at Wetsus, and your voluntary contribution to facilitate and make the eleven cities tour a pleasant day. I would like to thank Hardy for the nice scientific discussions about EPS. In a more social media and events organization matters, I want to thank Hester for making Wetsus visible and share that I'm impressed by your running skills. Still on the 2nd floor, I want to thank Gerrit for processing all the orders on time and without mistakes, and Rienk for help using VPN and bringing more laptops to the lab when needed. Nynke, Anke, and Alexander for helping in the hiring process for new students, Jannette for always finding a time slot to have a meeting with Bert, and Marnejaeike, Linda, Roely, and Trienke for their organization skills for always planning meetings and printing posters on time. I want to extend my thanks to Wies and Liesbeth (working at ETE) for their keenness to plan trips to attend conferences, always solving financial challenges, and dealing with money refunds.

Now that we are all in Bert's office, I would like to thank this fantastic team. Looking back, I realize I was very lucky to be able to join a team that had a solid past in research together and personal relationships. I see this as a very advantageous point that made my PhD journey smoother than the one of the other candidates. Bert, I'm thankful for the times I was there listening when you were brainstorming, and for always finding a way to challenge me. Your fast way of learning and reading people made me enjoy our meetings a lot. Tom, I knew you before starting the PhD and what I liked about you back then is the same I'm thankful for at the end of the PhD journey. Your chilled and funny way of thinking and doing science really helped change my perspectives on research, while still maintaining the quality of the outcomes. Besides, I want to thank you for always being available and for your more regular presence to talk about personal matters. Annemiek, first of all, I want to thank you for choosing me as the best candidate for this position. Even though my hurdles at the beginning of the project related to so much freedom in the research, your supportive style and maximiser talent turned out to be crucial later in the project. I'm very proud that after so many meetings, and after so

many professional and some personal topics discussed, we could always come to a consensus and kept a healthy and harmonized team until the very end. For both Annemiek and Tom, I also want to thank the opportunities you gave me to grow in the BES world by introducing me to your friends at conferences and by allowing me to collaborate with people working in the field. Besides work, I really liked joining your runs in Leipzig, Creta, Haren, and Wageningen, and I hope we can still plan more runs together in the future.

16:00h – 17:00h: Even though working in The Netherlands, collaboration with other institutes and meeting other people at conferences is also an important moment in the PhD journey. I would like to thank Falk and Benni for our collaborative work, and Heleen for the nice talks during the conferences at Aarhus University and in Arnhem. Finally, I would like to thank Fran for the efforts and help interpreting impedance data. I really liked spending a week in Castellón de la Plana and seeing the beautiful garden at your summer house.

17:00h – 18:30h: Sports help you keep a sane mind, and some believe it is crucial to finish your PhD (I'm one of them). During sports, I also got to know better some people. Sifis and Vanessa, thank you both for planning the exercises and for all the times we trained together at the gym. Yicheng, without you I would probably not be alive at this moment. Thank you very much for belaying me and for all the nice moments we spent climbing/bouldering walls in Leeuwarden and playing badminton. Yujia, thanks for the climbing evenings, playing ping-pong, and thanks for the nice time spent in Scandinavia during the ETE trip. Liang-Shin, thank you for bringing me to the badminton club, and Mu Lin thank you very much for showing us all how to properly play badminton. I want to thank Felipe, Hector, Filipe, GJ, Chris, Ángel, Alexander, and Marcus, for the Friday evenings playing indoor football and trying to become champions. Besides, thanks to Thomas, Sophie, Marteen, and all the students for the afternoons playing volleyball outside. Also in Wageningen, thanks Micaela and Jos for the nice beach volleyball afternoons. Finally, to the cycling group, Roel, Jolanda, Antony, Ruizhe, Qingdian, Carlo, Ángel, Sophie, Lisette, Marlene, Pim, Marijn, Dainis, for the practices and the eleven cities tour.

18:30h – 20:30h: To recharge and increase energy levels after sporting, it is key to have a healthy dinner. But even more importantly, it is crucial to share the dinner with people among whom you can be yourself. I would like to thank "North goes south" for the countless times we had pleasant evenings. Mariana, even though we are very different, our relationship has made us understand that people can think differently and that we can accept that. I want to thank you for checking up on me when I was first assembling IKEA furniture until the day you left Leeuwarden, for the advice exchanged, for the walks to and back from Wetsus, for the time spent in the gym, for helping me mingling with others, for the meals, and, more importantly, to always sharing your strong (but honest)

opinion. Qingdian, you turned out to be the person I spent the most time with in Leeuwarden and with whom I've shared the most about myself. We never really talked much about science, but I'm thankful for the way we always looked after each other. Thanks for the guitar sessions, for the time spent puzzling, for the cycling practices and the cycling tour to Groningen and Steenwijk, for the holiday together, for all the birthdays celebrations, and for all the lunches/dinners we had together. Margo, after meeting each other at Wetsus six years ago, I'm happy to see that our relationship remained and has actually grown to a more mature stage. Still, I want to thank you for always bringing simplicity and nature-based answers to our more recent grown-up talks. Coming back to dinner and food, I want to thank Catarina and Gijs for always providing tasty barbecues and for the nice evenings eating with Rita, Emanuel (also thanks for the tasty francesinha and the karts racing), Marianne, Barbara, Sara, and Rodrigo. Finally, thanks to Micaela and Miguel, Milan, Yme, Sha, and others for the nice office dinners in Wageningen.

20:30h – 22:00h: Stepping out of the comfort zone is needed for personal development, but stepping back into the comfort zone can be very rewarding. To my parents and family in Switzerland, and to the family and friends living in Portugal, with whom I occasionally talk, the coming thank words are for you. Mãe, obrigado por tudo, por tudo mesmo! Tu és a mulher mais forte que eu conheço, e eu tenho muito orgulho em ser teu filho e ter sido criado com os teus valores. Pai, obrigado por me ensinares a ser disciplinado e por sempre apelares ao meu lado mais racional para encarar a vida. Família, obrigado por todo o apoio desde sempre! Sofia e Patrícia, apesar de não termos ido de férias por causa do Covid, quero agradecer o facto de sempre arranjarem tempo para estamos juntos quando faço aquelas 'visitas á doutor' ao Porto. Mafalda, muito obrigado por todas as chamadas, por estares sempre lá para me apoiar, e por nos entendermos tão bem. Diogo, Joãozinho, Tony, Bekas, Zé, obrigado pelas boas gargalhadas e por fazerem sentir que o tempo passado á distância nunca existiu. Joana, Sara, e Pedro, obrigado pelos encontros em Matosinhos e em Bruxelas, e pela escapadinha em Valência.

22:00h: As a foreign, it is important to feel home and integrated after a couple of years in the new country of residence. Here, I would like to thank my partner and her family for always making me feel at home. Sanne, je bent de enige person waarvoor ik met mijn hart beslissingen neem ipv met mijn hoofd. Je bent grappig, slim, behulpzaam, sportief, en super lief. Ik ben extreem blij dat ik je heb leren kennen tijdens mijn PhD en ik kan niemand anders bedenken om de rest van mijn leven bij te zijn. Ik bb wat onze volgende avonturen worden maar ik heb er zeker veel zijn in. Naar de schoonfamilie, Piet Bos, Ingrid, Rudi, Ilse, Jan, Stijn, Coen, en Palle bedank voor de gasvrijheid en voor de mooie weekends en vakanties samen.

… - 7:00h: For the people I forgot to mention, I'll probably dream about you!

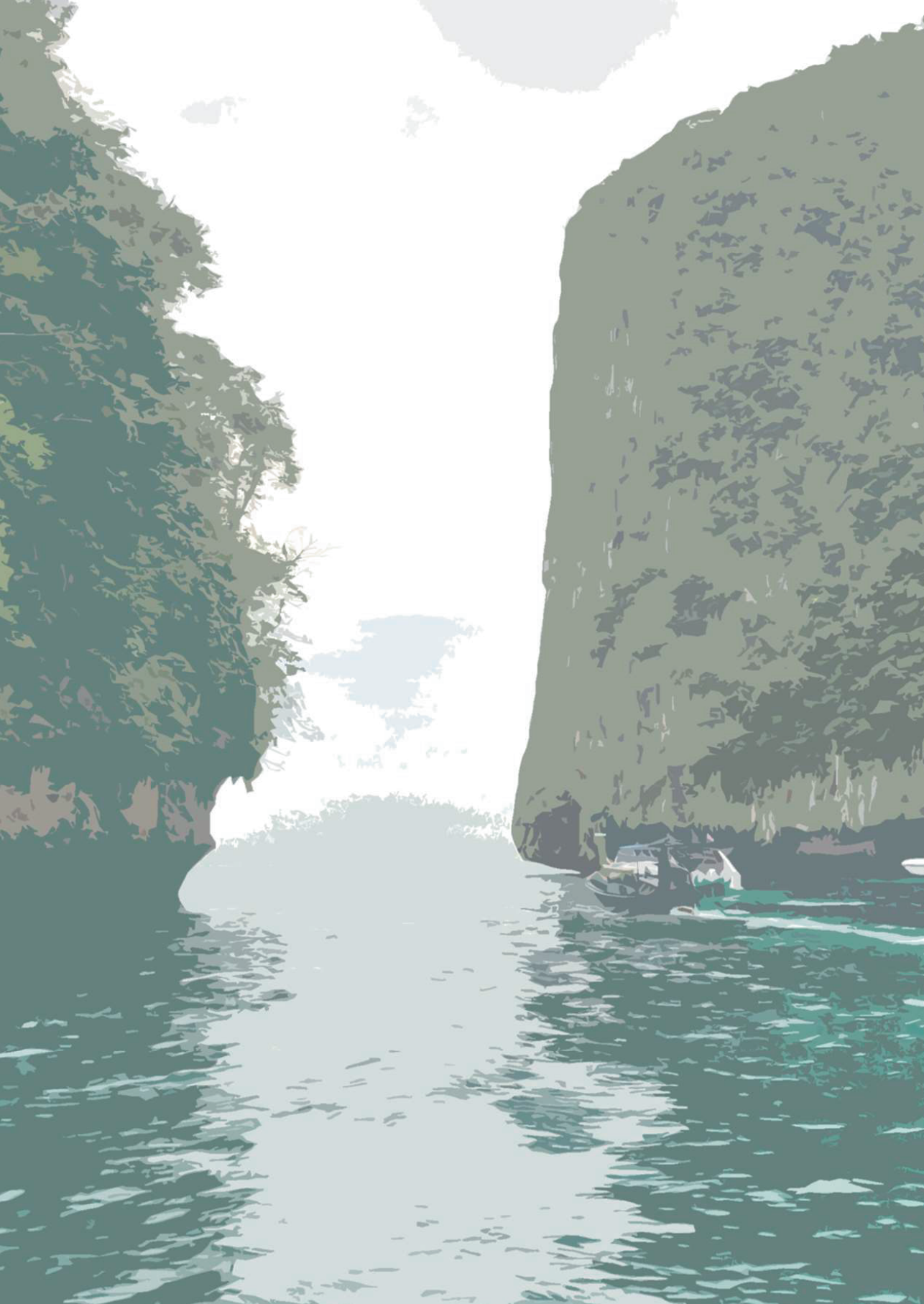

About the author

João Pereira was born in Porto (Portugal) on the 5th of September 1995. He started his Master's in Bioengineering at the Faculty of Engineering of the University of Porto in 2013 and graduated in 2018. During his Masters, he did an Erasmus+ internship at Wetsus on the development of a methodology to quantify electro-active biofilms using Optical Coherence Tomography. For his master's thesis, he joined Allmicroalgae where he optimized *Nannochloropsis* spp. biomass growth for feed application.

After graduating, he started a Trainee Program at Lactogal (a dairy company) and worked as a Bioprocess Engineer at Allmicroalgae. In between, he worked as a tutor on math and chemistry subjects to help primary and high-school students. His ambition to challenge himself and enthusiasm about biological processes made him apply for a Ph.D. at Wageningen University & Research (and Wetsus) in November 2019. Here, he used the method developed during his Erasmus+ internship to further study electro-active microorganisms' growth and electron storage capacity. He had the chance to work in collaboration with Pure Water Group, and he grew both professionally and personally by being exposed to an international environment, supervising students, and presenting his work at several conferences.

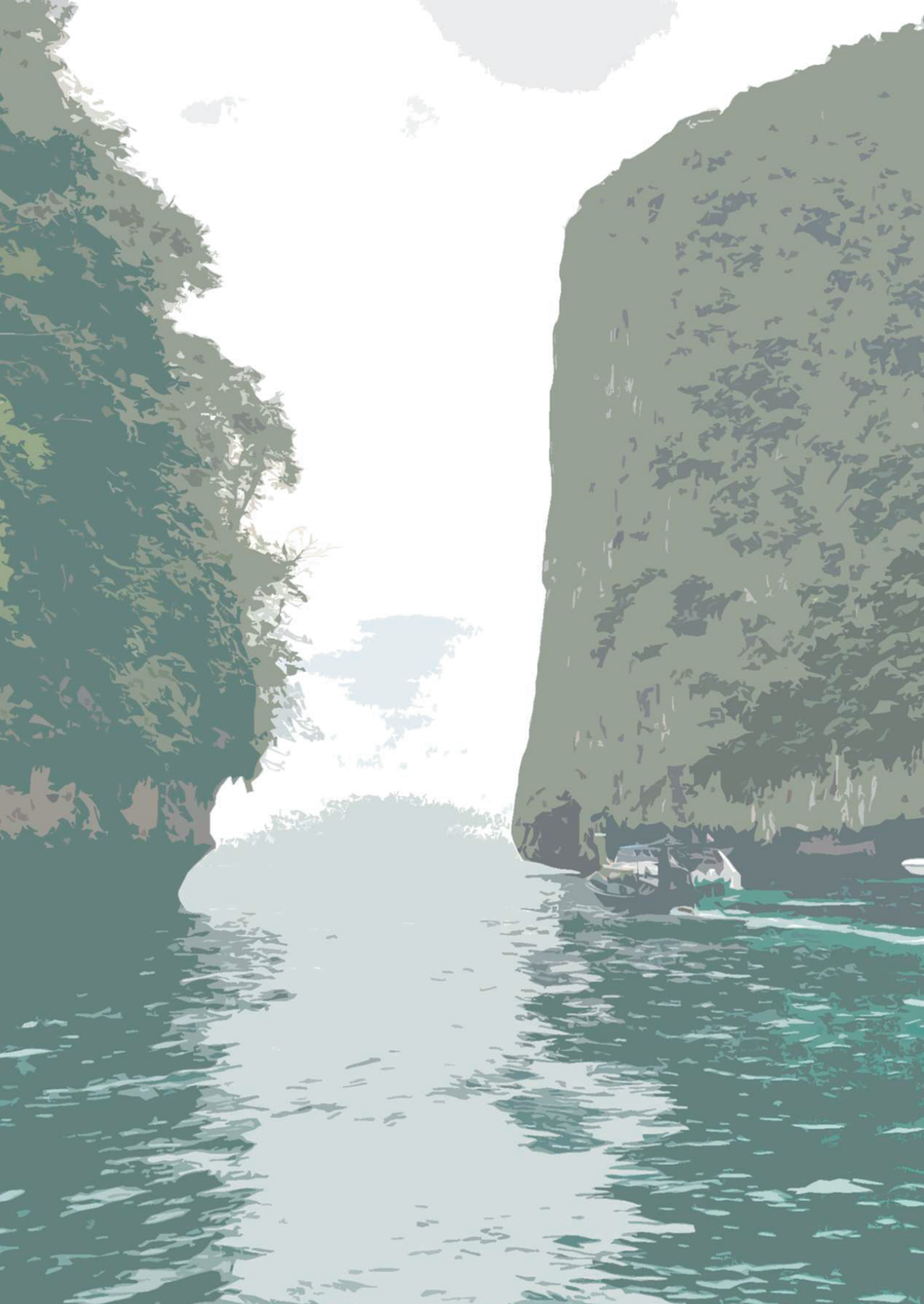

List of publications

Pereira J, Mediayati Y, van Veelen HPJ, Temmink H, Sleutels T, Hamelers B, et al. *The effect of intermittent anode potential regimes on the morphology and extracellular matrix composition of electro-active bacteria*. Biofilm 2021;4:100064. https://doi.org/10.1016/j.biofilm.2021.100064.

Pereira J, Pang S, Borsje C, Sleutels T, Hamelers B, ter Heijne A. *Real-time monitoring of biofilm thickness allows for determination of acetate limitations in bio-anodes*. Bioresour Technol Reports 2022;18:101028. https://doi.org/10.1016/j.biteb.2022.101028.

Pereira J, de Nooy S, Sleutels T, ter Heijne A. *Opportunities for visual techniques to determine characteristics and limitations of electro-active biofilms*. Biotechnol Adv 2022;60:108011. https://doi.org/10.1016/j.biotechadv.2022.108011.

Pereira J, Wang G, Sleutels T, Hamelers B, ter Heijne A. *Maximum thickness of non-buffer limited electro-active biofilms decreases at higher anode potentials*. Biofilm 2022;4:100092. https://doi.org/10.1016/j.biofilm.2022.100092.

Pereira J, Neves P, Nemanic V, Pereira MA, Sleutels T, Hamelers B, ter Heijne A. *Starvation combined with constant anode potential triggers intracellular electron storage in electro-active biofilms*. Water Research 2023;242, 120278. https://doi.org/10.1016/j.watres.2023.120278

Korth B, **Pereira J**, Sleutels T, Harnisch F, & ter Heijne A. *Comparing theoretical and practical biomass yields calls for revisiting thermodynamic growth models for electroactive microorganisms*. Water Research, 2023;120279. https://doi.org/10.1016/j.watres.2023.120279

ter Heijne A, Pereira MA, **Pereira J**, Sleutels T. *Electron Storage in Electroactive Biofilms*. Trends Biotechnol 2020;39:34–42. https://doi.org/10.1016/j.tibtech.2020.06.006.

Molenaar SD, Sleutels T, **Pereira J**, Iorio M, Borsje C, Zamudio JA, et al. *In situ biofilm quantification in bioelectrochemical systems by using optical coherence tomography*. ChemSusChem 2018;11:2171–8. https://doi.org/10.1002/cssc.201800589.

Cunha P, Pereira H, Costa M, **Pereira J**, Silva JT, Fernandes N, et al. *Nannochloropsis oceanica cultivation in pilot-scale raceway ponds-from design to cultivation*. Appl Sci 2020;10. https://doi.org/10.3390/app10051725.

Pereira J, Simões M, Silva JL. *Microalgal assimilation of vitamin B12 toward the production of a superfood*. J Food Biochem 2019;43:1–15. https://doi.org/10.1111/jfbc.12911.

Netherlands Research School for the
Socio-Economic and Natural Sciences of the Environment

D I P L O M A

for specialised PhD training

The Netherlands research school for the
Socio-Economic and Natural Sciences of the Environment
(SENSE) declares that

João Pedro Fontes Pereira

born on the 5th of September 1995 in Porto, Portugal

has successfully fulfilled all requirements of the
educational PhD programme of SENSE.

Wageningen, 11th of September 2023

Chair of the SENSE board

Prof. dr. Martin Wassen

The SENSE Director

Prof. Philipp Pattberg

The SENSE Research School has been accredited by the Royal Netherlands Academy of Arts and Sciences (KNAW)

KONINKLIJKE NEDERLANDSE
AKADEMIE VAN WETENSCHAPPEN

The SENSE Research School declares that **João Pedro Fontes Pereira** has successfully fulfilled all requirements of the educational PhD programme of SENSE with a work load of 47.9 EC, including the following activities:

SENSE PhD Courses

- Environmental research in context (2020)
- Research in context activity: 'Organizing ESEE 2021' (2021)

Other PhD and Advanced MSc Courses

- Personal development courses Wetsus (2019-2021)
- Illustrations for Scientific Publications, Wetsus (2019)
- Industrial Biotechnology, TU Delft (2020)
- Computational Methods in Water Technology, Wetsus (2021)
- Scientific writing, Wageningen Graduate Schools (2021)
- Business Development Course, Wetsus (2022)
- Career perspectives, Wetsus (2023)

Management and Didactic Skills Training

- Supervising 4 MSc students with thesis (2020-2022)
- Supervising 2 BSc students with internship (2020-2022)
- Making lab instruction videos for Wetsus employees (2021)
- Teaching practicals in the MSc course 'Environmental Electrochemical Engineering' (2021 - 2022)

Oral Presentations

- *Real-time monitoring of biofilm thickness allows for the determination of acetate limitations in bio-anodes.* ISMET8 19-23 September 2022, Creta, Greece
- *Real-time monitoring of biofilm thickness allows for the determination of acetate limitations in bio-anodes.* IWA biofilms, 6-8 December 2022, Phuket, Thailand
- *The effect of intermittent anode potential regimes on the morphology and extracellular matrix composition of electro-active bacteria.* Scientific Spring Meeting KNVM & NVMM, 5-6 April 2022, Arnhem, The Netherlands
- *The effect of intermittent anode potential regimes on the morphology and extracellular matrix composition of electro-active bacteria.* Electromicrobiology, 3-5 November 2021, Aarhus, Denmark

SENSE coordinator PhD education

Dr. ir. Peter Vermeulen

This work was performed in the cooperation framework of Wetsus, European Centre of Excellence for Sustainable Water Technology (www. wetsus.nl). Wetsus is co-funded by the Dutch Ministry of Economic Affairs and Ministry of Infrastructure and Environment, the European Union Regional Development Fund, the Province of Fryslân, and the Northern Netherlands Provinces. The authors thank the participants of the research theme “Resource Recovery” for the fruitful discussions and their financial support. This thesis is part of the project “Understanding and controlling electron flows in electro-active biofilms” with project number 17516 of the research program Vidi which is (partly) financed by the Dutch Research Council (NWO).

Financial support from Wageningen University and Wetsus for printing this thesis is gratefully acknowledged.

Thesis cover was designed by João Pereira

Printing: Ridderprint, The Netherlands